Chair of Energy Network Technology

Doctoral Thesis

REVERSIBLE SOLID OXIDE CELL SYSTEMS AND THEIR APPLICATION

David Banasiak, MSc

August 2024

MONTANUNIVERSITÄT LEOBEN
www.unileoben.ac.at

AFFIDAVIT

I declare on oath that I wrote this thesis independently, did not use any sources and aids other than those specified, have fully and truthfully reported the use of generative methods and models of artificial intelligence, and did not otherwise use any other unauthorized aids.

I declare that I have read, understood and complied with the "Good Scientific Practice" of the Montanuniversität Leoben.

Furthermore, I declare that the electronic and printed versions of the submitted thesis are identical in form and content.

Date 30.07.2024

David Banasiak

Signature Author
David Banasiak

ABSTRACT

The main share of greenhouse gas emissions is related to energy production and usage. Therefore, meeting the climate targets of mitigating global warming, set by the United Nations and the European Union, requires a strong expansion of renewable energy production and using this energy efficiently. However, energy from wind and photovoltaic is not controllable and only partly predictable. Therefore, these energy sources are challenging the electrical energy transmission and storage systems. A sector coupling between electricity and gas infrastructure can make the transmission and storage capacities of the gas grid available for the balancing of spatial and temporal mismatch between renewable production and demand. The plans for transforming the natural gas grid to a hydrogen grid, the need for providing carbon free industry feedstock and high temperature heat makes hydrogen an important future energy carrier.

Reversible Solid Oxide Cells (rSOC) are a bidirectional electrochemical conversion technology for converting electricity to hydrogen and back. Therefore, they can enable a coupling of electricity and gas grid. Furthermore, the operation at high temperatures allows for thermal coupling with industrial waste heat and district heating, which enables high conversion efficiencies of above 55%. Another strength of this technology is the fuel flexibility. This allows the fuel cell to operate with natural gas from current grids but also with hydrogen.

In the present thesis, the energy conversion system based on rSOC cells and its application in energy systems is investigated. Firstly, the effect of system parameters in this rSOC system is studied based on a detailed system model. This allows for the determination of important parameters and their values of an optimally designed rSOC system. Secondly, the possibilities and benefits of thermal coupling for both conversion directions are investigated. It allows deriving the characteristics of good integration sites for this system. Thirdly, the application of the rSOC system is simulated, in different ambient energy systems and market conditions, by means of operational optimisation. This gives an understanding of the economic conditions that are necessary to allow rSOC systems to be profitable. Finally, the system's application potential is studied considering grid supportive operation. This makes the identification of most promising installation sites for large scale rSOC systems possible. Thereby, this thesis enables a deep understanding of processes within the rSOC system, proposes approaches for simplified models, shows a simulation option of its application and gives insights into the application potentials.

KURZFASSUNG

Der größte Anteil von Treibhausgasemissionen entsteht im Zusammenhang mit Bereitstellung und Verbrauch von Energie. Um die Klimaziele der Vereinten Nationen und der Europäischen Union zu erreichen, benötigt es daher einen starken Ausbau von erneuerbarer Energieerzeugung und eine Effiziente Nutzung dieser Energie. Die Produktion von Wind und Photovoltaik ist allerdings nicht steuerbar und nur teilweise vorhersehbar. Das führt zu Herausforderungen für das elektrische Übertragungsnetz und für Speichersysteme. Eine Sektorkopplung von Strom- und Gasinfrastruktur kann die Übertragungs- und Speicherkapazitäten des Gasnetztes zum Ausgleich, von räumlichen und zeitlichen Abweichungen von Verbrauch und erneuerbare Erzeugung, zur Verfügung stellen. Die Pläne, zur Transformation des Gasnetzes zu einem Wasserstoffnetz, die Notwendigkeit CO_2 freie Ausgangsstoffe und hoch-temperatur Wärme für Industrie zur Verfügung zu stellen, machen Wasserstoff zu einem zukünftig wichtigen Energieträger.

Reversible Solid Oxide Zellen (rSOC) sind eine bidirektionale elektrochemische Technologie zur Wasserstoffumwandlung, für Strom zu Wasserstoff und zurück. Deshalb ermöglichten sie die Kopplung zwischen Strom- und Gasinfrastruktur. Weiters erlaubt ihr Betrieb bei hohen Temperaturen vielseitige thermische Integrationsmöglichkeiten für industrielle Abwärme und Fernwärmebereitstellung. Dadurch können hohe Gesamtumwandlungseffizienzen von über 55% erzielt werden. Eine weitere Stärke von rSOC-Systeme ist die Brenngasflexibilität, welche einen Brennstoffzellenbetrieb mit Erdgas, von derzeitigen Gasnetzen und auch Wasserstoff, ermöglicht.

In dieser Arbeit werden rSOC-Systeme zur Energieumwandlung und deren Anwendung im Energiesystem untersucht. Zuerst werden wichtige Systemparameter und ihre Werte für ein optimal ausgelegtes System, bestimmt. Danach werden die Möglichkeiten und die Vorteile der thermischen Kopplung für beide Umwandlungsrichtungen analysiert. Daraus werden Charakteristika guter Integrationsstandorte abgeleitet. Weiters wird die Anwendung von rSOC-Systemen über eine Optimierung der Betriebsweise, für unterschiedliche Energiesystemintegrations- und Marktpreisszenarien, untersucht. Daraus ergeben sich die notwendigen wirtschaftlichen Voraussetzungen für einen profitablen Betrieb von rSOC-Systemen. Abschließend werden räumlich aufgelöste Anwendungspotentiale und geeignete Standortcharakteristika für den netzdienlichen Betreib von bidirektionalen Wasserstoffumwandlungstechnologien bestimmt. Durch die Untersuchungen in dieser Arbeit wird ein besseres Verständnis rSOC-System interner Prozesse ermöglicht, eine Vorgehensweise zur Modellvereinfachung und eine Simulation der Anwendung demonstriert. Dadurch ist es möglich die Anwendungspotentiale von rSOC-Systemen abzuleiten.

FOREWORD

Here I would like to thank the people who helped me during the time of working on this thesis and who made its start possible in the first place. The biggest influence which led to this work came from my parents Sigrid and Josef Paczona and my brother Martin Paczona, who were a big help and orientation for choosing this path which includes the work on a dissertation. Also, my wife Natalia was a key ingredient in the success of this work. She decided to move with me to Leoben, allowed for the space required to work on this thesis, was my office mate during one year of Covid-19-virus related home office and was supportive in many scientific discussions.

I am happy that my decisions led me to the Chair of Energy Network Technology (EVT), where I found a place for applying and expanding my skills, which lead to this thesis. At this place I would like to express my gratitude to my supervisor Thomas Kienberger for giving me this chance. Also, the colleagues at the EVT deserve my gratitude, since they were a key ingredient for staying with the topic of my thesis in hopeless times, for diving into seas of unknown depth and discussing dreams, failures und successes.

CONTENTS

NOMENCLATURE

Abbreviations

AEM	Anion exchange membrane electrolysis technology
BoP	Balance of plant
CAPEX	Capital expenditures
EC	Electrolysis cell
EX	Exergy
FC	Fuel cell
fu	Fuel utilisation
G	Gibbs free Energy
GtP	Gas to Power
H	Enthalpy
HX	Heat exchanger
IC	Industry case
IDH	Industry and district heating case
LCOE	Levelized cost of energy
LCOH	Levelized cost of hydrogen
LCOS	Levelized cost of storage
LHV	Lower heating value
LOHC	Liquid organic hydrogen carriers
O/C	Oxygen carbon ratio
P	Power
PEM	Polymer electrolyte membrane / Proton exchange membrane
PtG	Power to Gas
PtH	Power to Hydrogen
Q	Thermal energy

RC	Reference case
rr	Recirculation rate
rROL	Relative return over lifetime
rSOC	Reversible solid oxide cell
rSOC-H2	Reversible solid oxide cell which is operated in FC only with H_2
S	Entropy
s	Specific entropy
SOEC	Solid oxide Electrolysis cell
SOFC	Solid oxide Fuel cell
U	Voltage
WAM	With additional measures
η	Efficiency

Indices

Indices	Description [Unit]
$\dot{E}_{sys}$	Energy stream into or out of the system [W]
$\dot{M}$	Molar flow rate [1/s]
$\dot{M}_f$	Molar flow rate of fuel [1/s]
p_a	Annual profit [€/y]
P_{el}	Electric power flow [W]
P_N	Nominal electric power [W]
$\dot{Q}_{th}$	Thermal power flow [W]
rav_i	Relative average volatility of the electric residual load in the grid node i [-]
y_{H2}	Molar fraction of specie hydrogen [-]
$\Delta_{el,H}$	Price spread of electricity and hydrogen [€/MWh]
η_E	Efficiency in the energy system scenario [-]

η_I	Efficiency in the industry thermal integration scenario [-]
η_S	System efficiency in application scenarios [-]
η_{is}	Isentropic efficiency [-]

LIST OF FIGURES

LIST OF TABLES

PART I

BACKGROUND AND OVERARCHING ANALYSIS

1 INTRODUCTION

The increase of wind and photovoltaic power generation are for many countries one of the main pillars to achieve net zero emissions by 2050 as set by the European "Green Deal" [1].

The first challenge connected with renewable power production comes from the high temporal volatility of wind and photovoltaic production. In contrast, the more stable energy production based on fossil energy or tidal, hydro, geothermal and biomass energy, were the main production technologies of the past. The newly introduced temporal fluctuations of production are challenging because the current energy system is designed based on fossil fuels, which can be stored cheaply in great amounts [2] and therefore it is not designed for storing electrical energy. Pumped hydro storages can provide flexible storage demand [3], however with geographical limitations. Therefore, especially the monthly to seasonal long-term fluctuations require pathways to store renewable energy in a similar manner like fossil energy. The second challenge connected with renewable energy is its inhomogeneous spatial distribution, as shown by Sejkora et al. for the case of Austria [4]. Actually, the global distribution of renewable energy potentials is, according to Overland et al. [5], more uniform than for fossil energy carriers. However, the problem for renewably produced energy is again, that energy is available mostly in the form of electricity, which is much harder to transport than fossil energy carriers with high energy density, like gas, oil and coal.

The gas grid fulfils already nowadays the need for balancing energy demand and availability on large spatial and temporal scales. Power-to-Gas (PtG) and Gas-to-Power (GtP) sector coupling technologies can make the gas grid's storage capacities available for the electricity grid and thus address the two challenges of renewable energy mentioned in the paragraph above. In Europe there are already plans for the transformation of the natural gas grid into a hydrogen gas grid [6], which allows for a more efficient sector coupling by avoiding an additional transformation step of H_2 to CH_4. With the cheap underground storage capacities of aquifers, hard rock and salt caverns, hydrogen can satisfy a big part of the long-term energy storage demand.

The PtG, especially the non-fossil-based Power-to-Hydrogen (PtH), route is possible through different water electrolysis technologies, which include alkaline electrolysers, proton-exchange-membrane (PEM) electrolysers, anion exchange membrane (AEM) electrolysers and solid oxide electrolysers (SOEC). According to the IEA [7] in 2023 a total electrolysis capacity of 2.2 GW was installed and if all the projects in pipeline get realized the capacity will be 175-420 GW by 2030. SOEC's offer the highest conversion efficiencies [8] and additionally low environmental life-cycle impact [9]. In SOECs a part of the required electrical energy can be

replaced by industrial waste heat, which allows already in today's systems for electrical conversion efficiencies of 84%, as is shown by Schwarze et al. [10].

GtP is already realized in large scale by CH_4-gas turbines, with an installed power of 313 GW in Europe in 2021 [11], which can potentially be operated with H_2 as well. Combined cycle gas turbines reach electric efficiencies of around 60% [9]. PEM fuel cells (FC) reach similar electric efficiencies and Solid oxide fuel cells (SOFC) can reach 65% [12, 13]. Fuel cell based combined cycles can increase the efficiency even further to 74% [14]. The capacity of installed SOFC fuel cells was 150 MW in 2020 [15] and IEA reports a future overall fuel cell capacity for power generation of around 500 MW in 2030 [7]. Not only are fuel cells highly efficient, but they are also applicable for smaller power scales, which allows better integration to electricity consumers with on-site waste heat utilisation for heating purposes. The SOFC operates at high temperatures of above 600°C, which allows to provide thermal energy to district heating systems and to industrial processes. The industrial heat demand up to medium high temperatures of 400°C presents a significant amount of heat [16] that could be covered by this technology. Another speciality of this fuel cell technology is the fuel flexibility, which allows systems to operate besides pure H_2 with various H_2 rich fuels, such as hydrocarbons like CH_4 [17] or NH_3 [18]. This is especially useful when considering the transition of gas grids from natural gas to H_2, where the rSOC technology can transform together with the grid. Furthermore,

Reversible Solid Oxide Cells (rSOC) are an electrochemical conversion technology that can produce H_2 in electrolysis operation (SOEC) and electricity and heat in fuel cell operation (SOFC) with the same electrochemical stack. Thus, they combine both PtG and GtP in one unit which reduces the environmental impact connected with the production of bidirectional system types. The rapid increase of installed electrolysis and fuel cell technologies, expected by the IEA [7], shows the high interest in these H_2 conversion technologies. Both conversion directions can be addressed by rSOC systems. Because of all the above-mentioned coupling possibilities and the high conversion efficiencies, the rSOC technology is a key enabler for a CO_2-emission free energy system.

1.1 Structure of this work

The present thesis investigates the application of rSOC technology in the future energy system. It is composed as a cumulative work consisting of this manuscript and the connected peer reviewed journal articles, which can be found in section 9 (page 75). This manuscript deals with the overarching questions concerning reversible hydrogen conversion technologies based on rSOC systems and aims at giving an overview of the performed research activities. Therefore, it refers to the connected publications of Chapter 9 and reproduces main

approaches and results which are needed to understand the higher-level conclusions that are drawn in this work.

This manuscript starts in Chapter 2 by deriving the research need from recent literature and stating the research questions that are answered by the present thesis. In Chapter 3 an overview of the methodological approach is given, including the connections between the different scientific publications, which constitute the core of this work. Chapter 4 provides the insights into theory and applied methods with a discussion of uncertainties and limitations of the different approaches. In Chapter 5 one finds the results produced with these approaches. This leads to the answers to the research questions which are presented in Chapter 6. Finally, Chapter 7 gives an outlook for future work that can improve the accuracy of the investigated system application potentials. The peer reviewed journal articles which are an integrated part of this work, can be found in the three sections B1, P1, P2 of Chapter 9. An overview of the connected conference contributions is given in section 10 (Appendix A).

2 DERIVATION OF THE RESEARCH NEED

This Chapter derives the research need based on publications concerning recent advances in the context of rSOC systems and their application in different energy systems.

2.1 Gaps in studies concerning the rSOC system internal parameters and thermal interaction

The electrochemical processes within the rSOC stack can be understood based on different published research activities, where stacks are placed in laboratory settings to investigate the behaviour under different influences. Ferrero et al. [19] validated a cell model, which can predict the voltage for fuel cell (FC) and electrolysis cell (EC) operation for different gas mixtures at the fuel electrode. Here the focus lies on rSOC systems, including Balance-of-Plant (BoP) components, and not single electrochemical cells. The performance of such a system, for SOEC operation, was investigated by Chen et al. [20]. They studied the influence of temperature, pressure, air flow and steam utilisation and optimize the parameter settings. The considered system does not include recirculation of the outlet gases. According to Frank et al. [21], who study internal heat recovery and ideal parameter settings for an rSOC system with recirculation on the fuel/steam outlet, the recirculation increases the efficiency in both operation modes. They optimized the recirculation rate at fixed values for fuel utilisation. The employed 0D stack model, however, cannot represent the influence of spatial change of concentrations. An improved representation including the stack geometry as shown by Subotic et al. [22] would be necessary. The lack of described connection between different modelling levels of the rSOC system leads to the research question (1) of section 2.3. Furthermore, Giap et al. [23] found that the recirculation with a blower is more exergy efficient than with a steam driven ejector. With the mentioned system studies the influence of internal parameters on the system's performance can be understood. However, the consequences of this understanding for modelling of rSOC systems needs further clarification to answer research question (2).

Other research groups included in their investigations of the rSOC system thermal coupling with heat storages or external systems. Thermal energy storages allow the EC operation to be supplied with heat from the FC operation in the study of Perna et al. [24]. They investigate a rSOC system as energy storage with a closed system for all reactants and products (H_2, H_2O and O_2). Giap et al. [25] and [23] included, in their parameter study for rSOC systems, waste heat used for steam production in EC operation. They found that the waste heat temperature is of little relevance for the performance. Also the thermal coupling to metal hydride H_2 storage is studied by Giap et al. [26]. Heat storage by phase change materials and exothermic

methanation of H_2 are considered as thermal system improvements by Mottaghizadeh et al. [27]. Schwarze et al. [28] have shown that a real installation of a 720 kW_{EC} SOEC system can reach an electrical efficiency of 84%, if industrial waste heat is available. Earlier, the operation of a 150/30 kW rSOC system was shown to have an electrical EC efficiency of 80% and FC efficiency of 50%, when operated with natural gas. From these studies, it is not yet clear how the heat demand in EC operation can be provided and a detailed investigation of the coupling to district heating is not present. This results in research question (3), concerning good application sites and their benefits for the rSOC systems.

2.2 Gaps in studies concerning the rSOC system integration and application in energy systems

Peters et al. [29] have shown that the reversible operation of rSOC systems with fast mode switching is possible. This makes the investigation of such systems as flexible units in energy systems interesting. Hutty et al. [30] considered a microgrid application of rSOC systems together with PV to increase the self-sufficiency ratio and found that the lifetime of the system's stack must be above 10 years to reach parity with the grid electricity price. Furthermore, they found that the economics depend strongly on the geographical location, since the storage need arises from PV production and the electric energy demand. Singer [31] considered the application of rSOC in energy systems based on time resolved operation optimisation and found that the operation share and profitability depends on future energy prices and system investment cost. Lamagna et al. [32] suggests that the application of rSOC systems as back up and H_2 production technology and combined desalination capability by off-shore wind parks is promising. In their investigations they employ a rule-based simulation with different operational strategies. Also, Mattaghizadeh et al. [33] uses rule-based simulation for the integration to buildings. Motylinski et al. [34] study the compatibility of the rSOC system's dynamic operation to the production profiles of wind turbines on the basis of a detailed stack model and given time-series for operation. Research question (4) arises in this context of different approaches used for simulating the time resolved operation of a rSOC system.

Reznicek et al. [35] calculated the levelized cost of storage (LCOS) with a rSOC system and compressed H_2 storage. They conclude that the levelized cost of energy (LCOE) of this technology are approaching the costs of electricity grid managing technologies like gas peak plants. Their approach does not include variability of energy prices and resulting choice of system operation but is based on given time shares of the different operation modes and static energy prices. Therefore, research question (5) was found to be insufficiently answered in available literature.

Research question (6) arises as a continuation of question (5). Further investigations in this direction of electricity grid influence are already proposed by Motylinski et al. [34] and Reznicek et al. [36]. Question (7) derives from the answers to the previous questions and their implications for finding application sites for rSOC Systems.

2.3 Research questions

In this section the overarching research questions, answered in this thesis, are summarized. Question (1) to (5) arise in the literature survey of section 2.1 and 2.2 and the question (6) and (7) are logical continuation.

Research questions:

(1) How are the simulation models for the low-level of the electrochemical cell, the mid-level of the stack and the high-level of the reversible system sequentially building up?
(2) What are good simplifications in the simulation of the rSOC system regarding the optimal operation parameters and the flowsheet?
(3) What are the possibilities and the benefits of coupling the rSOC system thermally to waste heat sources and heat sinks? What should good sites for the integration of rSOC systems offer?
(4) How can the operation of the rSOC system be simulated in different scenarios, what kind of system models are necessary and how can these be built-up most efficiently?
(5) Which economic and application conditions make the operation of reversible H_2 systems and rSOC systems profitable?
(6) What are the application potentials for locally concentrated reversible H_2 systems considering electricity grid service by smoothing residual loads?
(7) What are characteristics of the most promising application sites for rSOC systems?

3 METHODOLOGY

The presented thesis gives answers to all research questions highlighted in section 2.3. For this purpose, it refers to the author's works published in three peer-reviewed scientific journals in Chapter 9 and the conference contributions in Chapter 10. This Chapter provides an overview of the topics that are answered in this thesis based on the connected publications.

3.1 Approach and outline of the thesis

The methodology applied in the literature connected to this thesis can be divided into the three main parts that are followed by a study of system application potentials in the energy grid and accompanied by studying recent literature, as illustrated in Figure 1.

1. Firstly, **the rSOC system is studied** on a basis of models for the rSOC stack, the balance of plant components and the H_2 storage. With these models different configurations of the system-flowsheet are investigated and a study of the influence of operational system parameters is performed, as described in detail in B1 [37]. The processes in the rSOC stack and consequences for the internal heat recovery, as discussed in this thesis, were presented at the "New Energy for Industry" (NEFI) conference in 2021. In a next step, the physical model of the stack is exchanged to a data driven model for the electrolyte supported rSOC stack provided by Fraunhofer Institute for Ceramic Technologies and Systems (IKTS). This adapted model is used for investigation of the influence of operational system parameters, as shown in the conference contribution to the EnInnov conference in 2022.
2. Secondly, the application of **rSOC systems in industrial sites** is investigated, as described in P1 [38] and presented at the conference on sustainable development of energy, water and environmental systems (SDEWES) in 2022. The basis for this investigation is a simplified model for the rSOC system, that represents the part-load conversion behaviour from electricity to hydrogen and heat. This model is based on the insights created by the physical models of point 1. Furthermore, waste heat availability in different industrial processes and the process interdependence is studied.
3. Thirdly, the **Techno-economic performance of the rSOC system** in the energy system is studied, based on P2 [39] and the conference contributions C4 to C6. The operation of the system is simulated by an optimisation model, which minimizes the energy costs and connects the system models with time-series for integration scenarios (industry, district heat) and energy market prices. The mixed integer linear formulation of the optimisation problem demands for a suitable model of the rSOC system. This model is generated by piecewise linearization of the part load conversion curves, for electricity to hydrogen and electricity to heat, from point 2.

4. Finally, the **application of two spatial types of bidirectional H_2 conversion systems** in the Austrian electrical energy grid are studied. As a basis for this investigation, it is considered that the purpose of the systems' operation is to provide grid service by smoothing the electrical residual loads. This approach was presented at the "Symposium Energieinnovation" (EnInnov) conference in 2024.

The models used for the investigation of the rSOC system evolve from the description of stack internal processes in point 1, to a full system model allowing the investigation for the interaction with ambient systems in point 2. The Techno-economic assessment of point 3 is based on a simplification of the system model, which allows the optimisation of operation in a representation of the application scenarios by time-series .

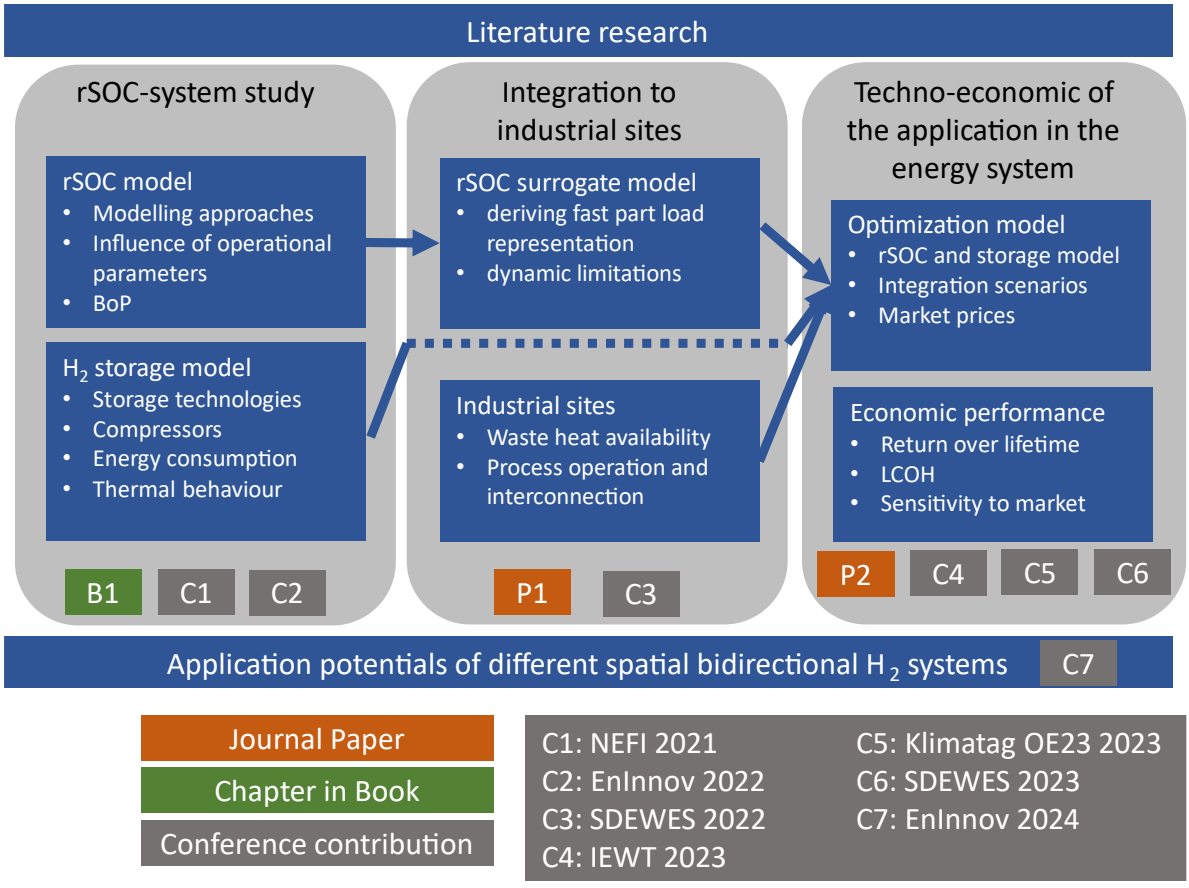

Figure 1: Illustration of methodology and its interconnections in this work: including publications in scientific journals and conference contributions.

4 THEORETICAL BACKGROUND AND METHODS

This Chapter provides the theoretical background and methods that are applied in the research connected with the four methodological sections of Chapter 3. It comprises the underlying processes of rSOC systems and H_2-storage systems and the approaches used for modelling these systems, which are necessary to understand the results and conclusions drawn in this thesis.

4.1 rSOC-system study

In this section the fundamentals of electrochemical rSOC systems are introduced, which are necessary for modelling the system from cell to system level. Furthermore, important results from the investigation in the scientific book Chapter B1 [37] and conference contributions C1 and C1 are discussed.

4.1.1 Electrochemical cell and thermodynamic description

The planar rSOC stack consists of a fuel channel, an air channel, an electrode in both channels which are separated by an electrolyte allowing ion selective charge transport from one electrode to the other. This layered structure can be seen in Figure 2. During the stack's operation the reactive species are transported from the gas bulk phase of the channels to the catalytic electrode surfaces by fluid transport mechanisms that include turbulence and diffusion. At the oxygen electrode surface the catalytic reaction from molecular to ionic oxygen takes place. In fuel cell operation electrons are released (cathode) and in electrolysis operation consumed (anode). In fuel cell operation the O^{2-}-ions are transported through the electrolyte from air to fuel channel due to the electrochemical potential difference between the electrodes. This potential difference can be used in the external electron conducting circuit. At the hydrogen electrode the reaction of hydrogen and oxygen ions to water takes place (equation (1) reacting from left to right). In electrolysis operation the reaction in equation (1) runs from right to left and the oxygen ions move from the hydrogen electrode to the oxygen electrode due to the externally applied voltage. The operation temperature for rSOC-cells in EC and FC operation is above 600°C, as one can see for different stacks studied by Preininger et al. [40], since the electrolyte's conductivity for oxygen ions increases with temperature. Upper limits for the operation are given by structural limits of materials at around 1000°C.

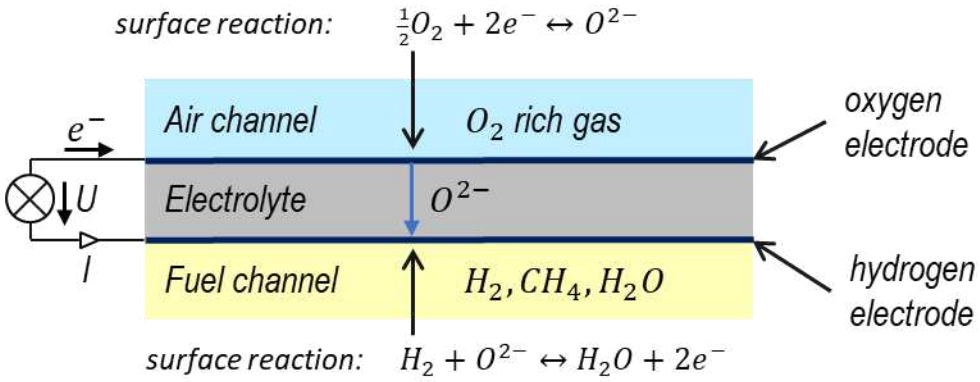

Figure 2: Layers of the stack and electrochemical reactions (directions for fuel cell operation, based on [41]).

$$H_2 + \frac{1}{2}O_2 \leftrightarrow H_2O \qquad (1)$$

The operation of the cell at high temperatures allows for flexibility of hydrocarbon-based fuels and ammonia as shown by Rabuni et al. [17] and Rathore et al. [18]. The hydrocarbon based fuel flexibility of SOFCs is reported on by Rabuni et al. [17], who gave a review on hydrocarbons as fuel and on direct and indirect pathways for its utilisation. The indirect way is most common, where the hydrocarbons are at first undergoing reactions for creating hydrogen, which is then converted in the electrochemical reaction. The reformation of hydrocarbons to H_2 is possible since the chemical equilibrium shifts with high temperatures to H_2. Figure 3 illustrates the temperature dependence of the equilibrium concentrations of important species for a mixture of H_2O and CH_4, which was calculated with the Python package of Cantera [42]. At above 600°C the equilibrium for the mixture shifts to H_2, which can occur under normal operation conditions of the rSOC-cell, while the metallic nickel electrodes act as catalysts. Due to the possible catalyst deactivation by formation of solid coke and the necessity of controlling the stack's internal temperature gradients, an additional pre-reformer is beneficial. A more detailed discussion of the formation of solid coke and other operation limits is presented in section 4.1.2, since this is critical in the operation of the stack.

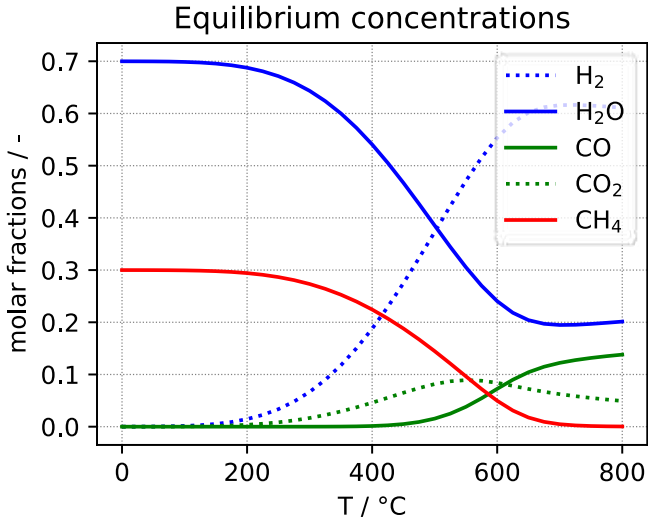

Figure 3: Temperature dependence of the molar equilibrium concentrations for a 70 % H_2O and 30% CH_4 gas mix.

The potential difference that appears between the oxygen and hydrogen electrode in open circuit can be calculated with the Nernst equation (equation (2)). The convention for the sign of the potential is such that a spontaneous occurring reaction yields a positive voltage. U_N is also referred to as the open circuit voltage.

$$U_N(T,p) = -\frac{\Delta G(T,p)}{2F} = -\frac{1}{2F}\left(\Delta G^0(T,p^0) + \Delta G(y_i,p)\right) \qquad (2)$$

$$\Delta G(y_i,p) = RT \cdot \ln\left(\frac{y_{H_2} y_{O_2}^{0,5}}{y_{H_2O}}\right) + \frac{RT}{2} \cdot \ln\left(\frac{p}{p^0}\right) \qquad (3)$$

The change of the Gibbs free energy (ΔG), as defined in equation (4), is equal to the reversible free reaction energy, while the change of enthalpy (ΔH) reflects the total released energy and the Entropy connected term (TΔS) the released heat.

$$\Delta G = \Delta H - T\Delta S \qquad (4)$$

By replacing the Gibbs free energy in the Nernst equation with enthalpy and the entropy term, the corresponding energies were calculated as electrical potential together with the Nernst potential, as shown in Figure 4, with the help of the Python package of Cantera [42] and using the equations (2), (3) and (4). The energy related to ΔG is the electrical potential (U_N), whereas the difference to the total reaction energy ($U_{\Delta H}$) is the thermal share ($U_{T\Delta S}$). At the transition from water to steam region, a step appears in the thermal reaction energy share which relates to the phase transition energy. This poses an advantage especially for electrolysis of steam, since the thermal phase transition energy to produce the feed steam can be provided from outside of the stack. This enables an increased electric efficiency.

The Gibbs free energy of the reaction decreases slowly with increasing temperature, while the share of thermal energy below and above the evaporation point increases. This means that at higher temperatures fuel cells produce less electrical but more thermal energy.

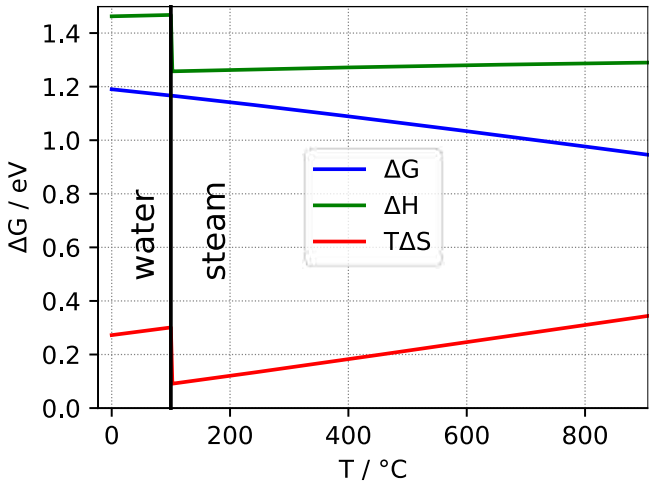

Figure 4: Change of the total (ΔH), reversible (ΔG) and irreversible (TΔS) reaction energy for the reaction of equation (1).

The so far discussed Nernst potential (equation (2)) yields, as mentioned, the open circuit voltage of the electrochemical cell (U_N). In any application, the transport of ions through the electrodes and the electrolyte, the transport of reactive molecules to the reactive centres and the overcoming of activation energies, contribute to the actual potential difference that is available in the fuel cell or must be applied in the electrolysis cell. These contributions are ohmic, diffusion, and activation overpotential as described by Srikanth et al. [43], Costamagna et al. [44], Ferrero et al. [19] and Kazempoor et al. [45]. The resulting cell voltage is given by equation (5) and Figure 5 shows how the resulting polarization curve for cells looks like.

$$U_{cell}(j) = U_N - U_{act}(j) - U_{ohm}(j) - U_{diff}(j) \qquad (5)$$

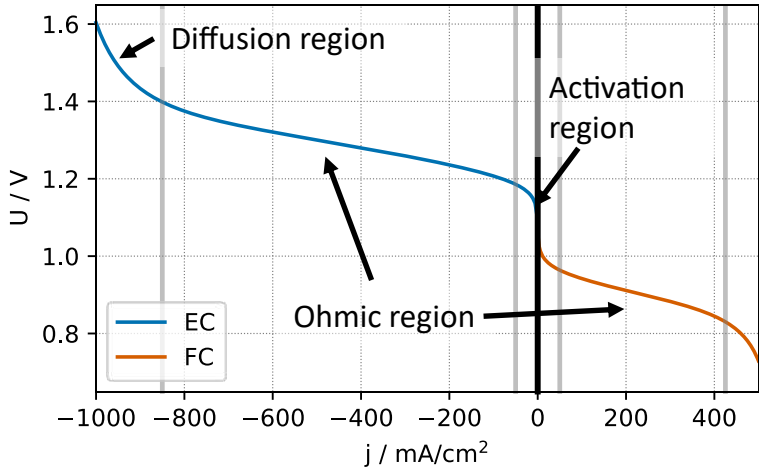

Figure 5: Schematic polarization curve of an rSOC cell operated with the same fuel mix in EC and FC operation.

The ohmic overpotential is caused by the ohmic resistance for the charge transport in the electrolyte and the electrodes. In solid oxide cells this resistance is highly dependent on the temperature. The activation overpotential is a result of the temperature dependent reaction kinetics at the electrode surfaces and relates to the gas concentrations at the active phase boundary. Similarly, the gas concentration at this boundary determines the diffusion overpotential, which relates to the concentration change from gas bulk to electrode surface and triple phase boundary. The gas concentrations at the triple phase boundary are a result of fluid transport mechanisms that depend on the concentration gradient between bulk and triple phase boundary concentrations and electrode material properties, which describe the permeability for gas molecules. Furthermore, the concentration gradients are connected to the electric cell current so that higher current causes higher concentration gradients and thus an increased transport of reactive molecules to the reactive recentres. The transport processes can be spatially resolved by computational fluid dynamics as shown by Yang et al. [46], Du et al. [47] and Wang et al. [48]. Subotic et al. [22] show in their investigations the current dependent contributions to the over voltage for different spatial resolutions of the stack.

In electrolysis operation, the overpotentials during the operation of the electrochemical cell can lead to three thermally different cases, which are illustrated in Figure 6. The cell voltage ($U_{\Delta H}$) calculated according to equation (2), considering the enthalpy (ΔH) instead of Gibbs energy (ΔG), divides these regions, which are:

1) Endothermic operation: The potential difference applied to the cell is smaller than $U_{\Delta H}$. This means that in addition to the electric energy, thermal energy must be provided for a thermally stable operation.
2) Thermoneutral operation: The potential difference applied to the cell is equal to $U_{\Delta H}$. In this case the thermal demand of the reaction is exactly covered by the internal losses.
3) Exothermic operation: The potential difference applied to the cell is larger than $U_{\Delta H}$. Here, the cell produces more thermal energy than is required in the reaction and a cooling of the cell is necessary to operate the cell thermally stable.

As Figure 4 shows, the thermal share of the reaction energy increases with temperature. This means that the thermoneutral operation shifts to higher overvoltage and thus a higher cell current.

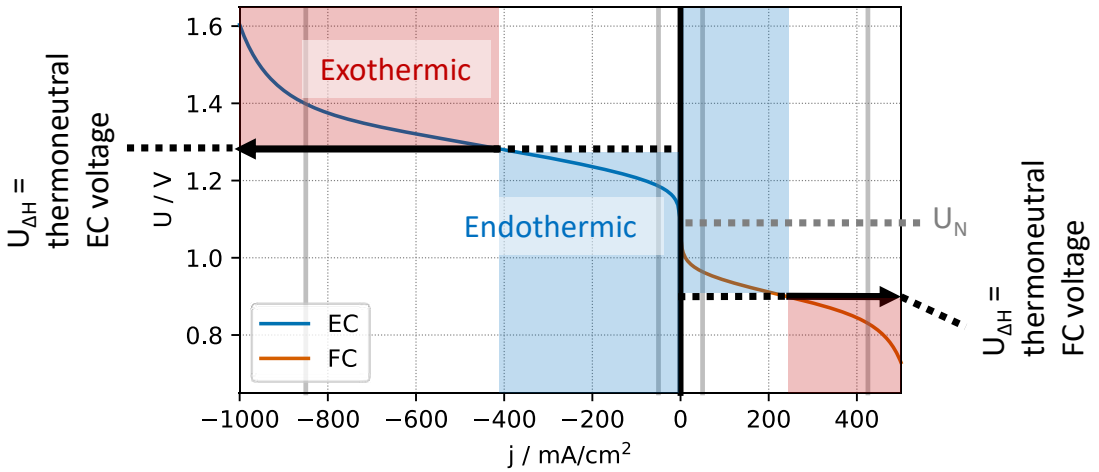

Figure 6: Thermal operation regimes for EC and FC operation.

The electrical efficiency of the cell is the quotient of energy produced by and provided to the cell. These energy streams are hydrogen rich fuel and electrical power, which switch role in EC and FC operation as shown in (6) and (7).

$$\eta_{FC} = \frac{P_{electric}}{P_{fuel}} \qquad (6)$$

$$\eta_{EC} = \frac{P_{fuel}}{P_{electric}} \qquad (7)$$

The electrical energy, that is required or produced by the cell, can be calculated from the cell voltage and the charge current transferred in the reaction (see equation (8)). The transferred charge relates to the molar flow of the fuel that reacts in the cell ($\dot{M}_{react}$), the Faraday constant for single charged ions (F) and the charge number of the ions taking part in the reaction ($n_{react,H2} = 2$).

$$\begin{aligned} P_{electric}(j) &= U_{cell}(j) \cdot j \cdot A_{cell} \\ &= U_{cell}(j) \cdot \dot{M}_{react} \cdot F \cdot n_{react} \end{aligned} \qquad (8)$$

The energy stream related to the fuel can be calculated from the fuel's molar ($\dot{M}_{react}$) or mass flow rate that is reacting in the cell and the respective heating value, as shown in equation (9). The present study considers the lower heating value (LHV) as the specific energy content of the fuel.

$$P_{fuel}(j) = \dot{M}_{react} \cdot LHV \qquad (9)$$

Inserting the definitions for both energy streams to equation (6) and (7) results in equation (10) and (11) for the electrical efficiency in EC and FC operation. One can see clearly that the cell voltage is the single variable defining the conversion efficiency.

$$\eta_{cell,FC} = \frac{U_{Cell} \cdot F \cdot n_{react}}{LHV} \qquad (10)$$

$$\eta_{cell,EC} = \frac{LHV}{U_{Cell} \cdot F \cdot n_{react}} \qquad (11)$$

4.1.2 The path from electrochemical cell to stack level

The distribution of the gas concentration and temperature varies along the gas flow direction within the stack and depends on the geometrical design of the stack's gas flow fields. Therefore, the Nernst voltage also varies within the stack, according to equation (2) and (3), as is visualized in Figure 7 for assumed concentration changes of O_2 and H_2 in counterflow arrangement.

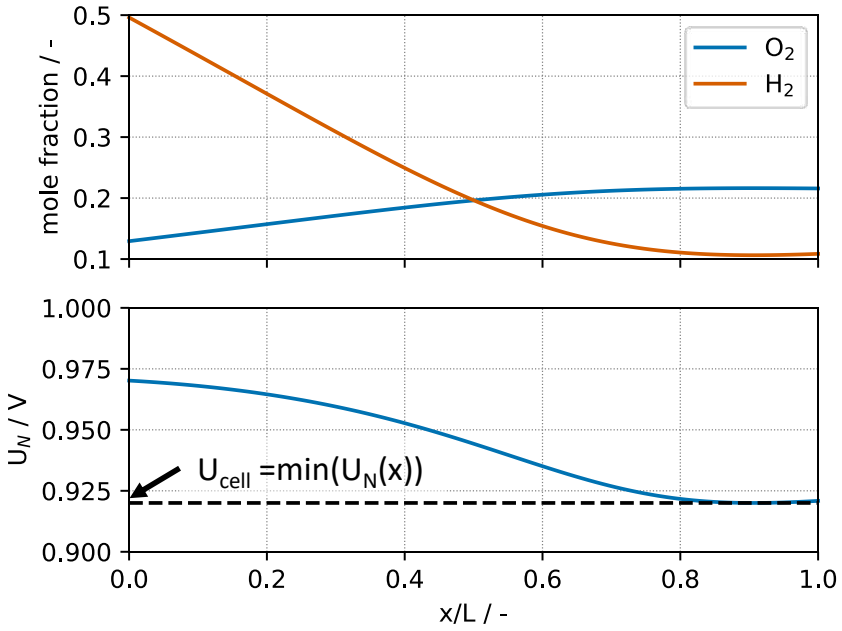

Figure 7: Change of gas concentrations and Nernst voltage along the flow direction (x) of a stack with length L, with H_2 and air provided in counterflow.

The flow fields of the stack may be designed in different ways of flow path layouts and assemblies for fuel and oxidant flow fields, which have different consequences for the stack performance, as shown by Saied et al. [49]. Possible flow field layouts include helical, parallel and serpentine flow and assemblies can be co-, counter- and crossflow or combinations of these. The equation for the cell voltage (equation (5)) allows us to derive the voltage in a single point of the stack, for given local temperature and gas concentrations. Since the metallic electrodes pose equipotential plates on both sides of the solid electrolyte, the actual operation voltage for a stack is determined by the most critical point of the electrochemical reaction according to equation (12) with the cell potential difference given in equation (5). The point with lowest potential difference determines the stack voltage in fuel cell operation and the point with highest potential difference determines the stack voltage in electrolysis operation.

$$U_{stack}(j) = U_{cell,criticalpoint}(j) \qquad (12)$$

The location of the most critical point is influenced by gas concentrations, temperature distribution, by the flow field and flow directions. The difference of the gas concentration and temperature between stack inlet and the critical point (close to the outlet) is connected to the stack's fuel utilisation. The fuel utilisation (*fu*) is the share of reactant gas (e.g. H_2) that is used in the process and can be defined according to equation (13), where $\dot{M}_i$ is the molar flow rate of the fuel at the inlet, outlet and in the reaction of the stack.

$$fu = \frac{\dot{M}_{f,in} - \dot{M}_{f,out}}{\dot{M}_{f,in}} = \frac{\dot{M}_{f,react}}{\dot{M}_{f,in}} = \frac{\dot{M}_{f,react}}{\dot{M}_{in} \cdot y_{fuel,in}} = \frac{I_{stack}/(F \cdot n_{react})}{\dot{M}_{in} \cdot y_{fuel,in}} \qquad (13)$$

Due to the equipotential electrodes the critical point (see equation (12)) determines the local potential difference to the Nernst voltage for all the other points. This local overpotential determines the local current density in the way that the current dependent contributions in equation (5) create a potential that is the same for the whole electrode. The electric energy connected with this local overpotential is converted to heat, which influences the heat gradients in the stack. Increased fuel utilisation lowers the concentration of the reactant in the critical point and thus increases the overpotentials for other points in the stack, which results in the desired increased reaction rates. Thus, also the thermal energy generated increases and varies stronger within the stack resulting in higher temperature gradients. Temperature gradients are problematic for layered structures of different materials. Differences in thermal expansion coefficients of the materials induce mechanical stress which leads to enhanced degradation and in the worst-case full delamination of the electrode-electrolyte layers. Therefore, stack manufacturers set limits for the maximum allowed fuel utilisation.

There is no way of estimating the distribution of temperature and concentrations over the stack by zero dimensional models. The evolution of concentrations in connection with the local overpotentials, which results from the fuel utilisation is not trivial. The spatial modelling of the gas transport together with the electrochemical reaction and thermal behaviour is necessary for a simulation of the electrochemical stack based on fundamental physics. Such a model in two dimensions for a single flow channel is employed by Yang et al. [46] for investigating the H_2 concentrations along and orthogonal to a flow channel. Du et al. [47] employ a three dimensional model for investigating the internal reformation and temperature distribution within the stack. As shown by Saied et al. [49] different flow field configurations lead to different polarization curves for the stack. Therefore, in spatial modelling the detailed geometry and flow fields are required in addition to the material parameters, which describe the local physics.

The mains steps of solving a spatially resolved stack model require iterative solution and include:

- Set a stack voltage and the initial distribution for gas concentrations and temperature
- Perform the calculation of local Nernst voltage, overpotential and resulting local current density (from equation (5)) for discretized sections from the beginning to the end of the fuel flow path.
- Check the resulting critical point of the stack voltage and the distribution for gas concentrations and temperature and modify the initial assumptions.

The design and engineering parameters required for such a calculation include material properties and geometric assumptions, which are still undergoing development. The detailed spatial modelling and investigation of influences in the stack is a wide research field for itself. The focus in the present study is not on developing a model which reflects detailed processes within the stack but on investigating the whole rSOC-system and its application. Therefore, the present study is based on the numerical data driven model, based on measurement data, of a stack from Frauenhofer IKTS, which is described in detail in B1 [37] including important limits for operation.

The numeric stack model used here allows to connect the stack voltage to the electrical current and the gas inlet properties including concentrations, temperatures and mass flows.

$$U_{stack}(I) = f(I, T_{gas,in}, y_{gas,in}, \dot{m}_{gas,in}) \qquad (14)$$

The stack voltage in return defines the stack's electrochemical conversion efficiency analogously to the cell equations (10) and (11). However, on the stack level the fuel utilisation also needs to be included. When inserting for the used molar flow of fuel in equation (9) the flow into the stack and by using the definition of the fuel utilisation according to equation (13), the stack efficiency for both FC and EC operation results in equation (15) and (16).

$$\eta_{stack,FC} = \frac{U_{stack} \cdot F \cdot n_{react}}{LHV} \cdot fu \qquad (15)$$

$$\eta_{stack,EC} = \frac{LHV}{U_{stack} \cdot F \cdot n_{react}} \cdot fu \qquad (16)$$

On one hand higher fuel utilisation trivially increases the conversion efficiency but on the other hand the fuel concentration in the critical point decreases the cell voltage (see equation (13)) and thus the electric efficiency decreases (see equation (3)). As mentioned earlier in this section, high fuel utilisation has detrimental effects. Therefore, this parameter cannot be increased beyond the manufacturer's limit.

4.1.3 The path from stack to system level

The electrochemical stack is not a stand-alone unit, but it is embedded in the balance of plant (BoP) components. These BoP components ensure the stack's safe and efficient operation and provide the gas streams with parameters in the allowed stack operation range for temperatures, concentrations and pressures.

In B1 [37] it was found that the BoP usually includes recirculation of the stack-outlet gas on the fuel and/or on the air side. This publication continues with the investigation of the fuel-recirculation and three possible ways of its realization:

- Hot gas recirculation
- Cold gas recirculation
- Cold gas recirculation with recirculation condenser

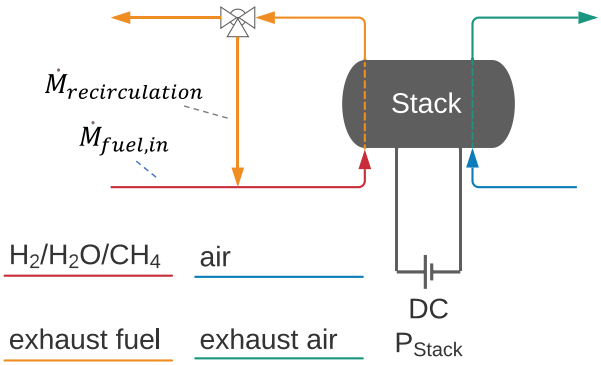

Figure 8: Fuel recirculation in the rSOC system.

The basic principle for fuel recirculation is illustrated in Figure 8. For further consideration the recirculation rate (rr) is defined according to equation (17).

$$rr = \frac{\dot{M}_{recirculation}}{\dot{M}_{fuel,in}} \qquad (17)$$

The recirculation of fuel decouples its utilisation on stack and on system level. On both levels the equation (13) is valid. However, with recirculation the molar share of fuel at the stack inlet is lower than at the system inlet. By taking into account the flow schematics of Figure 8 and equation (17) the fuel utilisation on stack level can be related to the fuel utilisation on system level as shown in equation (18).

$$fu_{stack} = \frac{fu_{system}}{1 + rr \cdot (1 - fu_{system}) \cdot \left(1 + fu_{system}\right)^{-1}} \qquad (18)$$

The relation between these two levels of the fuel utilisation is visualized in Figure 9. In this figure one can see that at high recirculation rates of above three, a significant decrease of the fu_{stack} in comparison to fu_{system} can be observed, especially at fu_{system} below 0.9. The stack considered in the present research has a manufacturers' limit of 0.75 for fu_{stack}. In this case

the fu_{system} with recirculation rate of 5 can be increased to 0.92 which corresponds to a hydrogen concentration at the stack inlet of 20.4% and 4.4% at the outlet.

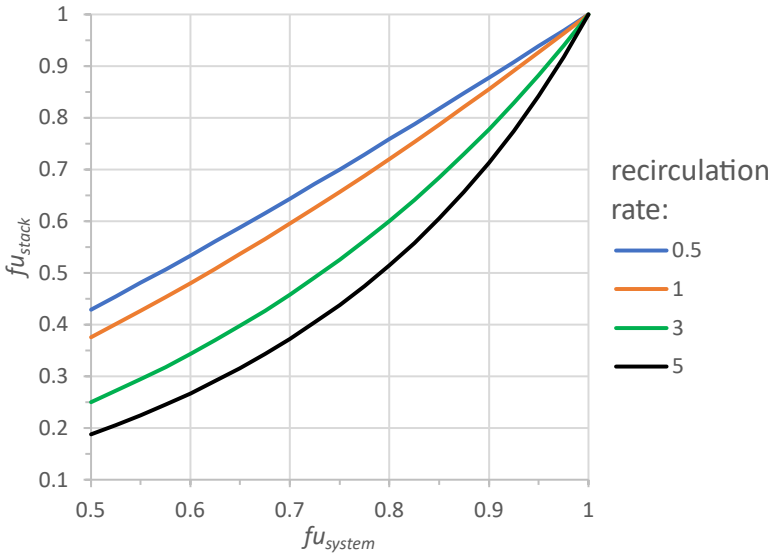

Figure 9: Dependency of the stack fuel utilisation on the system fuel utilisation for different values of the recirculation rate.

In principle there is no limit for the recirculation rate. However, in order to prevent oxidation of the metallic nickel, Preininger et al. [40] maintained a H_2 content of at least 20% at the steam/fuel inlet during EC operation, while Zhang et al. [50] assume that 10% of H_2 is sufficient. A 10% H_2 limit at the outlet would limit the system fuel utilisation to 82% in FC operation. In the research of Königshofer et al. [51] no degradation with high steam contents was observed. Due to the uncertainty for this limit in real systems, the min value of 4.4%, as calculated before, was chosen. In addition to this material limit a design limit is given by the mass flow through the stack which, in the case of high recirculation rates, can be a multiple of the mass flow without recirculation. The stack needs to be designed for such operation to avoid a high pressure drop. Furthermore, the recirculation requires energy for the blower or higher compressed fuel in case of an ejector.

When the FC operation is provided with CH_4 or other carbon rich fuels, an additional limitation for the recirculation arises. The generation of solid carbon within the stack or external reformer must be avoided. Solid carbon deposition on the catalytic surface of the electrodes or in the reformer would lead to deactivation of the catalyst as investigated by Subotic et al. [52]. Also Li et al. [53] describes the degenerative effects caused by carbon rich fuels and carbon deposition. Biert et al. [54] introduces in their work a limit of 2.5 for their defined oxygen carbon ratio (*O/C*) (equation (19)) at 500°C, which shall prevent carbon deposition during operation. Another thorough investigation of the carbon activity in CH_4 rich fuels is given by Ribeiro et al. [55].

$$O/C = \frac{y_{H2O} + y_{CO} + 2\,y_{CO2}}{y_{CO} + y_{CO2} + y_{CH4}} \qquad (19)$$

Generally, the generation of solid carbon can be calculated for the thermodynamic phase equilibrium considering all important reactions that can contribute to carbon formation. Typical reactions that must be considered are the Boudouard reaction, reverse coal gasification and cracking of long-chain hydrocarbons, as Schäfer et al. [56] describe. The calculation of equilibrium composition considering these reactions can be achieved for example with the Python package of Cantera [42]. Figure 10 shows the results for the solid carbon formation limit in a ternary diagram of carbon, hydrogen and oxygen. In this diagram one can see that the line defined by *O/C* equal 1.25 coincides almost exactly with the limit calculated from phase equilibrium. The line for *O/C* equal 2.5 is a safe distance away from the theoretical limit. A distance to the limit is in real application always required since non-uniform mixture, temperatures and pressures are present, which can favour the formation of solid carbon in certain points. Also, during load changes and system start-up more critical states than in theory can be reached and must be avoided. Additionally, Figure 10 includes the line on which the fuel mixed with recirculated gas can move on, depending on the recirculation rate. One can see that recirculation with a recirculation rate above one can effectively move a CH_4 fuel to the safe region for solid carbon formation. The model for the rSOC-system employed in the present work considers a maximum *fu* at stack level of 80%, a recirculation ratio of 5 and an *O/C* ratio of 2.5.

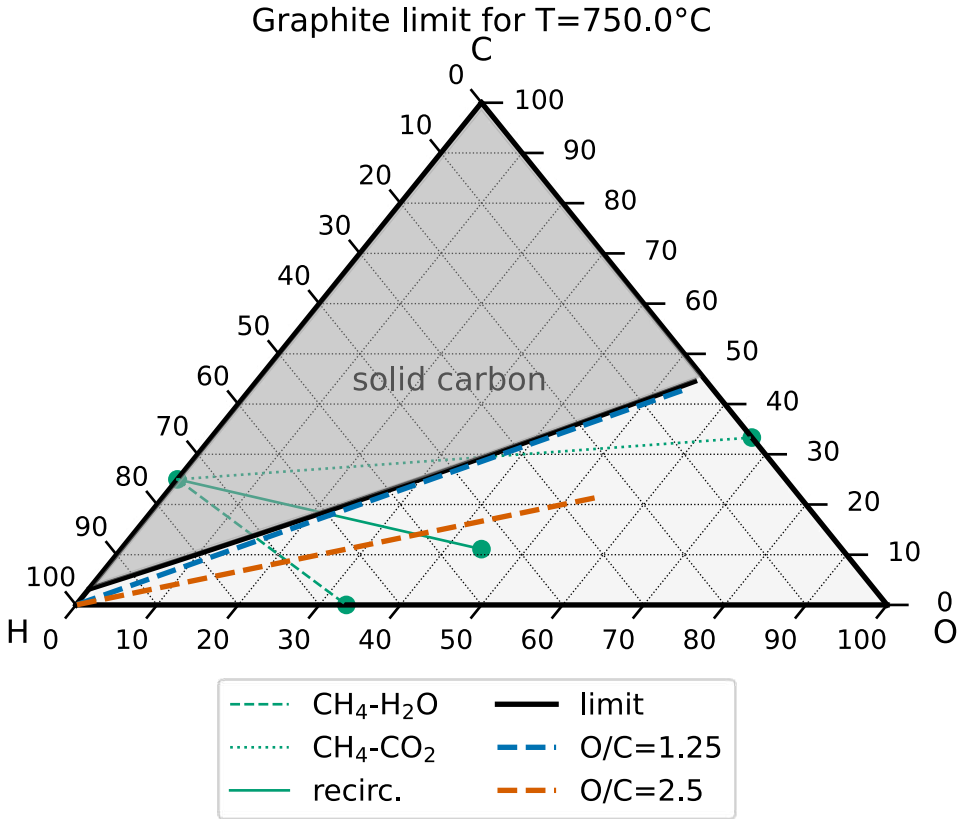

Figure 10: Ternary diagram for carbon, hydrogen and oxygen with the theoretical limit for the region of solid carbon formation (limit). The line between CH_4 and recirculation-gas (recirc.) shows how critical points can be moved below the solid carbon formation limit through off-gas recirculation.

4.1.4 Model of the rSOC-system

The model for the rSOC system, which is used in the present investigations, is set up in the modelling environment of Dymola [57] and is described in detail in B1 [37]. This model includes the numerical representation for the 5/15 kW (FC/EC) rSOC stack, as described in section 4.1.2. The BoP components are modelled on the basis of thermodynamic principles in steady state and include heat exchangers, recirculation blower, condensers, electric heaters, air fan and evaporator.

For all investigated flowsheet configurations (basic flowsheets in Figure 11), the operation temperature of the stack is kept constant at 750°C. In the exothermic fuel cell operation this is achieved by controlling the air mass flow, with the stoichiometric mass flow needed for the stack reaction as lower minimum. The electrolysis is operated in the endothermic region for current densities and the heating of the stack is controlled by electric heaters on the fuel and air side (Fuel e-heater and Air e-heater). Additionally, the air mass flow can be varied in order to ensure the delivery of thermal power, as described in more detail in B1 [37]. Therefore, the air mass flow is determined through the thermal control in both operation modes and the fuel mass flow is related to the fuel utilisation according to equation (13). The remaining main free

parameters of the model are: stack temperature, pinch point temperature differences of heat exchangers, condensation and separation efficiencies.

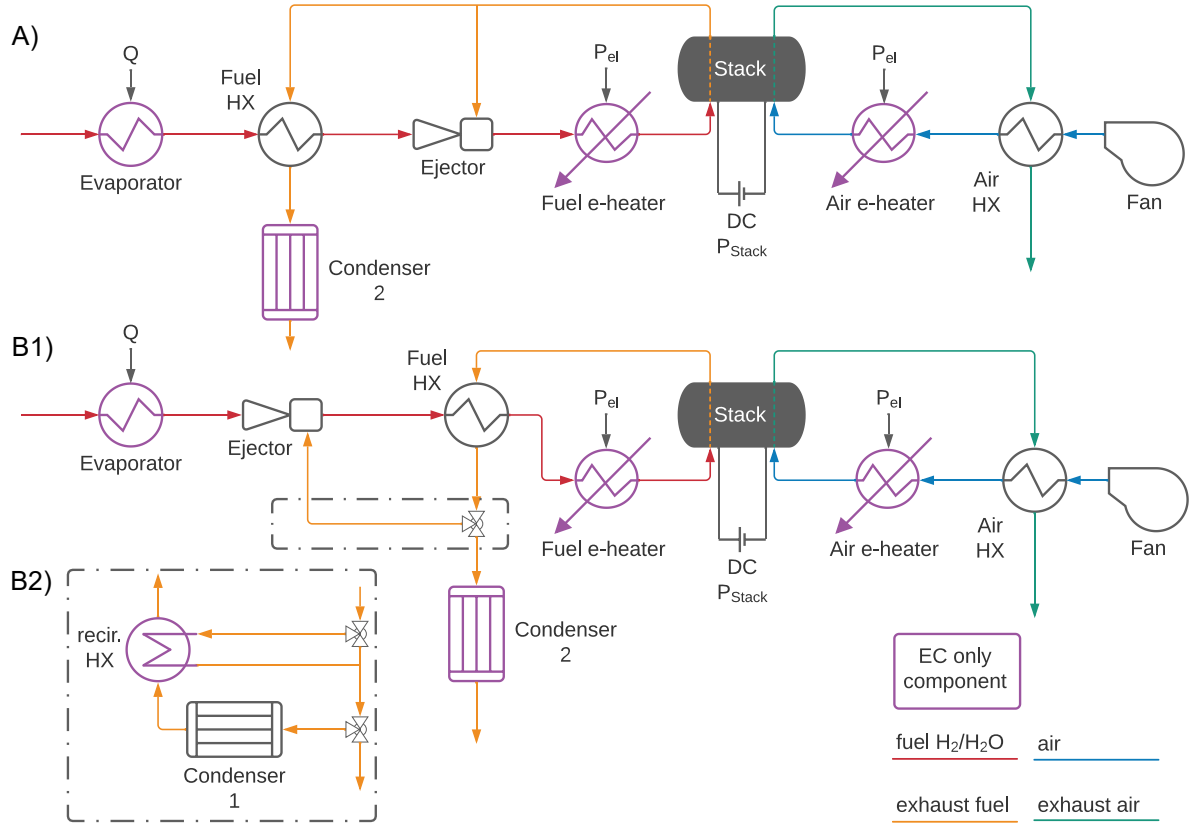

Figure 11: Flowsheets for A) hot gas recirculation, B1) cold gas recirculation and B2) cold gas recirculation with recirculation condenser, as presented by Paczona et al. [37] in Figure 19.4.

The considered system configurations in B1 [37], with the two main possibilities of hot- or cold-gas recirculation as mentioned in the previous subChapter, are reproduced in Figure 11. In A), the flowsheet with hot-gas recirculation, exhaust gas at stack's fuel side is recirculated directly to the stack inlet with a high temperature ejector or blower. In the case of cold-gas recirculation B1) the exhaust fuel is recirculated after the fuel heat exchanger (Fuel HX). This precooled gas allows easier utilisation of blowers that cannot withstand the high operation temperature of the stack. However, the fuel heat exchanger (Fuel HX) works in this case with the by recirculation increased flow rate. The heat exchanges on fuel and air side (Fuel HX and Air HX) are necessary to reduce heat losses with the exhaust gas streams. The flowsheet option B2) extends B1) by an additional condenser and recirculation heat exchanger in the recirculation path. This condenser ensures that the operation limits for the recirculation drive are met, with an upper limit of 80°C, and thus leads to condensation of the fuel exhaust when crossing the dew point. The cold-gas recirculation with condensation (option B2) in Figure 11) is the only flowsheet that allows for a standard recirculation blower instead of high temperature blower or ejector. The condenser in the recirculation is beneficial in FC operation

since it reduces the dilution of the fuel. However, in EC operation it means a loss of heat by draining steam.

With the definition for the exergy content of heat (equation (20)), the efficiency of the system can be defined for two scenarios. In the energy system scenario (E) heat streams are not used and the heat demand of the evaporator ($\dot{Q}_{evaporator}$) must be covered electrically. In this case the system efficiency is given by equation (21) and (22). The industry scenario considers utilisation of the system's waste heat in FC operation by adding its exergy content to the energy generated as can be seen in the numerator in equation (24). For the EC operation the evaporation heat demand is replaced by its exergy demand when heat from an external source is available, as shown in equation (33).

$$EX = Q \cdot \left(1 - \frac{T_{ambient}}{T_{released}}\right) \quad (20)$$

$$\eta_{E,EC} = \frac{P_{Fuel}}{P_{stack} + P_{Fan} + P_{e-heater} + \dot{Q}_{evaporator}} \quad (21)$$

$$\eta_{E,FC} = \frac{P_{stack} + P_{Fan}}{P_{Fuel}} \quad (22)$$

$$\eta_{I,EC} = \frac{P_{Fuel}}{P_{stack} + P_{Fan} + P_{e-heater} + \dot{EX}_{evaporator}} \quad (23)$$

$$\eta_{I,FC} = \frac{P_{stack} + P_{Fan} + \dot{EX}_{gas,out} + \dot{EX}_{condenser2}}{P_{Fuel}} \quad (24)$$

4.2 Integration to industrial sites and model simplification

In this section the integration to industrial sites and the construction of the surrogate models for the rSOC system are presented. The surrogate model is a mathematical simplification of the physical rSOC system model. Therefore, the model's calculation run-time is reduced, the stability is enhanced and a better reusability for systemic investigations is given. This simplified model developed here is a basis for the investigations in P2 [39], which is described in section 4.4.

4.2.1 The rSOC system's coupling possibilities to industrial sites

The flowsheet considered for the investigation of the rSOC system integration to industrial sites is based on the flowsheet with fuel cold gas recirculation and condensation, which is presented in section 4.1.3 and 4.1.4. This flowsheet is extended by an external CH_4-reformer, a catalytic burner for utilisation of non-reacted fuel to produce more heat and a heat exchanger for extracting high temperature heat, as suggested in section 5.1.2. In Figure 12 this improved flowsheet is shown together with heat flows, that can be used for thermal coupling

to industrial sites. Thermal interaction with industrial sites can arise from the heat demand of the evaporator in EC operation or the heat that can be extracted in FC operation after the catalytic burner. Furthermore, in EC operation the endothermic reaction requires electric heaters. Another option, which is not considered here, is the operation at or above the thermoneutral point, at which stack internal losses generate the thermal energy. The heat demand for controlling the stack temperature in endothermic operation could also be covered by external high temperature sources, to replace the electric heaters. However, such a controlled high temperature stack-heating with process waste heat poses big technical challenges and risks for the stack safety and is therefore not considered in the present work.

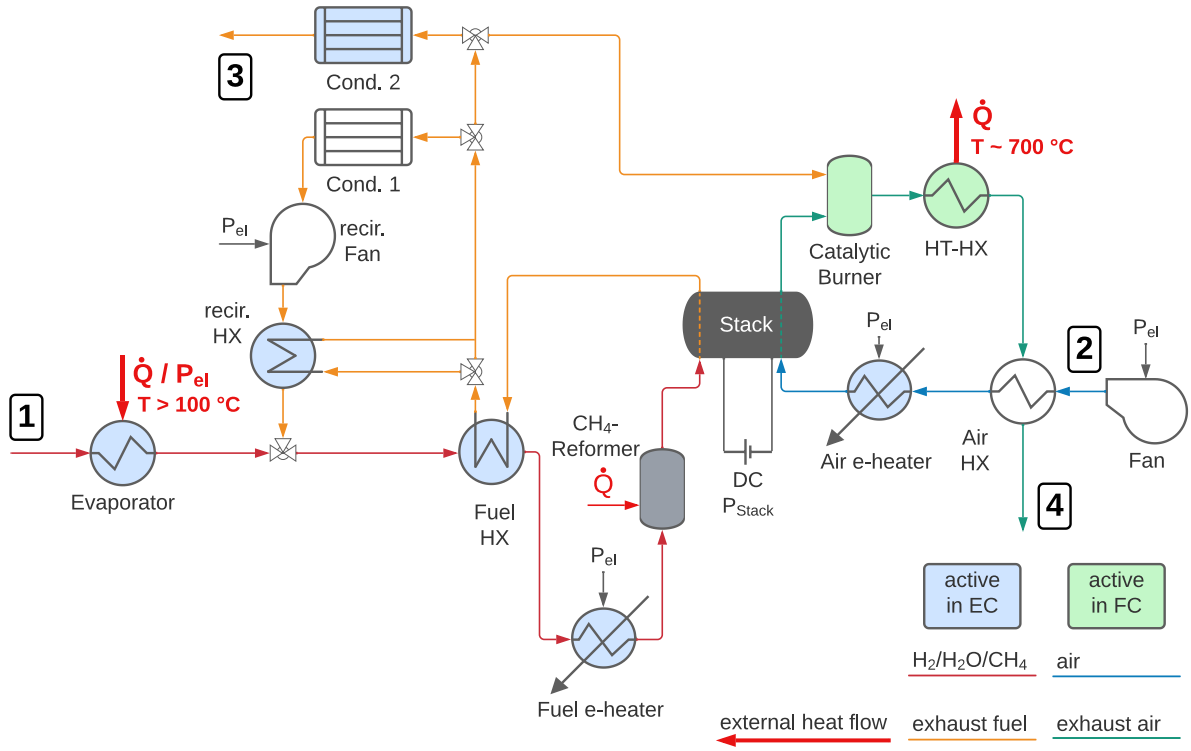

Figure 12: Flowsheet with cold-gas recirculation and catalytic burner used for generation of the surrogate model and basis for further investigations in P1 [38] and P2 [39].

Highly suitable industrial candidates, which can provide waste heat above 100°C for the steam production and cover the thermal demand shown in Figure 26 B) are steel, cement, glass, refractory, lime, and brick production. Also, breweries, grain mills, textile and food industry have waste heat suitable for steam production. In case the industrial waste heat does not meet the required temperature, a heat pump can be employed. This gives a coupling advantage to industry but requires additional electrical power, which slightly lowers the efficiency compared to the direct heat integration. Another application for thermal coupling that appears in industrial contexts are district heating networks, which can be used as a heat sink for the rSOC system's FC operation.

The model proposed in B1 [37] and discussed in section 4.1.3 to 4.1.4 includes thermodynamic models for the components that are shown in Figure 12 and has a variety of parameters that are partly fixed by optimisation (fuel recirculation and utilisation) and thermal control of the system. Further parameters defining the design are chosen for the heat exchangers pinch point temperature difference, cooling in the recirculation and stack operation temperature (750°C). In this way the part load fraction is the only variable left. By calling the Dymola model through the Dymola-Python interface parameter sweeps and postprocessing of results becomes easy to accomplish.

4.2.2 Model simplification: surrogate model

The aim of the model simplification is to derive a computational inexpensive fast model representing the rSOC system in sufficient detail for the simulation of the integration to energy systems with an operational optimisation. The model proposed in B1 [37], which is discussed in section 4.1.4 includes thermodynamic models for the components that are shown in Figure 12 and has a variety of parameters (Table 2). Figure 13 shows the model's results for the variation of three parameters of the model.

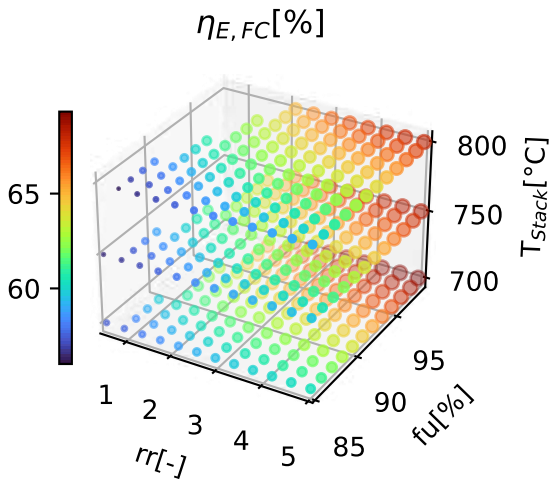

Figure 13: System efficiency in FC operation according to equation (21)(22) calculated with the Dymola system model. The varied parameters are: fuel utilisation (fu), stack temperature (T_{stack}) and recirculation rate (rr).

With highly flexible machine learning approaches one can find a computational inexpensive representation (surrogate model) of the rSOC system model including all the model parameters. Artificial neural networks, boosted trees and random forests are methods that can be applied for such a general approach, which is described by Alizadeh et al. [58] and Kudela et al. [59]. In any case Alizadeh et al. [58] suggest an analysis of the necessary variables to reduce the dimensionality for any approach applied later. Such an analysis will be described for the present model in section 5.1. By including all the relevant parameters in the surrogate model, the analysis for system integration can derive the ideal parameter set up for operational and design parameters for optimal performance in the integration. However, the

feasibility of such a combined analysis is depending on the level of detail of the simulation for system integration. In section 4.4.1, an optimisation-based approach for time resolved simulation of a yearly time-series is used. In this case a multivariate non-linear model leads to non-feasibility of ideal solutions for combined integration and system design. Therefore, the result for optimal system parameters is taken from a preceding investigation (see section 5.1.1) for the fuel utilisation and recirculation. The other relevant system variables are design parameters, which can be fixed as described in B1 [37]. For example, the design pinch point differences of heat exchangers are set to 10 K. By fixing these system internal parameters the variability is limited to the load fraction of each operation mode. This variability can be fully described by part load curves that reflect the dependence of all necessary output variables on the net electric system power (P_{el}). Therefore, a surrogate model of the rSOC system, which is suited for the time resolved simulation, is a representation of these curves. This part-load surrogate model can be obtained by combining spline interpolation for all necessary output variables, as shown in Figure 14 for the system heat production.

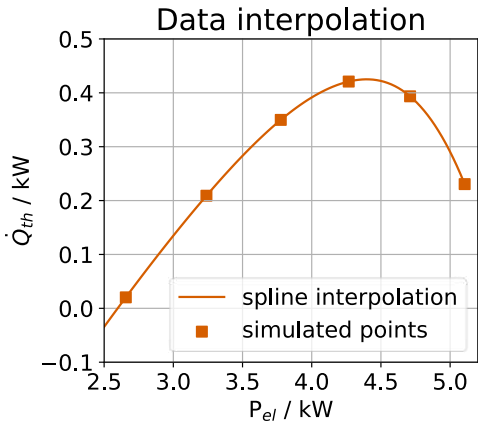

Figure 14: Example for spline interpolation of simulation points for FC-CH4 part load heat production.

Spline interpolation includes the knowledge from all points of the detailed system simulation and connects them in a smooth manner, reflecting physics without abrupt transitions. This approach of mathematic interpolation is justified, since no abrupt changes of physics and thus smooth conversion curves are expected between the simulated points. This spline representation of the part load behaviour can be easily extended by variables for other system internal parameters but requires a densely space filling dataset. It is important to notice, that the extrapolation beyond the data points for creating this spline surrogate model is not allowed. This is not a problem in our case since the limits of calculated datapoints are chosen in a way to reflect system limitations. Similarly, a spline interpolation can be applied for the H_2 compression model, which is shown in Figure 18. The biggest uncertainty of the surrogate model for the rSOC system derives from the uncertainty in the underlying system flowsheet. Another source of uncertainty comes from assumptions in the modelling of BoP components

that may have additional technical limitations and the thermal losses to ambient, which are discussed in P1 [38].

For the time resolved simulation described in section 4.4.1 the surrogate model must include, in addition to the static conversion, the dynamic system behaviour and limitations. These dynamic limitations and load change costs are derived in P2 [39] from literature and are given in Table 1. Since in the literature significant variations of these limits are present, a considerable uncertainty is also connected with the values stated here. These limits and costs are mostly connected to degradation processes in the stack as described in section 4.1.2 and to the unstable start-up of the steam generator [29].

Table 1: System dynamic parameters according to P2 [39].

Parameter	rSOC	PEM
Heatup power kW/kW_{EC}**	0.365	0
Warm standby in kW/kW_{EC}**	0.008	0
Heat-up and cool-down time in min	120	0
Ramp-to-EC time in min	13 [10, 29, 60]	0
Ramp-to-FC time in min	3 [10, 29, 60]	0
Ramp warm cost in €/kW_{EC}**	0.25*	0
Ramp EC cost in €/kW_{EC}**	0.01*	0
Ramp FC-H2 cost in €/kW_{EC}**	0.005*	0
Ramp FC-GG cost in €/kW_{EC}**	0.005*	0

**Schefold et al. [61] suggests no degradation due to cycling of the rSOC-stack, however low costs to prevent unrealistic optimisation results are included*

***kW/kW_{EC} - power relative to installed electrolysis power*

4.3 H_2-Storage possibilities and model for compressed H_2-storage

This section opens the side topic of local hydrogen storage possibilities and the modelling approach used in this work. The local storage of H_2 is in competition to a future existing H_2 grid, which offers storage capacities in the pipes of the gas grid and in future underground H_2-storage facilities, as illustrated in Figure 15. Therefore, a representation for local H_2-storage is necessary to compare these two possibilities.

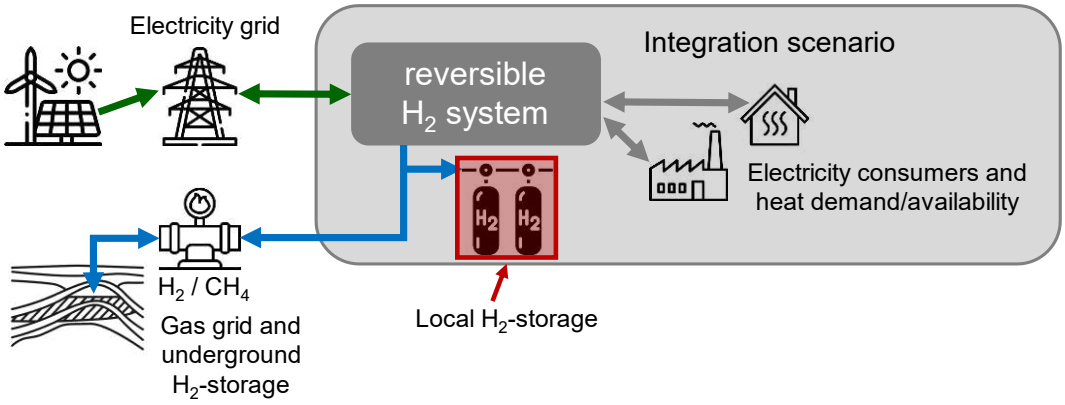

Figure 15: Role of H_2-storage possibilities for the reversible H_2 system and highlighted local H_2 storage.

Hydrogen can be stored in different ways based on chemical and physical principles. The most prominent chemical options are chemical hydrides such as ammonia, methanol or Liquid Organic Hydrogen Carriers (LOHC) and metal hydrides. One main advantage of chemical hydrides is the high energy density and specific energy as can be seen in Figure 16. The disadvantage of storing hydrogen in chemical compounds is the release of heat by the reaction from H_2 to a compound, which in case of being unused, reduces the storage efficiency significantly. The same amount of heat also must be provided when the H_2 is recovered. Furthermore, the reactions usually take place at elevated pressures, which requires a compression of the feed gases. Due to the higher energy demand for storing, but also higher energy densities, chemical hydrogen storage is especially suitable for energy transport and mobile applications with demand for large amounts of energy being stored, as described by Ishimoto [62] when comparing liquid H_2 to ammonia. Ammonia is also considered by Micco et al. [63] to be a promising way to replace diesel fuelled propulsion systems in cargo ships. The storages based on physical principles include high pressure, liquid and physically adsorbed hydrogen. The liquefaction process consumes, according to Peschel et al. [64], more than 22% of the LHV of H_2. The liquid H_2 has a high energy density, which is suitable for energy transport. In the present studies the stationary storage of H_2 is in the focus, which does not require outstanding energy density or specific energy but demands an efficient technology. Compressed hydrogen at moderate pressures of 200 bar to 300 bar fulfils exactly these requirements, with an energy consumption for the compression of below 10% of the LHV of H_2. Therefore, the following subchapter analyses compressed hydrogen storage in more detail.

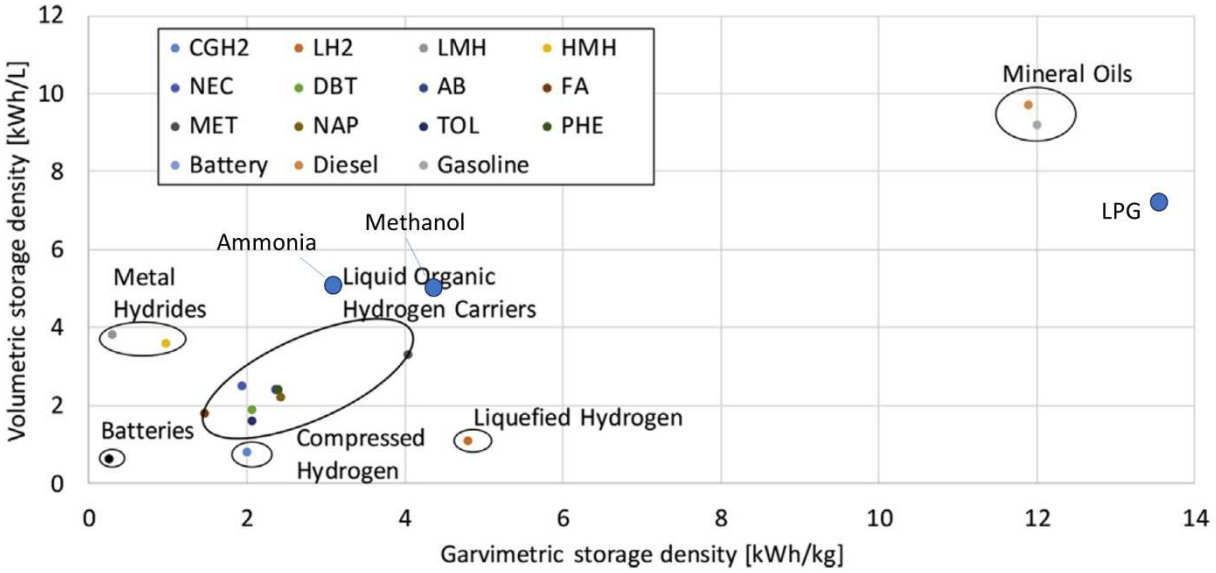

Figure 16: Energy densities of different hydrogen carriers according to [65] with additional points in blue for Ammonia, Methanol and LPG.

4.3.1 Models for H_2-compression

There are many possibilities to obtain high pressure H_2, as are described by Sdanghi et al. [66]. These options include metal hybrid compressors, where heat in combination with metal hydrides is used. Another interesting technology under development are electrochemical compressors, which are based on the principle of electrochemical cells and can theoretically reach high efficiencies but have a low technology readiness. In this work, mechanical positive displacement compressors, in particularly piston compressors, are considered due to their high technological readiness. The investigation here is based on the presentation at the NEFI conference in 2021 (C1 in section 10.1).

The ideal process of positive displacement H_2 compression can be described thermodynamically as an isentropic process, where during the process of compression no heat is added nor exchanged with the environment. In the real compression process heat is generated by friction and non-reversible processes in the fluid. This can be described by introducing an isentropic efficiency (η_{is}) which is defined according to equation (25) and allows the calculation of the real change of enthalpy in the fluid.

$$\eta_{is} = \frac{\Delta h_{is}}{\Delta h_{real}} \qquad (25)$$

The ideal and real compression process is visualized in a TS-diagram in Figure 17. One can see that a real compression from 40 to 200 bar causes a heating of the gas from 0°C to almost 200°C. The temperature in mechanical compressors is limited due to the material limits of sealings. Therefore, too high temperatures must be avoided, which is possible by dividing the compression process into multiple stages, with a H_2-compression ratio around 3 per stage and

intermediate cooling. Another desired effect of multistage compression is the increase of the efficiency of the process.

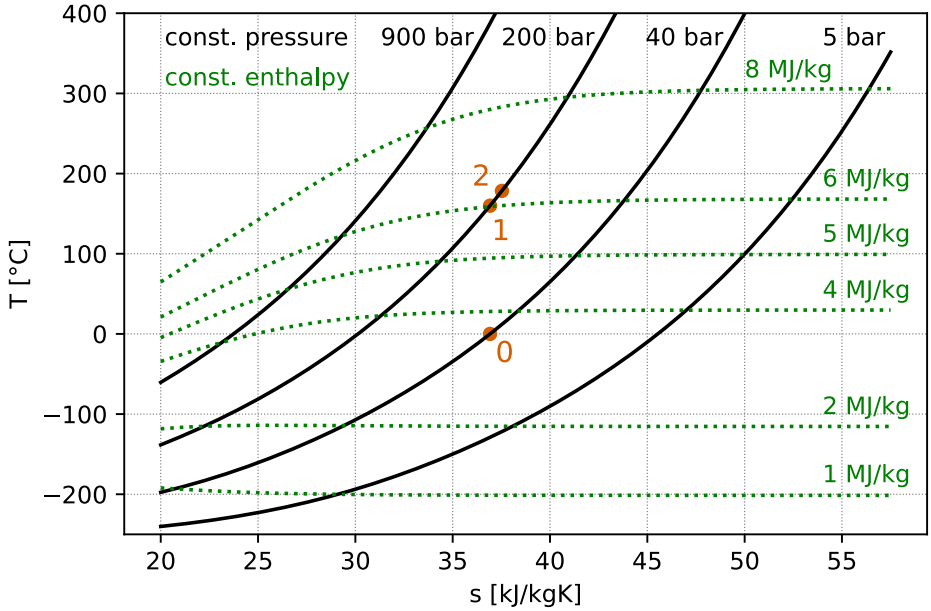

Figure 17: TS diagram for H_2 with point 0 start of compression, point 1 end of isentropic compression and point 2 end of real compression with isentropic efficiency of 0.9.

The compression model used in this work is created with the Python interface of CoolProp [67] and calibrated with the 5-stage Linde ionic piston compressor [68] for H_2 fuel station applications, which uses an ionic liquid above the pistons to reduce the heat-up of the gas and thus increases the isentropic efficiency. In reciprocating piston compressors, the outlet valve is usually spring loaded, so it opens when the pressure within the piston crosses the pressure of the next stage [69]. Therefore, the compression energy demand depends on the outlet pressure as shown in Figure 18 for different compression pathways. The isothermal compression line shows the thermodynamic limit which can be reached only with an infinite number of stages and an ideally isentropic compression process, which means that the gas stays at constant temperature.

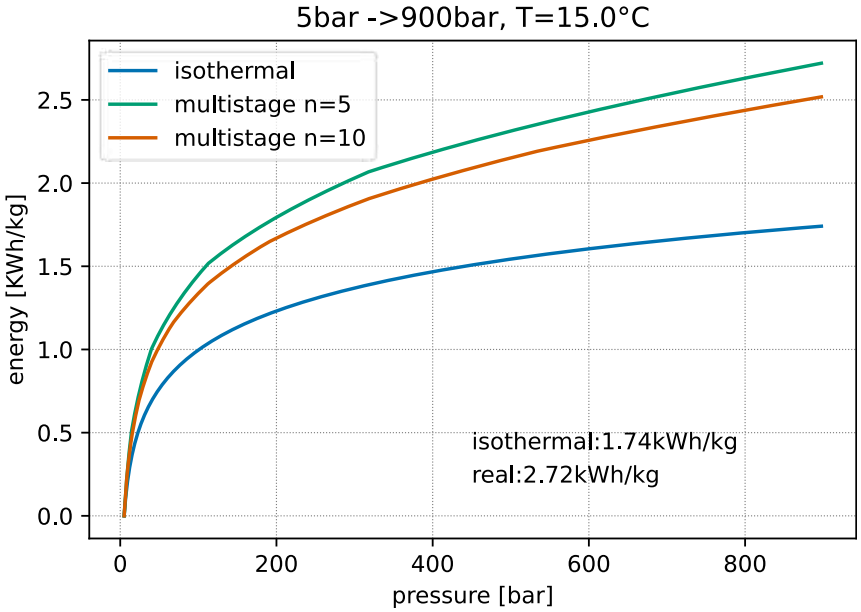

Figure 18: Energy demand for compression from 5 bar to them maximum outlet pressure of 900 bar in isothermal limit and modelled real multistage compression.

The energy that is necessary for filling a storage vessel from a given starting pressure to a desired end pressure can be calculated by integrating the specific energy consumption of the compressor, as shown in equation (26). The specific energy consumption for charging a storage from start to end pressure is given by equation (27).

$$E_{store}\left[\frac{kWh}{m^3}\right] = \int_{\rho(p_{start})}^{\rho(p_{end})} e_{compressor} \cdot d\rho \qquad (26)$$

$$e_{store}\left[\frac{kWh}{kg}\right] = \frac{E_{store}}{\rho(p_{end}) - \rho(p_{start})} \qquad (27)$$

Figure 19 visualises the specific energy consumption and pressure for charging a pressure vessel from starting to end pressure. When starting from a higher pressure of the storage vessel, the specific energy consumption of the H_2 stored during this charging process increases. The energy consumption for storing a certain amount of H_2 depends strongly on the starting pressure of the storage. This means that cycling the storage at elevated pressure significantly decreases the storage efficiency. For a storage cycle from 100 bar to 120 bar almost the same energy is consumed per stored kg of H_2 as in a cycle from 5 bar to 300 bar (Figure 19 point 1 and point 2). This shows that the cycling pressure of the storage is highly significant when evaluating the efficiency of compressed H_2 storage.

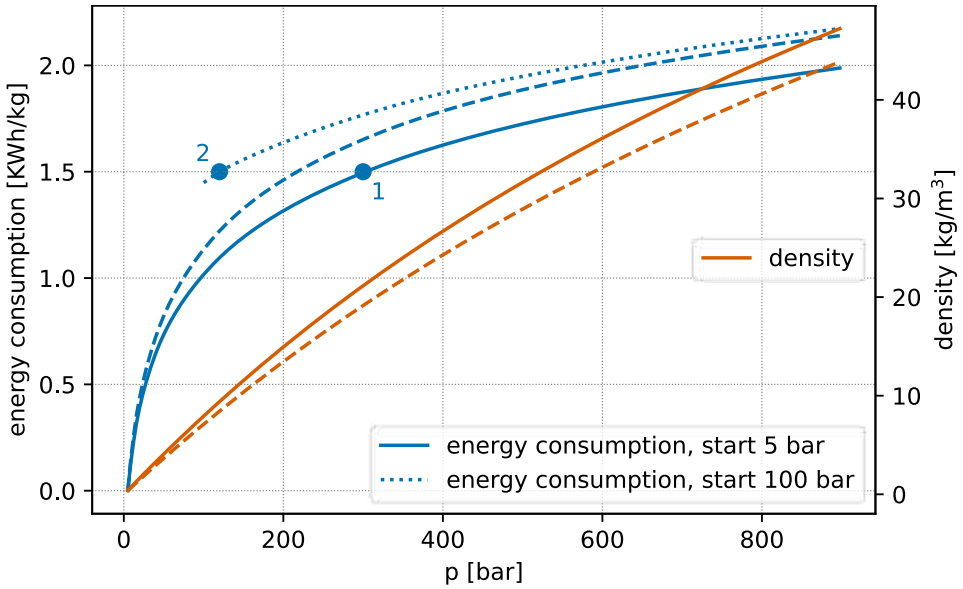

Figure 19: Energy consumption for charging a vessel with a 5-stage compression at 15°C start, intercooling and storage temperature and with two different starting pressures of 5 bar and 100 bar. The dashed line shows energy demand and density for a gas storage temperature of 50°C.

Another important parameter in compressed H_2 storage is the storage temperature, which influences the density at which H_2 is stored and thus also influences the energy required for storing a certain amount of H_2. Figure 19 shows in dashed lines the decrease of the density in the storage and thus the increase of energy consumption for storing a certain amount of H_2. The gas of the storage can change temperature due to ambient temperature changes and during the charging or discharging of the storage. The charging of the storage increases the storage temperature by two mechanisms. Firstly, the gas, that is already in the storage, is compressed when new gas is added. Secondly, the H_2 produced in electrolysis is not cooled to ambient temperature and is connected therefore with a heat flow to the storage. During fast charging processes like in mobile application, these storage heat-up processes are highly important, not only for the energy demand of the compression but also for the structural safety of the pressurized storage, as is described by Li et al. [70] and Zhang et al. [71]. In stationary applications with charging times of many hours, this effect is much less important and of similar magnitude like daily and yearly ambient temperature variations.

4.4 Techno-economic analysis of the application in the energy system

This section describes the approach to the techno-economic evaluation, which was published in P2 [39] and presented with different perspectives at C4 to C6. This investigation is based on the surrogate model for the rSOC system and its thermal coupling possibilities, which is

discussed in section 4.2.2. Furthermore, time-series for energy prices, industrial waste heat and district heat demand are considered in three integration scenarios. Figure 20 shows the interaction of the rSOC system with the environment, which includes electrical and thermal energy flows from/to industry and district heating and electric and gas flows from and to the respective grids.

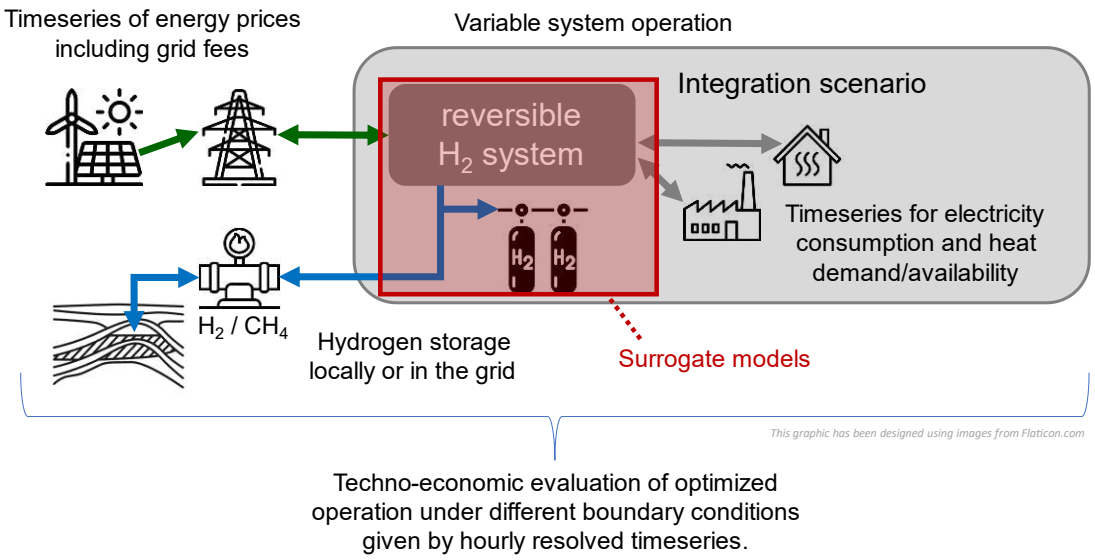

Figure 20: Embedding of the rSOC system to the energy system.

4.4.1 Optimisation model

In this section the main characteristics of the optimisation model are given, which is described in detail in P2 [39]. The model for the optimisation of the rSOC system's operation fulfils the following three tasks:

- Simulation of the rSOC system's cost optimal behaviour in given energy price scenarios
- Determination of the cost optimal H_2 storage size
- Connection of the model components as shown in Figure 21: rSOC system, H_2 storage system and one-hourly resolved time-series of the system boundary, which includes the waste heat of industrial sites and the energy prices of the gas, electricity and district heating grid

Therefore, this model allows for an investigation of the best rSOC system operation strategies in different energy price scenarios and the integration into different industrial and district heating systems.

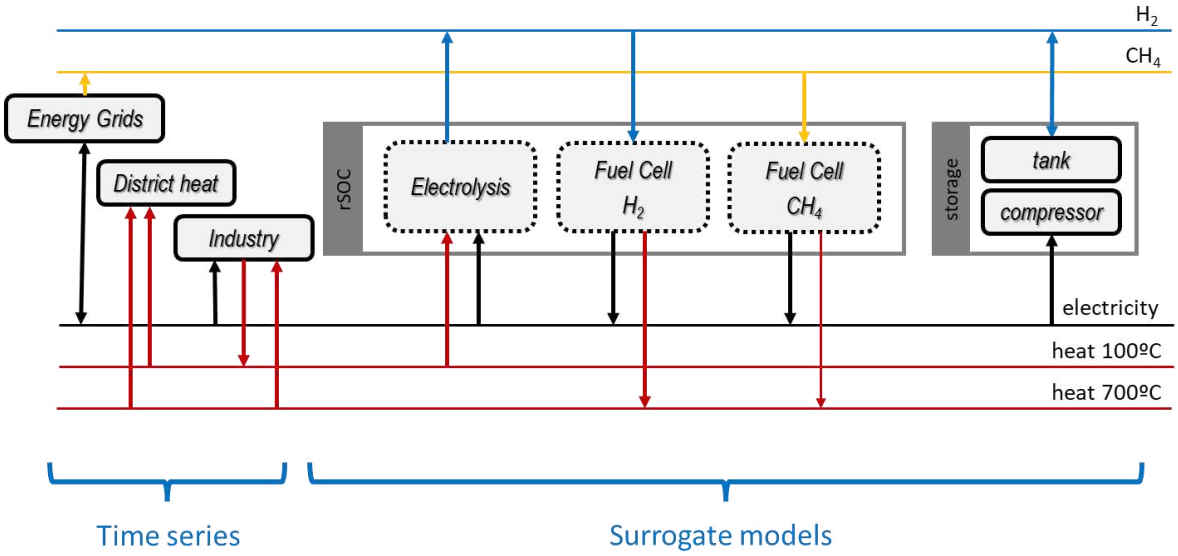

Figure 21: Structure of the optimisation model.

The simplified models for describing the behaviour of the rSOC system and the H_2 storage are taken from section 4.2.2 and section 4.3.1, respectively. The 5-stage compressor model is applied to a rSOC outlet pressure of 1 bar and a maximal storage pressure of 200 bar. The conversion curves of the rSOC system (surrogate model, Figure 26) and the pressure-energy curve of the compressor (Figure 18) are furthermore converted to a piecewise linearisation with 2, 3 and 4 support points, as described in P2 [39]. In this way the optimisation model can be formulated as a mixed integer linear problem (MILP), which can be solved efficiently by standard mathematical optimisation routines.

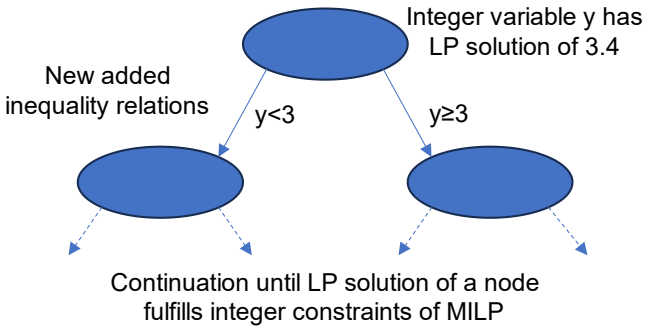

Figure 22: Branch-and-Bound algorithm for finding optimum of mixed integer linear problems (MILP) by transforming them into linear problems (LP).

The Branch-and-Bound algorithm is a standard approach for MILP problems, which is employed also by Gurobi Optimization LLC [72]. At first the integer conditions are removed, so that a linear problem is created, as illustrated in Figure 22, which can be solved by the Simplex algorithm [73]. If the LP solution by accident fulfils all original integer conditions the solution to the MILP is found. Otherwise, two new inequality equations are introduced for each integer variable, which divides the variable space into two non-connected spaces, excluding the previously found LP solution. This means, that as many new LP problem

branches are created as there are integer variables. Solutions for these new LP problems can be obtained again by the Simplex algorithm and if necessary, the branching is continued until a LP solution, fulfilling the MILP integer constraints, is found which determines this branch. If the difference between the minimum objective value of all end-of-the-branch LP solutions and a determined MILP solution is zero, the optimum of the MILP is found. By bounding the value of the optimal objective, not all created branches need to be followed to the end. An upper bound exists by the so-far best determined MILP solution and the LP solution of any branch must be lower to allow for better MILP solutions within this branch. The lower bound of the MILP solution is given by the minimum value of all LP solutions at the end of the branches. Since good bounds strongly influence the computation time, a good first guess of the solution is important. In the here implemented MILP the dynamic thermal behaviour of the storage and the change of ambient temperature is neglected to limit the complexity of the optimisation problem. Including these two effects would need additional piecewise linearised equations, which are integrated by integer conditions and thus strongly increase the number of branching-nodes and thus the computation time.

The **objective** in the MILP's optimisation is the minimization of the total costs, including for every timestep of the yearly time-series the costs and revenue for:

- Purchase of electricity and CH_4
- Selling of electricity, H_2 and district heat

Furthermore, the objective function incorporates the costs for dynamic degradation according to Table 1 and the capacity-investment costs for the compressed-H_2 storage.

The integer and real variables of the optimisation problem are:

- The rSOC system's operation mode for each timestep which can be EC operation, FC operation with H_2 or FC operation with CH_4
- The Load fraction of the rSOC system for each timestep can be equal 0 or vary between 0.5 and 1.0.
- The size of the H_2 storage
- Decision between storing H_2 in the local pressure storage or selling it to a hydrogen grid.

The following input variables for the system's environment are fixed **boundary conditions** for the optimisation problem:

- Electricity price time-series according to Traupman et al. [74]
- Gas price time-series for the purchase from the gas grid according to Traupman et al. [74]
- H_2 price: one value for all timesteps
- Grid fees for electricity and gas

- District heating price and demand time-series
- Industrial waste heat time-series from Ganymed [75] according to Binderbauer et al. [76].

The formulated optimisation problem includes the following **constraints** that need to be fulfilled by the determined optimal solution:

- Upper and lower power limits for the rSOC system's EC and FC operation
- Operation in only one modus (EC, FC, cold standby or warm standby) in one timestep possible
- Cooldown, heat-up and mode change times according to Table 1
- Delivery of system's wate heat to district heating only possible for the amount demanded in the district heating network

4.4.2 Techno-economic evaluation in the energy system

Here an overview of the calculation process described in detail in P2 [39] is given. The Techno-economic investigations are based on the relative return of investment calculated for the whole system lifetime (lt). The system lifetime is chosen for the investment period since it allows the economic comparison of technologies with different lifetimes from a technical perspective. Using an investment time, as usually done for rating investments, would omit the influence of different system lifetimes. Due to this change of considered time horizon this specific return of investment is called the relative return over lifetime (rROL). For the calculation of the rROL the solution of the optimisation, for the MILP defined in section 4.4.1, is obtained by using the solver of Gurobi [72]. Then the annual profit of the rSOC system (p_a) can be calculated from the energy prices and the determined system operation. Since the influence of the system's degradation on this profit is not neglectable it is analysed and incorporated in the calculation of the rROL, as shown in equation (28) according to P2 [39].

$$rROL = -1 + \frac{1}{CAPEX} \sum_{t}^{lt} \frac{p_a\big(d(t)\big)}{(1+i)^t} \qquad (28)$$

In P2 [39] the relation between degradation state and the system's annual profit (p_a) is determined. Furthermore, an assumption for the degradation throughout the lifetime must be made. Here it is assumed that the degradation progresses linearly from non-degraded initial state to 10% at the end of the lifetime. The biggest uncertainty for the rROL comes from

the uncertain future system investment costs and limitations for the options of generating profit.[1,2]

4.5 Investigation of spatial types for bidirectional hydrogen systems

This section introduces an approach for analysing the effect of grid-service-oriented operation of bidirectional hydrogen systems. The aim is to compare the two spatial system arrangements, spatially delocalized and concentrated and conclude which systems will be needed where in our energy system. Figure 23 defines the two spatial types. In the concentrated reversible system both EC and FC units are in the same point of the energy system and thus make reversible operation in one location possible. This can be interesting for sites where electricity production and consumption are close to each other, like in industrial or settlement areas with high potentials of photovoltaic or wind. In the delocalized version EC and FC units are in different locations and the reversible character arises by connecting them through a gas and electricity grid. The EC unit can be placed close to renewable production sites, with significantly more production than is locally consumed. The produced H_2 can be transported through the gas grid to locations with little renewable production but high energy consumption, where FC units convert the H_2 to electricity.

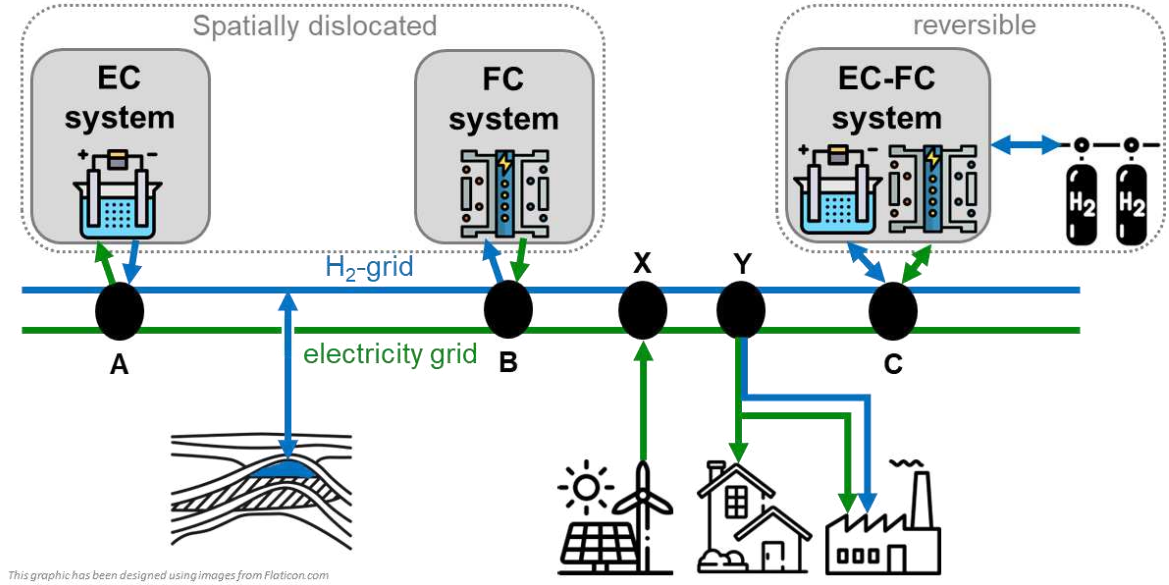

Figure 23: Spatially delocalized and concentrated Power-to-H_2-to-Power systems.

[1] Island applications and grid service operation are not included in this consideration.

[2] The present study considers the system costs according to Böhm et al. (Böhm et al. 2020) with an adaptation by Hans Böhm made for the reversible system.

4.5.1 Simulation of electricity grid load reduction by both spatial versions of reversible hydrogen systems

A reduction of the load for electricity grids, through the application of reversible hydrogen technologies, can be achieved by smoothing the electrical residual load in a given point of the grid. By smoothing the residual load, the peaks from consumption and production, that are the biggest challenges for electrical transmission infrastructure, are reduced. Spatially concentrated reversible hydrogen systems can reduce electrical load peaks in both directions, whereas spatially delocalized systems only allow for a unidirectional reduction.

The smoothing of the residual load in the present investigation is limited by the following assumptions in the simulation:

1) The amount of H_2 produced in EC operation is the same, that can be consumed in FC operation (only applied for the concentrated reversible system).
2) The system utilisation in the calculated yearly time-series is 50%. The utilisation (u) is defined according to equation (30), with the nominal electrical power (P_N), the length of the time-series (T) and system electrical power ($P_{el,t}$) in a specific timestep (t).
3) Delocalized electrolysis can only make use of negative residual loads and delocalized fuel cells can only operate when the residual load is positive. The resulting residual load must lie within the minimal and maximal value of the original residual load time-series .

$$u_i = \frac{\sum_t^T P_{el,t}}{P_N \cdot T} \qquad (29)$$

$$u = u_{EC} + u_{FC} \qquad (30)$$

The assumptions for the simulated reversible hydrogen systems are:

- Efficiency of 80% in electrolysis operation
- Efficiency of 60% in fuel cell operation
- Ratio of nominal electrolysis to fuel cell power of 3.0 (only for the concentrated reversible system)

The relative average volatility (rav) of the residual load (P_{res}) after applying different H_2 conversion technologies (i) is calculated according to equation (31). The average is calculated for all the nodes with H_2 grid connection and for the delocalized single mode units for the number of nodes where a system is employed.

$$rav_i = average_N \left(\frac{max\left(P_{res} + P_{i,el,t}\right) - min\left(P_{res} + P_{i,el,t}\right)}{max(P_{res}) - min(P_{res})} \right) \qquad (31)$$

5 RESULTS

This section comprises the main results of the studies shown in the three connected publications (B1 [37], P1 [38] and P2 [39]), which are necessary for answering the research questions raised in section 2.3. Furthermore, the calculation of LCOH for the multi revenue application of rSOC systems and the application of two different spatial system options is presented in this section.

5.1 Influence of operational parameters on the system performance

Here an overview of the most important influences of parameters on the system efficiency is given on basis of the model and efficiency definition of section 4.1.4. The parameter variations are performed by calling the Dymola model of the rSOC system through the Dymola-Python interface. A more detailed analysis can be found in B1 [37]. Table 2 contains the list of parameters and values that are included in this sensitivity analysis. In Figure 24 one can see that in FC operation fuel utilisation and recirculation rate are most important. In EC operation, the sensitivity is by a factor of five lower, with stack temperature and fuel utilisation being most important.

Table 2: Parameter range for sensitivity analysis

Parameter	**Minimal value**	**Middle value**	**Maximal value**
Stack temperature (T_{Stack}) [°C]	700	750	800
Recirculation rate (rr) [-]	0.5	2.75	5
Fuel utilisation (fu) [-]	0.85	0.918	0.985
Fuel HX (ΔT_{Pinch}) [°C]	5	10	15
Air HX (ΔT_{Pinch}) [°C]	5 (EC) / 70 (FC)	10 (EC) / 80 (FC)	15 (EC) / 90 (FC)
Air excess ratio (λ) [-]	0.5 (EC)	1.0 (EC)	1.5 (EC)
Subcooling temp. (ΔT_{SC}) [°C]	50 (FC)	60 (FC)	70 (FC)

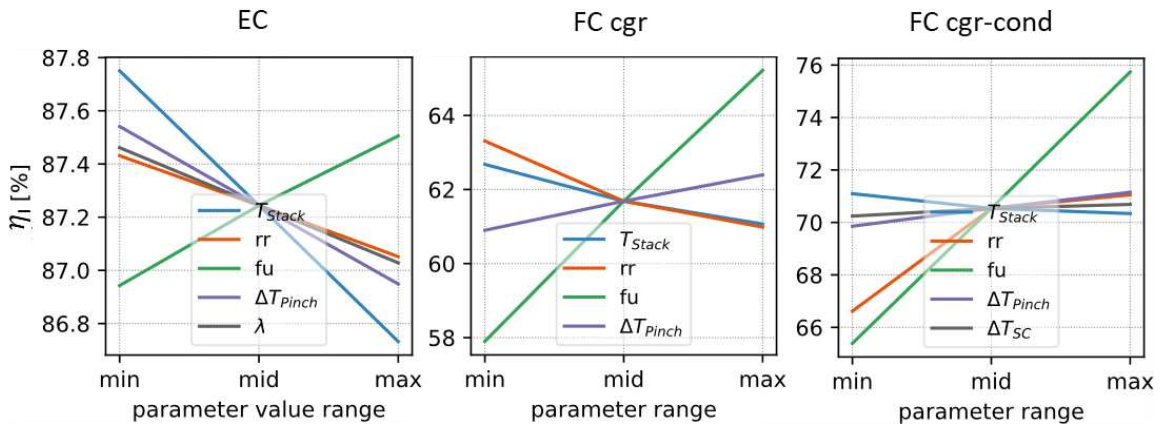

Figure 24: Sensitivity analysis for the flowsheet with cold gas recirculation in the industry scenario (efficiency according to equation (33) and (34)) as published in B1 [37].

The sensitivity analysis gives insights into the importance of the design parameters for the heat exchangers. It shows that low heat exchanger design pinch point temperature differences are beneficial for the system's efficiency, so that less heat is lost in EC operation and lower subcooling temperatures can be reached in FC operation. Furthermore, a low stack temperature is beneficial, since it decreases thermal losses in EC operation and increases the electric efficiency in FC operation, as is shown in the context of Figure 4. The fuel utilisation and recirculation are connected by the limitations described in section 4.1.3 and show opposite influence on the efficiency. Therefore, it is of high interest to investigate the change of efficiency more closely with respect to fuel utilisation and recirculation rate, which is subject of the next subsection. Only in the case of FC operation with condensation in the recirculation, an increase of both parameters results in an increase of efficiency.

5.1.1 Best operational parameters settings for recirculation rate and fuel utilisation

Here, the change of system efficiency, according to the definitions in equation (33) and (34), for variation of fuel utilisation and recirculation rate are discussed. In Figure 25 one can see that the best operation point in EC operation always lies on the limiting line of fuel utilisation, which corresponds to a stack fuel utilisation of 75% according to section 4.1.4. This was found to be the case for all flowsheets, also for FC operation, except for FC operation with a condenser in the recirculation loop. In FC operation with condensation in the recirculation, higher recirculation does not dilute the fuel much, since a big part of the steam content is condensed and drained. Therefore, the efficiency even rises with increased recirculation rate.

In all cases a recirculation on the fuel side has a positive impact on the system efficiency. Systems without fuel recirculation are highly limited by the maximum fuel utilisation rate of the stack in reaching high efficiencies. The influence of setting the parameters for the optimal values is highly significant in FC operation, yet in EC operation it is small. Therefore, it is more

important that the recirculation system is customized to the FC operation. Another important conclusion from this investigation is that the optimal parameter settings are different for the energy system and industry case. However, the influence of these settings on the system efficiency is marginal. Consequently, the optimal parameters for one scenario can be practically also used for the other.

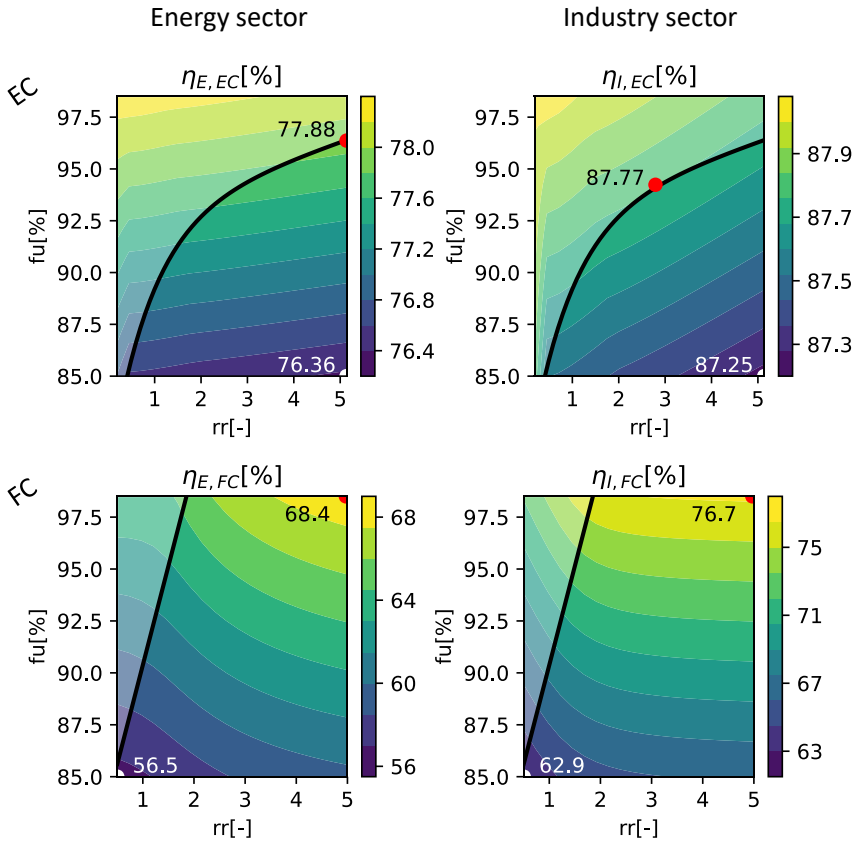

Figure 25: Optima of fuel utilisation (fu) and recirculation rate (rr) for the flowsheet with cold gas recirculation in EC and FC operation and in energy system and industry scenario as published in B1 [37]. The black limiting line divides the feasible operation regions from the not allowed operation region, with a maximum stack fuel utilisation of 75% according to section 4.1.3.

5.1.2 The best flowsheet considering round-trip operation

In B1 it was found that the flowsheets with the different types of recirculation (Figure 11) perform differently for the operation in EC and FC mode. In EC operation, the hot gas recirculation performs slightly better than the options with cold gas recirculation. On the other hand, in FC operation the cold gas recirculation with condensation has a significantly higher performance than other flowsheets. Therefore, B1 concludes that the cold gas recirculation with condensation is the preferred flowsheet for round-trip operation. Especially if the temperature reduction in the recirculation can be decreased in EC operation to avoid condensation. Furthermore, in B1 improvements for internal thermal recovery and increasing the system's waste heat temperature are proposed.

5.2 Integration to industrial sites and model simplification

This section is based on the results of the publication P1 [38] and starts by discussing the surrogate models for the thermal and fuel consumption part load behaviour. These models are then used in the investigation of industry integration scenarios.

5.2.1 Surrogate models for the integration to industrial sites

The simplified model for the rSOC system is given by the set of conversion curves for all desired properties in this representation, based on section 4.2.1 and 4.2.2. The part load behaviour obtained in this way for the conversion between electricity, fuel and heat is shown in Figure 26. In FC operation, the slightly convex trend for fuel consumption is a result of the increase of the stack losses with higher power. This can also be observed in the convex rise of thermal energy produced when operated with H_2. When operated with CH_4, the conversion curve for waste heat looks differently, since the reformer consumes a part of the heat generated in the endothermic steam reforming reaction. In EC operation, the conversion from electricity to fuel and thermal energy is nearly linear in Figure 26. This is a result of the modelled endothermic stack operation, in which case the temperature is maintained by electric heaters.

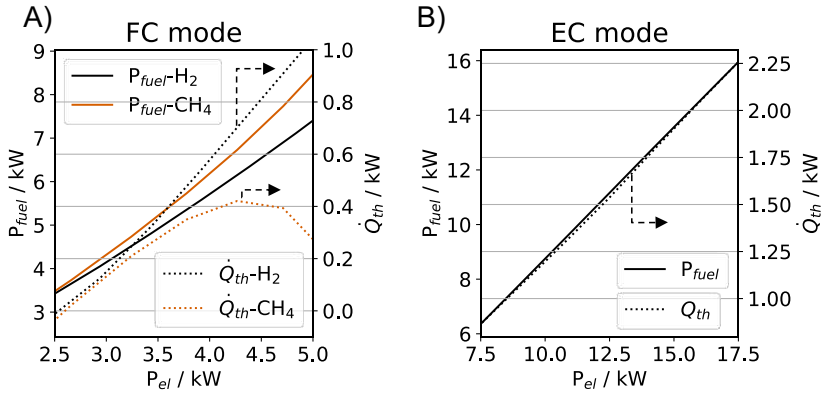

Figure 26: Conversion curves between electricity, fuel and heat for fuel cell (FC) and electrolysis cell (EC) operation of the rSOC system according to P1 [38].

The effect on the conversion efficiency of the thermal coupling in the different operation modes can be seen in Figure 27, when the conversion efficiency is defined according to equation (32) and (33). Here, the thermal coupling fraction f is introduced as a variable for the analysis and P_{el} is the net electric production of consumption of the system.

$$\eta_{FC} = \frac{P_{el} + f \cdot \dot{Q}_{th}}{P_{fuel}} \qquad (32)$$

$$\eta_{EC} = \frac{P_{fuel}}{P_{el} + (1 - f) \cdot \dot{Q}_{th}} \qquad (33)$$

In the FC operation, utilizing the waste heat (f=1) increases the efficiency in the nominal point of 5 kW electrical power by 15% when operated with H_2 and 3% when operated with CH_4. When the system load is reduced, the advantage decreases, since constant surface related losses to the environment take a bigger share. Below approximately 50% part load the system becomes endothermic and would require heating, so that $\dot{Q}_{th}$ becomes negative. Also, in EC operation the coupling advantage is the highest at nominal stack power of 15 kW (P_{el} equal to 17.5 kW) and increases the efficiency by 11%.

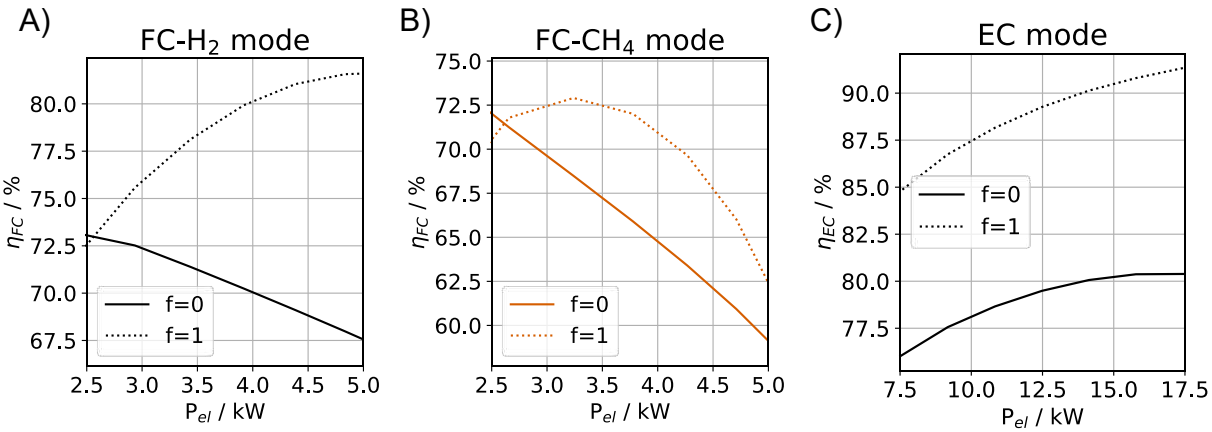

Figure 27: Conversion efficiency for thermal coupling (f=1) and no thermal coupling (f=0) according to equation (32) and (33), as published in P1 [38].

The investigation here is based on the system with a nominal power of 5 kW FC and 15 kW EC according to section 4.1.4. The system power demand in integrations to industries or district heating networks is much higher than the investigated system. There are two main strategies for scaling up the power of the investigated system. Firstly, a scale-up by number of system units which all have their own BoP components. Secondly, a scale-up of the stack and all the BoP components within the system. In our case we consider a mixed approach, where the stack is scaled by numbers, so that any power can be reached by making a pack of stacks, while the BoP components are scaled by size. When increasing the size of components or creating a pack of stacks, the most important changes comes from the change of surface to volume ratio and the connected thermal losses. The system model according to section 4.1.4. includes little thermal losses of 1 kW through the surface of stack and BoP components and therefore reflects the thermal isolation of large systems. This is discussed in detail in the validation of the simulation model in P1 [38] where the part load efficiencies of the present simulation is compared to the laboratory measurements on a stack conducted by Peters et al. [29]. By scaling the conversion curves of the 5/15 kW system to a higher power, the share of heat losses is constant. However, in a commonly insulated pack of cells the surface to volume ratio decreases with increasing size, which means that especially for very large systems, the thermal losses may be overestimated.

5.2.2 Scenario analysis of the integration to industrial sites

In the previous subsection the benefits of coupling a rSOC system to industrial sites was analysed qualitatively and quantitatively for the different operation modes of the system. However, the rSOC system combines both operation modes and therefore the system's conversion efficiency, defined according to equation (34), is relevant for the application. In this way the number of timesteps (t) for a chosen operation mode (i) can be considered.

$$\eta_S = \frac{\sum_{t,i} \dot{E}_{sys-out,i(t)}\,(t)}{\sum_{t,i} \dot{E}_{sys-in,i(t)}(t)} \qquad (34)$$

In P1 [38] an analysis of the coupling to industry with this definition of the system efficiency and the operation scenarios according to Table 3 was performed. In this way the effect of coupling to a generic industry, that can provide waste heat for the evaporation of feed water and can make use of waste heat from FC operation, is modelled. The main result of this investigation of different levels of coupling can be seen in Figure 28. The main conclusion of this analysis is that the influence of thermal coupling strongly depends on the operation time shares of the different modes. Furthermore, one can see that the thermal coupling for EC operation has a stronger influence on the system conversion efficiency than the coupling in FC operation. The biggest shortcoming of this approach is that operation shares must be known for this calculation. The operation times in real application are determined by economic conditions, which allow the operator to maximise the profit. This means that an operational optimisation is necessary to relate economic scenarios to the operation time scenarios discussed here. This approach will be followed in section 5.3.

Table 3: Scenarios for investigation of the rSOC system coupling to industrial sites.

Nr.	Operation time of mode in %		
	FC-H2	FC-CH4	EC
1		50	50
2		75	25
3	25	25	50
4	25	50	25
5	50		50

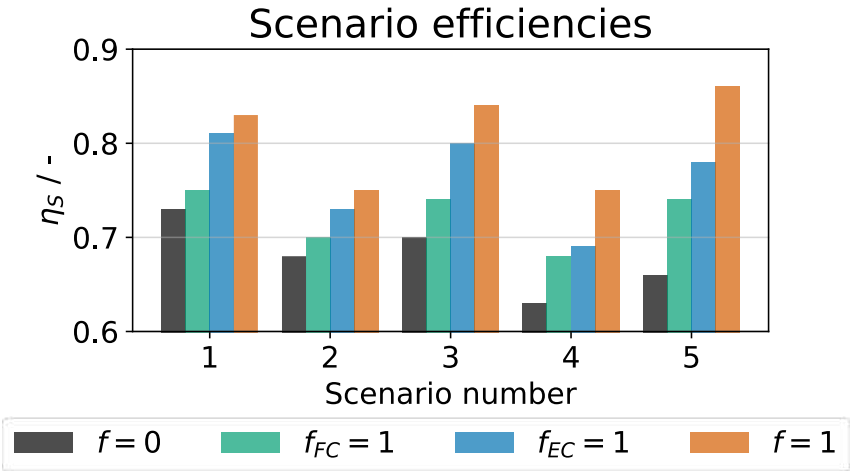

Figure 28: The system conversion efficiencies according to equation (34) for different scenarios, as published in P1 [38]: For no thermal coupling (f=0), thermal coupling in FC operation (f_{FC}=1), thermal coupling in EC operation (f_{EC}=1) and thermal coupling in both operation modes (f=1).

5.3 Techno-economic results of the application in the energy system

In this section the results of the techno-economic evaluation are shown, which are based on the optimisation approach for the system operation and H_2 storage size described in 4.4. Here the main results of the publication P2 [39] are revisited. Additionally, an idea for determining the levelized cost of hydrogen (*LCOH*) in this multi revenue set up, of electricity, hydrogen and heat markets, is introduced.

On the basis of the optimisation model the rSOC system's application in different levels of integration to the energy grid and industry can be simulated for the two selected scenario years 2030 and 2050. Furthermore, three scenario levels are implemented according to P2 [39] by adjusting the time-series of the optimisation model's boundary conditions as following:

- Reference case (RC): The time-series for industrial waste heat and district heat demand are set to zero. Thus, the rSOC system may interact only with the electricity and gas grid.
- Industrial case (IC): The time-series for district heating demand is set to zero. This allows thermal interaction with the energy grids and the industry's waste heat.
- Industry with district heating network (IDH): Allowing all interactions, that are shown in Figure 21.

The result of the *rROL* can be seen, for these three scenarios and depending on the scale of the rSOC system, in Figure 29. One can see that the IC scenario increases the *rROL* and thus the economics more than the IDH scenario. The reason is that the industrial waste heat availability has a bigger influence on economics, by increasing the profitability of EC operation

significantly, than the profit connected with providing district heat. The benefit of the coupling to industry is almost constant to a point of 23 MW in glass production and 9.5 MW in the brewery. After this point a decrease in the *rROL* follows which relates to the heat demand of the EC operation to be higher than can be provided by the industry. This sharp transition occurs due to the industrial heat time-series which have little variability as discussed in P2 [39].

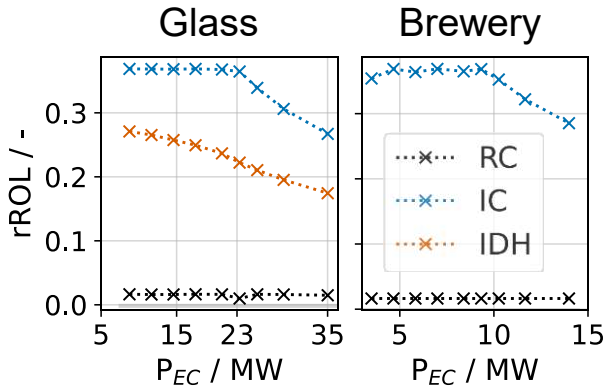

Figure 29: Influence of the rSOC system size given by the nominal electrolysis power (P_{EC}) in three application scenarios for the scenario year 2030: Reference case (RC), Industry case (IC), Industry with district heating network (IDH), as published in P2 [39].

In addition to the three coupling scenarios, the energy market prices are varied. The base time-series for the prices are forecasts for the years 2030 and 2050 both with uncertainties, as described in P2 [39]. To depict them, three variations are included in the analysis, as shown in Figure 30. These are:

- Constant shift of the electricity price and thus changing electricity-H_2-price spread.
- Amplitude of fluctuations of the electricity price on different domains of periodicity
- Gas grid fee

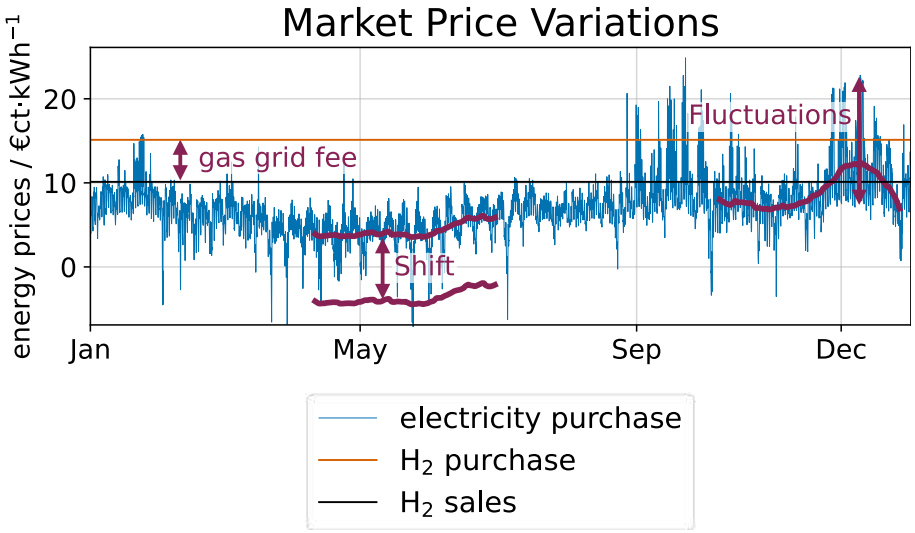

Figure 30: Variations of the energy market prices, to reduce the uncertainty of conclusions with respect to uncertain forecasts for future years.

The electricity-H_2-price spread is found in P2 [39] to be an interesting variable, which strongly determines the choice of operation mode of the rSOC system. This price spread is found in P2 [39] to be highly determinant for the so-called reversible zone. In the reversible zone both EC and FC operation are contributing at least 10% of operation time and only in this zone the rSOC system makes sense, since otherwise single mode systems are always more cost efficient. This reversible zone is visualized in Figure 31 for three reversible hydrogen technologies. In P2 [39] the influences of price fluctuations, grid gas price and industry coupling on this reversible zone are analysed. When fluctuations increase, the *rROL* strongly increases and they are found to have the strongest influence of the investigated parameters on the economics and on the width of the reversible zone.

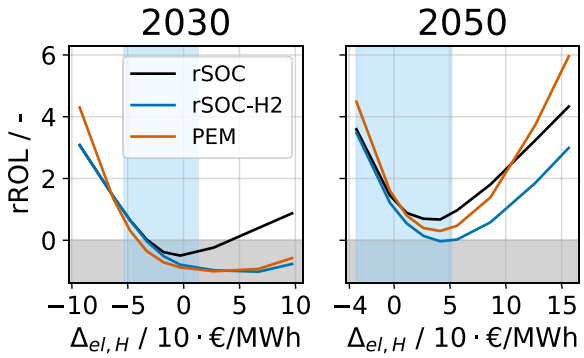

Figure 31: Change of rROL with electricity-H_2-price spread and reversible zone (highlighted in blue) for three versions of reversible systems, as published in P2 [39]: rSOC is the base system described in section 4.4.1, rSOC-H_2 does not include operation with CH_4 and PEM is a system for comparison and consists of a proton exchange membrane stack for electrolysis and fuel cell operation.

The influence of grid fees on the *rROL* and on the H_2 storage, analysed in P2 [39] and shown in Figure 32, has a strong impact on the economics and is most determining for the optimal size of local compressed H_2 storage. It is found that at today's grid fees, the economically optimal storage size only allows a buffering of H_2 for 3 h, which follows from Figure 32 B. The simulation of the H_2 storage in the optimisation model neglects the thermal storage behaviour, which would decrease the optimal storage size even further. Therefore, only large underground storages with storage-capacity costs of around 2 €/MWh according to Lord et al. [79], are a competitive solution for storing hydrogen. This conclusion points strongly to the need for the rSOC system to have a connection with the gas grid, so that an access to grid scale underground storage is given and long term H_2 storage becomes economically feasible. In this case, as discussed in P2 [39], the EC and FC unit do not necessarily need to be in the same location. For discussing the applications potentials of these spatially delocalized reversible systems in comparison to spatially concentrated reversible systems, the reduction of electrical grid load and the sites which offer coupling benefits for both EC and FC operation must be considered. An attempt to include the service for electricity grid load reduction is made in section 4.5.

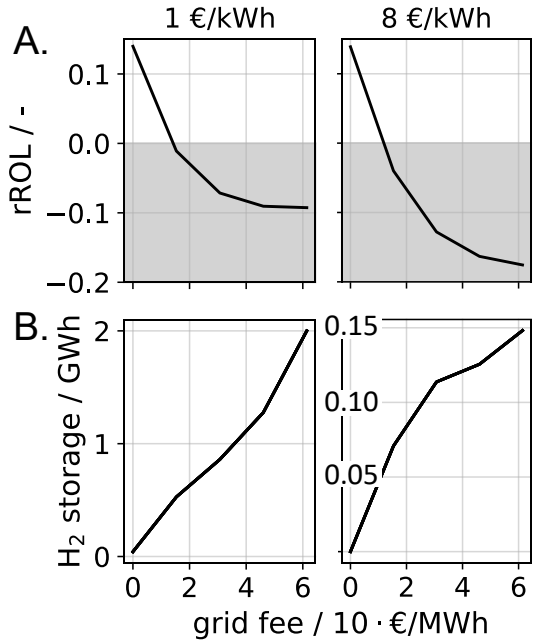

Figure 32: Influence of grid fee in the scenario year 2050 for two storage investment costs (1 €/kWh and 8 €/kWh) and a rSOC system operated in FC with H_2 only, as published in P2 [39]. A) relative return over lifetime (rROL), B) H_2 storage size.

Another interesting observation is possible when looking at the impact of the H_2 price on the *rROL*, which is shown in Figure 33. Depending on the scenario, the *rROL* may transit from negative to positive region. The H_2 price at this transition point, when *rROL* is equal to zero, can be interpreted as levelized cost of hydrogen (*LCOH*). In this way, the *LCOH* can be determined in the system with multiple revenue streams, for constant values of the other boundary conditions of the optimisation model. When interpreting the zero-transition point of the *rROL* in this way, it is also important to consider whether the reversible H_2 system is a net source or rather a sink for H_2. In the case of Figure 33, the EC operation is dominant which means H_2 can indeed be produced with at the *LCOH*.

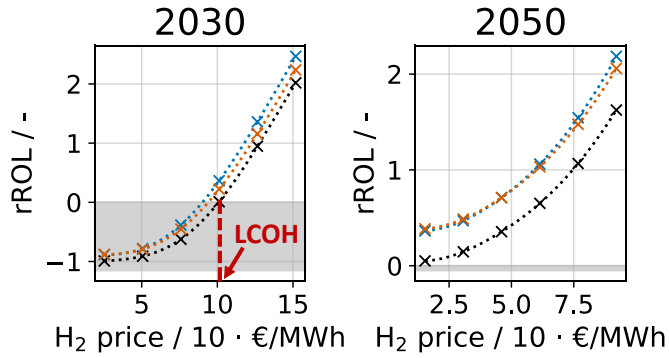

Figure 33: Influence of the H_2 price on the rROL and identification of the levelized cost of hydrogen (LCOH).

5.4 Investigation of spatial types for bidirectional hydrogen systems

Here the results for the investigation of the different spatial types of H_2-conversion systems, based on the modelling approach of section 4.5.1, are presented and discussed. Furthermore, a spatial visualization of the concentrated and delocalized types' applications is made. The results regarding the grid fee influence in section 5.3 suggests that a profitable operation of reversible hydrogen systems is only possible with the cheap storage capacities of underground formations and gas grids. Therefore, this work considers the future availability of H_2 gas grids according to the outlook in the ÖNIP [78] for the year 2040, to be the only sites where bidirectional hydrogen systems are installed.

5.4.1 Simulation results for the spatial system types in selected grid nodes

The simulated operation for the three systems options (concentrated reversible system, delocalized EC or delocalized FC) can be seen for three grid nodes with three different residual load characteristics in Figure 34, Figure 35 and Figure 36. These are the three possible main characteristics, which span, together with different magnitudes and temporal durations of fluctuations, the whole spectrum of possibilities. The limiting assumption for delocalized EC and FC operation, for H_2 production and utilisation and system utilisation (according to point 2) and 3) in section 4.5.1), causes either the delocalized EC or FC system to have a nominal power of zero.

Node type 1:

In Figure 34 one can see that both the delocalized EC system and the concentrated reversible system can highly smoothen the residual load. The nominal power of the concentrated reversible system, however, is 30% smaller. This means that a smaller concentrated system can provide the same grid service.

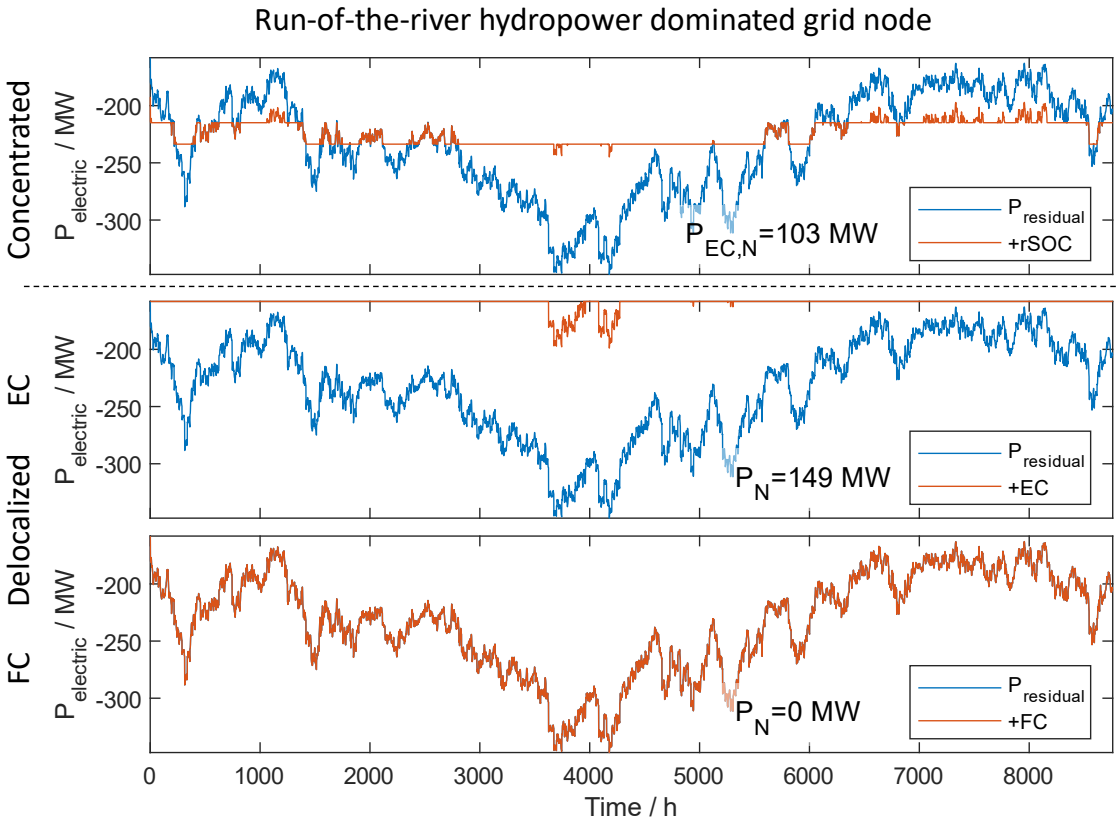

Figure 34: Simulation of reversible systems in production dominated grid node and resulting nominal system power (P_N).

Node type 2:

In the demand dominated node in Figure 35 one can see that the delocalized FC system with around 327 MW nominal power can flatten the residual load fully. The size of the concentrated system at 50% utilisation is much smaller and the smoothing is therefore less.

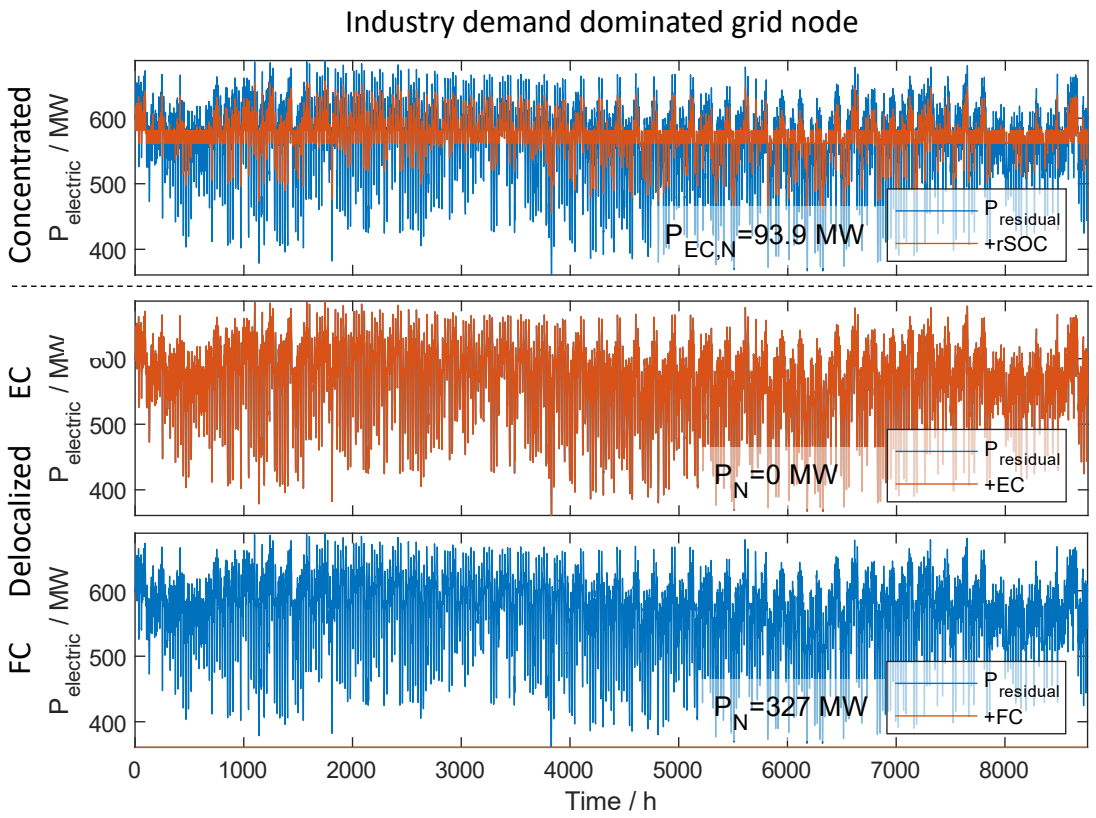

Figure 35: Simulation of reversible systems in an industry demand dominated grid node and resulting nominal system power (P_N).

Node type 3:

The node with frequently changing direction of residual load flow shown in Figure 36, has very little potential for both delocalized EC and FC systems. This is because the single mode delocalized systems are not allowed to cause a change of the residual load flow direction. The concentrated reversible system in this case can lead to a high degree of residual load smoothing.

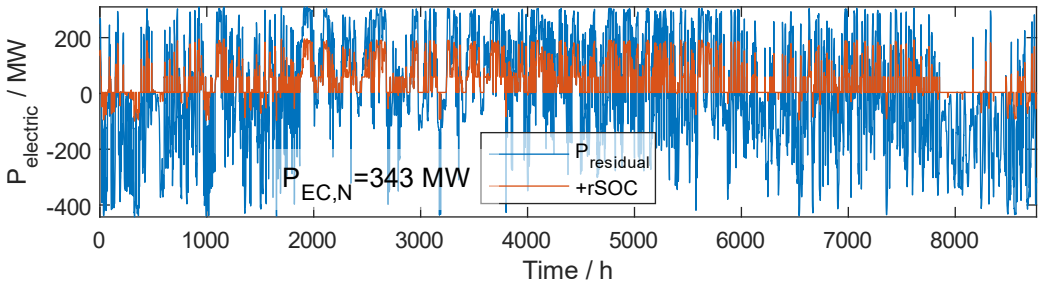

Figure 36: Simulation of reversible systems in a grid node with residual load changing its direction.

From the three node types discussed, one can conclude that delocalized systems (EC and FC) can flatten the residual load under the simulation constraints very well when the fluctuations are frequent, and the residual load does not change the flow direction. The strength of the concentrated system lies in places with bidirectional residual load flow, which limits the application of unidirectional systems. The proposed approach for simulating the different

spatial systems can be used for the calculation of system application potentials for given electrical residual loads.

5.4.2 Result and discussion of spatially resolved application potentials for both spatial system types

Here the results are analysed for applying the method of section 4.5.1 to the electrical residual loads predicted for 2040 for 136 out of 398 Austrian energy grid nodes that are expected to have access to a H_2 gas grid in 2040, according to the WAM scenario of the Infratrans 2040 project [80].

For these grid nodes one can see in Figure 37 the application potentials for smoothing the residual loads, when the only task of the reversible systems is this smoothing. Here one can see locations having the highest installed power for each of the three possible systems. Many sites with high potential for delocalized electrolysis systems have also significant potential for concentrated reversible systems. These locations are found especially by run-of-the-river waterpower plants and with lower potential also by wind and photovoltaic renewable production. These locations correspond to type 1, which is discussed in section 4.5.1. The locations with high application potential for delocalized FC system are close to residential or industrial areas, which cause positive electrical residual loads. These places therefore correspond to the type 2 of section 4.5.1. Locations that show the highest potential for concentrated reversible units are in places that are neither fully dominated by production nor by consumption. Thus, they have a residual load that has more balanced negative and positive times and thus corresponds to type 3 of 4.5.1. Such places can be found in regions with renewable production that is slightly larger than the demand and when high fluctuations of production are expected.

In this analysis, most nodes have higher installed system power of the unidirectional delocalized systems (EC or FC) than concentrated systems (rSOC). One of the possible reasons for this is, that the concentrated rSOC system needs lower nominal power to achieve a good smoothing of the residual load, as discussed for Figure 34. Another reason is that many grid nodes have a clear negative or positive electrical residual load, which makes the load smoothing highly compatible with the restriction for 50% system utilisation and allows for big unidirectional delocalized systems.

One limitation of the present analysis is the spatial resolution, where for each grid point the residual load is aggregated and thus in a certain region delocalized systems might be installed but visible on the grid point resolution as concentrated reversible systems.

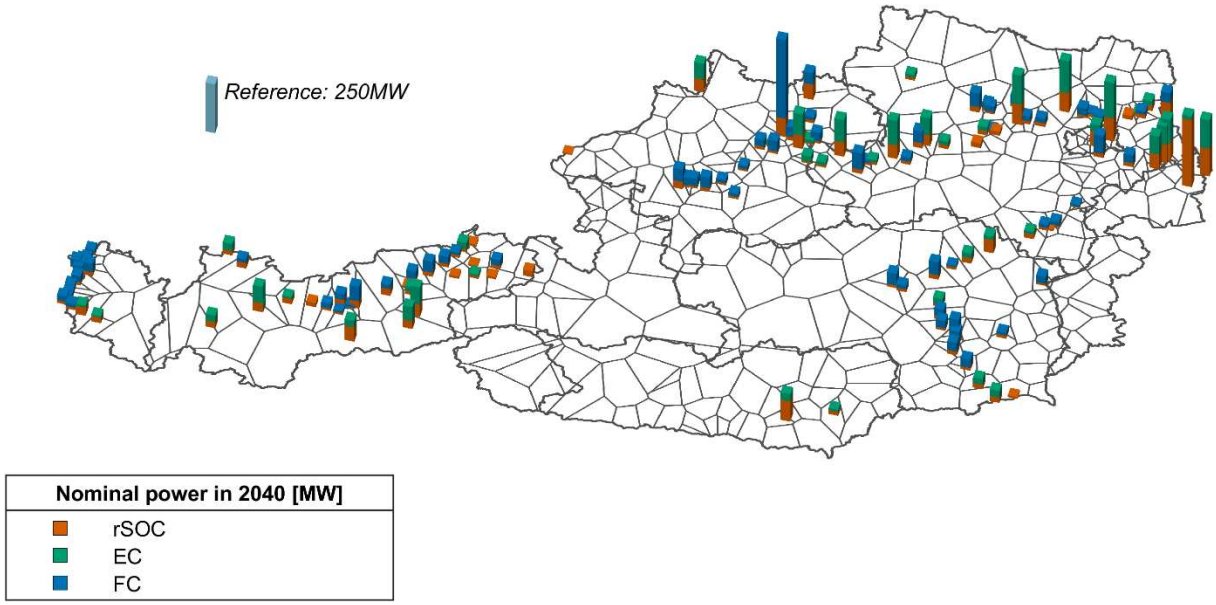

Figure 37: Nominal installed system power above 5 MW for concentrated (rSOC) and delocalized (EC and FC) systems in 136 Austrian grid nodes with expected H_2-grid connection in 2040 according to the WAM scenario [80].

In Table 4 one can see the sum up for the results of the simulation of the two spatial system types, which is visualized in Figure 37. One can see, that in almost all simulated grid node points, a rSOC system with more than 5 MW electrolysis power can be installed. Whereas pure EC and FC systems share the application places and these single mode systems are not used in 14 out of the 136 grid nodes. The installed power of rSOC units is larger than the sum of EC and FC units, when the FC units are only allowed to consume the hydrogen produced by the EC units. However, the converted energy is smaller for the rSOC units and the storage need is larger, even when balanced by the H_2 gas grid. When the grid is not used for balancing the temporal mismatch of electrolysis production and fuel cell consumption, the need for local H_2 storage to be stored locally is almost doubled. This is an important observation: H_2 grids are not only necessary to allow for cheap large scale H_2-storage, but also to reduce the need for storage capacity, by spatially balancing the H_2 demand and production. The total installed system power for the sum of EC and FC units is 26% larger than the installed capacities of the rSOC units. However, the costs of rSOC units are also around 25% higher than a single mode system with approximately 1000 €/kW (according to the assumptions in P2 [39]), which would result in very similar total system for the application of the two spatial types. In this case, when the H_2 consumption of FC units is not limited, the remaining volatility of electric residual loads for delocalised systems is 35.9%, which is lower for concentrated systems. When the FC units can consume only the amount produced by EC units, which is the same assumption like for rSOC systems, the volatility is 57.5%, which is higher than for rSOC systems. However, the smaller installed FC capacity makes the delocalized systems a cheaper option. Overall, the

decision whether concentrated or delocalized spatial hydrogen conversion systems are preferred, depends on the acceptable costs for reduction of residual load variability.

Table 4: Results of the simulation of spatial system types for an installed power above 5 MW.

	Nr. of nodes with system	Installed power in GW	Storage capacity in GWh	H_2 converted in GWh	Relative average volatility of the load (eq. (31))
rSOC	134	3.98	2 937 (loc.) 1 770 (grid)	5 590	48.5%
EC	46	2.33	1 487 (grid)*	8 156	54.0%
FC	74	1.11*			72.2% (57.5%**)
FC		2.71	-	19 856	32.5% (35.9%**)

*assuming that the FC units consume exactly the production of the EC units

**combined relative average volatility of EC and FC units for all H_2 grid node points

6 CONCLUSIONS

This Chapter provides answers to the research questions raised in section 2.3 regarding the modelling of the rSOC system, the coupling possibilities of this system, the time resolved techno-economic scenario analysis and the application potentials from the perspective of electricity grid service provided by two spatial system types.

(1) How are the simulation models for the low-level of the electrochemical cell, the mid-level of the stack and the high-level of the reversible system sequentially building up?

In section 4.1 the different stages from cell to system level are described in detail, based on the investigations published in B1 [37]. The modelling of the electrochemical zero-dimensional cell can be achieved by modelling fundamental processes that are dependent on material properties. In this stage the biggest uncertainty comes from material choices and the layer structure. For modelling an electrochemical stack continuing with fundamental principles, it is necessary to include the stack geometry. Especially, the gas flow fields, and the flow directions are important, since gas transport processes are determining the local behaviour of the electrochemical cell. Furthermore, the thermal inertia derives from this stack geometry. In addition to the model for the electrochemical stack, the full system model must include sub-models for the balance of plant components, which are necessary to operate the stack efficiently and safely. The arrangement of stack and balance of plant can be done in different ways resulting in different system flowsheets, as shown for three cases in Figure 11.

The focus of the present work is on studying influences on the reversible system and its integration to ambient energy systems. Therefore, it is not necessary to model the stack from fundamental principles, a numerical model for an existing stack can be employed. The shortcoming of this approach is that the influence of different stack designs on the system performance cannot be studied.

(2) What are good simplifications in the simulation of the rSOC system regarding the optimal operation parameters and the flowsheet?

The discussion in section 4.1.5 and 4.1.6 allows to conclude that most system parameters are independent from each other and show a clear direction of influencing the system efficiency. This allows for an independent determination of good parameters for the system design according to the sensitivity analysis in section 4.1.5. Only fuel utilisation and recirculation rate are found to be connected and need an optimisation to maximise the system efficiency, as can be found in section 4.1.6. The investigation shows that the optimal setting of these parameters only depends very slightly on the share of thermal interaction with industrial waste heat or district heating. Therefore, it is a good simplification to determine the optimal setting of fuel utilisation and recirculation independent from the thermal interaction scenario.

Based on B1 [37] the cold gas recirculation with condensation is found to be the best system flowsheet for a reversible round-trip system, as described in section 5.1.2.

(3) What are the possibilities and the benefits of coupling the rSOC system thermally to waste heat sources and heat sinks? What should good sites for the integration of rSOC systems offer?

The flowsheet of the rSOC system in Figure 12 shows the possibilities for heat integration and extraction, which can increase the conversion efficiencies by more than 10%, according to Figure 27. In FC operation thermal energy, with a temperature slightly below the stack temperature, can be extracted after the catalytic burner. In EC operation, waste heat can be used for steam production. Ideal integration sites for rSOC systems can offer a thermal coupling option for both the excessive heat of FC operation and heat demand in EC operation. This is possible for example in residential areas with district heating and a waste heat providing industry. The heating demand has a seasonal pattern, which can together with the industrial waste heat lead to availability of heat for EC operation in summer and demand for heat from FC operation in winter. Together with the seasonal production pattern of photovoltaic, this fits also very well to the availability of cheap electricity.

(4) How can the operation of the rSOC system be simulated in different scenarios, what kind of system models are necessary and how can these be built-up most efficiently?

This work implements two approaches for simulating the rSOC system's operation in implementation scenarios. In section 5.2.2 a static approach is used, which can evaluate the benefits of different coupling possibilities. In this approach, the operation time is not resolved but only the time share spent in different operation modes is considered. The biggest shortcoming of this approach is, that it is unclear how different distributions of the operation time correspond to economic conditions, however these operation shares are required for the calculation. The time-series based dynamic approach defined in section 4.4.1 determines the system's operation by mathematical optimisation based on given economic boundary conditions. The system models for this approach need to be simplified, so that they are suitable for the optimisation routine and the formulation of an optimisation model, here this is a mixed integer linear problem. Since the optimal system operation is based only on assumptions for the economic boundary conditions, different application scenarios can easily be considered. The optimisation establishes the link between choice of operation and economic conditions. The derivation of the required simplified models for the rSOC system and the H_2 storage system is described in section 4.2.2 and section 4.3.1 respectively. The simplification here is achieved by piecewise linearization of all part load conversion curves that are necessary to represent the rSOC system in the environment of the application scenarios.

(5) Which economic and application conditions make the operation of reversible H_2 systems and rSOC systems profitable?

The simulation of the optimal system operation described in section 4.4.1 can be used for performing a Techno-economic analysis which is discussed in section 5.3 based on the publication P2 [39].

The electricity - H_2 price spread is found to strongly determine the profitability and the operation choice of the system. A significant reversible operation is only observed in a limited range around zero for this spread, called in P2 [39] the reversible zone.

Price fluctuations are having the strongest influence on this reversible zone. Higher fluctuation increases the profitability and the width of the reversible zone. In low fluctuating price scenarios, no profitable operation is possible.

The thermal coupling to industrial sites and district heating barely influences the reversible zone, but increases the profitability significantly, especially when the system size matches the waste heat availability.

The grid fee investigations show that local H_2 storage is only for short time scales possible and reversible H_2 systems need a connection to cheap underground storage facilities, through H_2 gas grids, to be profitable. Therefore, the next question arises whether the system needs to combine both operation modes in one locally concentrated reversible unit or if spatial delocalized unimodal units can act reversibly through the H_2 gas and electricity grid connection.

(6) What are the application potentials for locally concentrated reversible H_2 systems considering electricity grid service by smoothing residual loads?

This question can only be answered considering electrical grid limitations and the benefits for the electricity grid connected with locally concentrated and spatially delocalized systems. By assuming grid supportive system operation for smoothing of residual loads, one can calculate the connected required system power. In this way, the ideal upper system size limit for grid supportiveness is determined. It turns out that there are three types of residual load characteristics that are connected to delocalized EC and FC or concentrated reversible systems. The locations most suited for rSOC systems have residual loads that have at least a partly balanced negative and positive load flow, as can be observed by renewable production sites in proximity of electricity consumers, like residential areas or industries. Assuming a balanced production and consumption of H_2 for EC and FC operation, the concentrated rSOC system allows a better smoothing or residual loads and thus stronger reduces the loads for electricity grids, as can be seen in Table 4. However, the nominal-power-related investment costs are higher for the concentrated than for the delocalized system type.

(7) What are characteristics of the most promising application sites for rSOC systems?

The conclusions regarding the questions (3) and (6) both point to application sites for rSOC systems that have the following characteristics:

- Changing load flow direction of the electrical residual load, which is usually connected to renewable production close to consumers like industries or residential areas
- Thermal coupling possibilities for both operation modes. In the presence of seasonal varying district heating demand and more constant industrial waste heat sources, heat can be available in summer for steam production in EC operation and heat from FC operation can be used in district heating in winter. However, to observe such a pattern, the available waste heat of the industry must be smaller than the district heating demand in winter and larger in summer.
- Photovoltaic in combination with residential heating and industries is promising, since it has a pronounced seasonal production periodicity which is almost exactly 180° shifted to the demand for residential heating. Therefore, the benefits of (3) and (6) are combined.

7 OUTLOOK

This Chapter concludes this thesis by giving ideas for future research works in the field of the application of rSOC systems. It is structured in three topics, which start with a general overview which is then divided into more precise points and detailed questions that are not yet answered or can be improved.

(1) Influence of new flexible technologies on the future volatility of the electricity market

The Merit-Order market clearing mechanism is responsible for the coupling of the electricity market price to volatile renewable production, as Traupmann [74] described in the future outlook for market prices. Renewable energy production and nuclear power have very low marginal operation costs, while the marginal costs for flexible operable powerplants like combined cycle gas turbines are by a multiple higher. Therefore, fluctuating renewable production, which will constitute a significant share of future energy generation, can lead to times of very low prices, when the renewables cover the demand and high prices when they are producing less than demanded. This arises because of the rigid demand cost relation, where the consumers hardly react to the momentary price of the electricity. This rigid response is especially pronounced when the energy contracts for consumers do not include dynamic price calculations. In the future, however, due to changed contracts for consumers, the increase of electric vehicle fleet and smarter operation of household appliances can increase the price responsiveness of the demand. New electric energy storage technologies on the energy system level, in addition to pumped hydro storages, can furthermore increase the demand responsiveness.

Interdependence of flexible technologies:

The reversible H_2 technologies can operate in electrolysis in times of low prices and as fuel cells in high-price times. Therefore, these technologies act in a way to stabilize the electricity price. The capability and magnitude of the stabilization is related to storage capacities and conversion efficiencies. Since the profitability of rSOC systems according to P2 [39] depends strongly on the price fluctuations, it is interesting to study the influence of future storage and conversion technologies on the price fluctuations. Also, the emerging Anion exchange membrane (AEM) electrolysis may play an important role in the future H_2 production. Questions that appear in this context are: Which technologies operate most profitably with fluctuations of certain periodicity and how does this influence the operation of less profitable technologies? What are fluctuation magnitudes that are needed by different storage and conversion technologies to be profitable and what is the connected electricity-H_2 price spread?

Influence of transformation of installed gas turbines on future economic chances of electrochemical systems:

The installed gas turbine power in Europe for 2021 was 314 GW as published by Statista [11]. The profitability is of these turbines is already nowadays depending on the electricity price volatility. It is widely believed that existing gas turbines can be converted with little effort to operate with hydrogen. This gives them a large importance for the hydrogen-to-power pathway without necessity of big new investments. When estimating future price volatilities, it is necessary to take this existing price-smoothing technology into account.

(2) Improved and new methodologies for evaluation of application potentials of bidirectional H_2 conversion technologies:

This point comprises suggestions for improving the methodology of simulating the application of the investigated bidirectional H_2 conversion technologies.

Spatial resolved application from both view perspectives of integrated systems and grid service:

The present thesis includes an investigation of the application of rSOC systems by industrial sites and district heating networks. It would be interesting to analyse the spatially resolved application potentials for this approach and to identify regions that match with the results for potentials based on electricity grid service approach, discussed in section 5.4.2. Such an approach demands for spatially resolved industrial waste heat and district heat demand time-series. Furthermore, this investigation should include future demands for hydrogen in industrial sites and in points of the energy grid. This can allow reversible H_2 systems to be more profitable by reducing H_2 transport and storage costs, since H_2 can be used fully or partly on-site during its production.

Improving the level of detail for the simulation of system integration:

The depth of the investigation of rSOC system application in industrial sites, as shown in section 5.3, is limited by the available time-series for industrial waste heat, which show little characteristic temporal behaviour. Therefore, the transition from system sizes with maximum to reduced coupling benefit has a kink (see Figure 29), which would be expected to be a smooth transition in time-series with more variability. A future study could investigate waste heat time-series with different temporal patterns and look for industries that are well suited to the dynamic limitations of rSOC systems. Therefore, the models in Ganymed [75] need to implement typical operation characteristic for different industrial sectors. Especially the temporal patterns of energy extensive sectors are not yet modelled to fulfil the described data demand.

Speed-up of scenario calculations:

The result of section 5.3, concerning the very small optimal storage size, can be used to speed up the simulation for future investigations. With a small storage the interaction across timesteps becomes small and can be neglected in many scenarios. This separates the optimisation problem in small non-connected problems for each timestep.

Include additional markets for determination of optimal operation, to reflect grid friendly operation:

Spatially resolved pricing mechanisms for the balancing and redispatch measures could be used in the approach via operation optimisation. An investigation considering such markets was performed by Traupmann et al. [81]. These markets for grid stability pose additional possibilities for rSOC systems to generate profit and can be easily integrated in an operation optimisation model as proposed in section 4.4.1. The optimisation model can then determine the cost optimal system operation and the resulting residual loads can be analysed with respect to grid supportiveness for both spatial system types. This approach can answer the question in which places concentrated reversible systems are interesting from both economic and grid perspective and which market incentives are necessary to achieve grid supportive operation.

(3) Wide view on bidirectional H_2 technologies:

An analysis concerning the applicability of different future H_2 conversion technologies should include Life-Cycle-Assessments (LCA) for environmental and economic parameters, in addition to the Techno-economic approach in P2 [39]. Also, niche applications can have a significant impact on the price development of conversion technologies and need to be considered.

Considering the environmental impact of technologies:

According to Zhao et al. [9] SOEC technology has the lowest environmental impact followed by AEM electrolysis and with a much higher impact PEM electrolysis. Also Salim et al. [82] and Gerloff et al. [83] found in their LCA investigations, that SOFC are superior in terms of environmental impact. The LCA by Smith et al. [84] show the reduction potential of the environmental footprint by new material in SOFC technologies. On the other hand, Mori et al. [85] found PEM to be less critical than SOFC which uses more rare elements that need importing to the EU. Also Lundberg [86] found the PEM electrolysis to have a lower environmental impact than SOEC, but expect a stronger decrease of the impact for the SOEC technology. Furthermore, the efforts for regulating the use of per- and polyfluoroalkyl substances (PFAS) can limit PEM and AEM technologies [87]. The rSOC technology offers advantages in this context, since both EC and FC operation can be combined in one asset and thus the related environmental impact is reduced for the single operation mode.

Niche applications:

A field of application, that was not investigated in the present thesis are reversible H_2 systems in island application. In this set up the rSOC system can possibly be beneficial through its thermal coupling possibilities.

8 REFERENCES

[1] The European Green Deal COM/2019/640 final. Brussels, 2019. https://eur-lex.europa.eu/legal-content/en/ALL/?uri=CELEX:52019DC0640 (accessed June 13, 2024).

[2] Crotogino F. Traditional bulk energy storage—coal and underground natural gas and oil storage, 2022. In *Storing Energy*, 633–49: Elsevier. https://doi.org/10.1016/B978-0-12-824510-1.00021-0.

[3] Hunt J.D., Byers E., Wada Y., Parkinson S., Gernaat D.E.H.J., Langan S., van Vuuren D.P., and Riahi K. 2020 Global resource potential of seasonal pumped hydropower storage for energy and water storage *Nature communications*, vol. 11, no. 1, p. 947. https://doi.org/10.1038/s41467-020-14555-y.

[4] Sejkora C., Kühberger L., Radner F., Trattner A., and Kienberger T. 2020 Exergy as Criteria for Efficient Energy Systems—A Spatially Resolved Comparison of the Current Exergy Consumption, the Current Useful Exergy Demand and Renewable Exergy Potential *Energies*, vol. 13, no. 4, p. 843. https://doi.org/10.3390/en13040843.

[5] Overland I., Juraev J., and Vakulchuk R. 2022 Are renewable energy sources more evenly distributed than fossil fuels? *Renewable Energy*, vol. 200, pp. 379–386. https://doi.org/10.1016/j.renene.2022.09.046.

[6] European Hydrogen Backbone: Implementation Roadmap - Cross Boarder Projects and Costs Update, 2023. https://ehb.eu/files/downloads/EHB-2023-20-Nov-FINAL-design.pdf (accessed December 12, 2023).

[7] Global Hydrogen Review 2023, 2023. https://iea.blob.core.windows.net/assets/cb9d5903-0df2-4c6c-afa1-4012f9ed45d2/GlobalHydrogenReview2023.pdf (accessed June 19, 2024).

[8] Zainal B.S., Ker P.J., Mohamed H., Ong H.C., Fattah I., Rahman S.A., Nghiem L.D., and Mahlia T.M.I. 2024 Recent advancement and assessment of green hydrogen production technologies *Renewable and Sustainable Energy Reviews*, vol. 189, p. 113941. https://doi.org/10.1016/j.rser.2023.113941.

[9] Zhao G., Kraglund M.R., Frandsen H.L., Wulff A.C., Jensen S.H., Chen M., and Graves C.R. 2020 Life cycle assessment of H2O electrolysis technologies *International Journal of Hydrogen Energy*, vol. 45, no. 43, pp. 23765–23781. https://doi.org/10.1016/j.ijhydene.2020.05.282.

[10] Schwarze K., Posdziech O., Mermelstein J., and Kroop S. 2019 Operational Results of an 150/30 kW RSOC System in an Industrial Environment *Fuel Cells*. https://doi.org/10.1002/fuce.201800194.

[11] Statista, *Gas electricity generation capacity in Europe from 2000 to 2021:* Statista, 2023. https://www.statista.com/statistics/1312537/gas-power-capacity-in-europe/ (accessed December 11, 2023).

[12] Jamal T., Shafiullah G.M., Dawood F., Kaur A., Arif M.T., Pugazhendhi R., Elavarasan R.M., and Ahmed S.F. 2023 Fuelling the future: An in-depth review of recent trends, challenges and opportunities of hydrogen fuel cell for a sustainable hydrogen economy *Energy Reports*, vol. 10, pp. 2103–2127. https://doi.org/10.1016/j.egyr.2023.09.011.

[13] Corigliano O., Pagnotta L., and Fragiacomo P. 2022 On the Technology of Solid Oxide Fuel Cell (SOFC) Energy Systems for Stationary Power Generation: A Review *Sustainability*, vol. 14, no. 22, p. 15276. https://doi.org/10.3390/su142215276.

[14] Salam M.A., Shaikh M.A.A., and Ahmed K. 2023 Green hydrogen based power generation prospect for sustainable development of Bangladesh using PEMFC and hydrogen gas turbine *Energy Reports*, vol. 9, pp. 3406–3416. https://doi.org/10.1016/j.egyr.2023.02.024.

[15] Cigolotti V., Genovese M., and Fragiacomo P. 2021 Comprehensive Review on Fuel Cell Technology for Stationary Applications as Sustainable and Efficient Poly-Generation Energy Systems *Energies*, vol. 14, no. 16, p. 4963. https://doi.org/10.3390/en14164963.

[16] The Future of Heat Pumps, 2022. https://iea.blob.core.windows.net/assets/4713780d-c0ae-4686-8c9b-29e782452695/TheFutureofHeatPumps.pdf (accessed June 13, 2024).

[17] Rabuni M.F., Li T., Othman M.H.D., Adnan F.H., and Li K. 2023 Progress in Solid Oxide Fuel Cells with Hydrocarbon Fuels *Energies*, vol. 16, no. 17, p. 6404. https://doi.org/10.3390/en16176404.

[18] Rathore S.S., Biswas S., Fini D., Kulkarni A.P., and Giddey S. 2021 Direct ammonia solid-oxide fuel cells: A review of progress and prospects *International Journal of Hydrogen Energy*, vol. 46, no. 71, pp. 35365–35384. https://doi.org/10.1016/j.ijhydene.2021.08.092.

[19] Ferrero D., Lanzini A., Leone P., and Santarelli M. 2015 Reversible operation of solid oxide cells under electrolysis and fuel cell modes: Experimental study and model validation *Chemical Engineering Journal*, vol. 274, pp. 143–155. https://doi.org/10.1016/j.cej.2015.03.096.

[20] Chen Y., Wu X., Hu H., and Zhang J. 2023 System level performance analysis and parameter optimization of hydrogen production based on solid oxide electrolytic cell *Applied Energy*, vol. 347, p. 121329. https://doi.org/10.1016/j.apenergy.2023.121329.

[21] Frank M., Deja R., Peters R., Blum L., and Stolten D. 2018 Bypassing renewable variability with a reversible solid oxide cell plant *Applied Energy*, vol. 217, pp. 101–112. https://doi.org/10.1016/j.apenergy.2018.02.115.

[22] Subotić V., Thaller T., Königshofer B., Menzler N.H., Bucher E., Egger A., and Hochenauer C. 2020 Performance assessment of industrial-sized solid oxide cells operated in a reversible mode: Detailed numerical and experimental study *International Journal of Hydrogen Energy*, vol. 45, no. 53, pp. 29166–29185. https://doi.org/10.1016/j.ijhydene.2020.07.165.

[23] Giap V.-T., Kim Y.S., Lee Y.D., and Ahn K.Y. 2020 Waste heat utilization in reversible solid oxide fuel cell systems for electrical energy storage: Fuel recirculation design and feasibility analysis *Journal of Energy Storage*, vol. 29, p. 101434. https://doi.org/10.1016/j.est.2020.101434.

[24] Perna A., Minutillo M., and Jannelli E. 2018 Designing and analyzing an electric energy storage system based on reversible solid oxide cells *Energy Conversion and Management*, vol. 159, pp. 381–395. https://doi.org/10.1016/j.enconman.2017.12.082.

[25] Giap V.-T., Kang S., and Ahn K.Y. 2019 HIGH-EFFICIENT reversible solid oxide fuel cell coupled with waste steam for distributed electrical energy storage system *Renewable Energy*, vol. 144, pp. 129–138. https://doi.org/10.1016/j.renene.2018.10.112.

[26] Giap V.-T., Lee Y.D., Kim Y.S., and Ahn K.Y. 2020 A novel electrical energy storage system based on a reversible solid oxide fuel cell coupled with metal hydrides and waste steam *Applied Energy*, vol. 262, p. 114522. https://doi.org/10.1016/j.apenergy.2020.114522.

[27] Mottaghizadeh P., Santhanam S., Heddrich M.P., Friedrich K.A., and Rinaldi F. 2017 Process modeling of a reversible solid oxide cell (r-SOC) energy storage system utilizing commercially available SOC reactor *Energy Conversion and Management*, vol. 142, pp. 477–493. https://doi.org/10.1016/j.enconman.2017.03.010.

[28] Schwarze K., Geißler T., Nimtz M., and Blumentritt R. 2023 Demonstration and scale-up of high-temperature electrolysis systems *Fuel Cells*. https://doi.org/10.1002/fuce.202300059.

[29] Peters R., Frank M., Tiedemann W., Hoven I., Deja R., Kruse N., Fang Q., Blum L., and Peters R. 2021 Long-Term Experience with a 5/15kW-Class Reversible Solid Oxide Cell System *J. Electrochem. Soc.*, vol. 168, no. 1, p. 14508. https://doi.org/10.1149/1945-7111/abdc79.

[30] Hutty T.D., Dong S., and Brown S. 2020 Suitability of energy storage with reversible solid oxide cells for microgrid applications *Energy Conversion and Management*, vol. 226, p. 113499. https://doi.org/10.1016/j.enconman.2020.113499.

[31] Singer D.V. Reversible solid oxide cells for bidirectional energy conversion in spot electricity and fuel markets, 2017 Doctoral Thesis, Columbia University.

[32] Lamagna M., Ferrario A.M., Astiaso Garcia D., Mcphail S., and Comodi G. 2022 Reversible solid oxide cell coupled to an offshore wind turbine as a poly-generation energy system for auxiliary backup generation and hydrogen production *Energy Reports*, vol. 8, pp. 14259–14273. https://doi.org/10.1016/j.egyr.2022.10.355.

[33] Mottaghizadeh P., Fardadi M., Jabbari F., and Brouwer J. 2021 Dynamics and control of a thermally self-sustaining energy storage system using integrated solid oxide cells for an islanded building *International Journal of Hydrogen Energy*, vol. 46, no. 49, pp. 24891–24908. https://doi.org/10.1016/j.ijhydene.2021.03.136.

[34] Motylinski K., Kupecki J., Numan B., Hajimolana Y.S., and Venkataraman V. 2021 Dynamic modelling of reversible solid oxide cells for grid stabilization applications *Energy Conversion and Management*, vol. 228, p. 113674. https://doi.org/10.1016/j.enconman.2020.113674.

[35] Reznicek E.P. and Braun R.J. 2018 Techno-economic and off-design analysis of stand-alone, distributed-scale reversible solid oxide cell energy storage systems *Energy Conversion and Management*, vol. 175, pp. 263–277. https://doi.org/10.1016/j.enconman.2018.08.087.

[36] Reznicek E.P. and Braun R.J. 2020 Reversible solid oxide cell systems for integration with natural gas pipeline and carbon capture infrastructure for grid energy management *Applied Energy*, vol. 259, p. 114118. https://doi.org/10.1016/j.apenergy.2019.114118.

[37] Paczona D., Sejkora C., and Kienberger T. Reversible solid oxide cell systems as key elements of achieving flexibility in future energy systems, 2023. In *High-Temperature Electrolysis*, ed. Werner Sitte and Rotraut Merkle, 19-1-19-32: IOP Publishing. https://doi.org/10.1088/978-0-7503-3951-3ch19.

[38] Banasiak D., Gallaun M., Rinnhofer C., and Kienberger T. 2023 Integration of a rSOC-system to industrial processes *Energy Conversion and Management: X*, vol. 20, p. 100425. https://doi.org/10.1016/j.ecmx.2023.100425.

[39] Banasiak D. and Kienberger T. 2024 A comparative analysis of the economic feasibility of reversible hydrogen systems based on time-resolved operation optimisation *Applied Energy*, vol. 371, p. 123639. https://doi.org/10.1016/j.apenergy.2024.123639.

[40] Preininger M., Stoeckl B., Subotić V., and Hochenauer C. 2020 Characterization and performance study of commercially available solid oxide cell stacks for an autonomous system *Energy Conversion and Management*, vol. 203, p. 112215. https://doi.org/10.1016/j.enconman.2019.112215.

[41] Wendel C.H., Kazempoor P., and Braun R.J. 2015 Novel electrical energy storage system based on reversible solid oxide cells: System design and operating conditions *Journal of Power Sources*, vol. 276, pp. 133–144. https://doi.org/10.1016/j.jpowsour.2014.10.205.

[42] Goodwin D.G., Moffat H.K., Schoegl I., Speth R.L., and Weber B.W., *Cantera: An Object-oriented Software Toolkit for Chemical Kinetics, Thermodynamics, and Transport Processes:* Zenodo, 2023.

[43] Srikanth S., Heddrich M.P., Gupta S., and Friedrich K.A. 2018 Transient reversible solid oxide cell reactor operation – Experimentally validated modeling and analysis *Applied Energy*, vol. 232, pp. 473–488. https://doi.org/10.1016/j.apenergy.2018.09.186.

[44] Costamagna P., Selimovic A., Del Borghi M., and Agnew G. 2004 Electrochemical model of the integrated planar solid oxide fuel cell (IP-SOFC) *Chemical Engineering Journal*, vol. 102, no. 1, pp. 61–69. https://doi.org/10.1016/j.cej.2004.02.005.

[45] Kazempoor P. and Braun R.J. 2014 Model validation and performance analysis of regenerative solid oxide cells: Electrolytic operation *International Journal of Hydrogen Energy*, vol. 39, no. 6, pp. 2669–2684. https://doi.org/10.1016/j.ijhydene.2013.12.010.

[46] Yang C., Shu C., Miao H., Wang Z., Wu Y., Wang J., Zhao J., Wang F., Ye W., and Yuan J. 2019 Dynamic modelling and performance analysis of reversible solid oxide fuel cell with syngas *International Journal of Hydrogen Energy*, vol. 44, no. 12, pp. 6192–6211. https://doi.org/10.1016/j.ijhydene.2019.01.068.

[47] Du Y., Qin Y., Zhang G., Yin Y., Jiao K., and Du Q. 2019 Modelling of effect of pressure on co-electrolysis of water and carbon dioxide in solid oxide electrolysis cell *International Journal of Hydrogen Energy*, vol. 44, no. 7, pp. 3456–3469. https://doi.org/10.1016/j.ijhydene.2018.12.078.

[48] Wang Y., Banerjee A., Wehrle L., Shi Y., Brandon N., and Deutschmann O. 2019 Performance analysis of a reversible solid oxide cell system based on multi-scale hierarchical solid oxide cell modelling *Energy Conversion and Management*, vol. 196, pp. 484–496. https://doi.org/10.1016/j.enconman.2019.05.099.

[49] Saied M., Ahmed K., Nemat-Alla M., Ahmed M., and El-Sebaie M. 2018 Performance study of solid oxide fuel cell with various flow field designs: numerical study *International*

Journal of Hydrogen Energy, vol. 43, no. 45, pp. 20931–20946. https://doi.org/10.1016/j.ijhydene.2018.09.034.

[50] Zhang X., O'Brien J.E., O'Brien R.C., Hartvigsen J.J., Tao G., and Housley G.K. 2013 Improved durability of SOEC stacks for high temperature electrolysis *International Journal of Hydrogen Energy*, vol. 38, no. 1, pp. 20–28. https://doi.org/10.1016/j.ijhydene.2012.09.176.

[51] Königshofer B., Boškoski P., Nusev G., Koroschetz M., Hochfellner M., Schwaiger M., Juričić Đ., Hochenauer C., and Subotić V. 2021 Performance assessment and evaluation of SOC stacks designed for application in a reversible operated 150 kW rSOC power plant *Applied Energy*, vol. 283, p. 116372. https://doi.org/10.1016/j.apenergy.2020.116372.

[52] Subotić V., Harter P., Kusnezoff M., Napporn T.W., Schroettner H., and Hochenauer C. 2021 Identification of carbon deposition and its removal in solid oxide fuel cells by applying a non-conventional diagnostic tool *Sustainable Energy Fuels*, vol. 5, no. 7, pp. 2065–2076. https://doi.org/10.1039/D0SE01914C.

[53] Li H., Wei W., Zhang T., Liu F., Xu X., Li Z., and Liu Z. 2024 Degradation mechanisms and mitigation strategies of direct methane solid oxide fuel cells *Applied Energy*, vol. 359, p. 122609. https://doi.org/10.1016/j.apenergy.2023.122609.

[54] van Biert L., Visser K., and Aravind P.V. 2020 A comparison of steam reforming concepts in solid oxide fuel cell systems *Applied Energy*, vol. 264, p. 114748. https://doi.org/10.1016/j.apenergy.2020.114748.

[55] Ribeiro T.R., Ferreira Neto J.B., Takano C., Poço J., Kolbeinsen L., and Ringdalen E. 2021 C–O–H2 ternary diagram for evaluation of carbon activity in CH4-containing gas mixtures *Journal of Materials Research and Technology*, vol. 13, pp. 1576–1585. https://doi.org/10.1016/j.jmrt.2021.05.033.

[56] Schäfer F., Egger S., Steiner D., Carré M., and Eichel R.-A. 2022 Control of oxygen-to-carbon ratio and fuel utilization with regard to solid oxide fuel cell systems with anode exhaust gas recirculation: A review *Journal of Power Sources*, vol. 524, p. 231077. https://doi.org/10.1016/j.jpowsour.2022.231077.

[57] ©2002 - 2022 Dassault Systèmes, *Dymola: Multi-Engineering Modeling and Simulation based on Modelica and FMI* Modelica version 3.2.3: 3DS Dassault Systems. https://www.3ds.com/products-services/catia/products/dymola/ (accessed November 18, 2022).

[58] Alizadeh R., Allen J.K., and Mistree F. 2020 Managing computational complexity using surrogate models: a critical review *Res Eng Design*, vol. 31, no. 3, pp. 275–298. https://doi.org/10.1007/s00163-020-00336-7.

[59] Kudela J. and Matousek R. 2022 Recent advances and applications of surrogate models for finite element method computations: a review *Soft Comput*, vol. 26, no. 24, pp. 13709–13733. https://doi.org/10.1007/s00500-022-07362-8.

[60] Srikanth S., Heddrich M.P., Gupta S., and Friedrich K.A. 2018 Transient reversible solid oxide cell reactor operation – Experimentally validated modeling and analysis *Applied Energy*, vol. 232, pp. 473–488. https://doi.org/10.1016/j.apenergy.2018.09.186.

[61] Schefold J., Brisse A., Surrey A., and Walter C. 2020 80,000 current on/off cycles in a one year long steam electrolysis test with a solid oxide cell *International Journal of Hydrogen Energy*, vol. 45, no. 8, pp. 5143–5154. https://doi.org/10.1016/j.ijhydene.2019.05.124.

[62] Ishimoto Y., Voldsund M., Nekså P., Roussanaly S., Berstad D., and Gardarsdottir S.O. 2020 Large-scale production and transport of hydrogen from Norway to Europe and Japan: Value chain analysis and comparison of liquid hydrogen and ammonia as energy carriers *International Journal of Hydrogen Energy*, vol. 45, no. 58, pp. 32865–32883. https://doi.org/10.1016/j.ijhydene.2020.09.017.

[63] Di Micco S., Cigolotti V., Mastropasqua L., Brouwer J., and Minutillo M. 2024 Ammonia-powered ships: Concept design and feasibility assessment of powertrain systems for a sustainable approach in maritime industry *Energy Conversion and Management: X*, vol. 22, p. 100539. https://doi.org/10.1016/j.ecmx.2024.100539.

[64] Peschel A. 2020 Industrial Perspective on Hydrogen Purification, Compression, Storage, and Distribution *Fuel Cells*, vol. 20, no. 4, pp. 385–393. https://doi.org/10.1002/fuce.201900235.

[65] Niermann M., Beckendorff A., Kaltschmitt M., and Bonhoff K. 2019 Liquid Organic Hydrogen Carrier (LOHC) – Assessment based on chemical and economic properties *International Journal of Hydrogen Energy*, vol. 44, no. 13, pp. 6631–6654. https://doi.org/10.1016/j.ijhydene.2019.01.199.

[66] Sdanghi G., Maranzana G., Celzard A., and Fierro V. 2019 Review of the current technologies and performances of hydrogen compression for stationary and automotive applications *Renewable and Sustainable Energy Reviews*, vol. 102, pp. 150–170. https://doi.org/10.1016/j.rser.2018.11.028.

[67] Bell I.H., Wronski J., Quoilin S., and Lemort V. 2014 Pure and Pseudo-pure Fluid Thermophysical Property Evaluation and the Open-Source Thermophysical Property Library CoolProp *Industrial & engineering chemistry research*, vol. 53, no. 6, pp. 2498–2508. https://doi.org/10.1021/ie4033999.

[68] Linde AG Datasheet: Hydrogen technologies. The Ionic Compressor 90 MPa – IC90. 43486081 0614 – 1.0,5 – Subject to change. http://donar.messe.de/exhibitor/hannovermesse/2017/A488848/hydrogen-technologies-the-ionic-compressor-90-fo-eng-358503.pdf (accessed October 19, 2022).

[69] Aigner R. Internal Flow and Valve Dynamics in a Reciprocating Compressor164277, 2007 Dissertation, Technische Universität Wien.

[70] Li J.-Q., Li J.-C., Park K., Jang S.-J., and Kwon J.-T. 2021 An Analysis on the Compressed Hydrogen Storage System for the Fast-Filling Process of Hydrogen Gas at the Pressure of 82 MPa *Energies*, vol. 14, no. 9, p. 2635. https://doi.org/10.3390/en14092635.

[71] Zhang J., Fisher T.S., Ramachandran P.V., Gore J.P., and Mudawar I. 2005 A Review of Heat Transfer Issues in Hydrogen Storage Technologies *Journal of Heat Transfer*, vol. 127, no. 12, pp. 1391–1399. https://doi.org/10.1115/1.2098875.

[72] *Gurobi Optimization:* Gurobi Optimization, LLC, 2023. https://www.gurobi.com (accessed July 31, 2023).

[73] Papageorgiou M., Leibold M., and Buss M., *Optimierung.* Berlin, Heidelberg: Springer Berlin Heidelberg, 2012.

[74] Traupmann A.M. Advanced Modeling and Analysis of Electrical Grids for Multi-Energy System Approaches, 2023, Montanuniversität Leoben.

[75] Binderbauer P.J., *Ganymed: Application for Industrial Load Profile Simulation:* Montanuniversität Leoben. www.ganymed.ga.

[76] Binderbauer P.J., Kienberger T., and Staubmann T. 2022 Synthetic load profile generation for production chains in energy intensive industrial subsectors via a bottom-up approach *Journal of Cleaner Production*, vol. 331, p. 130024. https://doi.org/10.1016/j.jclepro.2021.130024.

[77] Böhm H., Zauner A., Rosenfeld D.C., and Tichler R. 2020 Projecting cost development for future large-scale power-to-gas implementations by scaling effects *Applied Energy*, vol. 264, p. 114780. https://doi.org/10.1016/j.apenergy.2020.114780.

[78] Integrierter österreichischer Netzinfrastrukturplan. Wien, 2024. www.bmk.gv.at/themen/energie/energieversorgung/netzinfrastrukturplan (accessed May 30, 2024).

[79] Lord A.S., Kobos P.H., and Borns D.J. 2014 Geologic storage of hydrogen: Scaling up to meet city transportation demands *International Journal of Hydrogen Energy*, vol. 39, no. 28, pp. 15570–15582. https://doi.org/10.1016/j.ijhydene.2014.07.121.

[80] Energieinfrastruktur 2040: Szenarien und Ausbaupläne für ein nachhaltiges Wirtschaftssystem in Österreich, 2023. https://www.klimafonds.gv.at/wp-content/uploads/sites/16/240131_InfraTrans2040_2023_korr1.pdf (accessed June 11, 2024).

[81] Traupmann A., Greiml M., Steinegger J., Kühberger L., and Kienberger T. 2023 Analysing sector coupling technologies for Re-purposing coal-fired power plants–Case study for the ENTSO-E grid *IET Energy Syst Integration*, vol. 5, no. 1, pp. 95–118. https://doi.org/10.1049/esi2.12087.

[82] Salim K.M.A., Maelah R., Hishamuddin H., Amir A.M., and Ab Rahman M.N. 2022 Two Decades of Life Cycle Sustainability Assessment of Solid Oxide Fuel Cells (SOFCs): A Review *Sustainability*, vol. 14, no. 19, p. 12380. https://doi.org/10.3390/su141912380.

[83] Gerloff N. 2021 Comparative Life-Cycle-Assessment analysis of three major water electrolysis technologies while applying various energy scenarios for a greener hydrogen production *Journal of Energy Storage*, vol. 43, p. 102759. https://doi.org/10.1016/j.est.2021.102759.

[84] Smith L., Ibn-Mohammed T., Yang F., Reaney I.M., Sinclair D.C., and Koh S.L. 2019 Comparative environmental profile assessments of commercial and novel material structures for solid oxide fuel cells *Applied Energy*, vol. 235, pp. 1300–1313. https://doi.org/10.1016/j.apenergy.2018.11.028.

[85] Mori M., Stropnik R., Sekavčnik M., and Lotrič A. 2021 Criticality and Life-Cycle Assessment of Materials Used in Fuel-Cell and Hydrogen Technologies *Sustainability*, vol. 13, no. 6, p. 3565. https://doi.org/10.3390/su13063565.

[86] Lundberg S. 2019_Lundberg_LCA_H2Production_FULLTEXT01.

[87] Hydrogen Europe Position Paper on PFAS: The importance of fluoropolymers across the hydrogen value chain, and impacts of the proposed PFAS restriction for the hydrogen sector. Avenue Marnix 23, Brussels, Belgium. https://hydrogeneurope.eu/wp-content/uploads/2023/02/Hydrogen-Europe-position-paper-on-PFAS-ban_v12_FINAL.pdf (accessed June 12, 2024).

[88] Paczona D. and Kienberger T., *Determining best values of operational parameters for reversible Solid Oxid Cell Systems.* EnInnov 2022, Session D3: Wasserstoff III: Chair of energy networking technology, Montanuniversität Leoben, 2022. https://www.tugraz.at/fileadmin/user_upload/tugrazExternal/738639ca-39a0-4129-b0f0-38b384c12b57/files/pr/Session_D3/434_PR_Paczona.pdf (accessed July 22, 2024).

[89] Banasiak D., Gallaun M., and Kienberger T., *Untersuchung der Kopplung eines rSOC-Systems zur Industrie.* IEWT 2023, Session Industrie II: Chair of energy networking technology, Montanuniversität Leoben, 2022. https://iewt2023.eeg.tuwien.ac.at/download/contribution/presentation/155/155_presentation_20230216_055533.pdf (accessed July 22, 2024).

[90] Banasiak D., *H2-Produktion und Flexibilität: Hochtemperatur-Brennstoffzellensystem.* Österreichischer Klimatag 2023: Chair of energy networking technology, Montanuniversität Leoben, 2023. https://ccca.ac.at/fileadmin/00_DokumenteHauptmenue/03_Aktivitaeten/Dialogveranstaltungen/OEsterreichischer_Klimatag/P06_Banasiak.pdf (accessed July 22, 2024).

[91] Banasiak D. and Kienberger T., *Reversible und räumlich getrennte Elektrolyse-Brennstoffzellensysteme im Energienetz mit erneuerbarer Erzeugung.* EnInnov 2024, Session D3: Elektrolyseure und Brennstoffzellen: Chair of energy networking technology, Montanuniversität Leoben, 2024. https://www.tugraz.at/fileadmin/user_upload/tugrazExternal/f560810f-089d-42d8-ae6d-8e82a8454ca9/files/pr/431_PR_Banasiak.pdf (accessed July 22, 2024).

PART II

RESEARCH OUTPUT

9 PEER-REVIEWED PUBLICATIONS

9.1 B1 Chapter in scientific book [37]

Paczona D., Sejkora C., and Kienberger T. Reversible solid oxide cell systems as key elements of achieving flexibility in future energy systems, 2023. In *High-Temperature Electrolysis*, ed. Werner Sitte and Rotraut Merkle, 19-1-19-32: IOP Publishing. https://doi.org/10.1088/978-0-7503-3951-3ch19.

Published: January 2023

Table A. 1: Author statement to first peer-reviewed publication (B1)

Activity	**Contribution authors (main author is mentioned first)**
Conceptualization	Banasiak D., Kienberger T.
Methodology	Banasiak D., Kienberger T.
Data Curation	Banasiak D., Kienberger T.
Software Development and Validation	Banasiak D., Kienberger T.
Modelling	Banasiak D., Sejkora C., Kienberger T.
Visualization	Banasiak D., Sejkora C., Kienberger T.
Writing (Original Draft)	Banasiak D., Kienberger T.
Writing (Review and Editing)	Banasiak D., Kienberger T.

9.2 P1 Journal article [38]

Banasiak D., Gallaun M., Rinnhofer C., and Kienberger T. 2023 Integration of a rSOC-system to industrial processes *Energy Conversion and Management: X*, vol. 20, p. 100425. https://doi.org/10.1016/j.ecmx.2023.100425.

Submitted: 03.05.2023

Published online: 28.07.2023

Table A. 2: Author statement to second peer-reviewed publication (P1)

Activity	**Contribution authors (main author is mentioned first)**
Conceptualization	Banasiak D., Kienberger T.
Methodology	Banasiak D.
Data Curation	Gallaun M., Christoph Rinnhofer
Software Development and Validation	Banasiak D.
Modelling	Banasiak D.
Visualization	Banasiak D., Gallaun M., Christoph Rinnhofer
Writing (Original Draft)	Banasiak D., Kienberger T.
Writing (Review and Editing)	Banasiak D., Kienberger T.

9.3 P2 Journal article [39]

Banasiak D. and Kienberger T. 2024 A comparative analysis of the economic feasibility of reversible hydrogen systems based on time-resolved operation optimisation *Applied Energy*, vol. 371, p. 123639. https://doi.org/10.1016/j.apenergy.2024.123639.

Submitted: 31.01.2024

Published online: 15.06.2024

Table A. 3: Author statement to third peer-reviewed publication (P2)

Activity	**Contribution authors (main author is mentioned first)**
Conceptualization	Banasiak D., Kienberger T.
Methodology	Banasiak D.
Data Curation	Banasiak D.
Software Development and Validation	Banasiak D.
Modelling	Banasiak D.
Visualization	Banasiak D.
Writing (Original Draft)	Banasiak D.
Writing (Review and Editing)	Banasiak D., Kienberger T.

IOP Publishing

High-Temperature Electrolysis
From fundamentals to applications
Werner Sitte and Rotraut Merkle

Chapter 19

Reversible solid oxide cell systems as key elements of achieving flexibility in future energy systems

David Paczona, Christoph Sejkora and Thomas Kienberger

The application of reversible solid oxide cell (rSOC) systems in energy infrastructure allows cells to be reversibly operated as fuel cells (FCs) or electrolysis cells (ECs). Different levels of energy system integration and flowsheet options are possible. This chapter first derives the need for such energy conversion units in future energy systems and extracts ideas for the systems' flowsheets from the literature. Second, the main part of this chapter focuses on the operational parameters' influence on system performance, which is discussed for a chosen set of system flowsheets and application scenarios. In this process, general insights into the behavior of the system are generated. Finally, the chapter concludes with design suggestions for different rSOC operations in future energy systems.

19.1 Introduction

To meet the United Nations 1.5 °C climate target [1], society has defined ambitious objectives all around the globe, aiming at significantly reducing human greenhouse gas (GHG) emissions. Today, around 77% of them are energy-related [2]. As a result, a massive transformation of global energy systems needs to be brought about in the upcoming centuries in order to reach net zero GHG emissions on time. Three general fields of action must therefore be applied worldwide:

i) First and foremost, switching from fossil-fuel-dominated energy supply systems to systems based on renewable energies (REs) is vital. Since the fossil share in the global energy supply is around 81% [3], this can only be accomplished by massive and quick action.
ii) Technologies for energy efficiency must be introduced at all stages of the entire energy conversion chain to reduce energy losses. Waste heat potentials must be used to supply low-temperature demands.

doi:10.1088/978-0-7503-3951-3ch19

iii) The behavior of energy-consuming services, especially in the Organisation for Economic Co-operation and Development (OECD) member countries, must change to a more sparing and considered use.

Taking up these actions, the European Union's (EU's) 'Green Deal' [4], for instance, strives for net zero emissions by 2050. The intermediate target for 2030 aims to reduce EU greenhouse gas emissions by 55% compared to their 1990 levels. This should be achieved by reducing the European gross domestic consumption by 36%–39% through efficiency measures and by expanding REs to 40% to supply it [5].

Most of the REs to be exploited are hydro, wind, and photovoltaic (PV) potentials, which will lead to volatility in electricity generation; balancing demand and generation with appropriate flexibility and storage technology will become crucial. Multi-energy systems [6] (MESs), which connect various economic sectors (electricity, gas, heat transport, etc.) via grid-connected energy carriers, allow for both. Interlinking volatile electricity production with the gas sector or the heat sector, for instance, enables long-term storage [7] or mitigates the strain imposed on electricity grids by PV or wind power [8]. MESs may also be beneficial in terms of energy efficiency. They enable highly efficient technologies to be used for both the final energy applications (heat pumps, battery electric vehicles (BEVs), etc.) and the energy-sector conversion units (combined heat and power (CHP) units, power-to-X units, industrial waste heat use, etc). Figure 19.1 shows the general structure of MESs.

Both RE expansion and energy efficiency enhancement require proper energy strategies and coordinated, concerted energy policies to reach net zero emissions. On the level of implementation-oriented, time-phased actions, such plans are widely missing. Scenario-based MES studies may help us to deeply understand the interdependencies of energy systems and therefore foster their development [9].

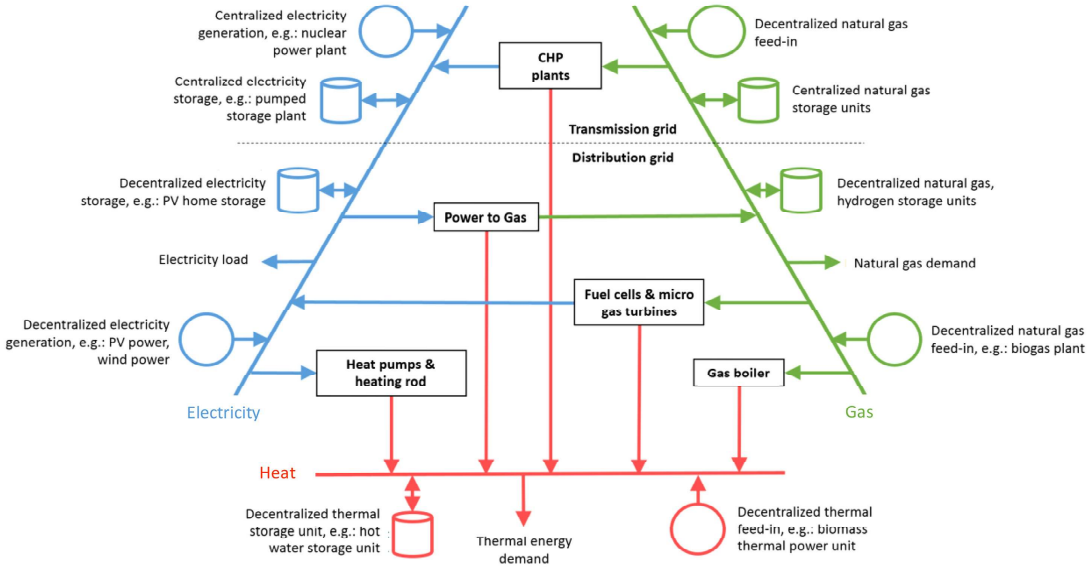

Figure 19.1. General structure of multi-energy systems (MES).

The authors of this work [10, 11] performed such investigations for Austria, an EU member state. Austria wants to reach net zero emissions by 2040 [12]—ten years ahead of the European Union. A quantum leap in this regard would be to achieve a decarbonized electricity system (on annual balance) by 2030 [13]. However, it is also true that no concrete action plans for Austria exist today. To facilitate policymakers in the process of identifying appropriate actions, the authors developed an exergy-based MES optimization methodology that minimizes the exegetic cost of supporting energy services for a given RE expansion. Exergy is the actual working capacity of any form of energy. Mechanical work and electricity are pure exergy. Chemical energy can be considered as 100% exergy. The exergy content of heat depends, according to Carnot's rule, on its temperature relative to the ambient temperature (see equation (19.7)). While energy is always conserved throughout all energy conversion processes (the first law of thermodynamics), exergy losses always occur whenever processes are irreversible (the second law of thermodynamics). In this sense, minimizing exegetic costs allows both the thermodynamic minimum energy demand of an energy system as well as the systemic location of system inefficiencies to be found. This approach uses data with high temporal resolution for both supply and demand. This enables us to show how future energy systems with high proportions of volatile REs can be fundamentally designed while considering an optimal technology mix that enables both energy efficiency and energy system flexibility.

For this calculation, the useful energy demands (space heating, process heat, light, mechanical work, etc) required to provide the energy services (space or process heat services, mobility services, lighting services, etc.) are first converted into useful exergy demands. Therefore, we apply exergy factors describing the thermodynamic energy quality required for the services [10]. Second, for REs, an analogous approach is taken: primary energies such as wind, PV, or biomass are considered to be exergy. For waste heat, we use corresponding temperature-dependent exergy factors. The subsequent minimization of exergy losses combines energy-efficient final energy application technologies with conversion and storage technologies in an optimal way to keep the exergy-related imports (in the case under consideration, electricity and gas imports) as low as possible (see equation (19.1)). In this case, we minimize the primary energy demand of the system under consideration.

$$\min\left(Ex_{\mathrm{Loss,tot}}\right) = Ex_{\mathrm{Sup,tot}} - Ex_{\mathrm{UED,tot}} = \sum_i Ex_{\mathrm{RES},i} + \left(\sum_j Ex_{\mathrm{Imp},j} - \sum_k Ex_{\mathrm{Exp},k}\right) - Ex_{\mathrm{UED,tot}} \tag{19.1}$$

$Ex_{\mathrm{Loss,tot}}$ The total exergy losses caused by both energy conversion and final energy applications
$Ex_{\mathrm{Sup,tot}}$ The total exergy used to supply the considered energy system
$Ex_{\mathrm{UED,tot}}$ The total useful exergy demand of all energy services to be covered
$Ex_{\mathrm{RES},i}$ RE generation of resource i

$Ex_{\mathrm{Imp},j}$ The exergy import of energy carrier j
$Ex_{\mathrm{Exp},k}$ The exergy export of energy carrier k

Figure 19.2 shows the results obtained by applying this exergy-based approach to a possible RE expansion in Austria for the year 2040. Using these results, the RE

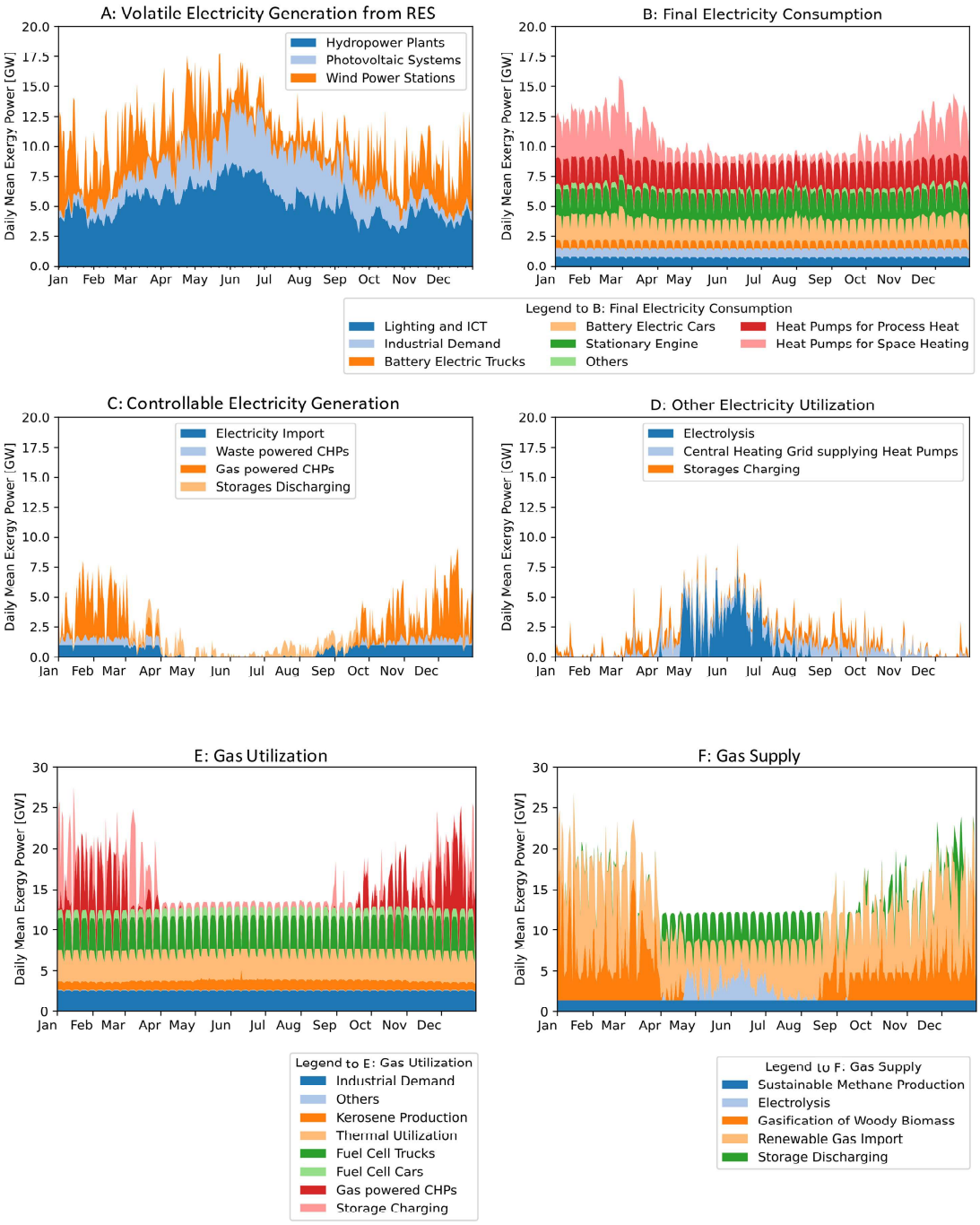

Figure 19.2. Exergy-optimized electricity system for 2040. (a) electricity generated by REs, (b) final electricity consumption, (c) deployment of undercoverages in the electrical energy system, (d) utilization of overcoverages in the electrical energy system, (e) final gas consumption, and (f) gas supply.

expansion target required to reach a decarbonized electricity system (on annual balance) in 2030 is linearly extrapolated. The useful exergy demand for 2040 is based upon the 2019 demand, adjusted by annual economic growth [14] and a decreased energy intensity within all sectors [15]. Figure 19.2(a) shows the expected seasonal effects, especially those due to PV and hydropower-based electricity generation. Panel (b) shows the final electricity consumption. Compared to today's figures, the exergy-optimized approach results in significant additional electricity demand, especially from BEVs and heat pumps used to supply both process heat and space heating. The latter naturally causes increased demand in the winter months, which results in an undercoverage of national REs (panel c). In the exergy-optimized case, national CHP units address this. They additionally provide waste heat that meets the space heat demand. In the summer months, RE overcoverage arises. This is used to operate electrolyzers and, to a minor extent, for pumped storage and process heat pumps (panel d). Due to the interaction between the electricity system and the gas system, there is a seasonal gas demand created by the CHP units (panels c and e). In addition, gas is used in an exergy-optimized system, in particular to supply high-temperature applications in industry and for various mobility needs in heavy transport (panel e). Those demands have a baseload character. Industrial waste heat and waste heat from CHP units reduce the primary energy demand for space heating in winter. Overall, optimizing exergy efficiency for final energy application and energy conversion and storage units can reduce primary energy use from about 400 TWh/a to about 240 TWh/a. Despite all this, imports, especially renewable gases, are to be expected in the future (panel f).

The results for Austria may be qualitatively valid for the future energy systems of other central European countries. Their RE-potential structures, as well as the structures of their energy service demands, are similar. In such modern energy systems with high proportions of REs, the application of both FCs and electrolysis is beneficial. Reversible FC systems and, in particular, rSOC systems combine their energy system advantages. For their future application, we can take away the following messages from the investigations shown above:

As a **conversion technology in the energy sector**, a possible rSOC application is first and foremost strongly influenced by the seasonal balance of RE generation and demand:

- FC operation is used to generate electricity mainly during the winter season. The high electric efficiency of the FC operational mode, compared to that of a classic combined cycle gas turbine (CCGT) power plant, is beneficial in this regard.
- EC operation is used to produce hydrogen during the summer season, using electricity from RE overcoverage. The hydrogen thus produced reduces renewable gas imports.

In an energy-sector application, an rSOC system must address rapid changes of load, but not fast switching between the electrolysis and FC operational modes. The combined-operation fuel–electrolysis cell allows for a large number of full-load hours (>5000 h/year), which improves the economics. Selling the rSOC's waste heat

to cover space heat demands at temperature levels below 100 °C can lead to further economic gains. This would mainly, but not exclusively, occur during winter time.

As a **conversion technology in the industrial sector**, a possible rSOC application is strongly influenced by the industrial baseload demands for electricity and gas as well by price signals in the electricity markets:

- FC operation generates electricity mainly during times of high electricity prices, or during times when energy system support measures (e.g. in the form of positive secondary control capacity) are needed.
- EC operation produces hydrogen during times of low electricity prices or during times when energy system support measures (e.g. in the form of negative secondary control capacity) are needed.

In an industry-sector application, an rSOC system also faces fast load changes, switching between the electrolysis and FC operational modes. The combined-operation fuel–electrolysis cell, together with the baseload demands of the industry, allows for an even higher number of full-load hours (>7000 h/year), compared to the energy-sector application. The rSOC's waste heat can supply process heat demands at temperature levels above 200 °C (e.g. process steam), reducing the gas demand on-site.

19.2 The state of research into rSOC systems

Reversible systems based on solid oxide cells (i.e. rSOCs) that can operate in FC mode and electrolysis mode have already been the subject of several investigations. Various ideas have been proposed for the system configuration. This subsection attempts to categorize current developments.

Pure hydrogen and mixtures with methane, carbon monoxide, and carbon dioxide have been investigated for use as fuels in FC operation mode. The oxidant can be pure oxygen (from storage vessels) or ambient air. In the electrolysis mode of operation, pure steam and mixtures with carbon dioxide are possible supply gases on the fuel side. Depending on the fuel composition, the system can either be open [16] (e.g. methane from the grid and ambient air), half open [17–24] (e.g. hydrogen from storage and ambient air), or closed [25–27] (e.g. hydrogen and oxygen storage). The layouts in figure 19.3, which will be further discussed, are of the half-open type, applying stored hydrogen and ambient air.

In many publications about half-open systems, the thermal management of the stack is ensured by the regulation of air temperature and air mass flow. Thermoneutral operation in the electrolysis mode and air cooling in the FC operational mode has been considered by others [21–24]. Different approaches have been followed by considering cooling by diathermic oils [25, 26], thermal integration of methanization reactors [27] and metal hydride storage systems [18].

Most flowsheets in the literature include a recirculation path for the fuel. This can be done in different ways, as shown in figure 19.3. The hot exhaust fuel of the stack is mixed with either the cold [16] (A2) or hot fuel (A1), which is called 'hot gas recirculation' (hgr) throughout this chapter [19]. A different option is 'cold gas recirculation' (cgr), in which cooled exhaust fuel is mixed with the cold fuel (after

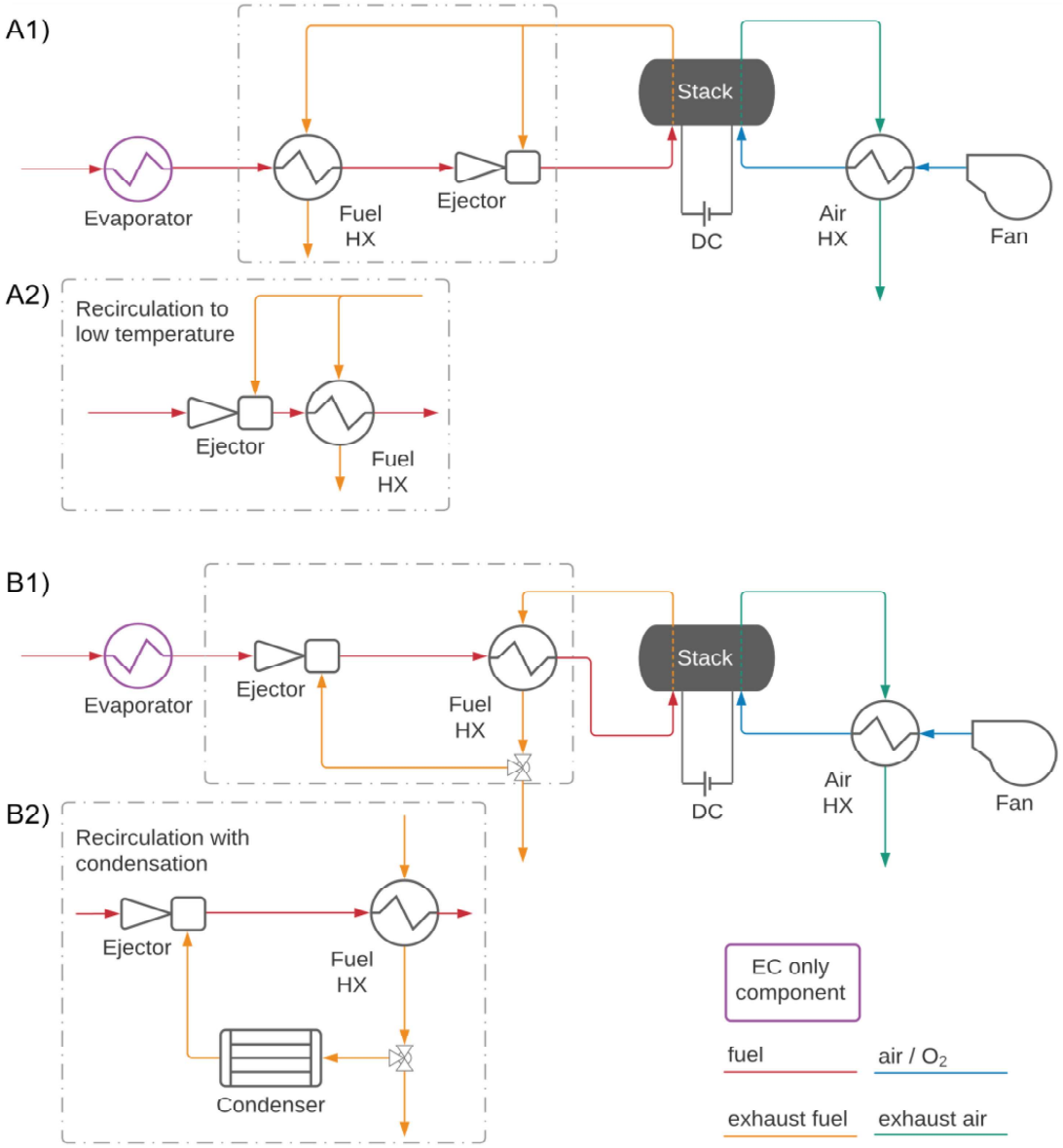

Figure 19.3. System layout ideas described in the literature: (A1) hot gas recirculation to cold (hgr), (A2) hot gas recirculation to the hot side of the fuel heat exchanger (HX), (B1) cold gas recirculation (cgr), (B2) cgr with condensation (cgr-cond).

passing through an evaporator) [19] (B1), which can be modified by adding a condenser (cgr-cond) of the recirculated stream [17, 19, 25, 26] (figure 19.3 B2). In the case of systems that operate with a synthesis gas mixture, which flows through the stack from one storage vessel to another, no circulation is used on the fuel side [27]. In this system, recirculation on the air side has been proposed by some studies [21–24, 27].

Commercial rSOC systems are already offered by SunFire [28], but little knowledge about their system layouts is publicly available. These systems are designed for applications in the energy, industry, and building sectors. In the latter two fields,

thermal coupling to heat sources and consumers is proposed to achieve high system efficiencies.

The abovementioned flowsheets have been investigated by research groups in different ways. Frank *et al* [17] studied how the system performance was influenced by changes of the recirculation rate at fixed values of the stack fuel utilization. In the research performed by Giap *et al* [19], the influence of the fuel's hydrogen concentration on efficiency was studied. These investigations are helpful in understanding the system behavior.

However, when talking about rSOC systems, it is more helpful to think in terms of system parameters. Low stack fuel utilization, a parameter which is often used in the literature, does not mean that a system with recirculation also has low fuel utilization. The difference in the definitions of fuel utilization at the stack and system levels can be seen from equations (19.2) and (19.3). Similarly, it is not easy to draw conclusions about the system from the effect of hydrogen concentration in the stack.

$$fu_{\text{stack}} = 1 - \frac{\dot{m}_{\text{fuel,stackout}} \cdot y_{H_2,\text{fuel,stackout}}}{\dot{m}_{\text{fuel,stackin}} \cdot y_{H_2,\text{fuel,stackin}}} \tag{19.2}$$

$$fu = 1 - \frac{\dot{m}_{\text{exhaustfuel}} \cdot y_{H_2,\text{exhaustfuel}}}{\dot{m}_{\text{fuel}} \cdot y_{H_2,\text{fuel}}} \tag{19.3}$$

So far, the literature has yielded little insight into the combined effects of parameter variations and their consequences for system design. The approach described in this chapter starts from the assumption that it is not enough to vary one parameter to investigate the effect on the system performance. Parameters should be varied across the whole multidimensional space in order to study combined effects and get deeper insights into system behavior. Instead of going into the details of possible changes in the configuration of one specific system layout, the influence of operational parameters should be investigated for a selection of different flowsheets, as displayed in figure 19.3. These configurations cover the core concepts of rSOC systems that include recirculation. The non-recirculation case can be seen as the limit with a zero recirculation rate. The performance dependence on operational parameters is studied for different operational modes and flowsheets. In this way one can learn about the preferred setup for round-trip operation and system limitations. The main outcomes of the investigations presented in this chapter are:

I) Understanding the combined influence of operational parameters on the system performance
II) Determination of the best operating points for the best system performance in different operational modes
III) Quantification of efficiency-increasing measures for different system flowsheets
IV) Determination of the best system flowsheets, for the use cases of the energy sector and the industry sector, to meet the demand for flexibility with the best system performance

19.3 Methodology

This section describes the steps and methods used to produce the results of section 19.4. First, the method used to choose the exemplary layouts for further investigations is described. This is followed by an explanation of the modeling approach. A description of the ideas used to progress from the analysis of individual operational modes to round-trip operation concludes this section.

19.3.1 Choice of system layouts

The system flowsheet used for further investigation was chosen in accordance with the basic concepts described in the literature (figure 19.3). These flowsheets are of the half-open type (i.e. hydrogen is stored in a vessel and ambient air acts as oxidant). The basic concepts are extended to include all the necessary components, as can be seen in figure 19.4. As before, these flowsheets can be divided into:

- Hot gas recirculation (hgr)
- Cold gas recirculation (cgr)
- Cold gas recirculation with condensation (cgr-cond)

Reversible solid oxide cell (SOC) systems can operate in two different modes:

- **The FC mode of operation:** the stack produces electricity from the reaction of hydrogen and oxygen to produce water. The fuel entering the system is pure

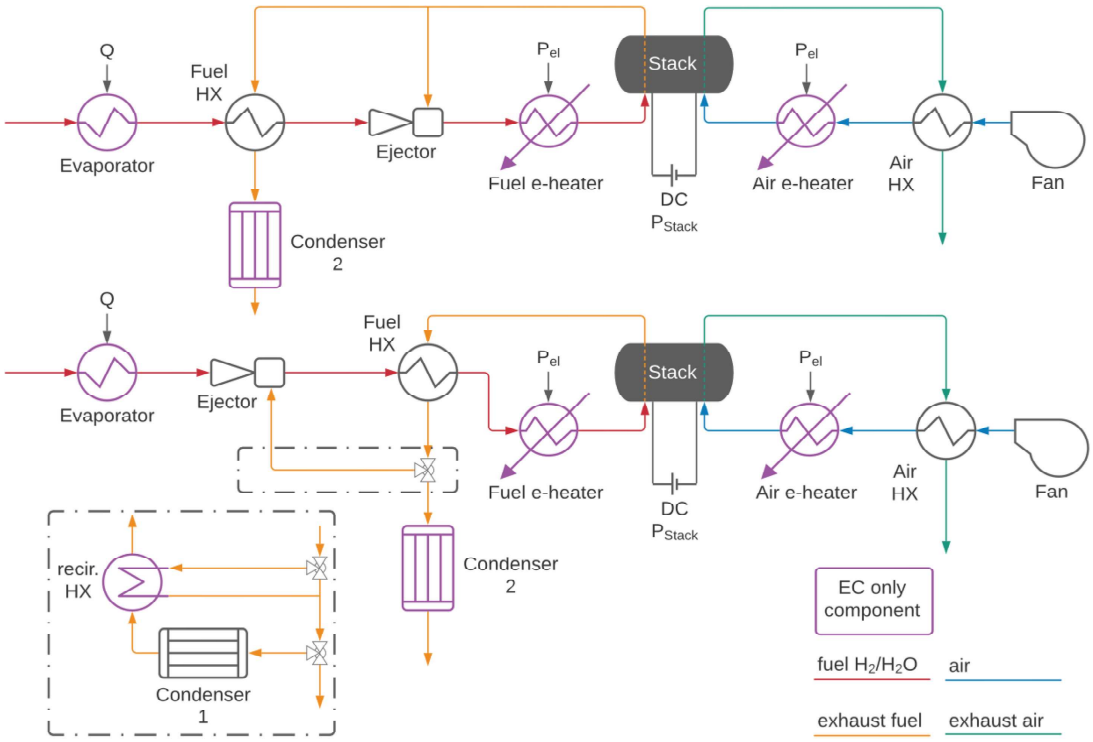

Figure 19.4. Extended system layout ideas: (A) hot gas recirculation (hgr) to the cold side of the fuel HX, (B1) cold gas recirculation (cgr), (B2) cgr with condensation in the cold gas recirculation (cgr-cond) path (Condenser 1) and a recirculation reheater after the condenser (recir. HX).

hydrogen, which is mixed with the recirculated exhaust fuel (which contains steam) before it enters the stack. Cooling of the stack is ensured by control of the air mass flow.

- **The EC mode of operation:** the stack consumes electricity for the water reaction, which produces hydrogen and oxygen. The fuel is pure water, which is mixed with the recirculated exhaust fuel (which contains hydrogen) before it enters the stack. The stack is operated below the thermoneutral voltage. For thermally stable operation, heating is required, which is ensured by electric heaters in the fuel (the fuel e-heater) and air streams (the air e-heater).

For the application of the system, two scenarios were chosen:

- **Energy-sector scenario (E):** no thermal interaction with other processes is considered. The rSOC waste heat, which may be used in other applications, does not influence the efficiency of the rSOC system and no industrial waste heat is available for integration. This reflects the possible real application of the system in the energy sector, in which no other facilities might be located nearby.
- **Industry-sector scenario (I):** in the FC operational mode, the system can provide generated waste heat to industrial consumers. Industrial waste heat sources are used for the evaporation of water in the electrolysis operational mode.

In the following paragraphs, the flowsheets of the rSOC systems capable of the two operational modes and ready for both application scenarios are separately described for hot and cold gas recirculation.

19.3.1.1 Hot gas recirculation

In systems that use hot gas recirculation (see figure 19.3(A1)), the exhaust fuel stream is recirculated before being cooled by the fuel heat exchanger (HX). The fuel HX only needs to handle the mass flow entering the stack, and an increased recirculation rate does not require a bigger heat exchanger area. This configuration means that the ejector is at almost the same temperature as the stack, which excludes the use of other components, such as mechanical fans, for recirculation. The best point at which to include the recirculated exhaust fuel is after the fuel heat exchanger, so that gases of similar temperatures are mixed. In figure 19.3(A2), we can see that systems have been proposed which recirculate the hot exhaust fuel to the cold incoming fuel. This is disadvantageous for two reasons. First, the ejector is operated with a big temperature difference, which causes thermal stress. Second, the recirculation increases the temperature of the fuel entering the fuel HX. This means that less of the heat can be recovered here and that the exhaust fuel entering Condenser 2 has higher temperatures. For these reasons we do not treat this recirculation option in the studies shown here.

19.3.1.2 Cold gas recirculation

Systems that use cold gas recirculation (see figure 19.3(B1)) employ an ejector to recirculate the cooled exhaust fuel after the fuel HX and mix it with the cold fuel

after the evaporator. In this configuration, fewer components are operated at high temperatures, but the mass flow through the fuel HX increases with higher recirculation rates, which inflicts higher requirements on this component. The cold gas recirculation can be modified by adding a condenser downstream from the recirculation (see figure 19.3(B2)), which lowers the temperature to less than the condensation point of water and separates the condensed water from the gas stream. Since even lower temperatures occur in this case, a fan can be used instead of an ejector. In the FC operational mode, the cooling in this condenser (Condenser 1) helps to cool the stack and consequently less airflow is needed. However, in the electrolysis operational mode, a loss of heat is disadvantageous. A simple additional heat exchanger in the recirculation that recovers heat from the exhaust fuel can compensate this heat loss, as also shown in the detail in figure 19.4. In the FC mode, the condenser has another very important advantage. Because it lowers the steam content, the hydrogen concentration in the fuel is less affected by the recirculation, and very high fuel utilization rates are possible at the system level .

Basically, to increase the fuel utilization in the FC mode, it would be possible to include a condenser in the high-temperature recirculation. To ensure permissible temperature differences between the gas entering the stack and the stack itself, it would be necessary to monitor the fuel temperature at the stack entry. Consequently, the recirculation flow could not be higher than just a fraction of the feed fuel flow. Overall, this flowsheet creates additional hurdles for system control without promising benefits. Therefore, it will not be discussed further.

19.3.2 Modeling

Thermodynamic zero-dimensional, time-resolved, steady-state models of the different rSOC system flowsheets according to figure 19.4 were set up in the software from Dassault Systèmes, Dymola. The model of the stack was provided by AVL List GmbH and is a virtual representation of a solid oxide cell stack from Fraunhofer IKTS. The important input and output variables of this model are summarized in table 19.1.

Table 19.1. Stack model: inputs and outputs.

Inputs	Outputs
Electric current	Electric voltage
	Electric power
	Stack temperature
Fuel composition	Exhaust fuel composition
Fuel temperature	Exhaust fuel temperature
Fuel mass flow	Exhaust fuel mass flow
Air composition	Exhaust air composition
Air temperature	Exhaust air temperature
Air mass flow	Exhaust air mass flow

In the simulations of all the other components, the Dymola-compatible Modelica library 'MixtureGasNasa' for media is used to determine the fluid properties. The approach used to model these components is described in the following paragraphs. A summary of the important parameters that must be set up in the calculation is given in table 19.2.

The heat exchangers (fuel HX, air HX, recirculation HX) are chosen to operate in counterflow, and they are modeled as 0D objects that exchange heat between two non-phase-changing fluids. The heat exchange is limited by the minimum set temperature difference at the pinch point (ΔT_{Pinch}) and the maximum transferable heat is given by the medium with the lower heat capacity flow. Given two of the four temperatures (those of the inputs and outputs) and the two gas compositions, the missing temperatures can be calculated. Additionally, the heat exchanger constant, which combines the area and the transfer coefficient, is calculated as a design dimension. In the off-design calculation, this constant can be set and ΔT_{Pinch} calculated for this specific design.

In the evaporator model (see figure 19.3), the incoming fluid is heated to more than the boiling point of water at a pressure of 1 bar. The superheating temperature must be specified. The energy required for this change is calculated in terms of sensible and latent heat.

The condenser model (used for Condenser 1 and Condenser 2) cools down the incoming fluid to below the boiling point of water. The subcooling value (ΔT_{SC}) must be set. The heat released in the process is then calculated by considering the sensible and latent contributions. The latent heat released is calculated by the condensation heat of the condensed share of the steam. The steam content leaving the condenser is determined using the saturation pressure of water at the subcooled temperature. A condensation efficiency of 95% is used and this share of the maximum condensable amount is liquified and drained in the component.

Table 19.2. Overview of the component and system parameters in the rSOC system model.

Component	Parameters
Heat exchanger	Pinch-point temperature difference or heat exchanger constant
Evaporator	Superheating temperature difference
Condenser	Subcooling temperature difference and efficiency
Electric heater	In electrolysis operational mode only: outlet temperature
Fan	Pressure rise, efficiency
Ejector	–
System parameter	**Description**
Electric current	Operational current of the stack
Stack temperature	Temperature that the stack shall operate at
Fuel composition	Mass fraction of species in fuel
Air composition	Mass fraction of species in air
Recirculation rate	Ratio of fuel volume flow and recirculated exhaust fuel flow
Fuel utilization	System fuel utilization as defined in equation (19.3)
Air mass flow	Set in electrolysis mode, controlled in FC mode

In EC mode, the electric heaters provide the stack with thermal energy. They heat the incoming fluid to a temperature above the desired operational temperature of the stack. This temperature difference is calculated such that the desired stack temperature is reached. The energy required to heat the fluid is calculated from the sensible heat difference.

The energy consumption of the fan on the air side is calculated from the volume flow, the pressure rise, and the efficiency, as can be seen in equation (19.4).

$$P_{\text{fan}} = \dot{V} \cdot \Delta p \cdot \eta \tag{19.4}$$

The ejector is assumed to provide the desired pressure drop in the recirculation for the set recirculation flow rate. This assumption is made so that component limitations, which are not physical limitations and that could be overcome by clever design, do not impair the theoretically best possible system efficiencies. The recirculation rate is calculated as defined in equation (19.5).

$$rr = \frac{\dot{V}_{\text{recirculation}}}{\dot{V}_{\text{fuel}}} \tag{19.5}$$

During the operation of the system, some parameters are controlled in order to operate in steady-state conditions. The control strategies and parameters depend on the operation, which can be FC mode or EC mode, as described below.

In the FC operational mode, the heat produced by the stack must be discharged. This can be achieved by varying the air mass flow. The lower limit for the air mass flow is given by the minimum oxygen stream that is required for the reaction in the stack. This minimum mass flow can be calculated from the set air composition and the set electric current. The air excess (λ) is defined in equation (19.6) as the ratio of the oxygen mass flow of the air stream and the reaction mass flow.

$$\lambda = \frac{\dot{m}_{\text{air}} \cdot y_{\text{air, } O_2}}{\dot{m}_{O_2,\text{ reaction}}} \tag{19.6}$$

The EC mode consumes heat, and λ can be set almost freely in this case. As the flow is lowered the oxygen concentration on the air side of the stack increases, which reduces the efficiency. This is not a hard limit, but another limitation is that the heating of the stack is ensured by the sensible heat of the air stream. The temperature difference at the stack is limited to around 100 °C. This means that below certain air flow rates, the desired stack temperature cannot be maintained. In EC operation, an air mass flow is set that obeys these limitations.

In the system simulation, in addition to all the state variables of the fluids leaving and entering components, the important outputs summarized in table 19.3 are calculated.

$$\text{Exergy} = \text{Heat} \cdot \left(1 - \frac{T_{\text{ambient}}}{T_{\text{stream, hot}}}\right) \tag{19.7}$$

The system efficiency can be calculated in different ways, which reflect the different application scenarios (i.e. the energy and industry sectors) of the system. In

Table 19.3. System outputs in the rSOC system model.

Output	Calculation
Electric power	Stack model output
Electric heater power consumption	Electric heater model
Fan power consumption	Fan model
Fuel power content	Hydrogen flow of the fuel stream (FC) or exhaust fuel stream (EC) multiplied by the lower heating value (LHV) of hydrogen (LHV_{H2} = 33.3 kWh kg^{-1})
Condenser heat release	Condenser model
Evaporator required heat	Evaporator model
Exhaust fuel heat	Calculated using the enthalpic difference from a gas at ambient temperature using the 'MixtureGasNasa' library of Modelica
Exhaust air heat	Calculated using the enthalpic difference from a gas at ambient temperature using the 'MixtureGasNasa' library of Modelica
Condenser exergy release	Calculated from equation (19.7) using the condenser heat and the boiling temperature of water
Evaporator required exergy	Calculated from equation (19.7) using the evaporation heat and the boiling temperature of water
Exhaust fuel exergy	Calculated from equation (19.7) using the exhaust fuel heat and the exhaust gas temperature
Exhaust air exergy	Calculated from equation (19.7) using the exhaust air heat and the exhaust gas temperature

both scenarios, it is possible to operate the rSOC system in EC mode and FC mode. The different ways of defining the efficiency for both operational modes and application scenarios can be seen in equations (19.8)–(19.11).

Energy-sector:

$$\eta_{E,\,\mathrm{EC}} = \frac{P_{\mathrm{fuel}}}{P_{\mathrm{Stack}} + P_{\mathrm{fan}} + P_{\mathrm{e-heater}} + Q_{\mathrm{evaporator}}} \tag{19.8}$$

$$\eta_{E,\,\mathrm{FC}} = \frac{P_{\mathrm{Stack}}}{P_{\mathrm{Fuel}} + P_{\mathrm{fan}}} \tag{19.9}$$

Industry-sector:

$$\eta_{I,\,\mathrm{EC}} = \frac{P_{fuel}}{P_{\mathrm{Stack}} + P_{\mathrm{fan}} + P_{\mathrm{e-heater}} + Ex_{\mathrm{evaporator}}} \tag{19.10}$$

$$\eta_{I,\,\mathrm{FC}} = \frac{P_{\mathrm{Stack}} + Ex_{\mathrm{air}} + Ex_{\mathrm{fuel}} + Ex_{\mathrm{Condenser1}}}{P_{\mathrm{Fuel}} + P_{\mathrm{fan}}} \tag{19.11}$$

19.3.3 Round-trip operation of an rSOC system

The idea behind an rSOC system is to run the same system in both operational modes. This round-trip operation requires the air FX and the fuel HX (see figure 19.4) to be designed for this purpose. The changed system design modifies the maximum efficiencies for both operations, compared to a single mode of operation (either EC or FC). The basic idea behind examining the round-trip operation is that the amount of hydrogen produced during electrolysis is the same as that consumed in the FC operational mode, as indicated in figure 19.5.

For this purpose, the heat exchanger constant of both HXs is determined in the respective critical operation mode by setting the pinch-point temperature difference to 5 °C in all cases except for the air HX in FC mode, for which 90 °C was used. In the FC mode, the reaction in the stack reduces the mass flow on the side of the air HX. This means that the air cannot be fully preheated to the stack exhaust temperature, because the heat capacity of the flow of air entering the system is higher than that of the exhaust air leaving the stack. The stack limitations for temperature differences must be fulfilled in any case. With this limitation it turns out that at all calculated points, the air HX in the FC operational mode has a higher exchanger constant than in the EC mode, even though a pinch-point temperature difference of 90 °C is used. Therefore, its geometry is determined for the best operational point in FC mode. Similarly, due to the increase in fuel flow in EC mode, the fuel HX is defined for the best operational point in EC mode. In the FC mode, the requirements for this heat exchange are much lower.

To obtain the round-trip efficiency, the energy content of the fuel (P_{fuel}) in equations (19.9) and (19.11) must be divided by the efficiency in the corresponding EC mode (equations (19.8) and (19.10)). This results in equations (19.12) and (19.13). It can also be interpreted in such a way that the fuel's energy content is replaced by the energy demand of the electrolysis scaled by the ratio of produced versus consumed fuel.

Energy sector round−trip

$$\eta_{E,\mathrm{RT}} = \frac{P_{\mathrm{Stack,FC}}}{\left(P_{\mathrm{Stack,EC}} + P_{\mathrm{fan,EC}} + P_{\mathrm{e-heater,EC}} + Q_{\mathrm{evaporator,EC}}\right)\cdot P_{\mathrm{fuel,FC}} / P_{\mathrm{fuel,EC}} + P_{\mathrm{fan,FC}}} \tag{19.12}$$

$$= \eta_{E,\mathrm{EC}} \cdot \frac{P_{\mathrm{Stack,FC}}}{P_{\mathrm{fuel,FC}} + \eta_{E,\mathrm{EC}} \cdot P_{\mathrm{fan,FC}}}$$

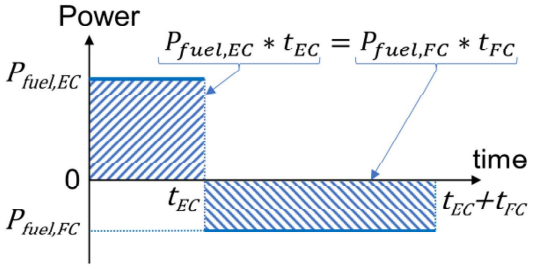

Figure 19.5. Full operating cycle of a reversible system that produces as much hydrogen in electrolysis as it uses in the FC operational mode.

Industry sector round−trip

$$\eta_{I,\mathrm{RT}} = \frac{P_{\mathrm{Stack,FC}} + Ex_{\mathrm{air,FC}} + Ex_{\mathrm{fuel,FC}} + Ex_{\mathrm{Condenser1,FC}}}{\left(P_{\mathrm{Stack,EC}} + P_{\mathrm{fan,EC}} + P_{\mathrm{e-heater,EC}} + Ex_{\mathrm{evaporator,EC}}\right)\cdot P_{\mathrm{fuel,FC}} / P_{\mathrm{fuel,EC}} + P_{\mathrm{fan,FC}}} \quad (19.13)$$

$$= \eta_{I,\mathrm{EC}} \cdot \frac{P_{\mathrm{Stack,FC}} + Ex_{\mathrm{air,FC}} + Ex_{\mathrm{fuel,FC}} + Ex_{\mathrm{Condenser1,FC}}}{P_{\mathrm{fuel,FC}} + \eta_{I,\mathrm{EC}} \cdot P_{\mathrm{fan,FC}}}$$

In these equations, we can see that the common way of calculating the round-trip efficiency (equation (19.14)) is only valid if either η_{EC} is equal to one or if $P_{\mathrm{fan,FC}}$ equals zero, which is a good approximation in all cases in which the product of η_{EC} and $P_{\mathrm{fan,FC}}$ is small compared to $P_{\mathrm{fuel,FC}}$.

$$\eta_{\mathrm{RT,\,approx}} = \eta_{\mathrm{EC}} \cdot \eta_{\mathrm{EC}} \quad (19.14)$$

The round-trip efficiency calculated in this approximative way is smaller than in the precise calculation, since $P_{\mathrm{fan,FC}}$ in the calculation of η_{FC} is not scaled by the electrolysis efficiency η_{EC} (compare the denominator of equations (19.9) and (19.11) with (19.12) and (19.13)).

19.4 Results and discussion of rSOC system behavior

In this section, the simulation results of the model described in section 19.3 are shown and analyzed. The content of the presented studies reaches from the effect of the stack temperature and an investigation of system layouts with cold and hot gas recirculation to an evaluation of efficiency measures and a discussion of round-trip operation.

19.4.1 Operational parameters for high efficiency in EC and FC mode

In this subsection, we try to understand the behavior of the rSOC system with respect to changing operational parameters. This is done separately for EC and FC mode, for both scenarios, and for the flowsheet options defined in section 19.3.2.

Before getting deeper into the effects of parameter changes, we investigate the influence of the rSOC temperature levels of figure 19.4. In the simulations, the ambient temperature at which fuel and air enter the system is 20 °C and the stack temperature is chosen to be 750 °C. The pinch-point temperature difference of the heat exchangers (air and fuel HXs) is set to 5 °C and in the FC operational mode, 90 °C is specified for the air HX. In EC mode and for all the flowsheet configurations of figure 19.4, this results in temperatures of around 110 °C at the fuel exhaust and 260 °C on the air exhaust side. In FC mode, the fuel exhaust temperature is the lowest in the cgr-cond flowsheet (figure 19.4(A)) at 105 °C and the highest in the cgr flowsheet (figure 19.4(B)) at 235 °C. The air exhaust temperature is 110 °C in all cases, since the pinch point of the air heat exchanger (air HX) is at its cold end and determines this temperature.

19.4.1.1 Operational parameter sensitivity analysis

19.4.1.1.1 Influence of the stack temperature

The main mechanisms through which the stack temperature affects the system efficiency are given by processes in the stack. One can see the change of the stack electric voltage (ΔG) and total reaction energy (ΔH) with its (mean) temperature in figure 19.6. In the steam region, an increased temperature reduces the electric stack voltage, which is given by the change in the Gibbs free energy (ΔG), while the total energy of the reaction increases slightly (ΔH). More heat ($T\Delta S$) is released as the share of ΔG decreases while ΔH grows.

$$\Delta G_r = \Delta H_r - T\Delta S_r \tag{19.15}$$

In FC mode, this means that the electric efficiency decreases with increased temperature, as can be observed in figure 19.7 (FC cgr and FC cgr-cond). Nevertheless, a high system efficiency can be achieved if an increased proportion of the high-temperature waste heat is utilized. In EC mode, the decrease in stack voltage would be beneficial for the efficiency. However, in SOCs, the reaction heat must be provided at a high temperature. Available high-temperature heat sources that can meet this demand can only be found in specific settings, such as steel mills or cement plants. Therefore, it is assumed in this chapter that the high-temperature heat must be provided using electric heaters. As a result, the advantage of a decreased stack voltage in EC mode is lost and the disadvantage of the increased total reaction energy demand (see figure 19.6 ΔH) remains.

In figure 19.6 we can see a step in thermal energy ($T\Delta S$) at the transition from the water region to steam region, which reflects the heat of evaporation of water. Nevertheless, in the steam region this energy must be also provided (EC) or can be extracted (FC) at some point in the system. Due to the use of two separate processes (stack reaction and vaporization), the heat of evaporation can be provided non-electrically. Low-temperature (>100°C) waste heat sources or coupling to exothermic processes (e.g. methanation) can be utilized (see chapter 15). The replacement of

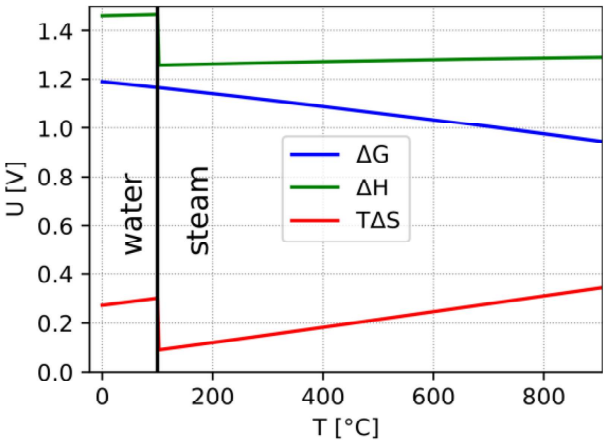

Figure 19.6. Change of the composition of the reaction energy with temperature for the reaction $2H_2 + O_2 \rightarrow 2H_2O$.

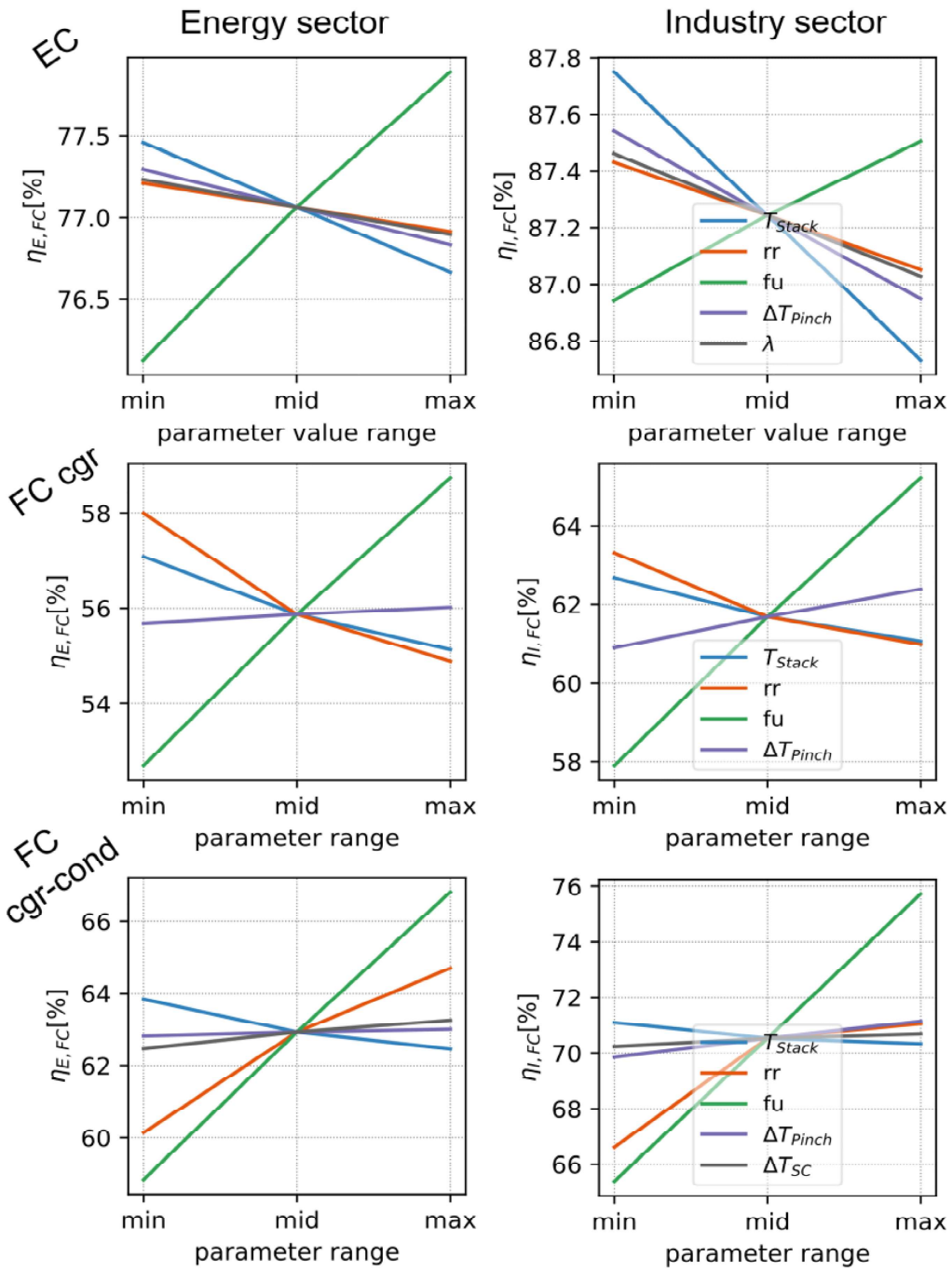

Figure 19.7. System sensitivity to parameters for the cold gas recirculation system; in the case of hot gas recirculation, the picture is similar. The range of efficiency variation in EC mode is factor of about five lower than in FC mode. The range of parameter variations can be seen in table 19.4.

high-quality energy (electricity) by lower-quality energy (heat) results in an increase in exothermic efficiency.

Another important process that affects the system performance through the stack temperature is the loss of heat to the environment. This loss increases with increasing process temperature, which reduces the efficiency in both operational modes but especially in EC mode.

19.4.1.1.2 The influences of recirculation rate (rr), fuel utilization (fu), HX pinch-point temperature difference (ΔT_{Pinch}), air excess ratio (λ), and subcooling temperature (ΔT_{SC})

In figure 19.7 a decrease in system efficiency with increased stack temperature can be seen in all cases. Furthermore, it can be observed that in EC mode, the efficiency decreases with an increase in any of the following parameters: rr, ΔT_{Pinch}, and λ. From this analysis, one might expect that small recirculation rates are preferred, and that systems without recirculation can be competitive with the ones that employ recirculation. However, the next two sections will disprove this conclusion and clarify the picture. The maximum value for the rr was chosen such (table 19.4) that it could be realized by ejectors and does not result in complete mismatch of system dimensions. While in FC mode, the efficiency increases with a higher ΔT_{Pinch} of the heat exchangers, it decreases in EC mode. The chosen ΔT_{Pinch} values in the air HX are much higher in the FC mode than in the EC mode (table 19.4). This is caused by the need for the air stream to provide cooling. In the condensed recirculation flowsheet, the effect of the recirculation rate is reversed, and higher subcooling temperatures (ΔT_{SC}) also increase the efficiency.

While, as mentioned, the stack temperature can only be varied within the limitations of the stack, the parameters λ, ΔT_{Pinch}, and ΔT_{SC} do not have strict limitations on their values. The fuel utilization (fu) is limited by the allowed range of stack fuel utilizations (fu_{Stack}, see equation (19.2)). Since fu_{Stack} depends on fu (see equation (19.3)) and rr, these two parameters cannot be investigated independently. Furthermore, the recirculation must provide a suitable gas composition for the stack. As can be seen in figure 19.7, in FC mode, these two parameters have the main impact on the efficiency and can be chosen from a wide range.

19.4.1.2 Cold gas recirculation: the influence of operational parameters

In this subsection, the parameter values are determined which lead to the best performance in a system with cold gas recirculation. Contour plots are used for the analysis. The region of the stack in which operation is infeasible, due to the limitations of fu_{Stack}, is separated by a black line and slightly grayed out. In the simulations used to generate figures 19.8 and 19.9, the stack temperature and ΔT_{Pinch} were set to the middle values of table 19.4. The minimum values of this table were chosen for the air excess ratio and the subcooling temperature.

Table 19.4. Parameter variation values

Parameter	Minimal value	Middle value	Maximal value
Stack temperature (T_{Stack}) [°C]	700	750	800
Recirculation rate (rr) [–]	0.5	2.75	5
Fuel utilization (fu) [–]	0.85	0.918	0.985
Fuel HX (ΔT_{Pinch}) [°C]	5	10	15
Air HX (ΔT_{Pinch}) [°C]	5(EC)/70(FC)	10(EC)/80(FC)	15(EC)/90(FC)
Air excess ratio (λ) [–]	0.5 (EC)	1.0 (EC)	1.5 (EC)
Subcooling temp. (ΔT_{SC}) [°C]	50 (FC)	60 (FC)	70 (FC)

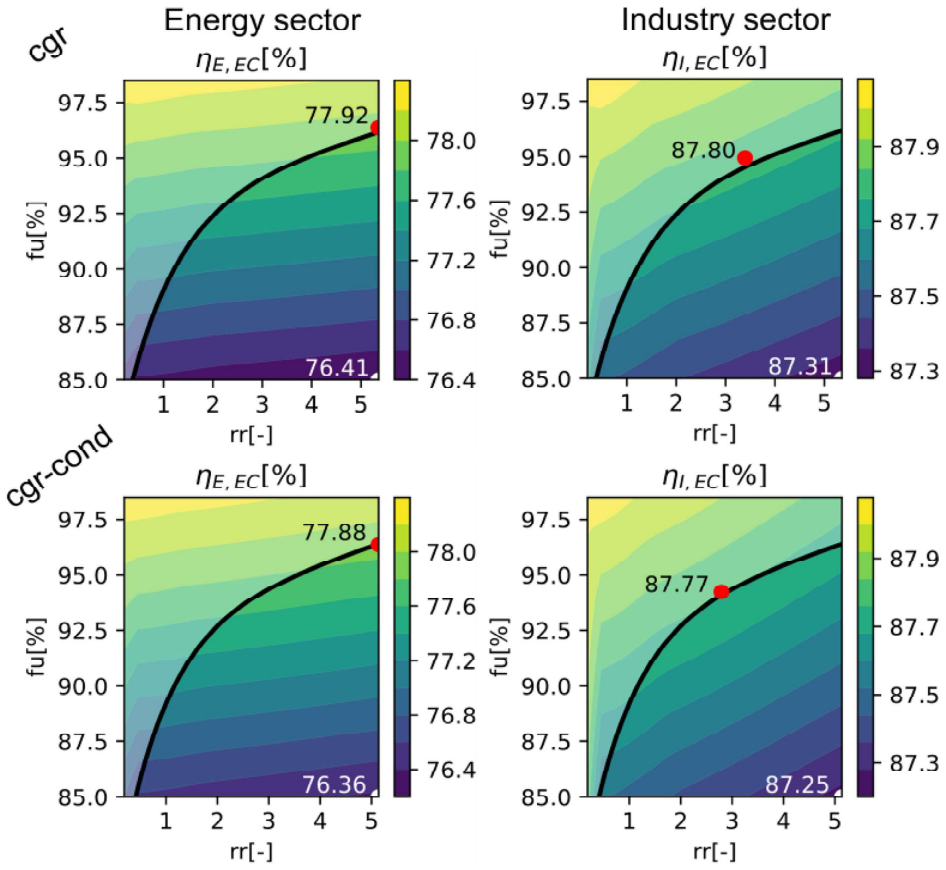

Figure 19.8. Efficiency of the cold gas recirculation flowsheet in EC mode, with (industry sector) and without (energy sector) heat integration/utilization and with (cgr-cond)/without (cgr) condensation in the recirculation. The black line separates the infeasible and feasible regions for the stack. The red points indicate the conditions of maximum efficiency.

Figure 19.7 gives a first overview of the system behavior, and we can see the difference in the magnitude of the performance influence for the EC and FC operational modes. Figures 19.8 and 19.9 provide closer insights. Here, we limit our investigation to the plane of the two parameters recirculation rate (rr) and fuel utilization (fu), because they strongly depend on each other and have a high impact on efficiency in all scenarios (see figure 19.7), as discussed in the previous section 19.4.1.1. By comparing both figures, we can see that in EC mode in figure 19.8 (white—minimum and black—maximum value), the influence of both parameters on the performance (0.5% ($\eta_{I,EC}$) and 1.5% ($\eta_{E,EC}$)) is much lower than in FC mode in figure 19.9 (4% ($\eta_{E,FC}$) to 14% ($\eta_{I,FC}$)). In the industry-sector scenario in particular, the effect in EC mode is very small. The reason is that as the stack power consumption (P_{Stack}) increases the heat produced in the stack increases as well; thus, the stack demands less electric energy from the electric heaters ($P_{e\text{-}heater}$). The increase in stack power and drop in electrical heating energy cancel almost exactly, which means that there is no influence on the efficiency, which can be concluded from equations (19.8) and (19.10).

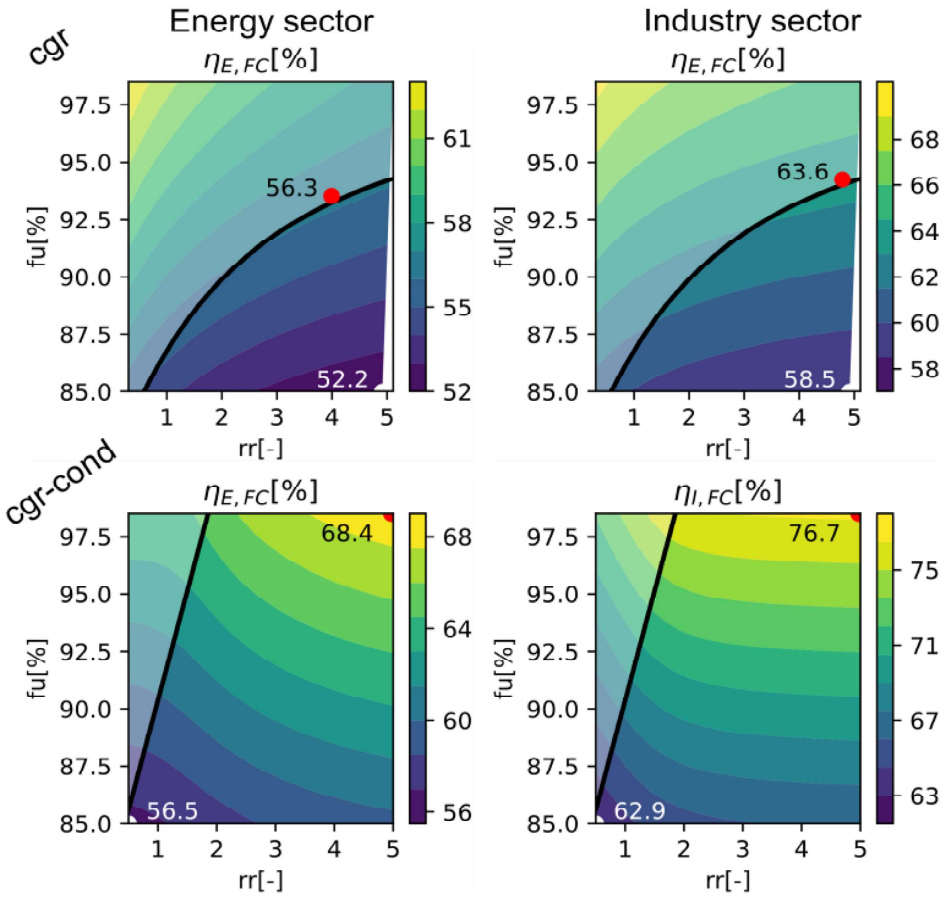

Figure 19.9. Efficiency of the cold gas recirculation flowsheet in FC mode, with (industry sector) and without (energy sector) heat integration/utilization and with (cgr-cond)/without (cgr) condensation in the recirculation. The black line separates the infeasible and feasible regions for the stack. The red points indicate the conditions of maximum efficiency.

19.4.1.2.1 Electrolysis cell operation mode

Although in EC mode, an increase in rr decreases the efficiency, the effect of better performance due to a higher possible fu moves the best operating points to considerable recirculation values. In the energy-sector scenario, the best fuel utilization and recirculation rates are higher than in the industry-sector scenario. One can see that this is caused by a smaller sensitivity to the rr (the slope of the contour lines). It is interesting that although the layout with condensation (figure 19.4(B2)) loses additional heat in the condensation step, the recovery of the fuel exhaust heat (recirculation HX, figure 19.4(B2)) can almost fully compensate this loss. The reason for this is that in the layout without condensation (figure 19.4(B1)), the heat of the exhaust fuel leaving the system is unused. In contrast, in the layout with condensation (figure 19.4(B2)), it is necessary to recover the heat to prevent mixing of a subcooled recirculation gas with the incoming steam from the evaporator. This is an important insight if a fan is used for recirculation instead of an ejector, since the temperature limit for fans is usually below 80 °C. From figure 19.8, we can see that the increase in efficiency from the grid scenario to the industry scenario is around 10% for both

system flowsheets. That means that thermal integration with ambient aggregates in the industry-sector scenario is highly beneficial.

19.4.1.2.2 Fuel-cell operational mode

The efficiency pattern in FC mode without condensation is similar to that in EC mode, as can be seen in figure 19.9. An increase of rr alone decreases the efficiency but allows higher fuel utilization (fu). This decrease due to higher rr is stronger in the energy-sector scenario ($\eta_{E,FC}$) than in the industry-sector scenario ($\eta_{I,FC}$). Therefore, the optimum operating point in the energy-sector operation is found at lower values of rr. However, in the case of the flowsheet with condensation (cgr-cond), a totally different picture can be seen. Here, in the energy-sector scenario, the efficiency increases in the direction of higher rr, as can be observed in figure 19.9. This is due to processes in the stack. The advantage of a spatially more homogeneous fuel composition over the length of the gas channels in the stack outweighs the disadvantage of lowering the average hydrogen concentration. In the flowsheets without condensation (cgr) the recirculation causes a larger drop in the hydrogen concentration, which is not compensated by the described mechanism. Another important difference can be observed in the flowsheet with condensation. The reduction of the steam content in the recirculation due to condensation almost cancels the fuel utilization limitations of the stack. The grayed-out zone for this case in figure 19.9 is small and does not exclude the theoretically best operational region of the system, which is not the case for all the other investigated flowsheet configurations and operation modes. The fuel utilization is, in this case, limited only for low rr. Using figure 19.9, the effect of condensation in recirculation can be quantified. It can increase the efficiency by 13% ($\eta_{E,FC}$) in the energy-sector scenario and 12% ($\eta_{I,FC}$) in the industry-sector scenario. Furthermore, the efficiencies of all scenarios can be compared. Upon changing from the energy-sector scenario to the industry-sector scenario, the efficiency with the cgr flowsheet (figure 19.4(B1)) increases by 7% and that of cgr-cond (figure 19.4(B2)) increases by 8%.

19.4.1.3 Hot gas recirculation: the influence of operational parameters

In this subsection, the hot gas recirculation flowsheet is examined similarly to the previous subsection on cold gas recirculation. The contour plots in figure 19.10 were made in the same way as described in section 19.4.1.2 for cold gas recirculation. Likewise, they show the minimum and maximum values (white and black numbers, respectively). From this we can see that the variation in efficiency in EC mode (0.6% ($\eta_{I,EC}$) and 1.6% ($\eta_{E,EC}$)) is much smaller than in FC mode (around 6% ($\eta_{I,EC}$) and 5% ($\eta_{E,EC}$)). The reason for this lower sensitivity in EC mode was already discussed in section 19.4.1.2. In figure 19.10, we can see that the efficiency of the best operation point (red dot, black number) grows by 10% in EC mode and by 7% in FC mode if we change from the energy-sector scenario to the industry-sector scenario.

19.4.1.3.1 Electrolysis cell operational mode

In both scenarios, the recirculation rate has a very small impact on system performance. An increased recirculation rate (rr) permits higher fuel utilization (fu).

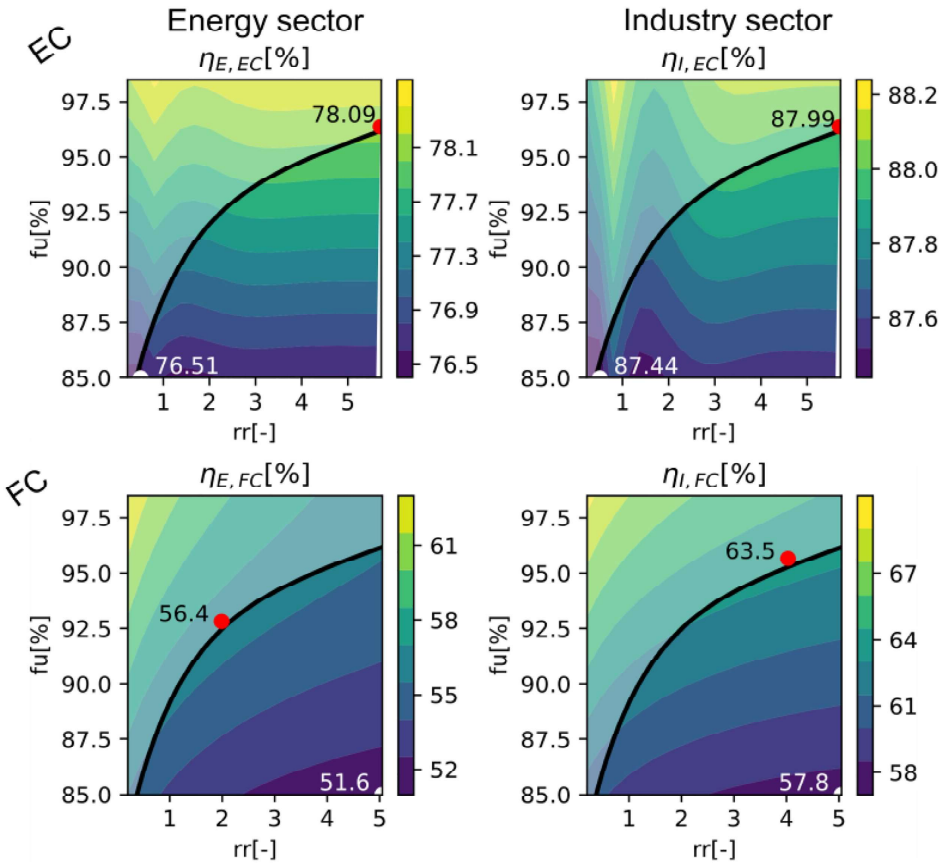

Figure 19.10. Efficiency of hot gas recirculation in EC (top) and FC (bottom) modes, with (industry sector) and without (energy sector) heat integration/utilization and with (cgr-cond)/without (cgr) condensation in the recirculation. The black line separates the non-feasible and feasible regions for stack operation. The red points indicate the conditions of maximum efficiency.

Consequently, the most efficient operation is found at high values of rr. The reasons for this behavior are two mechanisms that act on the efficiency in opposite ways. As is the case in any other flowsheet configuration, an increase in rr leads to a lower average steam concentration, which decreases efficiency. This lowered efficiency causes more heat generation in the stack, which reduces the need for external electric heaters by the same amount. Therefore, high rr are beneficial, as there is no downside, but they allow high values of fu. The electrolysis efficiency in this flowsheet configuration is slightly higher than with cold gas recirculation. In addition to the changed influence of the rr, another reason for this may be that less heat is lost from the system, as the recirculated gas stream does not have to pass the fuel HX.

19.4.1.3.2 Fuel-cell operational mode

The graphs of FC mode in figure 19.10 look almost identical to those of cold gas recirculation without condensation (cgr) in figure 19.9. Even the efficiencies of the most efficient points nearly match, although they lie at different values of the parameters. Thus, the discussion of cgr (section 19.4.1.2) applies here as well.

19.4.2 Evaluation of measures to increase efficiency

In this subsection, we explore the effect of two different options that extend the flowsheet in figure 19.4 to increase system efficiency in EC mode, and one possibility for FC mode:

- Heat recovery from exhaust air for preheating and evaporation in EC mode
- Heat recovery from exhaust fuel for preheating and exhaust air for superheating in EC mode
- Use of high-temperature heat potentials in FC mode

19.4.2.1 Heat recovery from exhaust air for preheating and evaporation in electrolysis mode

In the flowsheets of figure 19.4, the heat exchangers for internal heat recovery (the fluid HX and air HX) work with gas only on the respective system side. The fuel HX works with fuel and exhaust fuel and the air HX works with air and exhaust air. In EC mode, the mass flow of the air is increased by the transferred oxygen in the stack; thus, the exhaust air exceeds the incoming air mass flow. As a result, the pinch point in the air HX lies on the hot side and the exhaust air leaves the system at temperatures of up to 300 °C. For the fuel HX, the exact opposite applies: the pinch point lies on the cold side. To use this exhaust air heat, an additional heat exchanger can be added on the fuel side, as can be seen in figure 19.11.

In this configuration, the heat of the exhaust air stream can be recovered internally. This heat suffices to preheat the feed fuel (water) and produce a part of the steam needed (preheater/evaporator). In figure 19.12, one can see the increases in efficiency for the different scenarios (the energy and industry sectors) and flowsheets (cgr and hgr) in EC mode. By comparing this graphic with figures 19.8 and 19.10, we can see that an increase of around 2.8% ($\Delta\eta_{E,EC}$) is achieved in the energy-sector scenario and an increase of 0.8% ($\Delta\eta_{I,EC}$) is achieved in the industry-sector scenario in both flowsheet configurations (cgr and hgr).

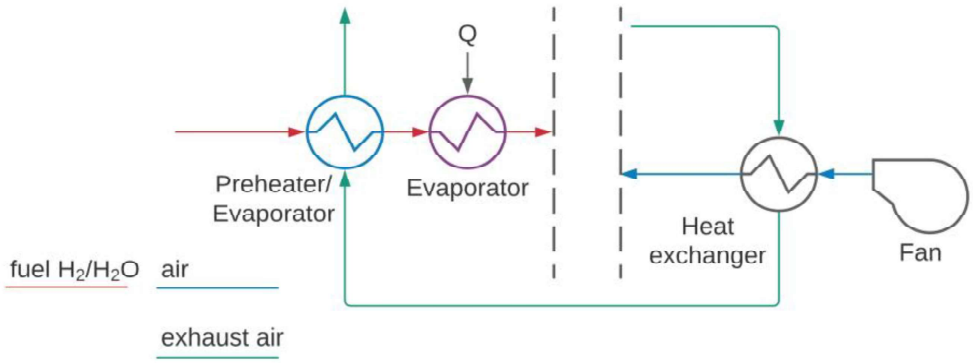

Figure 19.11. Flowsheet with heat recovery from exhaust air for preheating and evaporation in the electrolysis operational mode (an extension of figure 19.4).

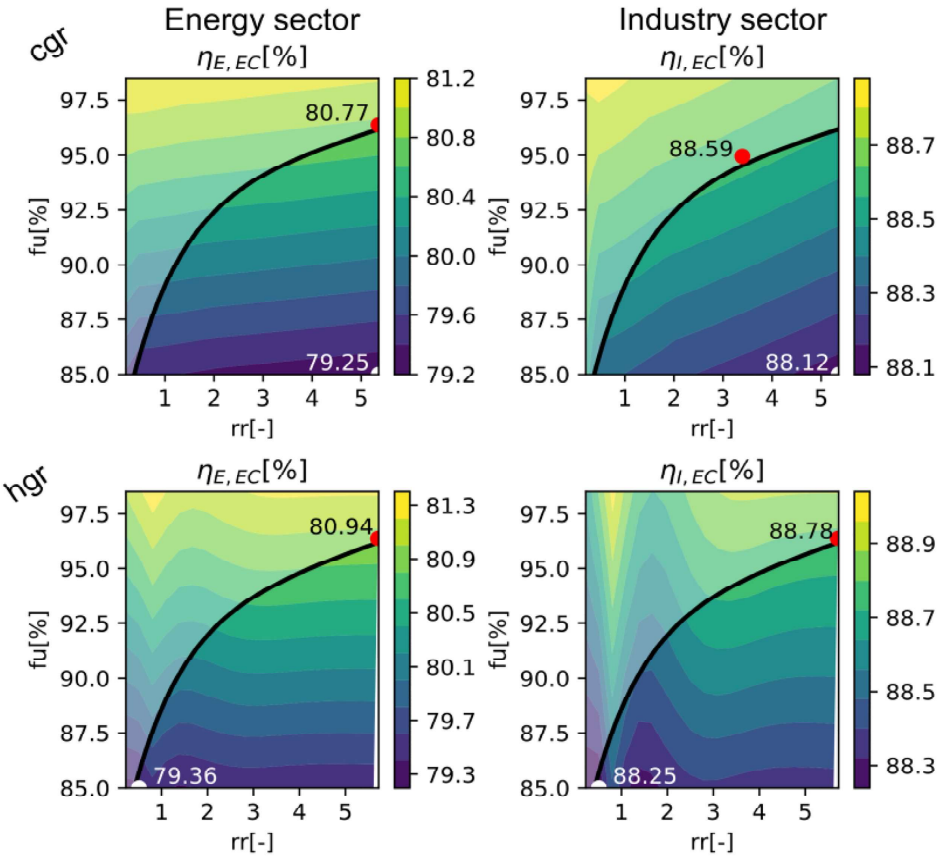

Figure 19.12. Changed efficiency pattern for the flowsheet of figure 19.11 in EC mode, with (industry sector) and without (energy sector) heat integration/utilization.

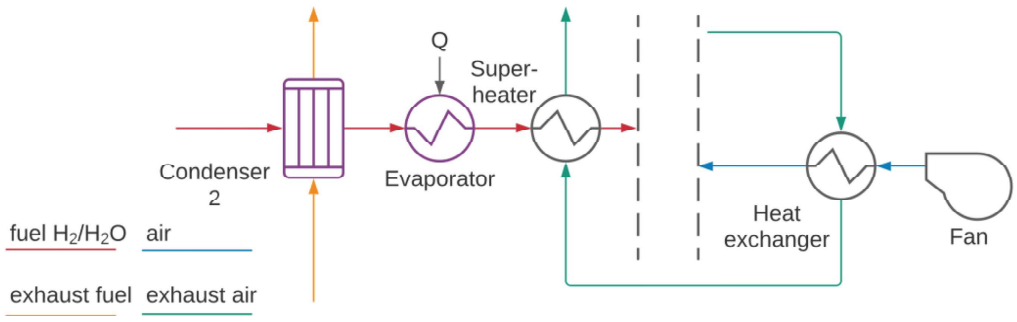

Figure 19.13. Flowsheet of heat recovery from the exhaust for preheating and exhaust air for superheating in EC mode (an extension of figure 19.4).

19.4.2.2 Heat recovery from exhaust fuel for preheating and exhaust air for superheating in electrolysis mode

A different version of heat recovery from the exhaust streams can also be realized. The condensing exhaust fuel stream contains more heat than that needed for preheating the feed fuel, so its heat can be used to preheat the fuel feed water to a temperature close to its boiling point (see figure 19.13 Condenser 2). The exhaust air has a temperature of more than 100 °C and it has a higher heat capacity stream than

the fuel feed gas. Therefore, part of its heat content can be used to superheat the evaporated fuel close to the exhaust air temperature (superheater). Since the internal fuel heat exchanger has its pinch point on the cold side, increasing the cold-side temperature can slightly increase the temperature of heat recovery for the fuel entering the electric heater on the fuel side. Consequently, less electric energy is used in this heater.

For the efficiencies at the most efficient points, with patterns like those shown in figure 19.12, increases of about 1.0% ($\Delta\eta_{E,EC}$) and 0.5% ($\Delta\eta_{I,EC}$) can be achieved in the energy-sector scenario and the industry-sector scenario, respectively. The efficiency increase is lower than that obtained using the previously proposed system improvement. The reason for this is that the exhaust fuel can only preheat the feed fuel and not evaporate it as in the previous case. Thus, the electricity demand in the evaporator is decreased much less. The reduction in the electric energy used to meet the high-temperature demand due to the superheating with exhaust air is only minor and cannot outweigh this disadvantage.

19.4.2.3 Use of high-temperature heat potentials in fuel-cell mode

The changes to the base scenarios related to both hot and cold gas recirculation shown in figure 19.4 consist of additional heat exchangers (HT-HX) that are added to extract high-temperature heat from the exhaust gases of the stack. This new configuration is shown in figure 19.14.

The usable high-temperature heat is calculated so as to ensure that the stack entrance temperature is exactly 100 °C lower than the stack temperature. The exergy content of this heat is calculated according to equation (19.7), and it is an additional contribution to the denominator in equation (19.11). If the amount of heat generated during operation stays the same, an increase in efficiency can be achieved by increasing the temperature and therefore the exergy. The changed efficiency patterns are shown in figure 19.15. We can see that in a cgr-cond system (according to figure 19.4(B2)), when compared to the results shown in figures 19.9 and 19.10, the efficiency has increased ($\Delta\eta_{I,EC}$) by 3.4%. The increase is 2.0% if heat is only extracted at the air side. In the case of a system with hot gas recirculation, the efficiency can be increased by 7.0% compared to the base case (figures 19.9 and

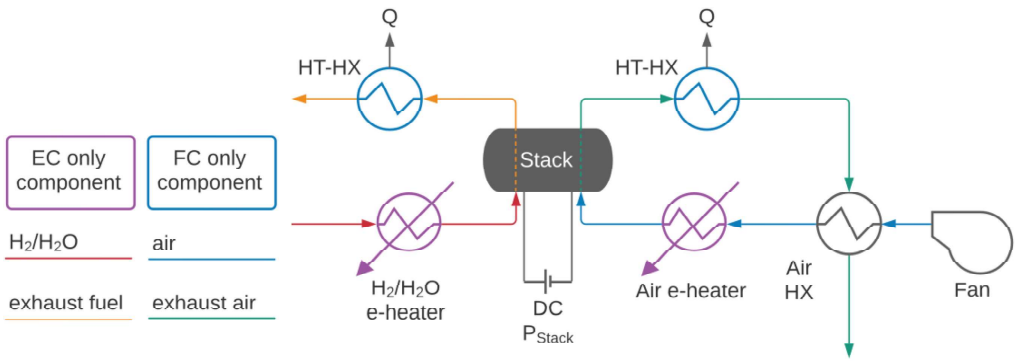

Figure 19.14. Flowsheet with high-temperature heat decoupling in FC mode (an extension of figure 19.4).

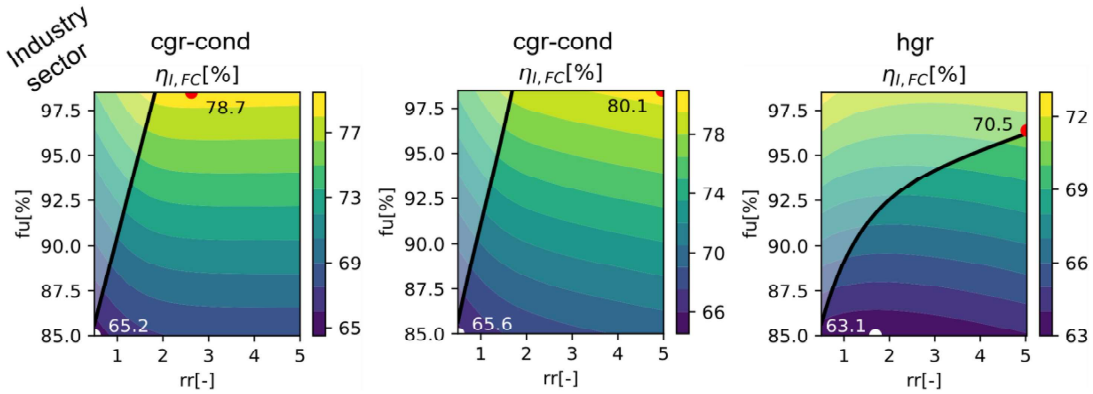

Figure 19.15. Efficiency patterns in industrial-sector application with high-temperature heat consumers. The left-hand graph for cgr-cond represents the case of high-temperature heat extraction on the air side only, while the other graphs refer to figure 19.14 and represent high-temperature heat extraction on both the air and fuel sides.

19.10). The amount of high-temperature heat was quantified. Its proportion of the stack's electric power is 15% for the cold gas and 30% for hot gas recirculation.

The configuration with high-temperature heat extraction can significantly increase the system efficiency in the industry-sector scenario ($\eta_{I,FC}$), according to equation (19.11) if there is a consumer for the high-temperature heat. For large systems, this could also be a steam boiler in a steam turbine cycle. At times without high-temperature heat extraction, other stack cooling mechanisms must be implemented. The simplest option is a valve in the exhaust air stream that bypasses the heat exchanger (air HX), so that the air entering the stack is heated less. In this case, the air exhaust system must be able to deal with temperatures above 300 °C.

19.4.3 Round-trip operation and the design of heat exchangers

Up until now, the two operational modes of the system (EC and FC) have been investigated independently. This means that the geometry of heat exchangers was chosen separately for each mode. We now analyze a system with maximized efficiency as it is switched from EC mode to FC mode as shown in figure 19.5. The system flowsheets for the cases under discussion are cold gas recirculation (cgr) in EC mode and condensation with condensation (cgr-cond) in FC mode.

Figure 19.16 shows the changed efficiency patterns if the heat exchanger constants are determined for the respective scenario (energy sector and industry sector). These results can be compared to the independent analyses of the EC and FC modes in figures 19.8 and 19.9.

The efficiency increased slightly in EC mode (by around 0.1% for both scenarios) due to the optimization of the heat exchangers (fuel HX and air HX) for the best operational point. The patterns changed, since the pinch-point temperature difference now varies with the recirculation rate (mass flows through the fuel HX). As the recirculation rate increases, the mass flow through the fuel heat exchanger increases as well. Thus, the pinch-point temperature difference increases, causing a higher electricity demand in the electric heater and lowering the efficiency. At scant

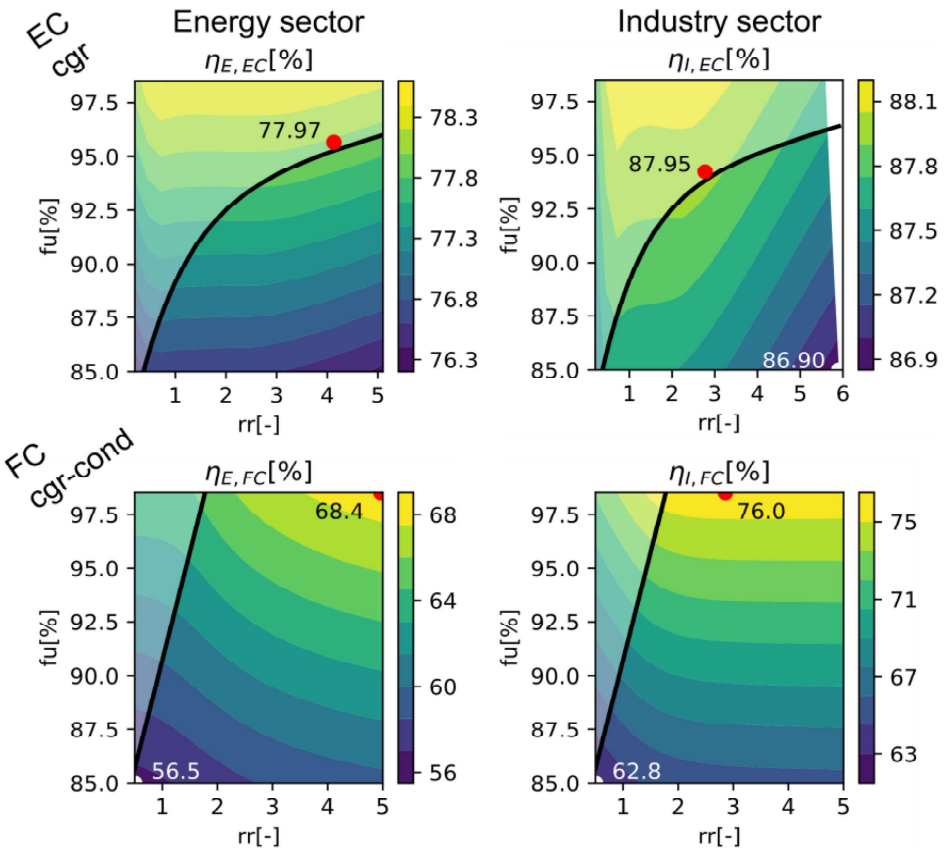

Figure 19.16. Efficiency pattern for system round-trip operation with cold gas recirculation flowsheets (FC with condensation in recirculation).

recirculation rates, the stack reactions produce too little energy and the stack temperature cannot be maintained. The latter effect causes the rise in efficiency at the left-hand ends of the EC graphs in figure 19.16.

In FC mode for the energy-sector scenario, the efficiency is unchanged compared to the pure FC mode in figure 19.9. However, the efficiency in the industry scenario is slightly decreased, by 0.7% ($\Delta\eta_{\mathrm{I,FC}}$). The reasons for this are the changed heat exchanger pinch-point differences, which decrease the exhaust temperature and therefore the waste heat exergy content of both the fuel and air streams. In this scenario, the design should probably be executed in a different way by making a better design compromise in the EC mode.

The efficiencies of the round-trip operation can be calculated using equations (19.11) and (19.12); they are 53.5% ($\eta_{\mathrm{E,RT}}$) in the energy-sector scenario and 67.0% ($\eta_{\mathrm{I,RT}}$) in the industry-sector scenario. Using the approximation of equation (19.14) we get the approximative efficiency values 53.3% ($\eta_{\mathrm{E,RT}}$) and 66.8% ($\eta_{\mathrm{I,RT}}$). This shows that the approximation is good and delivers (as expected) slightly lower efficiencies. To be precise, by taking the values for single-mode operation from sections 19.4.1 and 19.4.2, an additional approximation is used as a result of neglecting the effect of the round-trip heat exchanger design. This is a legitimate method, since the optimum round-trip design is close to the previously investigated single-mode designs.

The measures used to increase the system efficiency in the previous section can also be applied to the system in round-trip operation. If we limit ourselves to analyses of the efficiency at the best operational point, the approximation for the round-trip efficiency can be used to calculate the efficiency values for all combinations of different system flowsheets, improvements, and scenarios. This is justified by the small deviations that can be observed in the paragraph above for the case of cold gas recirculation. As an example, the round-trip efficiencies of the basic hot gas recirculation flowsheet from section 19.4.1.3 can be calculated in this way, which gives the values 44.0% ($\eta_{E,RT}$) and 55.9% ($\eta_{I,RT}$).

One hurdle in setting up a reversible system with recirculation shall be mentioned here. The volume flow for the system flowsheets of figure 19.16 in EC mode is larger by a factor of 2.5 than in FC mode. This means that two different ejectors or a mechanical fan must be used to achieve the required recirculation rates in both operations (EC and FC). There may be other solutions, but in any case, additional complexity is added to the system.

19.5 Concluding remarks

In the following, the main results are summarized and conclusions are drawn for the design of rSOC systems for different applications. During this process, questions I–IV of section 19.2 are considered and used to structure this section.

Message I. Understanding the combined influence of operational parameters on the system performance:

From the parameter sensitivity analysis in section 19.4.1.1, we can conclude that the stack temperature and the air excess ratio should be at the lower boundary of the possible operational range. For the system flowsheets of figure 19.4, the lower boundary for the air excess ratio could theoretically be removed by using a different method of stack heating. The heat exchanger pinch-point differences have opposite effects in the EC and FC modes. In the round-trip operation of the rSOC system, a good way of determining the heat exchanger area is to use the EC mode for the fuel HX and the FC mode for the air HX. There is a need for a more detailed investigation of the best heat exchanger dimensions for round-trip operation.

Message II. Determining the best operating points for the best system performance in different operational modes:

Figures 19.8–19.16 show the optimum operating points for both operational modes (EC and FC), application scenarios (the energy and industry sectors), and flowsheets (cgr, cgr-cond, hgr). These graphs strongly support the conclusion that high recirculation rates (>1) are beneficial in all cases, and are always better than a lack of recirculation. Therefore, the system flowsheet with fuel recirculation is preferred.

Message III. Quantification of efficiency-increasing measures for different system flowsheets:

Measures for increasing system efficiency are discussed in section 19.4.2. In the energy-sector scenario in particular, the options for EC mode have a significant impact on the system performance. Furthermore, it was found that simple heat recovery from exhaust air has the best outcome. In this case, the efficiency can only be increased by providing the heat of evaporation for the steam and by using high-temperature waste heat sources. For the FC mode, high-temperature extraction can make remarkable improvements to the flowsheet with hot gas recirculation. The effect is also noteworthy in the cold gas recirculation flowsheet with condensation. However, a limitation for this measure is implied by the ambient demand for high-temperature heat.

Message IV. Determination of the best system flowsheets, for the use cases of the energy sector and the industry sector, to meet the flexibility demand with best system performance:

Depending on the main operating mode, the best system flowsheet varies. If the EC mode is dominant, high-temperature recirculation may be used. Since, in this case, the recirculation rate can be higher in EC mode than in FC mode (see section 19.4.1.3), it is promising that the same ejector could be applied for both operating modes. This should be investigated further in simulations using detailed models of the ejector recirculation system. The cold gas recirculation flowsheet with condensation in the recirculation path is superior in terms of efficiency in FC mode. This is the preferred layout for systems without high-temperature extraction that spend a considerable proportion of their operational time in FC mode.

References

[1] 2015 United Nations Treaty Collection: Chapter XXVII Environment: 7. d Paris Agreement vol. 3156 Accessed 29.02.2022

[2] European Environment Agency, European Topic Centre on Climate Change Mitigation 2021 Annual European Union greenhouse gas inventory 1990–2019 and inventory report 2021: Submission to the UNFCCC Secretariat EEA/PUBL/20 Accessed 15 Dec 2021

[3] IEA 2021 Total primary energy supply by fuel, 1971 and 2019 https://iea.org/data-and-statistics/charts/total-primary-energy-supply-by-fuel-1971-and-2019 Accessed 29.02.2022

[4] European Commission 2019 The European Green Deal COM/2019/640 final Accessed 29.02.2022

[5] European Commission 2021 Fit for 55: delivering the EU's 2030 Climate Target on the way to climate neutrality COM/2021/550 final Accessed 28 Feb 2022

[6] Mancarella P 2014 MES (multi-energy systems): an overview of concepts and evaluation models *Energy* **65** 1–17

[7] Greiml M, Traupmann A, Sejkora C, Kriechbaum L, Böckl B and Pichler P *et al* 2020 Modelling and model assessment of grid based multi-energy systems *Int. J. Sustain. Energy Plan. Manage.* **29** 7–24

[8] Greiml M, Fritz F and Kienberger T 2021 Increasing installable photovoltaic power by implementing power-to-gas as electricity grid relief – a techno-economic assessment *Energy* **235** 121307
[9] Pfenninger S, Hawkes A and Keirstead J 2014 Energy systems modeling for twenty-first century energy challenges *Renew. Sustain. Energy Rev.* **33** 74–86
[10] Sejkora C, Kühberger L, Radner F, Trattner A and Kienberger T 2020 Exergy as criteria for efficient energy systems—a spatially resolved comparison of the current exergy consumption, the current useful exergy demand and renewable exergy potential *Energies* **13** 843
[11] Sejkora C, Lindorfer J, Kühberger L and Kienberger T 2021 Interlinking the renewable electricity and gas sectors: a techno-economic case study for Austria *Energies* **14** 6289
[12] Bundeskanzleramt Österreich 2020 Aus Verantwortung für Österreich (Out of a sense of responsibility for Austria): Regierungsprogramm 2020-24 https://bundeskanzleramt.gv.at/bundeskanzleramt/die-bundesregierung/regierungsdokumente.html (https://bundeskanzleramt.gv.at/en/federal-chancellery/the-austrian-federal-government/government-documents.html) Accessed 18 Feb 2022
[13] Bundesministerium für Klimaschutz, Umwelt, Energie, Mobilität, Innovation und Technologie 2022 Bundesgesetz über den Ausbau von Energie aus erneuerbaren Quellen (Erneuerbaren-Ausbau-Gesetz – EAG) (The Renewable Energy Expansion Act) StF: BGBl. I Nr. 150/2021 (NR: GP XXVII RV 733 AB 982 S. 115. BR: 10690 AB 10724 S. 929.) [CELEX-Nr.: 32018L2001, 32019L0944, 32019L0692]: EAG https://ris.bka.gv.at/GeltendeFassung.wxe?Abfrage=Bundesnormen&Gesetzesnummer=20011619 Accessed 18 Feb 2022
[14] Krutzler T, Kellner M, Heller C, Gallauner T, Stranner G and Wiesenberger H *et al* Energiewirtschaftliche Szenarien im Hinblick auf die Klimaziele 2030 und 2050 (Energy management scenarios with regard to climate targets 2030 and 2050): Synthesebericht 2015 Perspektiven für Umwelt und Gesellschaft REP-0535 Umweltbundesamt Wien
[15] Bundesministerium für Klimaschutz, Umwelt, Energie, Mobilität, Innovation und Technologie 2020 Energie in Österreich: Zahlen, Daten, Fakten (Energy in Austria 2020: Numbers, data and facts) https://bmk.gv.at/themen/energie/publikationen/zahlen.html Accessed 28 Feb 2022
[16] Singer D V 2017 Reversible solid oxide cells for bidirectional energy conversion in spot electricity and fuel markets *Doctoral Thesis* (Columbia University)
[17] Frank M, Deja R, Peters R, Blum L and Stolten D 2018 Bypassing renewable variability with a reversible solid oxide cell plant *Appl. Energy* **217** 101–12
[18] Giap V-T, Lee Y D, Kim Y S and Ahn K Y 2020 A novel electrical energy storage system based on a reversible solid oxide fuel cell coupled with metal hydrides and waste steam *Appl. Energy* **262** 114522
[19] Giap V-T, Kim Y S, Lee Y D and Ahn K Y 2020 Waste heat utilization in reversible solid oxide fuel cell systems for electrical energy storage: fuel recirculation design and feasibility analysis *J. Energy Stor.* **29** 101434
[20] Giap V-T, Kang S and Ahn K Y 2019 High-efficient reversible solid oxide fuel cell coupled with waste steam for distributed electrical energy storage system *Renew. Energy* **144** 129–38
[21] Reznicek E P and Braun R J 2018 Techno-economic and off-design analysis of stand-alone, distributed-scale reversible solid oxide cell energy storage systems *Energy Convers. Manage.* **175** 263–77

[22] Reznicek E P 2016 Design and simulation of reversible solid oxide cell systems for distributed scale energy storage *Master Thesis* (Golden, CO: Colorado School of Mines)
[23] Wendel C H and Braun R J 2016 Design and techno-economic analysis of high efficiency reversible solid oxide cell systems for distributed energy storage *Appl. Energy* **172** 118–31
[24] Wendel C H, Kazempoor P and Braun R J 2016 A thermodynamic approach for selecting operating conditions in the design of reversible solid oxide cell energy systems *J. Power Sources* **301** 93–104
[25] Perna A, Minutillo M and Jannelli E 2018 Designing and analyzing an electric energy storage system based on reversible solid oxide cells *Energy Convers. Manage.* **159** 381–95
[26] Spath S 2019 *Modellierung einer Power-to-Gas-(to-Power)-Anlage auf Basis einer RSOC mit Ebsilon® Professional* Montanuniversität Leoben https://pure.unileoben.ac.at/portal/en/publications/modellierung-einer-powertogastopoweranlage-auf-basis-einer-rsoc-mit-ebsilon-professional(f276dad8-81cd-4c3d-a2e3-0da0727a910f).html
[27] Mottaghizadeh P, Santhanam S, Heddrich M P, Friedrich K A and Rinaldi F 2017 Process modeling of a reversible solid oxide cell (r-SOC) energy storage system utilizing commercially available SOC reactor *Energy Convers. Manage.* **142** 477–93
[28] SunFire GmBH 2016 SunFire supplies Boeing with world's largest commercial reversible electrolysis (RSOC) system https://sunfire.de/de/news/detail/sunfire-liefert-weltgroesste-kommerzielle-reversible-elektrolyse-rsoc-an-boeing Accessed 12 Dec 2021

Energy Conversion and Management: X 20 (2023) 100425

Contents lists available at ScienceDirect

Energy Conversion and Management: X

journal homepage: www.sciencedirect.com/journal/energy-conversion-and-management-x

Integration of a rSOC-system to industrial processes

David Banasiak *, Markus Gallaun, Christoph Rinnhofer, Thomas Kienberger

Department of Environmental and Energy Process Engineering, Montanuniversität Leoben, Franz Josef-Straße 18, Leoben, Austria

ARTICLE INFO

Keywords:
Fuel cell
Electrolysis
Industrial waste heat
rSOC
SOEC
SOFC
Integrated energy system

ABSTRACT

The reversible operated high temperature solid oxide cell system (rSOC-System) seems to be a promising technology, enabling our future energy system to cope with the challenges of the transition to renewable electricity production and electrification. The rSOC-System provides energy storage capabilities and connects different energy carriers. This work provides insights into the coupling possibilities of such a system to industrial processes. Based on previously published investigations a flowsheet for the rSOC-System is chosen and described. To enable a quantitative analysis of the interaction with industries, a simulation model for this rSOC-System is created. This model is used for creating energy conversion and efficiency maps, which are then discuss with respect to the system behaviour. The increase of the system's conversion efficiency is determined for a selection of thermal coupling and operation scenarios. This work concludes with an analysis of the scenario dependent effect of heat coupling and the consequences for the integration of a rSOC-System to industrial processes.

1. Introduction

For reaching climate goals not only the expansion of renewable energy sources is crucial, but also to find ways for dealing with their volatile nature. Grid strengthening, storage solutions and a multi-energy-system with closely connected energy carriers will be inevitable in the future. Among others, reversible Solid Oxide Cell (rSOC) systems may be a key technology to provide flexibility for balancing volatile production and demand. They produce hydrogen in electrolysis cell (EC) and electricity in fuel cell (FC) mode. In FC operation either previously stored hydrogen or natural gas from the grid can be used as fuel, whenever the electricity prices are high enough to make this operation economical. In times of low electricity prices hydrogen can be produced. This high flexibility enables a high numbers of economical operation hours and reduces therefore the relative investment costs and the relative environmental impact connected with the system's manufacture.

Live cycle assessments were conducted by Gerloff et al. [1], Smith et al. [2] and Zhao et al. [3] for alkaline, PEM and SOEC electrolysis. They came to the same result, that for SOEC electrolysis systems, the impact on global warming is the lowest. The rSOC-System consist of the same core components as the SOEC electrolysis system but adds the possibility of the FC operation. Therefore, rSOC-Systems are of high interest for all efforts to reduce the CO_2 emissions connected to human activities, even though currently PEM electrolysers and fuel cells are clearly leading this transition.

The rSOC-Systems have already been subject of different scientific investigations. Here we give an overview on the different topics addressed by other research groups. Reznicek et al. [4] looked at the balance of plant components' off design performance and also considered floating piston tanks. In another publication of the same two authors [5] a synthetic gas production and reversible operation with an optimisation of levelized costs of product were considered in a setup with natural gas and CO_2 infrastructure. Srikanth et al. [6] made a study of transient operation strategies. Frank et al. [7] optimised internal waste heat recovery to reach high plant efficiencies. Sorrention et al. [8] determined the optimal plant configuration for microgrid application. Hutty et al. [9] investigated the rSOC-System as energy storage for a microgrid and its economic potential [10]. Zhang et al. [11] analysed the optimal dispatch of a rSOC-System in a scenario with wind production. Giap et al. [12] studied a system with a waste heat fuelled boiler and investigated different recirculation concepts. The same group of authors [13] investigated the thermal coupling to a metal hydride hydrogen storage system. Mottaghizadeh et al.[14] studied the importance of thermal energy storage in an rSOC-System and demonstrated the effect on the system efficiency. With a different group of co-Authors Mottaghizadeh [15] investigated an island application in a stand-alone building. Lamagna et al. [16] investigated the application of rSOC-Systems in buildings and with different co-Autors [17] the integration to wind parks. Königshofer et al. [18] performed measurements in the laboratory concerning the operation of a stack for a large-scale rSOC-plant. Posdziech et al. [19] reports on results from pilot plants connected

* Corresponding author.
E-mail addresses: david.banasiak@unileoben.ac.at (D. Banasiak), thomas.kienberger@unileoben.ac.at (T. Kienberger).

https://doi.org/10.1016/j.ecmx.2023.100425
Received 3 May 2023; Received in revised form 28 June 2023; Accepted 12 July 2023
Available online 16 July 2023

Nomenclature

rSOC-System	reversible Solid Oxide Cell System
EC	operation of the system in electrolysis cell
FC	operation of the system as fuel cell
P_{el}	system net electric power
P_{stack}	electric power of the electrochemical stack
$\dot{Q}_{th}$	thermal energy
H_2	molecular hydrogen
CH_4	methane, natural gas
f_i	thermal coupling factor in operation mode i
η_i	Efficiency in the operation mode i

to industries and the potential of such applications. Schwarze et al. [20] analysed a plant producing hydrogen and offering grid services by producing electricity, at the site of a steel plant. Singer et al. [21] rSOC operation strategies for market price time series in Denmark. This and further literature is discussed in section 2.1 with respect to the investigated system layouts, together with the here proposed flowsheet.

1.1. Remaining gap in the current state of research

The topic of many research groups, in the field of rSOC-System application, is its good integration to energy systems and the role of thermal energy storage or supply. This underlines the importance of understanding the coupling possibilities of the system. The industry integration enables strong coupling possibilities for different energy carriers (electricity, heat, hydrogen, oxygen). As a result, high system efficiencies as well as multi revenue-streams are possible and grid strain is reduced by being close to the consumer. Despite its attractivity, there is no detailed literature available on the rSOC-industry coupling and the quantification of its advantages for the system. In the research presented here we are focusing on the integration of a rSOC-System to industrial processes.

1.2. Open research questions and structure of this work

The aim of this work is to bridge the gap of knowledge related to the rSOC-industry coupling described in section 1.1.

The research questions addressed in this work are:

- How can the coupling of an rSOC-System with industrial sites look like?
- What is the thermal behaviour of the rSOC-System?
- How do the different coupling possibilities effect the efficiency of the rSOC-System?

Another aim of this work is to lay the foundation for a quantitative economic evaluation by means of operational optimisation based on time series.

This publication starts with an explanation of the coupling possibilities of rSOC-Systems and industries by streams of heat, hydrogen and electricity (section 2). Secondly, the methods for studying this integration are explained (section 3). This is followed by the results and the discussion (section 4) for the simulation of the rSOC-System behaviour. In this section the advantage of thermal coupling to waste heat is quantified. The conclusion section (section 5) contains the most important messages that can be drawn from the presented results. Finally, an outlook is given on how this present work can be a basis for future studies.

2. The RSOC-System and interaction with industrial waste heat

2.1. Basics of the rSOC-System and its coupling possibilities to industrial processes

The here investigated rSOC-System consists of a high temperature electrolyte supported electrochemical cell stack and the balance of plant components necessary for the operation. This system setup was already described by Paczona et al. [22,23] in detail and is illustrated in Fig. 1. Similar designs were already proposed in Literature. Reznicek et al. [4,5] investigated a system operated with syngas, that is cycled in a closed system, and with methane from the gas grid. This system is based on earlier concepts of Kazempoor et al. [24]. Their system includes on the air side a recirculation system and they modelled the internal heat recovery of the fluids in detail. Frank et al. [7] used pure hydrogen and air, with a fuel recirculation system and investigated different heat recovery possibilities including a catalytic afterburner. Giap et al. [13] studied with his colleagues a rSOC-system where waste steam is used in electrolysis operation and a part of the produced hydrogen stream is recirculated. In their system the hydrogen is stored in a metal hydride hydrogen storage and the released waste heat is utilized for production of steam. In fuel cell operation hydrogen is dried and recirculated and heat of the air stream is used to supply the endothermic discharge of the metal hydride storage. Motylinski et al. [25] use a system operating with hydrogen, water and air, that has a fuel recirculation system. Singer [21] addition included the possibility of operating the system with methane from a gas grid, which is making this system most similar to the one investigated in this work. The rSOC-System studied here (Fig. 1) is operated with hydrogen or methane in FC operation, while oxygen from air acts as oxidant. A recirculation path on the side of the exhaust fuel, active in both operation modes and driven by fan, ensures high system efficiencies and within fuel utilisation limits of the stack.

The different system operation modes considered in this work are:

- Fuel Cell operation (FC)
  - o FC operation with hydrogen as fuel (FC-H_2)
  - o FC operation with methane from a gas grid as fuel (FC-CH_4)
- Electrolysis Cell operation (EC), with the option of storing the hydrogen or providing hydrogen to external processes or market.

In FC operation, hydrogen (H_2) or methane (CH_4) are considered as fuel gas entering from the point 1 in Fig. 1, while air enters at point 2. Both gas streams are preheated in internal heat recovery heat exchangers (Fuel HX and Air HX) before entering the electrochemical cell stack. In the stack the oxygen ions are transported through the electrolyte at around 750 °C from air to fuel channel. The driving force is the difference of the electrochemical potential of the two electrodes in the gas streams. This potential difference multiplied by the ion charge transfer equals the externally utilizable electrical energy. In the fuel channels, on the electrode surface, the exothermic reaction of hydrogen and oxygen to steam is taking place. A part of the released reaction heat is used for preheating the incoming gas streams. However the overall system is net exothermic and heat can still be extracted for external use (e.g. industrial processes or district heating) at temperatures of up to 700 °C at the high temperature heat exchanger (HT-HX), as indicated in Fig. 1. When operated with natural gas, a larger share of the reaction heat is used internally, to supply the endothermic methane steam reformation. This reaction takes place in an external reformer just before the fuel enters the stack (CH_4-Reformer). The depleted fuel gas, after the stack and passing the heat exchanger (Fuel HX), is mainly recirculated. The recirculation path includes a condensing heat exchanger (Fig. 1, Cond. 1), where cooling below the dew point takes place. The condensation and removal of water from the recirculation stream has a positive effect at the system efficiency, as the hydrogen partial pressure stays high. A mechanical fan (recir. Fan) is considered as driver for the recirculation. In FC operation depleted exhaust fuel gas is burned

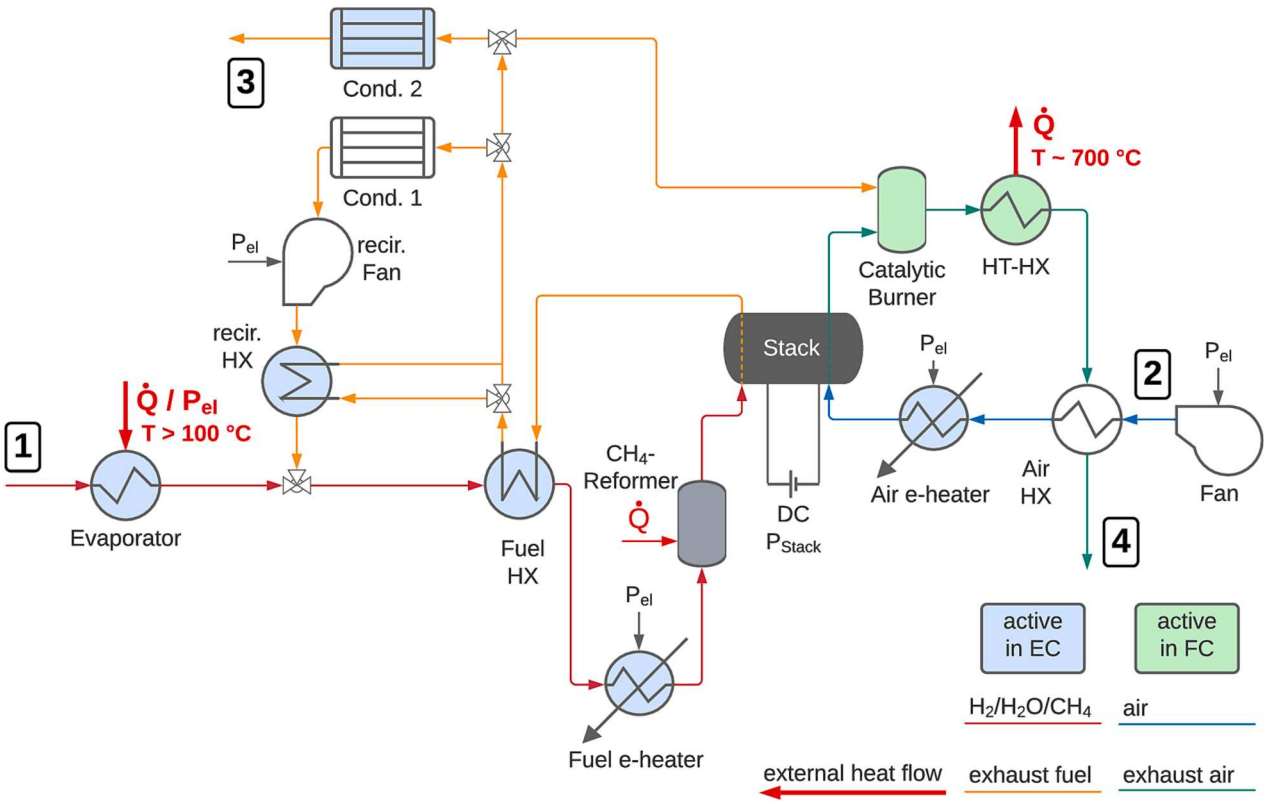

Fig. 1. Flowsheet of the considered rSOC-System with recirculation of the stack exhaust fuel and its thermal coupling possibilities: industrial waste heat can be integrated in electrolysis cell operation (EC) for steam production at the evaporator, replacing an electric energy demand, then hydrogen is generated with high electric efficiency. In fuel cell operation (FC) heat can be extracted from the HT-HX heat exchanger at high temperatures (>700 °C) and is utilizable additionally to the generated electricity.

together with exhaust air (Catalytic Burner Fig. 1) to increase the extractable waste heat. The combined exhaust gas stream after this combustion is used to preheat the incoming air, before leaving the system at point 4.

In EC operation, which is the reverse of FC-operation, water enters the system at point 1 in Fig. 1. An air stream, entering at point 2, is not needed as a reactant, but is used to control the stack temperature. The water is evaporated either by electric heat generation or other heat sources. If waste heat (e.g. from industrial processes) is available, it can be utilized here to significantly increase the system efficiency. In electrolysis operation the preheating of the incoming gases with heat recovery exchangers (Fuel HX and Air HX in Fig. 1) is not sufficient and electric heaters for fuel (Fuel e-heater) and air (Air e-heater) must further increase the temperature. In the stack, at the electrode surface, the steam molecules are dissociated. The oxygen ions can then be transported to the air side of the stack by applying an electric field, that is higher than the electrochemical potential difference of the electrodes. This potential difference and the electric current associated with the transport of oxygen ions is the electric power that must be applied to the system. Due to this oxygen transport, the air becomes enriched with oxygen. Hydrogen together with steam stays on the steam side of the stack. If the electric power applied to the stack in EC operation would be increased, at some point the stack internal losses generate enough heat to equal the thermal energy demand in the stack. This point is known as the thermoneutral point. Above this point no thermal energy input from additional components (electric fuel and air heater) is necessary. The hydrogen enriched steam, that is generated in the stack can be recirculated. In electrolysis operation it is advantageous to cool the recirculated stream only slightly in the condenser (Fig. 1 Cond.1). Ideally the steam should not fully condense but be reused for another pass through the electrochemical stack. However, the recirculation blower demands a temperature limitation to 80 °C, which causes significant condensation. Before the hydrogen can be stored or consumed by industrial processes (Fig. 1 point 3), the water content must be reduced by another condenser (Fig. 1 Cond.2).

2.2. Industries waste heat availability and coupling possibilities

The energy intensive industries shown in Table 1 and the energy extensive industries in Table 2, in accordance with results from the project “Abwärmekataster Steiermark” [26], are determined as suitable candidates for the integration of an rSOC-System. Furthermore, other metal producing industries besides steel were identified as promising, as they have large waste heat potentials at temperatures above 100 °C. In Table 1 the source of heat, that can be used for steam production in electrolysis mode, is shown together with the corresponding temperature and typical heat flow rate. In cement, glass, refractory and steel production the waste heat, which is available in form of gas streams, can be used directly to produce steam at 1 bar for the electrolysis operation.

Table 1
Energy intensive industry key heat sources for coupling with rSOC-System and temperature and heat flow for typical plant sizes in Austria.

	Cement	Glass	Lime	Refractory	Steel
Heat source	Clinker cooler, raw gas	Flue gas: before/after e-filter, annealing oven	Flue gas	Flue gas	Flue gas: Sinter, LD-converter
Temperature in °C	300	380 – 500	70 – 100	180 – 300	110 – 140
Heat flow in MW	10.4	3.8			3 – 7

Table 2
Typical heat flow for waste heat above 100 °C of selected energy extensive industries.

	Meat-processing	Brewery	Textiles	Grain mill
Heat flow in kW	51	1200	75	47

In lime production the temperatures are slightly below 100 °C, so that high temperature heat pumps would be required. However, in this case one must consider additionally the efficiency of the heat pump and its investment costs.

The industries presented in Table 1 are in first order running constantly all year long with interruptions only by scheduled maintenance. This means, that the waste heat is available nearly constantly. However, there are batch processes involved, for example the LD-converter in a steel plant. In this case the waste heat flow must be delivered continuously to the rSOC-System, since constant cycling of the rSOC-System would lead to fast degradation. In comparison, the costs of steam storage systems are low. Similar fluctuations appear in the cement industry, the internal heat demand increases when the raw material mill is operating. That means, whenever this mill is operating, the available waste heat is reduced. Simultaneously, the raw material mill causes high peaks in electricity consumption. The rSOC-System's FC operation can be used in this case for peak shaving. Similar mills are used in lime-, refractory- and steel (sinter plant) production. A different reason for fluctuations in availability of process waste heat was identified in the refractory production. Here, depending on the product type, an additional cooler is activated after the cooling zone in the tunnel oven. This non continuously operating cooler is generating additional utilizable waste heat.

Energy extensive industries can also be interesting for the coupling with an rSOC-System especially if the waste heat is above 100 °C. A selection of investigated industries fulfilling this criterion is shown in Table 2. The heat flow rate of these industries is significantly lower than of energy intensive industries.

The integration to industries, of Table 1 and Table 2, allows the utilisation of process waste heat by the evaporator of Fig. 1. Additionally, many locations of energy intensive industries, especially the ones shown in Table 1, have a connection to a district heating network. This utilization of the process waste heat in a district heating network reduces the heat, that is available for integration in the rSOC-System's evaporator. From a first point of view, a district heating network is therefore competing with the heat demand of the rSOC-System's EC operation. However, the fuel cell operation with natural gas can be the main operational mode in winter, so that even more heat for district heating can be provided. In such an operation strategy other heat generation units like gas boilers or heat pumps can be replaced. In summer on the other hand the heat demand in district heating is low, allowing an unreduced waste heat utilization in electrolysis mode. Furthermore, it is predicted that in future there will be an excess of renewable electricity during summer months while there will be a shortage of renewable energy during the winter months. This matches perfectly this industrial pattern of a favourable EC operation mainly in summer months and FC operation mainly in wintertime. This implies, that industries which can provide waste heat at a suitable temperature and are connected to a district heating network, are very likely to enable a highly beneficial thermal coupling both in FC and EC operation mode.

Theoretically, it would be interesting to find industries, that offer both a waste heat source for steam production and processes with high temperature heat demand. In this case the EC operation could be operated with steam produced by industrial heat and the heat produced in FC operation could be utilized by another industrial process with a minimized loss of exergy. The rSOC-System can consume heat at ~100 °C at times of EC operation and providing heat at 700 °C during FC operation. In this way the system can provide the service of a high temperature heat pump together with the time decoupling of a storage. However, such pattern of processes was not found in the investigated industries.

In the future many industrial high temperature processes, in the effort of becoming climate neutral, will switch from fossil energy sources to hydrogen (e.g. hydrogen direct reduction in steel plants). This means that an efficient hydrogen production on site is of high interest.

3. Methods

In this section we discuss the methods employed in our investigations of the impact of thermal coupling on the efficiency of the rSOC-System. It is divided into two subsections. At first is presented the approach used in modelling the rSOC-System (shown in Fig. 1). This model allows us to perform system simulations, understand the behaviour and create performance maps. Secondly, we describe the calculation of the system efficiency for single operation modes, the round-trip operation and in scenarios. This is used to quantify the effect of the thermal coupling to industries.

3.1. Modelling approach of the rSOC-System

In our study we made use of computer simulations to reproduce the behaviour of a 5 kW FC and 15 kW EC System. The simulations were based on thermodynamic steady state models of the rSOC's components like heat exchanges, condensers, the recirculation system and a semi-empirical model of the electrochemical stack, that was provided by AVL List GmbH. A detailed description of this model, enabling design and off-design calculations, with all relevant parameters was already published by Paczona et al. [22,23]. The modelling was done in the environment of Dymola [27] from Dassault Systems. The data for the gas mixtures was taken from the NASA ideal gases data implementation in Dymola. We determined the design parameters for the system components through a parameter sweep which includes engineering knowledge (e.g. the design pinch point temperature difference of the heat exchangers was set to 10 K). The optimum setting of internal system parameters (recirculation rate and fuel utilization) within the allowed operation range were determined for different part load points through an optimization algorithm which maximizes the system's efficiency. The fuel utilization at stack level was limited to a maximum of 0.8 according to the stack limitations and in accordance with literature [28–31]. By optimising the recirculation rate and fuel utilization, these parameters are fixed, so that a real-world system at the end of its development cycle, is represented most accurately. The stack operation temperature for all simulations was set to 750 °C. Furthermore, assumptions about the thermal control strategy had to be made: In our model, by controlling the air mass flow and its temperature, we can ensure a maximum temperature difference, between any two of the in- and outcoming gas streams of the stack and the stack itself, of below 100 K. This thermal control strategy for the stack is used also by Preininger et al. [30,32]. It ensures that the stack does not experience spatial temperature differences of more than 10 K/cm [29] in order to avoid high degradation or destruction. As a result of this constraint, the heating and cooling rates in the here considered planar stacks must be limited to 1 K/min up to 10 K/min [18,29,33]. This means that a cold start for these systems most likely takes one to two hours. However, as the system reached its operational temperature of 750 °C the change of operation mode (EC, FC) can happen in a few minutes [6,19,28].

The energy consumption of the compressor in the hydrogen storage system was simulated in Python with the help of the PropSI function of the CoolProp package [34]. In this model the temperatures for start, intercooling and end of the compression were chosen to be equal. Four compression stages were chosen for the compression from 1 bar to 300 bar. In each stage an adiabatic process is simulated and an isentropic efficiency of 0.92 and electric efficiency of 0.98 is considered. These efficiency values were obtained from the calibration with the datasheet of the ionic piston compressor (IC90) of the Linde Hydrogen FuelTech GmbH [35].

3.2. System efficiency in different operation modes

The effect of thermal coupling between the rSOC-System and industries is investigated based on the steady state efficiencies which are defined in this section. The efficiency of the rSOC-Sytem is given by the ratio of useful energy output divided by the needed energy input.

In fuel cell operation the energy input is solely the energy stream of the fuel (P_{fuel}), which can be hydrogen or natural gas. The useful electricity output (P_{el}) in this operation is the electric power produced by the stack (P_{stack}), which is decreased by the system self-consumption for the air fan (P_{fan}) and the recirculation blower ($P_{rec.}$). An additional useful energy output can be the heat stream from the HT-HX heat exchanger ($\dot{Q}_{HT-HX}$, see Fig. 1). In case of operation with natural gas, a part of this heat stream is used to supply the steam reformer ($\dot{Q}_{reformer}$). This is needed to pre reform the natural gas into hydrogen before entering the stack, where internal reformation takes place as well. The net heat stream leaving the system ($\dot{Q}_{th}$). is the difference of those two heat streams. By multiplying this heat flow with a thermal coupling factor (f_{FC}), that is equal to zero in case of no and one in case of full heat utilization, we end up with equation (1) for the system efficiency in fuel cell operation (η_{FC}).

$$\eta_{FC} = \frac{\dot{E}_{out,FC}}{\dot{E}_{in,FC}} = \frac{P_{el} + \dot{Q}_{th}}{P_{fuel}} = \frac{P_{stack} - P_{fan} - P_{rec.} + f_{FC} \bullet \left(\dot{Q}_{HT-HX} - \dot{Q}_{reformer}\right)}{P_{fuel}} \tag{1}$$

By setting the thermal coupling factor to one, we assume explicitly that the excessive heat and produced electricity are equal in quality. This is well justified for high temperature processes acting as heat sinks or in any other case where chemical energy, which has an exergy content almost equal to electricity, is converted to heat. In some cases, one might prefer to weight the heat by using the Carnot-factor, in which case the used energy is the exergy content. This is a good approach especially in case when there are low temperature heat consumers connected, like a district heating grid.

In electrolysis cell operation, the efficiency (η_{EC}) is almost the inverse of the one in fuel cell operation. However, an additional term must be added to the total electric energy consumption (P_{el}), the consumption of the electric high temperature heaters ($P_{e\text{-}heater}$), which are only active in the endothermic electrolysis mode. Furthermore, the net thermal energy demand ($\dot{Q}_{th}$) is the difference of the heat demand of the evaporator ($\dot{Q}_{Evaporator}$) and the internal available heat ($\dot{Q}_{HT-HX}$). By introducing another thermal coupling fraction for EC operation (f_{EC}) we arrive at equation (2). This thermal coupling fraction is introduced in such a way, that it reflects no waste heat availability for evaporation in case being equal to zero and fully coverage of heat demand in case of being equal to one.

$$\eta_{EC} = \frac{\dot{E}_{out,EC}}{\dot{E}_{in,EC}} = \frac{P_{fuel}}{P_{el} + \dot{Q}_{th}} = \frac{P_{fuel}}{P_{stack} - P_{fan} - P_{rec.} - P_{e-heater} + (1 - f_{EC}) \bullet \left(\dot{Q}_{Evaporator} - \dot{Q}_{HT-HX}\right)} \tag{2}$$

Again, we assume here, that the quality of heat and electricity is equal. This is perfectly justified, if the energy demand in the evaporator is covered electrically, in case there is no suitable waste heat source available.

With the definitions of the efficiency in the operation modes in equation (1) and equation (2), the round-trip efficiency is simply the product of the efficiency in fuel cell operation and electrolysis operation as can be seen in equation (3).

$$\eta_{RT}(f_{FC}, f_{EC}) = \eta_{FC}(f_{FC}) \bullet \eta_{EC}(f_{EC}) \tag{3}$$

This definition is only applicable to the case of a closed hydrogen side, where hydrogen is produced via electrolysis and the same amount is consumed in FC operation. However, this is not a round-trip efficiency of a closed system, as the origin and destination of the heat streams is not accounted for. In this way we assume, that no additional energy is needed to provide external available waste heat or to further use the heat extracted at the high temperature heat exchanger (HT-HX).

In case of an open system, methane can be taken from a gas grid and hydrogen can be also sold to a market instead of converting it back to electricity. Then the overall scenario system efficiency (η_S) can be defined as the quotient of the sum of the energy produced and leaving the system in all timesteps and the energy imported over the system boundaries, according to equation (4). This corresponds to the real conversion efficiency, that can be reached in specific scenarios. Introducing operation hours (h_i) for all possible operation modes allows us to derive the explicit form for calculating scenarios, as shown in the continuation in equation (4). Here it is not explicitly written that one operation modes can also have different efficiencies, these contributions must simply to be added accordingly to the summations in the numerator and denominator. It shall be also noted that the consumption of hydrogen in FC operation reduces the output of hydrogen produced in EC operation, as self-consumed hydrogen does not leave the rSOC-System, as is visible in the numerator in equation (4). In this way we do consider explicitly the case that, the consumed hydrogen of FC operation is previously produced by EC operation.

$$\eta_S = \frac{\sum_{t,i} \dot{E}_{sys-out,i(t)}(t)\,\dot{E}}{\sum_{t,i} \dot{E}_{sys-in,i(t)}(t)} = \frac{h_{FC,H2} \bullet \eta_{FC,H2} \bullet \dot{E}_{in,FC} + h_{FC,CH4} \bullet \eta_{FC,CH4} \bullet \dot{E}_{in,CH4}}{h_{FC,CH4} \bullet \dot{E}_{in,CH4} + h_{EC} \bullet \dot{E}_{in,EC}} + \frac{h_{EC} \bullet \eta_{EC} \bullet \dot{E}_{in,EC} - h_{FC,H2} \bullet \dot{E}_{in,FC}}{h_{FC,CH4} \bullet \dot{E}_{in,CH4} + h_{EC} \bullet \dot{E}_{in,EC}} \tag{4}$$

In the calculations in section 4.2 four different possibilities for the coupling to industrial waste heat sources and sinks are considered. In the case $f = 0$ there is no thermal coupling present. For the case $f_{FC} = 1$ there is a heat sink present but no heat source and in case $f_{EC} = 1$ it is exactly the other way around, with an available heat source but no sink. In the case $f = 1$ both, thermal couplings for EC and FC operation, are considered.

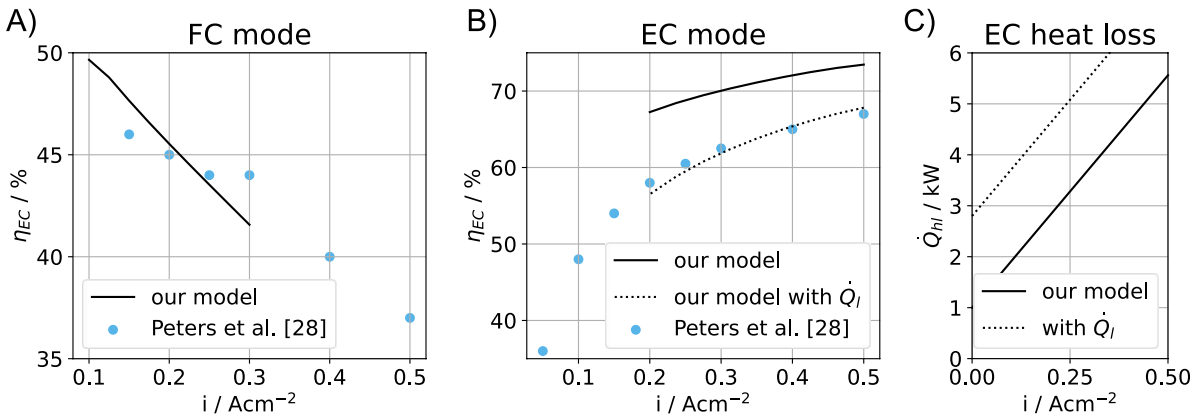

Fig. 2. Validation of the part load behavior in A) FC mode and B) EC mode. In B) it can be seen, that the model used by us in this work can be adjusted to the values obtained by Peters et al. by using an additional constant heat loss factor $\dot{Q}_l$ which is set here to 1.8 kW. C) shows the heat loss behaviour in our system and the heat losses if an additional constant value of 1.8 kW is added.

3.3. Validation of the model part load behaviour

The model validation was performed by analysing the agreement of the part load efficiency curve with the laboratory measurement data of Peters et al. [28], as can be seen in Fig. 2. The date of our model was calculated for the same conditions (fuel side recirculation rates and fuel utilisation) as in the laboratory set up of Peters et al. However, the electrochemical stacks under investigation are different. This results in lower maximum current densities for our system of 0.3 A/cm^{2}compared to 0.5 A/cm^2 for the system used by Peters et al. In Fig. 2 A) we see that the slope of our curve and the slope of the measurement points of Peters et al. is very similar and the absolute values are in good agreement. The shift of the points of Peters et al. towards higher current densities, can be due to slightly different electrical properties of the cell stack. In EC-mode, which can be seen in Fig. 2 B), the efficiency of our model is higher than in the case of the reference system. If we would add an additional constant term of$\dot{Q}_l = 1.8$ kW to our considered heat losses, as is illustrated in Fig. 2 C), the efficiency curve calculated by our model resembles the laboratory measurements of Peters et al. very well, as can be seen in Fig. 2 B). A constant heat loss term, that does not change with the system's operation power is related to heat transfer through the system surface to ambient. Our model is aimed at depicting a future commercial system with good thermal insulation, this justifies this discrepancy between our model and the laboratory system of Peters et al.

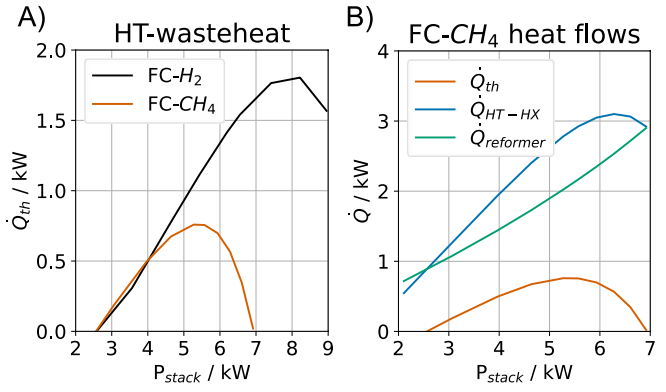

Fig. 3. A) Dependency of the high temperature net waste heat ($\dot{Q}_{th}$) on the stack power in the two different FC operations, B) The HT-HX heat ($\dot{Q}_{HT-HX}$) is reduced by the reformer heat ($\dot{Q}_{reformer}$) demand to the extractable high temperature heat ($\dot{Q}_{th}$) in FC-CH$_4$ operation.

4. Results and discussion

The results of the steady state simulations, described in section 3.1, were used to create efficiency- and performance maps for the different operation modes (see Fig. 4 and Fig. 5). These performance maps enable the comparison of a standalone application to thermal coupling, to waste heat sources and heat consumers. Based on these results the influence of thermal coupling is investigated in different scenarios. This subsection is divided into, firstly, the overall system operational behaviour and conversion rates and, secondly, the influence of thermal coupling on the rSOC-System efficiency.

4.1. Operational behaviour of rSOC-Systems

The operation of the rSOC-System is characterized in FC operation by the conversion of fuel (H$_2$ or CH$_4$) to electricity. In EC operation the conversion of electricity and thermal energy to hydrogen is of interest. These conversion rates are shown in Fig. 4 for the three operation modes of the rSOC-System. Additionally, the relation between electric power and heat flow as well as the compression energy consumption of a hydrogen storage can be seen in Fig. 4.

In FC operation (see Fig. 4 A) the fuel consumption (P_{fuel}, solid lines) is a convex function of the electrical system output power (P_{el}). This means as the power increases the specific fuel consumption increases as well. This results in the decrease of electric efficiency as the electric power output increase, which is visible in Fig. 5 A and B. The reason for this convexity is an increasing internal resistance of the rSOC stack, as the load increases. This internal resistance increase is connected to the transport of hydrogen to the active electrode surface (concentration losses [24,36]). The heat generation of the stack is shown in dotted lines. In hydrogen operation the generated heat follows a similar trend as the fuel consumption ($\dot{Q}_{th}$, black dotted line), as the increased internal resistance causes higher heat generation. However, in an operation with methane the high temperature waste heat, is lowered by the reformer's heat consumption and does not show the same characteristics. The reason is that in the operation with CH$_4$ the concentration losses increase sharper and therefore more cooling air is needed, which in return increases the low temperature heat loss while more high temperature heat is needed for preheating the higher mass flow of incoming air. In Fig. 3 the dependency of the extractable high temperature waste heat is shown for a wider operation range. Here in graph A it is visible, that in FC- H$_2$ operation as well as in FC-CH$_4$, the trend is similar. Which underlines the argument that a higher air mass flow needed for cooling reduces the high temperature extractable heat. However, with CH$_4$ the decrease of waste heat happens already at a lower stack power of around 5 kW compared to 7 kW in operation with H$_2$. In Fig. 3 B the decrease of

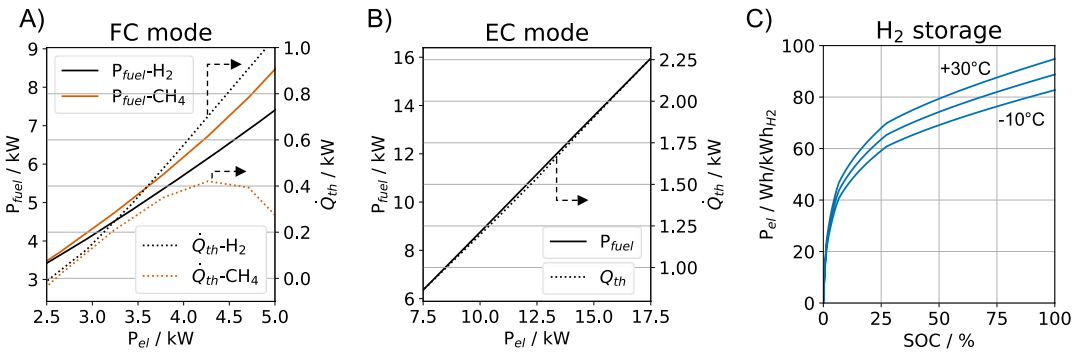

Fig. 4. Performance of a 5 kW / 15 kW rSOC-System, in its operation range for A) fuel cell mode with hydrogen and methane and B) electrolysis cell mode. Graph C) shows the energy demand at different temperatures relative to the hydrogen energy, for a storage allowing up to 300 bar at state of charge (SOC) equal to 1, for compression start temperatures of −10 °C, +10 °C and 30 °C.

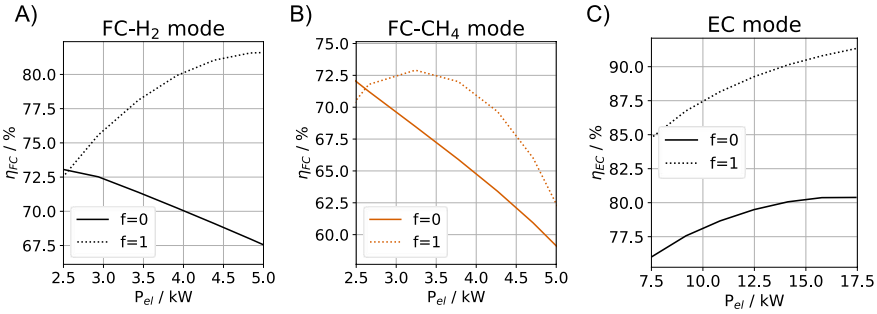

Fig. 5. Influence of thermal coupling on the efficiency (calculated according to equation (1) and (2)) of a 5 kW / 15 kW rSOC-System A) in fuel cell mode with hydrogen, B) in fuel cell mode with natural gas and C) in electrolysis mode.

the HT-HX heat is visible at high stack power of above 6 kW. However, the reformer heat consumption still increases, which results in the observed sharp decrease of extractable high temperature heat. The reformer heat demand increases in this model linearly with the stack current and since the power increases slower than linearly, the reformer heat increases faster than linearly with respect to the stack electric power.

In electrolysis mode (Fig. 4 B) the hydrogen production (P_{fuel}) is linear with respect to the electric system power consumption (P_{el}). In the illustrated case the thermal energy demand of the evaporator is shown separately from the system electric power consumption. The reason for the linear relationship is the here investigated operation below the thermoneutral point (described in section 2.1). In the thermoneutral point the heat generated by electric losses in the stack would be equal to the heat demanded by the endothermic electrolysis reaction and thus not require any additional electric heaters. An operation below this point means that heat must be provided to the stack by such external heaters, to maintain a constant operation temperature. An increased electrolysis power means higher internal heat production through electrical losses and by the same amount the power demand of electric heaters is reduced. Therefore, the slope of the curve stays constant, which is approximately equal to the constant inverse specific electricity consumption of stack plus heater. However, the heat losses of the system consist of a constant surface related part and a gas stream related part. The surface related part only depends on the geometry and temperature of the system. This means that it is a constant value decreasing the system efficiency. The gas stream related part, on the other hand, depends only on the flow rate, which is related to the system power. Therefore, it effects the slope of the efficiency-power curve but not its shape. The constant surface part of the heat losses makes the operation at high powers, close to the maximum limit of the system, favourable for reaching high efficiencies, since the relative contribution of the surface related constant heat loss decreases. This can be seen in Fig. 5 C. The thermal heat requirement ($\dot{Q}_{th}$, black dotted line) in the evaporator is mainly a function of the water mass flow, as the specific evaporation energy stays constant, influenced only by the internal heat recovery system. It shows the same trend as the hydrogen production however by a factor of 7.5 smaller.

Fig. 4 C shows the energy consumption in a hydrogen storage system as a function of the state of charge (SOC). The curves for different storage temperatures show a nearly logarithmic behaviour, although the compression is composed of four stages with intercooling. Furthermore, the increase of energy demand with increasing temperature is visible. A temperature increase from −10 °C to + 30 °C increases the compression energy demand by 25%.

4.2. Influence of thermal coupling on the efficiency of the rSOC-System

According to equation (1) and (2) the efficiency of the rSOC-System for the two extreme cases of thermal coupling, reflecting no and full coupling ($f = 0$ and $f = 1$), can be calculated. In hydrogen fuel cell operation, there is almost no difference in the efficiency at low electric power between the case of pure electric ($f = 0$) and fully thermally coupled efficiency ($f = 1$) as can be seen in Fig. 5 A. The reason is that, at low power all heat generated by the stack is needed to cover the system heat losses. As the load increases, the efficiency without thermal coupling ($f = 0$) decreases, as the internal stack resistance increase, which causes more generation of unused heat. However, if the generated heat can be used ($f = 1$) the system efficiency increases significantly with higher load, since the relative impact of heat losses decreases.

The FC-CH_4 operation (Fig. 5 B) looks for low powers like the hydrogen case. Right from the point where the two lines ($f = 0$ and $f = 1$) intersect (at 2.6 kW), there is waste heat available for external use ($\dot{Q}_{HT-HX} - \dot{Q}_{reformer}$ in equation (1) is positive), which increases the efficiency notably. However, the increase in efficiency is not as pronounced as in the case of hydrogen, as there is much less excessive heat available.

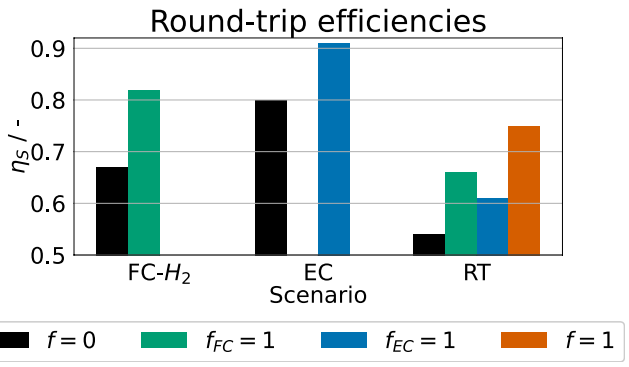

Fig. 6. Change of efficiency with thermal coupling for the operation as fuel cell (FC-H_2), electrolysis cell (EC) and in round-trip operation. The round-trip (RT) efficiency is calculated according to equation (4).

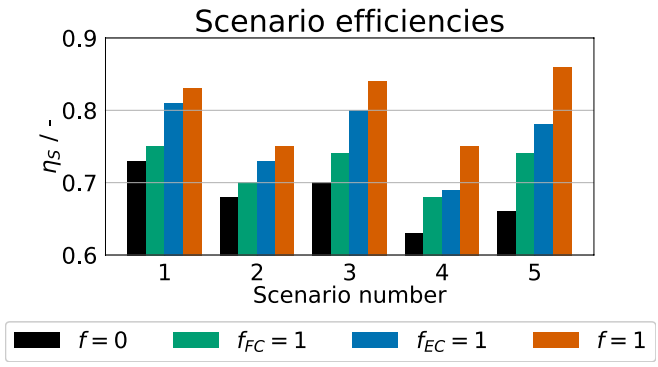

Fig. 7. Change of efficiency with different thermal coupling in scenarios of Table 3.

The reforming of methane to a hydrogen-rich gas mix uses most of the available heat. As discussed in 4.1 the available high temperature excess heat decreases at higher electric power and therefore the advantage of thermal coupling is the highest at moderate system load of 3.2 kW. At an operation below the intersection point at 2.6 kW, the internally generated heat is not sufficient to cover heat losses and the demand of the steam reformation. Therefore, this heat requirement reduces the efficiency in $f = 1$, while in $f = 0$ it is not taken into account.

In contrast to FC operation, the situation is different in EC operation. Here in both cases of thermal coupling the efficiency increases with increasing electrical system power, as can be seen in Fig. 5 C. This increase is because of the operation below the thermoneutral point, if this point would be crossed, the efficiency would start decreasing if the power is increased further. Below the thermoneutral regime the electrical losses, present as heat, reduce the electricity consumption of the high temperature heaters by the same amount. In addition, the relative contribution of losses to ambient have smaller impact and therefore the efficiency increases with increasing power.

In all cases of Fig. 5, besides low power in FC operation, the thermal coupling significantly increases the system efficiency. However, the benefit of thermal coupling in the FC- CH_4 operation is less pronounced.

With the definition for the round-trip efficiency according to equation (3) we can calculate the efficiencies of a system, that is operating in a closed hydrogen cycle. The results for this calculation are shown in Fig. 6, together with the efficiency in the nominal points from the Fig. 5 A and C. It is interesting that the round-trip efficiency, for the case of thermal coupling only in FC-H_2 operation (66%), is higher than in the case where there is a thermal coupling only in EC operation (61%). The efficiency increased by + 12% and + 7% respectively compared to the case $f = 0$. When we consider a thermal coupling in both operation modes ($f = 1$) the round-trip efficiency increases to 75%. Which is an increase of + 21% compared to an efficiency of 54% in $f = 0$. In case the rSOC-System's heat is used in district heating, heat pumps are a competing heat providing technology. In this case the efficiency increase of the FC operation is decreased by the factor of the heat pump's coefficient of performance, which is usually in the range of 2 to 3.5 depending on ambient conditions. This would result in a lower efficiency increase in FC operation of only + 4% to + 8% and the increase of the round-trip efficiency would be only + 3% to + 6%.

Table 3
Operation times in the different operation mode of the rSOC-System for the different scenarios for calculation of the scenario system efficiency.

Nr.	Operation time of mode in %		
	FC-H_2	FC-CH_4	EC
1		50	50
2		75	25
3	25	25	50
4	25	50	25
5	50		50

The calculation of open system scenarios is possible with the approach in equation (4) and the operation mode efficiencies from Fig. 5. For the scenarios of Table 3 the corresponding scenario efficiencies can be seen in Fig. 7. The scenario operation times in the different modes in Table 3 were chosen in a way that FC and EC operation are represented with similar shares. Basically, these operation times would have to be determined by an economic evaluation. The influence of the thermal coupling depends strongly on the share of operation time of the different modes in the different scenarios. In scenario 1 the impact of thermal coupling in FC operation ($f_{FC} = 1$) has a much smaller impact on the efficiency than in scenario 5. Since in scenario 1, with the FC-CH_4 operation, much less waste heat is available, than in scenario 5 where FC-H_2 operation is used. Scenario 2 shows the lowest increase of efficiency (+6%) due to thermal coupling, since the system is 75% of the time operated in FC-CH_4 mode, where the least coupling potential is present. Similarly, the FC coupling effect in scenario 1 is less pronounced. The efficiency increase, from $f = 0$ to $f = 1$, in all other scenarios than 2 is larger than + 10%. The scenarios where the FC-H_2 operation is present (3, 4 and 5), the presence of a heat sink ($f_{FC} = 1$) can significantly improve the efficiency in comparison to $f = 0$. In contrast of the here calculated scenarios to the round-trip efficiency, the impact of the thermal coupling in EC operation is more important than in FC operation. This is a consequence of the power difference of the FC (5 kW) and EC (15 kW) operation, which means that in the same timeframe bigger amounts of energy are converted. The round-trip scenario of Fig. 6 corresponds to approximately 70% FC-H_2 operation and 30% EC operation.

5. Conclusion

The results for the behaviour of the rSOC-System and the coupling to industrial processes allows us do make general conclusions on the operation of this system as well as on the implications for industrial integration. The possible conclusions drawn from these insights and results are structured here in the three most important categories.

Conclusion 1: Surrogate models. The results presented in Fig. 4 and discussed in section 4.1, gives a deeper understanding of the processes, that influence the efficiency of the rSOC-System. Furthermore, these curves can be used as computational inexpensive surrogate models in a steady state time series simulation. By including the dynamic system limitations, that are discussed in section 3.1, a quasi-dynamic simulation on basis of time series is possible for the rSOC-System.

Conclusion 2: Round-trip and scenario system efficiencies. In Fig. 5 we can see the high significance of the increase in efficiency caused by thermal coupling, of up to + 15%. This efficiency increase in the single operation modes leads to a high impact on the round-trip efficiency, which is shown in Fig. 6. From here we can conclude that a high

temperature heat sink in FC-H_2 operation is more important for the round-trip efficiency, than the availability of industrial waste heat in EC operation. However, having both couplings result in the highest round-trip efficiency. Furthermore, it could be economically beneficial at some times to operate the system in FC-H_2 operation at lower powers as the efficiency without thermal coupling is higher in this case. In addition, if there is only a low temperature heat sink present, the EC thermal coupling is of higher importance. In case of an open system no round-trip efficiency can be defined. However, in such a case the scenario system efficiency of equation (4) can be used. The calculations for different scenarios of Table 3 result in Fig. 7. Here it is worth to note, that in case of a high share of electrolysis time, the availability of a waste heat source is most important. The impact of waste heat utilisation from FC-H_2 operation is of a similar magnitude. In case of FC-CH_4 operation, the heat utilisation plays a much smaller role for the scenario system efficiency. This means, that according to the economical boundary conditions of the integration of an rSOC-System, the importance of an appropriate heat sink and heat source can vary tremendously. However, even with a low share of electrolysis time, the availability of a heat source is still important.

Conclusion 3: Implications for the integration of a rSOC-System to industry. Industries with suitable waste heat are discussed in section 2.2 and the important role of district heating networks as heat sinks is elaborated on. As the results of section 4.2 show, this possible thermal coupling in both operation modes (EC and FC), will result in high system efficiencies in all possible scenarios. This makes the integration of rSOC-Systems to industrial sites, from a viewpoint of efficiency, much more interesting, than nodes in the energy grid, where little thermal coupling can be achieved. In addition, if there is an industry with moderate temperature (>100 °C) waste heat, that operates also processes with high temperature heat demand, the rSOC-System could act as a heat pump and storage. Such a coupling would equal the scenarios of section 4.2 with $f = 1$, which means a significant increase of the conversion efficiency of +8% to +20%. However, such a pattern was not found in the investigated industries.

6. Outlook

In the results presented in section 4.2 the dependence of the thermal coupling efficiency on the operation scenarios is clearly visible. Throughout a whole year of operation, the possibilities for thermal couplings in industries vary, as the waste heat availability changes with production plans and due to batch processes. Furthermore, the heat demand in district heating networks, that can be used as a sink for the heat generated in FC operation, have a pronounced seasonal pattern. Not only the coupling availabilities, but also the energy prices decide which operation is most economical at each point in time. The scenarios of Table 3 are chosen in a way covering a wide spread of possible operation, that can occur in real life application. However, it is not clear how these operation scenarios correspond to the time dependent behaviour of heat availability and market prices. A future approach shall be based on a dynamic time series calculation for the coupling possibilities and energy prices. Here, for example a decision tree or an optimisation routine can decide for the most lucrative operation mode and system power. Also, the dynamic rSOC-system behaviour described in section 3.1 and the energy demand of the hydrogen storage system from Fig. 4 C must be integrated. Such a representation of the real application can determine the share of the different operations and correct the scenarios of Table 3 to be corresponding to real conditions. In addition, such a setup of the model enables the investigation of the impact of the dynamic constraints of the rSOC-system and a techno-economic assessment. To be able to perform these calculations, additional to the here presented data and models, the time series of electricity, heat and gas flow in industries (from work of Binderbauer et al. [37,38]) and time series for energy prices must be known.

CRediT authorship contribution statement

David Banasiak: Conceptualization, Methodology, Software, Validation, Formal analysis, Investigation, Writing – original draft, Writing – review & editing, Visualization. **Markus Gallaun:** Formal analysis, Investigation, Data curation, Visualization. **Christoph Rinnhofer:** Formal analysis, Data curation, Visualization. **Thomas Kienberger:** Conceptualization, Resources, Writing – original draft, Writing – review & editing, Supervision, Project administration, Funding acquisition.

Declaration of Competing Interest

The authors declare the following financial interests/personal relationships which may be considered as potential competing interests: Thomas Kienberger reports financial support was provided by Austrian Research Promotion Agency. Thomas Kienberger reports a relationship with Austrian Research Promotion Agency that includes: funding grants.

Data availability

Data will be made available on request.

Acknowledgements

The authors gratefully acknowledge the cooperation and exchange of knowledge with partners in the project FIRST, the Chair of Physical Chemistry at the Montanuniversität Leoben and the Institute of Thermal Engineering at the Technical University Graz.

Funding

This work was financially supported by the Austrian Research Promotion Agency (FFG) with public money from the Austrian Climate and Energy Fund, in the context of the project FIRST (Project Nr. 871700).

References

[1] Gerloff N, 2021. Comparative Life-Cycle-Assessment analysis of three major water electrolysis technologies while applying various energy scenarios for a greener hydrogen production, J Energy Storage 43 102759. doi: 10.1016/j.est.2021.102759.
[2] Smith L, Ibn-Mohammed T, Yang F, Reaney IM, Sinclair DC, Koh SL. Comparative environmental profile assessments of commercial and novel material structures for solid oxide fuel cells. Appl Energy 2019;235:1300–13. https://doi.org/10.1016/j.apenergy.2018.11.028.
[3] Zhao G, Kraglund MR, Frandsen HL, Wulff AC, Jensen SH, Chen M, et al. Life cycle assessment of H2O electrolysis technologies. Int J Hydrogen Energy 2020;45(43):23765–81.
[4] Reznicek EP, Braun RJ. Techno-economic and off-design analysis of stand-alone, distributed-scale reversible solid oxide cell energy storage systems. Energ Conver Manage 2018;175:263–77. https://doi.org/10.1016/j.enconman.2018.08.087.
[5] Reznicek EP, Braun RJ. Reversible solid oxide cell systems for integration with natural gas pipeline and carbon capture infrastructure for grid energy management. Appl Energy 2020;259:114118. https://doi.org/10.1016/j.apenergy.2019.114118.
[6] Srikanth S, Heddrich MP, Gupta S, Friedrich KA. Transient reversible solid oxide cell reactor operation – experimentally validated modeling and analysis. Appl Energy 2018;232:473–88. https://doi.org/10.1016/j.apenergy.2018.09.186.
[7] Frank M, Deja R, Peters R, Blum L, Stolten D. Bypassing renewable variability with a reversible solid oxide cell plant. Appl Energy 2018;217:101–12. https://doi.org/10.1016/j.apenergy.2018.02.115.
[8] Sorrentino M, Adamo A, Nappi G. Optimal sizing of an rSOC-based renewable microgrid. Energy Procedia 2019;159:237–42. https://doi.org/10.1016/j.egypro.2018.12.063.
[9] Hutty TD, Dong S, Lee R, Brown S. Long term energy storage with reversible solid oxide cells for microgrid applications. Energy Reports 2021;7:24–33.
[10] Hutty TD, Dong S, Brown S. Suitability of energy storage with reversible solid oxide cells for microgrid applications. Energ Conver Manage 2020;226:113499. https://doi.org/10.1016/j.enconman.2020.113499.
[11] Zhang Z, Zhou J, Zong Z, Chen Q, Zhang P, Wu K. Development and modelling of a novel electricity-hydrogen energy system based on reversible solid oxide cells and power to gas technology. Int J Hydrogen Energy 2019;44:28305–15. https://doi.org/10.1016/j.ijhydene.2019.09.028.

[12] Giap V-T, Kim Y S, Lee Y D, Ahn K Y 2020 Waste heat utilization in reversible solid oxide fuel cell systems for electrical energy storage: Fuel recirculation design and feasibility analysis J Energy Storage 29 101434. doi: 10.1016/j.est.2020.101434.
[13] Giap V-T, Lee YD, Kim YS, Ahn KY. A novel electrical energy storage system based on a reversible solid oxide fuel cell coupled with metal hydrides and waste steam. Appl Energy 2020;262:114522. https://doi.org/10.1016/j.apenergy.2020.114522.
[14] Mottaghizadeh P, Santhanam S, Heddrich MP, Friedrich KA, Rinaldi F. Process modeling of a reversible solid oxide cell (r-SOC) energy storage system utilizing commercially available SOC reactor. Energ Conver Manage 2017;142:477–93. https://doi.org/10.1016/j.enconman.2017.03.010.
[15] Mottaghizadeh P, Fardadi M, Jabbari F, Brouwer J. Dynamics and control of a thermally self-sustaining energy storage system using integrated solid oxide cells for an islanded building. Int J Hydrogen Energy 2021;46:24891–908. https://doi.org/10.1016/j.ijhydene.2021.03.136.
[16] Lamagna M, Groppi D, Nastasi B. Reversible solid oxide cells applications to the building sector. Int J Hydrogen Energy 2023. https://doi.org/10.1016/j.ijhydene.2023.03.387.
[17] Lamagna M, Ferrario AM, Astiaso Garcia D, Mcphail S, Comodi G. Reversible solid oxide cell coupled to an offshore wind turbine as a poly-generation energy system for auxiliary backup generation and hydrogen production. Energy Reports 2022;8:14259–73.
[18] Königshofer B, Boškoski P, Nusev G, Koroschetz M, Hochfellner M, Schwaiger M, et al. Performance assessment and evaluation of SOC stacks designed for application in a reversible operated 150 kW rSOC power plant. Appl Energy 2021;283:116372.
[19] Posdziech O, Schwarze K, Brabandt J. Efficient hydrogen production for industry and electricity storage via high-temperature electrolysis. Int J Hydrogen Energy 2019;44:19089–101. https://doi.org/10.1016/j.ijhydene.2018.05.169.
[20] Schwarze K, Posdziech O, Mermelstein J, Kroop S 2019 Operational Results of an 150/30 kW RSOC System in an Industrial Environment Fuel Cells. doi: 10.1002/fuce.201800194.
[21] Singer D V 2017 Reversible solid oxide cells for bidirectional energy conversion in spot electricity and fuel markets Doctoral Thesis Columbia University doi: 10.7916/D8V988P6.
[22] Sitte W, Merkle R (eds) 2023 High-Temperature Electrolysis IOP Publishing.
[23] Paczona D, Sejkora C, Kienberger T 2023 Reversible solid oxide cell systems as key elements of achieving flexibility in future energy systems. In: Sitte W, Merkle R (eds) High-Temperature Electrolysis. IOP Publishing, 19-1-19-32. https://doi.org/10.1088/978-0-7503-3951-3ch19.
[24] Kazempoor P, Braun RJ. Model validation and performance analysis of regenerative solid oxide cells for energy storage applications: Reversible operation. Int J Hydrogen Energy 2014;39:5955–71. https://doi.org/10.1016/j.ijhydene.2014.01.186.
[25] Motylinski K, Kupecki J, Numan B, Hajimolana YS, Venkataraman V. Dynamic modelling of reversible solid oxide cells for grid stabilization applications. Energ Conver Manage 2021;228:113674. https://doi.org/10.1016/j.enconman.2020.113674.
[26] Gruber-Glatzl W 2021 Abwärmekataster III Steiermark: Öffentlicher Kurzbericht https://www.aee-intec.at/awkst-abwaermekataster-steiermark-p278 Accessed 24 Aug 2022.
[27] ©2002 – 2022 Dassault Systèmes Dymola: Multi-Engineering Modeling and Simulation based on Modelica and FMI Modelica version 3.2.3 3DS Dassault Systems https://www.3ds.com/products-services/catia/products/dymola/.
[28] Peters R, Frank M, Tiedemann W, Hoven I, Deja R, Kruse N, et al. Long-term experience with a 5/15kW-class reversible solid oxide cell system. J Electrochem Soc 2021;168(1):014508.
[29] Zeng Z, Qian Y, Zhang Y, Hao C, Dan D, Zhuge W. A review of heat transfer and thermal management methods for temperature gradient reduction in solid oxide fuel cell (SOFC) stacks. Appl Energy 2020:280 115899. https://doi.org/10.1016/j.apenergy.2020.115899.
[30] Preininger M, Stoeckl B, Subotić V, Mittmann F, Hochenauer C. Performance of a ten-layer reversible Solid Oxide Cell stack (rSOC) under transient operation for autonomous application. Appl Energy 2019;254:113695.
[31] Saarinen V, Pennanen J, Kotisaari M, Thomann O, Himanen O, Di Iorio S et al. 2021 Design, manufacturing, and operation of movable 2 × 10 kW size rSOC system Fuel Cells. doi: 10.1002/fuce.202100021.
[32] Preininger M, Stoeckl B, Subotić V, Hochenauer C. Characterization and performance study of commercially available solid oxide cell stacks for an autonomous system. Energ Conver Manage 2020;203:112215. https://doi.org/10.1016/j.enconman.2019.112215.
[33] Khan MZ, Mehran MT, Song R-H, Lee S-B, Lim T-H. Effects of applied current density and thermal cycling on the degradation of a solid oxide fuel cell cathode. Int J Hydrogen Energy 2018;43:12346–57. https://doi.org/10.1016/j.ijhydene.2018.04.175.
[34] Bell IH, Wronski J, Quoilin S, Lemort V. Pure and pseudo-pure fluid thermophysical property evaluation and the open-source thermophysical property library CoolProp. Ind Eng Chem Res 2014;53:2498–508. https://doi.org/10.1021/ie4033999.
[35] Linde AG Datasheet: Hydrogen technologies.The Ionic Compressor 90 MPa – IC90. 43486081 0614 – 1.0,5 – Subject to change. http://donar.messe.de/exhibitor/hannovermesse/2017/A488848/hydrogen-technologies-the-ionic-compressor-90-fo-eng-358503.pdf Accessed 19 Oct 2022.
[36] Ferrero D, Lanzini A, Leone P, Santarelli M. Reversible operation of solid oxide cells under electrolysis and fuel cell modes: Experimental study and model validation. Chem Eng J 2015;274:143–55. https://doi.org/10.1016/j.cej.2015.03.096.
[37] Binderbauer PJ, Kienberger T, Staubmann T. Synthetic load profile generation for production chains in energy intensive industrial subsectors via a bottom-up approach. J Clean Prod 2022;331:130024. https://doi.org/10.1016/j.jclepro.2021.130024.
[38] Binderbauer P J Ganymed: Application for Industrial Load Profile Simulation www.ganymed.ga.

Applied Energy 371 (2024) 123639

Contents lists available at ScienceDirect

Applied Energy

journal homepage: www.elsevier.com/locate/apenergy

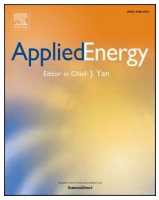

A comparative analysis of the economic feasibility of reversible hydrogen systems based on time-resolved operation optimisation

David Banasiak *, Thomas Kienberger

Montanuniversitaet Leoben, Chair of Energy Network Technology, Franz-Josef-Straße 18, Leoben, AUSTRIA

HIGHLIGHTS

- Techno-economics of reversible hydrogen systems in uncertain market conditions.
- Mathematical optimisation of system operation including dynamic limitations.
- Market price range allowing the application of reversible hydrogen systems.
- Effect of fluctuations, gas grid fees, storage costs, integration and degradation.
- Analysis of two possible spatial system configurations for rSOC and PEM systems.

ARTICLE INFO

Keywords:
rSOC
PEM
Power-to-gas-to-power
Sector coupling
Energy efficiency
Techno-economic

ABSTRACT

The expansion of fluctuating renewable energy production, such as wind and PV, increases the mismatch to consumption. Power-to-Hydrogen-to-Power (PtHtP) systems are believed to be a key for balancing under and overproductions. PtHtP systems can provide temporal and spatial flexibilities and among them reversible solid oxide cells (rSOC) are a promising technology. They combine production of hydrogen and power in the same electrochemical stack. This generates a financial and environmental benefit since less resources are necessary for enabling both Power-to-Hydrogen and Hydrogen-to-Power. This work investigates the application of rSOC systems in comparison to reversible PEM systems consisting of electrolysis and fuel cell unit. In the present studies time-resolved optimization is employed for simulation of the optimal operation of the PtHtP technologies in different market price conditions for electricity, hydrogen and natural gas and with coupling to industry and district heat. Both systems have a zone of market prices, that allows for a positive economic performance over lifetime. The electricity-hydrogen price difference in this zone is in the range from −83 €/MWh to 133 €/MWh depending on the scenario. Furthermore, the electricity price fluctuations are found to have the major impact on the profitability. By studying the influence of gas grid fees, one finds that local compressed hydrogen storages can be used only for very short storage timescales up to a few hours. Finally, the derivation of application conditions, that are suitable for the two different spatial kinds of reversible hydrogen systems – spatially concentrated and delocalized and the two technologies – rSOC and PEM, is made.

1. Introduction

Many countries committed to reducing the emissions of anthropogenic greenhouse gases [1] and limiting the global rise of average temperature [2]. The increase of renewable production is undoubtedly one of the major pillars, allowing a transition of the energy sector towards low greenhouse gas emissions and thus building a foundation for the transition of industry, transport, and building sectors.

In many regions wind and PV-power will play a major role in renewable production, as e.g. Sejkora et al. showed in the analysis of technical renewable potentials for the case of Austria [3]. Sources, like tidal, run-of-river hydro, wind and solar energy, may have partly predictable production. However, these predictions relate to uncertainties of weather forecasts requiring dispatchable generation to balance the mismatch of predicted production and demand. The potential for performing such dispatch actions by pumped hydro and dispatchable renewable sources, like geothermal and biomass, is much smaller than needed. This leads to over or under production that must be covered by

* Corresponding author.
E-mail addresses: david.banasiak@unileoben.ac.at (D. Banasiak), thomas.kienberger@unileoben.ac.at (T. Kienberger).

https://doi.org/10.1016/j.apenergy.2024.123639
Received 30 January 2024; Received in revised form 23 April 2024; Accepted 2 June 2024
Available online 15 June 2024

different strategies.

For dealing with short-term fluctuations, we need strong electrical energy grid enhancement. Short-term imbalance requires technologies like pumped hydro, compressed air or batteries. The long-term fluctuations with a monthly to seasonal periodicity require for both power-grid expansion and seasonal storage capacities. Also pumped hydro storages can contribute to this long-term balancing, however with geographical limitations [4]. The gas grid is already nowadays fulfilling exactly this job of balancing differences in energy demand and availability on large spatial and long temporal scales. Therefore, many believe that the coupling of electricity and gas grid can provide the needed future flexibilities. Traupmann et al. [5] studied Power-to-Gas (PtG) and PtGtP in former coal-fired power plant sites and concluded, that overloads in the grid can be mitigated by adjusting operations to the volatile generation situation in the grid. In Europe, there are plans to transform the natural gas grid partly into a hydrogen grid [6]. Cerniauskas et al. [7] conclude that a reassignment of the natural gas grid to hydrogen can be done and is the cheapest option to offer a hydrogen distribution system. Nazir et al. [8] review storage, transport and distribution in a H_2-economy. They identified compressed H_2 on the road as the early-stage transport path, followed by pipelines as underground storages and more consumers appear. Lord et al. [9] estimate the costs of hydrogen underground storage to be 0.04–0.06 $/kg for aquifers and 1.61–2.76 $/kg for hard rock and salt caverns. These cheap storage capacities enable underground gas storages to provide long-term and seasonal cycling economically. Due to the flexibilities that PtGtP offers to the energy supply system and the plans to transform the natural gas grid to a hydrogen grid the focus in the present study is on GtP and Power-to-Hydrogen-to-Power (PtHtP) systems. This sector coupling can be achieved by fuel-cell (FC) and electrolysis cell (EC) technologies.

1.1. State of the research with respect to flexible sector coupling technologies

The electrical efficiency of electrochemical fuel cells depends on the technology and can reach 50% up to 60% [10] for Polymer Electrolyte Membrane (PEM) and up to 65% [10,11] for Solid Oxide (SOFC). The advantage of electrochemical fuel cells is their applicability for smaller scales than gas turbines. Thus, they are enabling a better integration to the energy system close to consumers, making the waste heat accessible for heating purposes even in the absence of district heating grids. This potential for integrations is also shown by Salam et al. [12] who investigate a combined cycle power plant based on fuel cells and report electrical efficiencies of 74%. Also Scaccabarozzi et al. [13] attested efficiencies of 75.7% for a natural gas operated system based on a SOFC in combination with a Brayton cycle for CO2 capture.

The production of hydrogen can be accomplished on different paths. Zainal et al. [14] conclude that solid oxide electrolysis cells (SOEC) outperform other technologies in terms of electric efficiency, but yet have drawbacks in terms of technological readiness and costs. Furthermore, they find anion exchange membranes (AEM) and electrified steam methane reforming to be promising alternatives. Mohebali et al. [15] compare alkaline electrolysis (AEL), PEM electrolysis and SOEC in an integrated system to produce H_2, electricity and desalinated water. Schwarze et al. [16] report on the upscaling plans for a SOEC system to 2.5 MW, with an electrical efficiency of 84%. The ramp rates of the system considered by Schwarze et al. [16] is below 3 min for shutdown and below 15 min for switching from part to full load.

These works lead us to the conclusion that PEM and SOEC/SOFC technologies seem very promising to be efficient sector coupling technologies.

The combination of EC systems with FC systems or gas turbines enables PtHtP and a variety of such systems was already proposed in the literature. However, Rad et al. [17] employed an optimisation of technology choice based on timeseries to studied optimal energy supply solutions for rural areas. They found EC and FC systems to be not yet competitive and may only be used as backup technologies. Skordoulias et al. [18] investigated PEM electrolysis and combined heat and power gas turbine plants as PtHtP technologies. They conclude on the price limits for natural gas and CO_2 necessary to make the integration of green hydrogen into the gas turbine plant economically viable by using static prices. Furthermore, support and market schemes to boost the implementation of the technology are proposed. Bukhari et al. [19] studied PtHtP employing PEM electrolysis and combined cycle gas turbines as conversion technologies on basis of time resolved operational and design optimisation. They found that hydrogen is economically better suited for large-scale energy storage than batteries. Yue et al. [20] review the PtHtP path including H_2 storage. They conclude that capital and H_2-production costs are not yet competitive for a wide introduction. Reduced system costs, improved efficiency and durability are keys for enabling an economical operation. Risco-Bravo et al. [21] reviewed the development of power-to-hydrogen-to-power (PtHtP) technologies and attested that high efficiency, sector coupling capability and reduction of grid dependency can help to exploit the potentials of these systems. Escamilla et al. [22] make static investigations of three electrolysis technologies (PEM, AEL and SOEC) and three H_2 storage pathways (compressed, liquefied and in metal hydrides) with a gas turbine closing the PtHtP cycle. They conclude that the round-trip efficiency is critical for the viability of the H_2 energy storage path.

Not only separated EC/FC systems can perform PtGtP operations. Reversible solid oxide cells (rSOC) systems combine both power and hydrogen production in one system and are thus a very promising conversion technology. Furthermore, rSOC systems offer fuel flexibility, allowing them to operate with H_2 as well as CH_4. These system employs the same electrochemical stack as SOEC systems. However, additional and different BoP components and a more sophisticated design process are required. The heat exchangers and blowers must be able to operate under both electrolysis and fuel cell conditions, with very different mass flows and the power electronics must allow a bidirectional operation. The rSOC systems enable PtHtP with round trip efficiencies above 50%.

A report on the operation of a highly efficient rSOC pilot system by Schwarze et al. [23] with a power of 150/30 kW in EC/FC operation gives high hopes for the technological readiness and the integration to industrial environment. It is shown that with steam being fed to the electrolysis an efficiency of 84% is possible. In fuel cell operation the natural gas was converted to electricity with an efficiency of 50%. Laboratory measurements for quantification of the performance of rSOC stacks were performed by Königshofer et al. [24]. Peters et al. [25] performed long-term experiments with a 15/5 kW rSOC-system, with fuel side recirculation to reach high efficiencies of 70% in EC and above 60% in FC operation. Furthermore, they determined the time required for switching between operation modes as 3 min from EC to FC and 13 min from FC to EC. Santhanam et al. [26] arrived at round trip efficiencies of 53%–60% based a model that implements the stack performance through measurement data. These works have proven, that rSOC systems can act as large-scale flexible load and power source in the energy grid and that they can effectively combine both conversion directions of PtHtP in one unit with high round-trip efficiencies. Hutty et al. [27] investigated the economic application abilities of reversible solid oxide cells for microgrids and performed a techno-economic comparison to battery energy storage systems. They used time resolved operational and design optimisation and found that H_2 storage systems for microgrids may be favoured only if a high self-sufficiency ratio is required and low PV capacities are available. Wang et al. [28] investigate PtXtP based on rSOC systems, where different forms of the hydrogen carrier are compared. They attested that the rSOC system is a key enabling the penetration of fluctuating renewable production, coupling of energy sectors and decarbonization of the transport sector and chemical industry. Similarly, PEM stacks may be used in reversible systems as Paul et al. [29] reports and Ito et al. showed with a laboratory system [30]. However, there are no recent reports on the progress of reversible PEM systems, which is why they will not be considered

further in the present work.

Electrochemical-cell-based PtGtP systems are today hardly economical due to the high investment costs. However, the systems are still undergoing rapid progress in development and the costs are expected to drop soon. This investment cost development was studied by Böhm et al. [31] for AEL, PEM and SOEC based on technological learning. They show that the investment costs for these three technologies will decrease significantly with market penetration in the future. Soon PEM will have lower costs than AEL and SOEC shows the largest potential for cost reduction, making them competitive in investment cost around 2050. Furthermore, SOEC, according to Zhao et al. [32] and Gerloff et al. [33], is the more environmentally friendly electrolysis technology in comparison to AEL and PEM. Since they base on the same electrochemical stack, the costs for a rSOC system are expected to be only slightly higher than the ones for SOEC [34].

1.2. Structure of the work and research questions

We found that literature covering reversible electrochemical systems, based on different technologies and evaluations of economics are present. The before mentioned investigations on economic system performance either employ static methods or time resolved operational optimisation. A shortcoming of these approaches is the lack of a systematic investigation of the uncertain market prices' influence on the techno-economic performance. That is why the present study analyse the influence of different market prices on the techno-economic results obtained from optimized plant operation. Furthermore, most studies concern PtGtP technologies that employ either hydrogen and power generation in separate locations (delocalized reversible systems) or having them concentrated in one location (concentrated reversible systems). Nevertheless, no comparison of the applicability of these approaches for energy system level is done.

The present study aims at investigating the economic application limits for PtHtP systems based on rSOC and PEM-EC/FC electrochemical stacks. The The PEM system with short reaction time, for changing load and operation mode, is chosen in contrast to the slow rSOC systems. The latter systems have fuel flexibility due to high temperature, therefore CH_4 and H_2 are considered. CH_4 operated rSOC systems are not carbon neutral, but have a high potential for CO_2 capture, which can be easily separated from the CO_2-H_2O flue gas stream, as shown by Scaccabarozzi et al. [13]. The methodology in this publication is based on the techno-economic analysis of the optimal operation found for different variations of future hourly resolved energy market prices. In this way system dynamics and temporal price fluctuations can be investigated. With given hourly-resolved timeseries for industrial electricity consumption, waste heat availability and district heat demand, the influence of different integrations to such industrial and residential energy systems is investigated. A novelty of the present methodology is the computational inexpensive implementation of the system degradation, which decreases the profitability within the system's lifetime. Furthermore, the optimal sizing of the local H_2 storage in the presence of a gas grid is investigated. Thus, the conditions which would be necessary for enabling local H_2 storage can be derived. This is fundamental for concluding on the applicability of delocalized and concentrated reversible systems.

The three research questions the present study aims to answer are:

(1) What are the influences on the reversible zone?

The reversible zone is introduced as the market price range for which the electrochemical PtHtP systems are economically viable. Followed by investigating different influences on this reversible zone, which allows us to answer questions (2) and (3).

(2) Do we need spatially concentrated or delocalized reversible systems?

The benefits related to placing EC and FC unit in one site (concentrated) in comparison to a placement in different locations (delocalized) are analysed. The distinction for reversible systems into concentrated and delocalized will be made in the conclusion. Connected to this question is the analysis of the local storage of H_2 in comparison to a connection to a gas grid infrastructure.

(3) Do rSOC or PEM-EC/FC systems perform better?

A holistic picture of the performance of rSOC and PEM-EC/FC systems is created. Enabling a conclusion on the best ways of utilizing both technologies.

(4) What is important for rSOC system engineering?

This question concerns the importance of dynamic parameters for the application of the rSOC-system.

The present work starts by presenting the modelling approach used to represent both the rSOC and PEM-EC/FC based PtHtP system with compressed local H_2 storage and gas grid connection. The rSOC system model includes the ramp dynamics, as the transition from cold to warm state and between different operation modes is much slower than in PEM systems. This is followed by an explanation of the PtHtP system's interactions with energy markets for electricity, CH_4, H_2 and district heat and with industrial sites. Consequently, the market prices and industrial energy streams, that play a role thereby are shown. The quantitative evaluation of the proposed PtHtP systems is performed based on simulations of the optimal unit-commitment for lowest energy prices, via mathematical optimization on an hourly basis. Based on these optimal energy costs, the economics of the PtHtP systems, including degradation, are evaluated by means of the net present value method. The results section starts by identifying the market price zone, when the operation of rSOC systems is economically viable, which is called the reversible zone. Furthermore, the influence on this reversible zone is studied for: electricity price fluctuations, the gas grid fee, H_2-storage costs and the integration scenario. Additionally, the sensitivity of the techno-economic calculation concerning the investment parameters is discussed.

2. Methodology

This section describes the employed models, calculation scenarios and the approach for quantitative evaluation of rSOC and PEM based reversible systems.

2.1. The model of the reversible systems

As reversible systems, that can generate hydrogen and reversibly convert it back to electricity, PEM-EC/FC- and rSOC-systems, which are shown in Fig. 1, are considered. The PEM-EC/FC system consists of two sets of electrochemical stacks with separate balance of plant components, one for electrolysis (EC) and the second for fuel cell (FC) operation. The rSOC system is based on a bidirectional electrochemical cell stack and bidirectional balance of plant components. Both systems include a compressed H_2 storage system and access to a gas grid providing CH_4 or H_2.

In FC operation these reversible systems are supplied on the stack's hydrogen side with either H_2 and in the case of the rSOC system optionally also with CH_4. The option in which the rSOC system operates only with H_2 is denoted as rSOC-H2. When CH_4 is used, denoted as rSOC, a reformer upstream the stack entrance provides a pre-reformed synthetic gas mix. There are two pathways of providing fuel to the system:

- FC-H2 – operation as fuel cell using hydrogen from a pressure vessel that was produced in electrolysis operation.

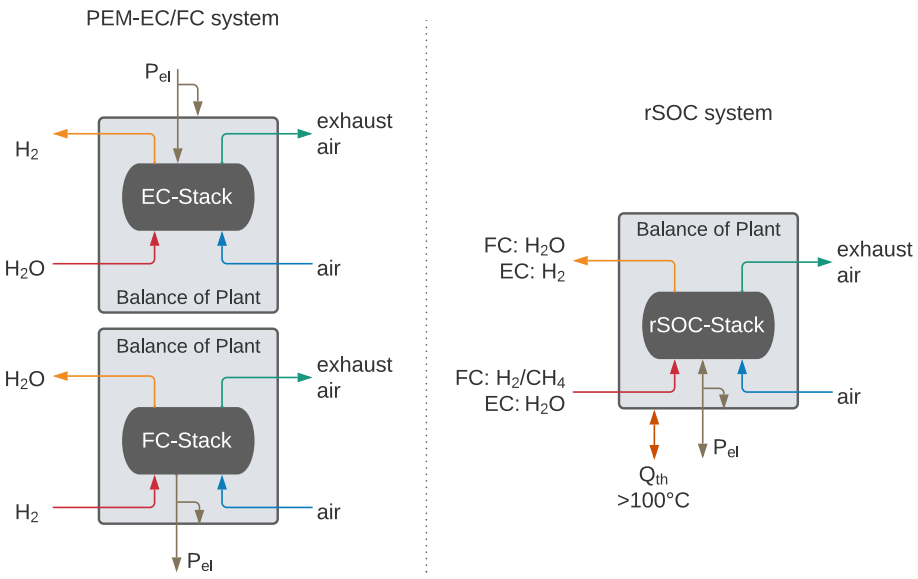

Fig. 1. Flowsheet of the considered reversible systems: PEM-EC/FC and rSOC system.

- FC-GG – operation as fuel cell with fuel gas from gas grid infrastructure: In the case of the rSOC system the grid gas is methane and for the rSOC-H2- and the PEM-EC/FC system it is hydrogen.

In EC operation, water is supplied on the hydrogen side and ambient air is used for thermal management on the oxygen side of the stack.

- EC - operation as electrolysis cell: Hydrogen is produced with electrical energy from the grid. The produced hydrogen can either be sold to a market with an assumed constant H_2 price or stored in a compressed gas storage on site for later FC operation.

In addition to these active operation modes, the system can be either in a cold standby (CSB) or warm standby (WSB) mode. For the PEM-EC/FC system CSB and WSB are equal and do not include any energy consumption. It is assumed in the calculations with hourly time resolution, that the PEM-EC/FC system has no dynamic limitations (Table 1 column PEM). However, start-up times of up to a few minutes are realistic. The rSOC systems needs a cooldown phase for a switch to CSB. In this time the operation temperature (750 °C) is decreased to ambient temperature, during which 20% of the WSB electric power is used. A heat-up phase, for changing to warm operation modes, with related energy consumption, is required (Heat-up and cool-down time in Table 1). Furthermore, costs for this transition (ramp warm cost) are assigned, which are fixed to a value that corresponds to reaching the end of the stack lifetime after 6000 such cycles at system costs of 1500 €/kW. In the WSB mode, the system is electrically kept at the operation temperature (see Table 1 for warm standby). In WSB the system can be switched to an active operation (EC, FC-H2 and FC-GG) within a few minutes, while consuming electricity or hydrogen like in operation but without output. For the transition between any two warm states transition costs (Ramp EC, Ramp FC-H2 and Ramp FC-GG in Table 1) are inclueded, representing a system devaluation at costs of 1500 €/kW for 150.000 and 300.000 transitions. These low values are based on Schefold et al. **[35]** who describe that only little or no degradation is expected for load switching and transitions. The effect of transition to EC is higher according to Nuggehalli **[36]**.

A detailed description of the model of the rSOC system in Fig. 1 is given by Paczona et al. **[38]**. In this publication, the detailed modelling process and choice of engineering parameters can be found, including heat exchanger design pinch point difference, considered pressure drops and thermal and electrical control strategies. In addition to modelling details, the application in industries and the thermal coupling possibilities with conversion curves and underlying processes are described by Banasiak et al. **[39]**. Further ideas concerning the system coupling possibilities are described by Vialetto et al. **[40]** who investigate a rSOC system in a paper mill.

The part load conversion curves considered here were calculated by Banasiak et al. **[39]** for a modelled system with a nominal power of 5/15 kW in FC/EC operation, with EC operation below the thermo-neutral point. This model was validated with the results of Peters et al. **[25]** and shows a similar behaviour as reported by **[41]**. This rSOC system determines the systems' EC/FC power ratio for the calculations. The efficiency in FC-H2 operation at nominal power of 5 kW is 65%, considering only the produced electricity, and 79% when the high-temperature waste heat is additionally utilized, as can be derived from Fig. 2 A). One can see in Fig. 2 B) that at the nominal power of 17.5 kW the efficiency is 81%, if P_{el} and Q_{th} are met electrically, and 91% when Q_{th} is provided by free waste heat. The part-load energy conversion behaviour of the PEM stack is represented by the three points of the piecewise linearization given in Table 2. These part load data sets are scaled up to the nominal EC system power of 23.0 MW, which is used in the simulations (see subsection 2.5). The system dimension of 23.0 MW electrical power in electrolysis operation arises from the integration to the industry and district heating network (see discussion in section 3.2.3) and is considered in all scenarios, if not explicitly stated differently.

Table 1
System dynamic parameters.

Parameter	rSOC	PEM
Heatup power kW/kW$_{EC}$**	0.365	0
Warm standby in kW/kW$_{EC}$**	0.008	0
Heat-up and cool-down time in min	120	0
Ramp-to-EC time in min	13 [23,25,37]	0
Ramp-to-FC time in min	3 [23,25,37]	0
Ramp warm cost in €/kW$_{EC}$**	0.25*	0
Ramp EC cost in €/kW$_{EC}$**	0.01*	0
Ramp FC-H2 cost in €/kW$_{EC}$**	0.005*	0
Ramp FC-GG cost in €/kW$_{EC}$**	0.005*	0

* Josef Schefold et al. **[35]** suggests no degradation due to cycling of the rSOC-stack, however low costs to prevent unrealistic optimization results are included.

** kW/kW$_{EC}$ - power relative to installed electrolysis power.

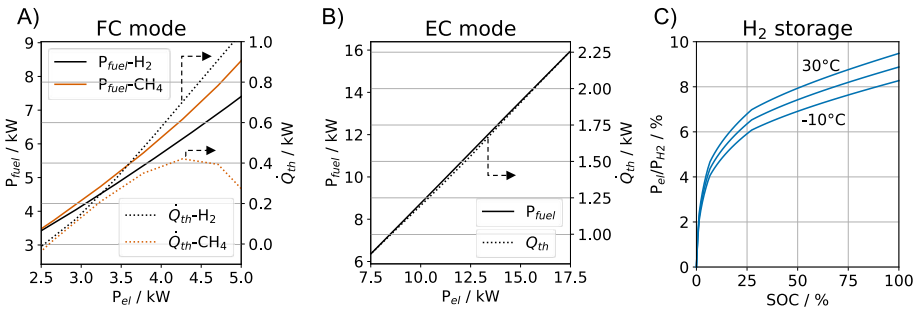

Fig. 2. Energy conversion curves for the rSOC-System and specific energy consumption of the compressor for the H_2 storage [39].

Table 2
PEM part-load points for conversion efficiency from electricity to H2 and back (estimated on a report of the Danish energy agency and Siemens Energy [42,43]).

Parameter		Value	
Load-fraction	0.15	0.4	1.0
efficiency	0.27	0.71	0.51

2.2. Interaction of the PtGtP system with grid infrastructure and industrial sites

The present research considers reversible systems with a H_2 storage that can interact with grid infrastructure for electricity, natural gas, hydrogen, and district heating. Furthermore, the systems can interact with industrial sites with given electrical and district heat demand as well as with available industrial waste-heat. In such a setup, multi-revenue streams are possible by using fluctuations in energy prices, selling hydrogen, self-consumption of produced electricity and providing heat to a district heating grid.

The considered PtHtP systems have different ways of interacting with district heat infrastructures and industry. In the present work, three coupling scenarios are considered, representing three levels of interaction between the rSOC system and peripheral systems, as illustrated in Fig. 3 and described below. The reversible system can either be a single plant combining EC and FC operation or spatially separated plants with specific EC or FC units.

Reference case (RC): In this scenario, the reversible system interacts solely with the grid for electricity and gas. The system is subject only to the volatility of the energy market for electricity and grid gas. It can be operated in EC operation to produce hydrogen at low electricity prices and FC operation during high prices. The FC operation can be fuelled by either previously produced and stored hydrogen or gas from the gas grid. The grid gas is CH_4 in the case of the rSOC system and H_2 for the rSOC-H2 and the PEM-EC/FC system. In the case of rSOC-H2 and PEM-EC/FC systems, the hydrogen price for gas bought from the grid is equal to the remuneration for hydrogen sold to the market. The price for electricity or gas purchased from the grid includes the fee for the grid operation (for further details on the considered energy prices see section 2.3)

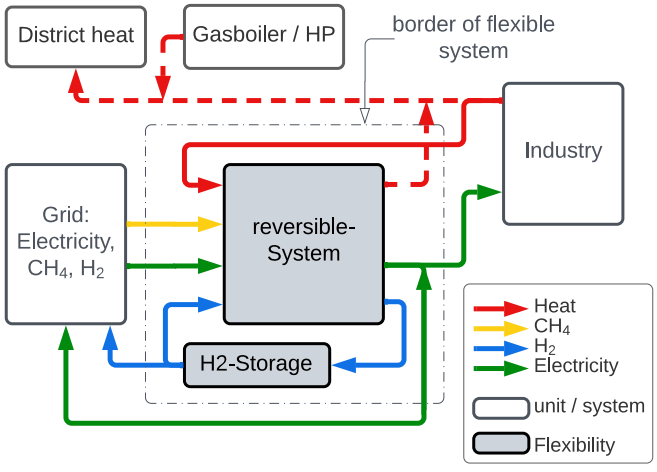

Fig. 3. Illustration of the energy flows to and from the rSOC system in a set up with energy grid, local H_2 storage, industry and district heating network.

Industrial coupling (IC): This scenario extends the RC scenario by adding the timeseries for electricity demand and waste heat availability of an industrial site, which are described in section 2.4. The direct industrial consumption of FC produced electricity reduces the amount of grid electricity which includes grid fees and therefore generates a higher profit than selling it to the market. Furthermore, industrial waste heat, if available at a given timestep and of suitable temperature, can be used for providing steam to the EC operation of the rSOC and rSOC-H2 system. This increases the electric efficiency by >10% [44]. Systems with a nominal FC power larger than the power consumed by the industry cannot fully benefit from the self-consumption. Similarly, a nominal EC power that requires more steam, than can be produced by industrial waste heat, loses advantage of the coupling.

Industry with district heating network (IDH): The IDH scenario extends the IC scenario by including the heat demand of a district heating system (the timeseries is discussed in section 2.4). In this scenario heat generated by the rSOC- and rSOC-H2 system can be utilized if the district heat demand is not fully covered by industry. However, the district heat demand reduces the available waste heat from the industry, which reduces steam production for electrolysis operation.

An overview of the variations of the calculation scenarios, including investigated technologies, market prices and integration cases, is given in Table 3 and illustrated in Fig. 4. A more detailed description is given in Appendix A.

2.3. The energy market and district heat prices in the base price scenario

In this section, the scenario base prices for electricity (c_{el}), grid gas

Table 3
Scenarios for the investigation of reversible systems.

Nr.	Name	Description
1	Technology	• rSOC – FC operation with CH_4 • rSOC-H2 – FC operation with H_2 • PEM-EC/FC
2	Shift Electricity-price	Variation of electricity price by a constant shift, the H_2 sales price is unchanged. This results in a change electricity-H_2-price spread.
3	Fluctuation Modification	Amplitude in Fourier spectrum of electricity price multiplied by a factor (fm)
4	Gas grid fee	Difference between H_2 sales price and H_2 purchase price (ggf). This difference can arise from grid fees, governmental support and H_2 storage costs in the grid.
5	Integration	RC, IC and IDH

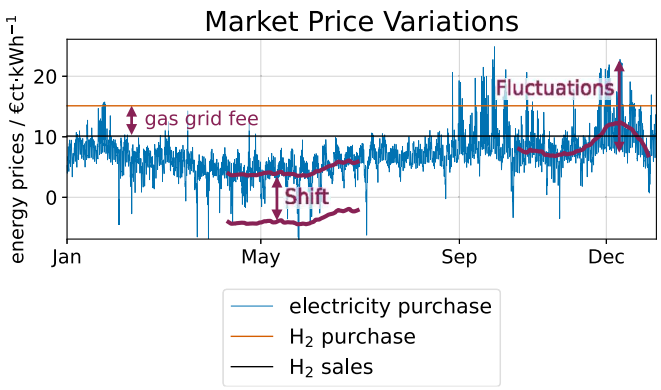

Fig. 4. Illustration of the variations performed for the energy market price (Nr. 2,3 and 4 in Table 3).

(c_{gg}) and hydrogen (c_{H2}) is discussed. The prices are considered in hourly resolution for the location of Austria. Furthermore, the approach used to derive the district heating price from these time series is shown. The energy market prices can be seen in Fig. 5 for the considered price-scenario years 2030 and 2050. Traupmann et al. **[5,45]** provide more details about modelling these electricity and natural gas prices, which are considered as base scenario in this work. Historic timeseries for the year 2020 **[46]** are modified to match the expected development of the average electricity price **[47]**, which are influenced by CO_2-prices, the share of renewable energy sources, and extreme price events **[48]**. The time series for day-ahead spot-market electricity purchase prices in 2030 has a minimum of −72.6 €/MWh and a maximum of 249 €/MWh with a mean value of 68.2 €/MWh. In 2050 the minimum price is −101 €/MWh, the maximum 335 €/MWh and the mean value 87.8 €/MWh. The remuneration for electricity sold to the grid is lower than the purchase price. The difference is the grid fees, which is 9.08 €/MWh **[49]** for Styria in Austria. The reversible systems therefore can generate higher profits, by supplying self-demand in comparison to market trading. The electricity market in 2050 is expected to be more influenced by the volatility of renewable production, which results in a higher variation between minimum and maximum prices, whereas the mean price only slightly increases. The price for gas from the grid consists of a mixed price for natural gas, biogas and hydrogen according to Traupmann et al. **[5]**. The gas price modelling approach is based on quarter-hourly resolved historical data for 2020 **[50]** and includes scenario assumptions for future gas routes including renewable gases. This price has little variability from 32.4 €/MWh to 46.1 €/MWh and a mean value of 36.7 €/MWh in the scenario year 2030. In 2050 the price varies between 33.8 €/MWh to 48.1 €/MWh with a mean of 38.2 €/MWh. The price for hydrogen that can be sold by the operator of the rSOC system to a market is set to the constant value of 101.2 €/MWh and 61.4 €/MWh for the years 2030 and 2050 respectively. Due to the uncertainty of the H_2 price in future yet to be established markets, the analysis is based on the variation of the spread between hydrogen and electricity price. For the rSOC-H2 and the PEM FC/EC scenarios, the grid gas price is set equal to the H_2 price. For grid gas purchase todays gas grid fee of 1.059 €/MWh **[51]**, for Styria in Austria, is added on top of the gas market prices. The price duration cures in Fig. 4 show the increase of volatility for the electricity price. Furthermore, one can see here clearly, that in 2030 the H_2 price is mostly above the electricity price and in 2050 it is in the lower middle region.

In the scenario IDH, with the heat demand shown in Fig. 6, the price for heat (c_{dh}) sold to the district heating network is required. This price is determined by taking the minimum of the grid gas price (c_{gg}) and the electricity price (c_{el}) divided by the COP of a generic heat pump according to eq. (1) for each time step. In the calculations, the COP of the electric heat pump is set to the constant value of 3.0. By determining the district heat price in this way, a direct competition in the heat market is assumed, where the cheapest technology, either gas burners or electric heat pumps, define the heat price.

$$c_{dh} = min\left(c_{gg}, \frac{c_{el}}{COP}\right) \quad (1)$$

Due to the uncertainty of all future energy prices the sensitivity analysis in section 3.2 investigates the influence of average prices of all considered energy carriers and vary the magnitude of fluctuations as well as grid gas prices (for details about these variations see Appendix A).

2.4. Industrial electricity demand and waste heat implementation

Two industry types, with different operational patterns and magnitude of energy streams were chosen. This shall allow us to compare the influence of the industry type on the operational regime of the rSOC system. For the IDH scenario, a timeseries for the district heat consumption of a typical Austrian small city which is housing various industries is generated.

The time series for the electricity consumption and the waste heat were generated for the generic examples of a packaging glass-producing company with a production of 10 t/h and for a brewery with a beer

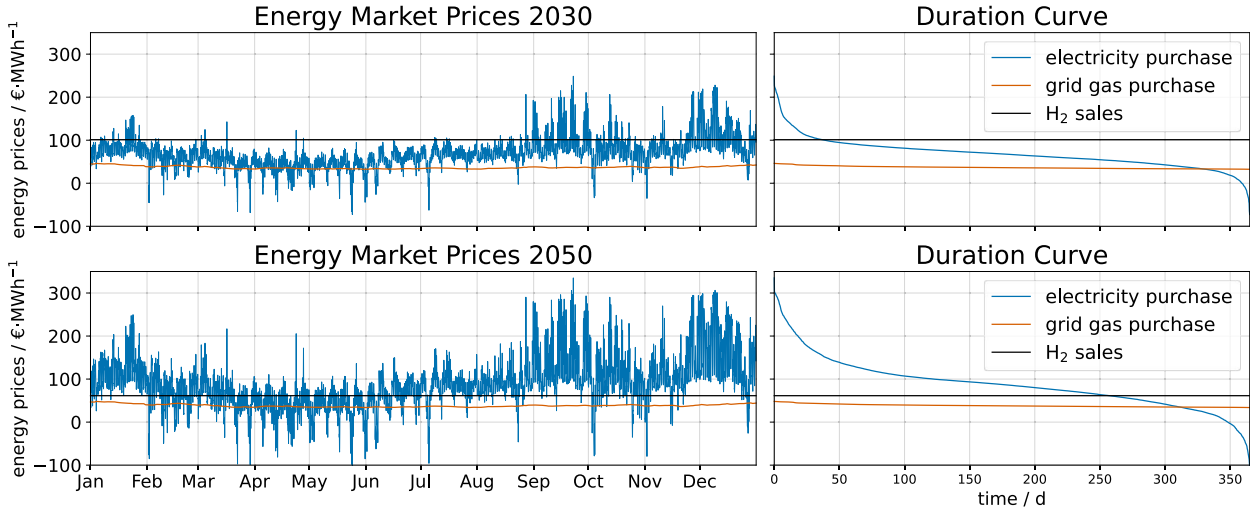

Fig. 5. Energy market prices and duration curves for the scenario years 2030 and 2050 for the energy carriers electricity (blue), grid gas (orange) and hydrogen (black) according to Traupmann et al. **[9]**. (For interpretation of the references to colour in this figure legend, the reader is referred to the web version of this article.)

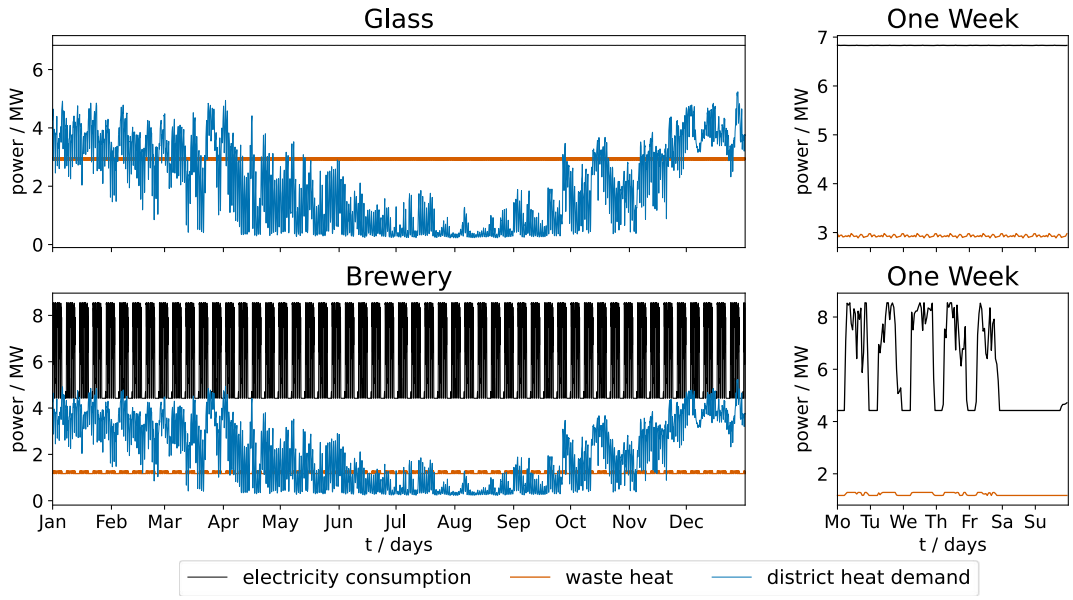

Fig. 6. Energy streams in the selected industrial sites of glass production and a brewery and the district heat demand of a residential area. The two graphs on the right show the weekly profile for the industries that was added up to obtain the total timeseries for a year.

production of 20,800 l/h and 80 employees. The synthetic energy time series were generated with the industrial load profile simulation software Ganymed **[52,53]**, which is based on surveys of industry sites in Austria and physical modelling of main aggregates. This software delivers the electricity consumption for the whole plant for one week as is shown in Fig. 6 on the right. This is considered a representative week and added up to represent the full year shown on the left in Fig. 6. The electricity consumption for glass is 6.83 MW with a variation of <0.01 MW and for the brewery on average 6.00 MW with a minimum of 4.42 MW and a maximum of 8.55 MW. The waste heat calculated by Ganymed is reduced to represent the utilizable heat for 1 bar (100 °C) steam production as a feed for the rSOC's EC operation. In this reduction, technical limitations of heat exchange, like pinch point temperature difference and dew points in flue gas, are included. This utilizable waste heat is shown in Fig. 6. For the glass production, a waste heat temperature of 380 °C with an energy stream of 2.90 MW varying only slightly between 2.89 MW and 2.98 MW, is considered. The brewery has an average waste heat stream of 1.20 MW varying between 1.17 MW and 1.29 MW. Unused waste heat is released to the environment, this means that the reversible system has the freedom but not necessity to use the available heat.

The time series for the district heat demand is calculated according to the guidelines for gas consumption for heating purposes **[54]**. For this approach, a temperature time series is required, which is generated with the web interface of renewables.ninja **[55]** for the year 2019 for the considered city in Austria. The yearly district head demand in this location is estimated to be 18 GWh. The resulting time series for the heat demand in the district heating network is shown in Fig. 6 on the left in blue. It is assumed here that industrial waste heat firstly covers this demand and only the reminder is available for integration to EC operation. One can see, that in the case of the glass industry, the industrial waste heat covers the base load of the district heating most of the time. From May to November a substantial amount of waste heat cannot be used by the district heating network. The picture looks different for the brewery, which produces much less waste heat. Therefore, the waste heat excess is much reduced.

2.5. Optimization model and model parameters

An optimization algorithm for simulating the optimal operation of the PtGtP system in different market price conditions is employed. The optimization model incorporates the following: the connection of the different assets, as shown in Fig. 3; the implementation of the conversion behaviour and dynamic limitations according to section 2.1; the implementation of the exogeneous energy prices from Fig. 4 and the exogeneous industry energy streams from Fig. 6 with a time resolution of 1 h.

It was decided to employ a MILP formulation to represent the system to be optimized. The conversion curves or Fig. 3 were transformed into piecewise linear sections with the number of points shown in Table 4. For the PEM system the 0.4 and 1.0 part load efficiency points from Table 2 are chosen. The number of points was chosen in such a way as to give a good run-time performance and accuracy. Test calculation runs have shown that including the point for the part load value of 0.15 does not have observable influence on the results. The limitations for the discrete choice of the operation mode and the way of hydrogen usage result in another set of integer linear equations. Furthermore, the dynamic limitations from Table 1 are formulated as integer linear boundary conditions. The boundary conditions for the H_2 storage are linear equations reflecting the limitations of being empty or full and the state of charge. The latter parameter is used for calculation of the corresponding compression energy demand. Due to the small overall contribution of the compression energy, the mass flow partial load behaviour of the compressor is not considered. The resulting model has the variables: system electrical power; operation mode (EC, FC-H2, FC-GG, WSB, CSB), hydrogen utilization (store or sell) and storage size. Depending on the interaction scenario (according to section 2.2), the EC operation can utilize industrial waste heat or provide heat from FC operation to district heating, according to the availability and demand at the specific point in the timeseries.

The target function (c_{energy}) of the optimization consists of a

Table 4
Parameters in the optimisation problem.

Parameter	Value	Variation tested
Timestep size in min	60	30
NPPL* for EC mode	2	3
NPPL* for FC and CH4 mode	3	2, 4
NPPL* for the compressor	2	3

* Number of Points in the Piecewise Linearization.

summation over all timesteps, as shown in eq. (2(2) and includes the following cost contributions: electrical energy consumption ($E_{el,con}$) times energy price (c_{el}) in EC-operation, WSB-phase and during heat-up- and cool-down-phase (according to Table 1); energy content (LHV) of consumed grid gas ($\dot{Q}_{gg,con}$) times its price (c_{gg}); energy content (LHV) of H_2 sold to market ($\dot{Q}_{H2,m}$) times its price (c_{H2}); thermal energy sold to a district heating grid ($\dot{Q}_{dh,g}$) times its price (c_{dh}); number of ramp events to a warm operation state (EC, FC-H2 and FC-GG, Table 1) times costs per ramp events ($c_{ramp,i}$) of the kind *i*. Furthermore, the annual specific storage investment costs (c_{st}) times the storage size (Q_{st}) are added to the target function. The specific storage investment costs need to be adjusted, so that the annual storage investment costs are adjusted to the length of calculated time series in relation to storage-lifetime.

$$c_{energy} = \sum_t \left(c_{el} \bullet E_{el,con} + c_{gg} \bullet \dot{Q}_{gg,con} - c_{H2} \bullet \dot{Q}_{H2,m} - c_{DH} \bullet \dot{Q}_{DH,g} \right) + c_{s+t} \quad (2)$$

$$c_{s+t} = \sum_i c_{ramp,i} \bullet n_i + c_{st} \bullet Q_{st} \quad (3)$$

The optimization aims to minimize the value of the target function (c_{energy}), which represents the total costs of energy supply including energy supply, storage investment and transition costs. The optimization model is formulated in Python in the language of Pyomo [56,57] and solved with Gurobi optimization [58]. From the found minimum for c_{energy} the storage costs and transitions costs (c_{s+t}) are subtracted, so that one arrives at the total energy costs in €/y which are used in further calculations ($c_{energy,rev\text{-}sys}$). The storage costs are investment costs and not revenue and therefore they are considered in the CAPEX costs of eq. (11).

2.6. Including degradation to the PtGtP systems

The curves of Fig. 2 and values in Table 2 are adopted in the following way to represent the conversion behaviour of a system that underwent degradation. For this purpose introduce the degradation parameter d is introduced. At d = 0 the system is at the initial non-degraded state. For d larger than zero, degradation reduces the electrical conversion efficiency.

In EC operation it is assumed that the electric power that can be applied to the stack stays the same, but the output of hydrogen is reduced (see eq. (4)). Therefore, also the production of steam can be reduced (see eq. (5)).

$$P_{fuel}^{EC,d} = P_{fuel}^{EC,0} \bullet (1 - d) \quad (4)$$

$$\dot{Q}_{th}^{EC,d} = \dot{Q}_{th}^{EC,0} \bullet (1 - d) \quad (5)$$

In FC-H2 and FC-GG operation a similar assumption is made as in EC operation, namely the input energy flow stays constant, which is in this case the fuel gas. As a result of degradation, the output electric energy is reduced by the degradation parameter, as is depicted in eq. (6). By the same amount, that the electric energy is reduced the amount of heat produced increases. By adding a heat utilization efficiency (η_{heat}) which is set to 0.8, one arrives at eq. (7).

$$P_{el}^{FC,d} = P_{el}^{FC,0} \bullet (1 - d) \quad (6)$$

$$\dot{Q}_{th}^{FC,d} = \dot{Q}_{th}^{FC,0} + P_{el}^{FC,0} \bullet d^* \eta_{heat} \quad (7)$$

Simulations for the optimized operation with parameter variation for the electricity-gas-price spread, grid gas price and degradation factor are performed. Based on these results one can fix the coefficient a_1 of the linear relation between the annual profit (p_a) and the operation time and degradation according to eq. (8). A more detailed description and the values for a_1 are given in Appendix B.

$$\Delta p_a(d, h) = a_1 \bullet h \bullet d \quad (8)$$

2.7. Investment calculation

For the economical evaluation, the method of the net present value for the investment costs and cash flows is employed. In this calculation, the investment costs of the different units in the system and the cashflow during the system's operation are needed. Furthermore, assumptions about the change in the value of money units over the operation time are made.

The scale-dependent investment costs of a SOEC system are taken from Böhm et al. [31]. The power-specific costs are fixed to 1000 €/kW (2030) and 400 €/kW (2050) which represents a system with a size of 20 MW. Similarly, the PEM-EC system is approached and the costs are fixed to 600 €/kW (2030) and 250 €/kW (2050). The costs for reversible systems are derived from the EC system costs and with a power ratio of three between EC and FC, according to the limitations of the chosen rSOC system. The resulting system investment costs in relation to the EC system costs are shown in Table 5. The costs for the rSOC system are lower than the sum of EC and FC system, since after adjustment stack, power electronics and balance of plant components can be used in both operation modes. The resulting price for the reversible systems is shown in Table 5.

The specific compressor cost is set to the value shown in Table 6 in accordance with Tahan et al. [59] adapted for the known power of electrolysis. The ultimate H_2 storage costs in Light-Duty Fuel Cell Vehicles are estimated by the U.S. Department of Energy [60] (see Table 6), this same value is applied as costs for specific investment costs of stationary H_2 storage.

The optimal operation of the reversible systems is determined by solving the optimization model of section 2.5. The annual profit (p_a) generated by the optimal operation of the reversible system is the difference between the annual energy costs with and without the application of such a system, according to eq. (9). The costs without a reversible system are the result of the costs from energy consumption without flexibility. In the RC scenario, this is zero and with industrial size it is equal to the industrial electricity demand times the price, summed for all timesteps. The costs with reversible system are calculated from energy consumption of the optimal operation according to the optimization model.

$$p_a(d) = c_{energy,no.rev-sys} - c_{energy,rev-sys}(d) \quad (9)$$

The optimization result for the annual profit depends on the degradation parameter d, as was discussed in section 2.6. The degradation (d_{lt}) over the system lifetime (lt) is set equal to 10% for all systems. Then the actual degradation (d) can be calculated according to eq. (10) by using a linear temporal behaviour.

$$d(t) = \frac{d_{lt}}{lt} \bullet t[y] \quad (10)$$

The return on investment with the method of the net present value is used for the evaluation of economics. In this way the system's economic performance over the lifetime (lt) of the main components can be evaluated. To stress the fact, that in this calculation not a deprecation period and interests but the lifetimes and inflation rate of money (i) are considered and called the Return on Lifetime (ROL, see eq. (11)). By

Table 5
Specific investment costs for EC-, FC system and reversible systems in percent of the EC system investment costs.

Technology Power	EC 20 MW	FC 6.7 MW	Reversible 20/6.7 MW
PEM in %EC	100	33	133
SOC in %EC	100	33	125

Table 6
Investment parameters.

	Parameter	Value
CAPEX	rSOC price in €/kW_{PEC}**	1250 (2030) 500 (2050)
	PEM-EC/FC price in €/kW	798 (2030) 333 (2050)
	Storage price* in €/kWh	8 [60]
	Compressor price in €/kW_{EC}**	100 [59]
	rSOC lifetime (lt_{stack}) in y	10 [43]
	PEM EC/FC lifetime in y	20 [43]
	Storage lifetime* (lt_{st}) in y	20
	Compressor lifetime (lt_c) in y	20
	Interest (inflation) rate (i) in %	5
	Degradation over liftetime (d_{lt}) in %	10

* The storage price and its lifetime is not only relevant for the investment calculation but also for the operational and design optimization, where the optimal storage size is determined.
** €/kW_{EC} – price relative to installed electrolysis power.

setting this ROL in relation to the investment cost of the system (CAPEX) one arrives at the relative Return on Lifetime (rROL) as can be seen in the eq. (12). The investment parameters used for the calculation of the ROL and rROL are compiled in Table 6. A rROL of zero or higher means that the system pays of its CAPEX during lifetime. A negative rROL-value leads to negative economics respectively.

$$\boldsymbol{ROL} = -\boldsymbol{CAPEX} + \sum_{t}^{lt} \frac{\boldsymbol{p_a}(\boldsymbol{d}(\boldsymbol{t}))}{(\boldsymbol{1}+\boldsymbol{i})^{t}} \tag{11}$$

$$\mathbf{rROL} = \frac{\boldsymbol{ROL}}{\boldsymbol{CAPEX}} \tag{12}$$

3. Results

In this section the definition of the reversible zone, scenario-specific influences on this zone and the results of the sensitivity analysis with respect to investment parameters, are presented.

3.1. Zone for reversible operation with respect to the electricity-hydrogen-price spread

The graphics in Fig. 7 show the change of the rROL and the operation-mode, with the average spread between electricity and hydrogen sales price ($\Delta_{el,H}$) according to eq. (13).

$$\Delta_{el,H} = \frac{\boldsymbol{1}}{\boldsymbol{8760}} \sum_{t=1}^{8760} (\boldsymbol{c_{el}}(\boldsymbol{t}) - \boldsymbol{c_{H2}}(\boldsymbol{t})) \tag{13}$$

This price spread was varied by increasing or lowering of the electricity price. A resulting positive spread means, that the average price for electricity is higher than for hydrogen and a negative spread means in average higher hydrogen than electricity prices. Consequently, for a positive spread the FC operation and for negative spread the EC operation is dominant (see Fig. 7 B to D). At electricity prices much lower than the hydrogen sales price ($\Delta_{el,H} < -60$ €/MWh for 2030) only systems for pure EC operations are economically viable, as the FC operation is rarely chosen. At a positive spread ($\Delta_{el,H} > 10$ €/MWh for 2030 and $\Delta_{el,H} > 50$ €/MWh for 2050) the FC operation dominates, as can be seen in Fig. 7 B, and a system only capable of operating in this mode is economically viable. In these market price regions, both reversible systems, the rSOC system and the PEM-EC/FC system are not economically competitive to single-mode systems since the investment cost are 25 (33) % higher for the rSOC (PEM-EC/FC) system than for single-mode systems (Table 5).

The region, in between the two regions of extreme operational choice of eighter pure EC or pure FC operation, was found to be the **reversible zone**. The limits for this reversible zone are determined in such a way,

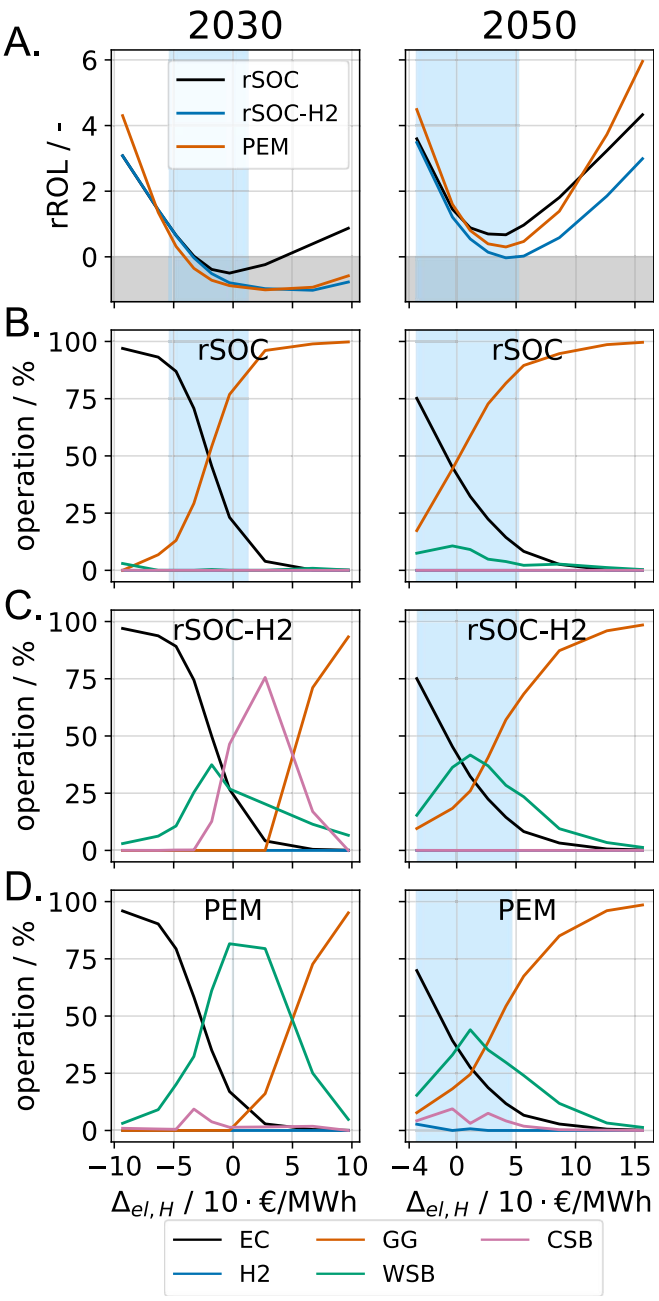

Fig. 7. Dependence of the rROL (A.) and operation shares (B.-D.) on the electricity-H_2-price spread ($\Delta_{el,H}$) for a rSOC, rSOC-H2 and PEM-FC-EC system, with blue highlighted reversible zones. (For interpretation of the references to colour in this figure legend, the reader is referred to the web version of this article.)

that EC and FC operation each is contributing 10% of the operation time, which does not yet say that it is economical.

For 2030 there is only a very small reversible zone and only for the rSOC system, from spreads between −50 €/MWh to 10 €/MWh and an even smaller zone with positive rROL. Since the positive rROL reversible zone is very small (Fig. 7 A), the probability that in 2030 exactly such spreads occur is small. Within this reversible zone the influence of the chosen technology is marginal.

In the year 2050 the PEM system performs better and beats the rSOC system for price spreads below 0 €/MWh, as is visible in Fig. 7 A. Even though the PEM system has a lower EC efficiency the high price fluctuations in 2050 and the fast reaction time, enables enough profitable operation time. Together with lower investment costs the PEM-system outperforms the rSOC systems up to 0 €/MWh. However above this

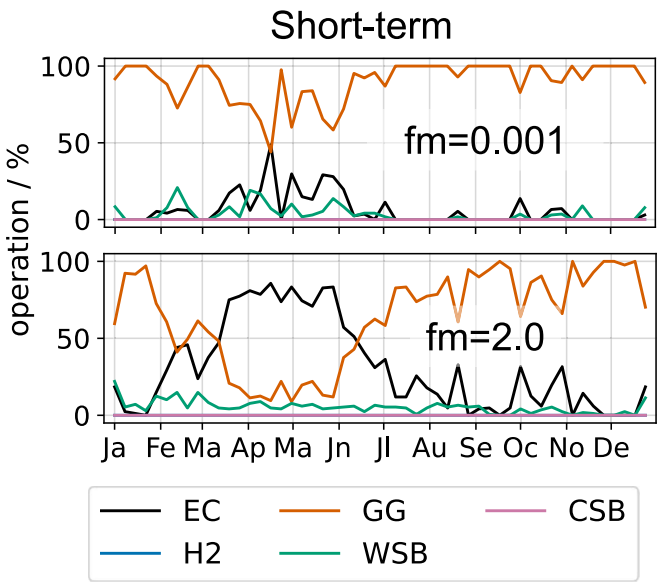

Fig. 8. Effect of fluctuation magnitudes (fm) in different time domains (periodicities: "Overalll" 1 h to 8760 h, "Long-term" 168 h to 8760 h, "Mid-term" 168 h to 12 h and "Short-term" 1 h to 12 h) on the rROL (top) and number of operation mode changes (bottom).

spread, the rSOC system performs better in the reversible zone (higher rROL), because it can operate with grid gas that is cheaper than H_2. Furthermore, it was found that in EC operation the system operates more than three-fourth in full load. In FC operation however the part load share varies from 0 to 100% in different scenarios.

Overall one finds that, for an electricity-H_2-price gap between −50 €/MWh and 10 €/MWh for 2030 and from −40 €/MWh to 50 €/MWh for 2050 a reversible zone exists. The reversible zone in 2050 is significantly wider than in 2030 which is because of price fluctuations. This means, that it is much more likely that future energy electricity and hydrogen prices will lie within this reversible zone.

Furthermore, it is found that PEM and rSOC technology perform differently under changed market price spreads and price fluctuations, which comes mostly from the conversion efficiencies and investment cost and not from the system dynamics. A contribution to the difference between the 2030 and 2050 scenarios comes from the different magnitudes of price fluctuations, which will be studied closer in section 3.2.1.

3.2. Influences on the reversible zone

In this section the influence of electricity price fluctuations and grid gas price on the reversible zone (introduced in section 3.1) and the competition between rSOC and PEM systems is investigated.

3.2.1. Influence of temporal fluctuations in the electricity price timeseries

Here the influence of the magnitude of periodical fluctuations in three different time domains on the rROL and on the numberer of switching events between operation modes is studied. The amplitude of the fluctuations in the base timeseries as introduced in section 2.3 is multiplied by the fluctuation multiplier (fm). This happens for the four respective time periods (overall, Long-term, Mid-term and Short-term) in the Fourier spectrum, as described in detail in Appendix A.

Exemplarily one can see in Fig. 8 that decreased short-term fluctuations (fm = 0.001) lead to less diversity in the choice of operation modes. In the shown specific scenario, FC-GG operation dominates. When increasing these fluctuations (fm = 2.0), the EC and FC operation are more balanced over the year. The same is true for mid- and long-term fluctuations. The yearly accumulated distribution of operation for overall increased fluctuations, can be seen together with the rROL in Appendix C, Fig. A3. Mid-term fluctuations have a very similar influence like short-term fluctuations. The more fluctuations, the more the overall diversity in operation choice increases. Increased long-term fluctuations increase the seasonal specialization for FC operation in winter and EC operation in summer.

Fig. 9 shows that higher fluctuations at any timescale lead to a strong increase of profitability (rROL). The effect of short-term is the strongest followed by long-term and then by mid-term fluctuations. The number of ramp actions from one operation mode to another correlates positively with mid- and short-term fluctuations and negatively with long-term fluctuations. The change of fluctuations on all timescales (Overall) has the strongest influence and is approximately the sum of the effect of the separately changed three timescales.

Furthermore, Fig. 9 shows that the effect on the PEM system is significantly stronger than for the rSOC systems. The reason is that the larger marginal gap for turning PEM systems on is less relevant at higher fluctuations. This marginal gap is a consequence of the efficiency gap between EC and FC operation.

One can see in Fig. 10 that the highlighted reversible zone is much wider and has a wider positive rROL-zone for increased fluctuations than for the base case shown in Fig. 7. Therefore, in the case of high fluctuations, it is highly likely that the future energy prices will lie in the reversible zone and installation of reversible systems will be lucrative. Furthermore, one can see that the PEM system profits stronger from increased fluctuations and is then the better choice for a wider region.

3.2.2. Influence of gas grid fees

This section discusses the influence of the cost difference between H_2 purchase and sales price which is equal to the gas grid fee. The gas grid fee is added on top of the energy base price (section 2.3) of H_2 and CH_4. This fee determines whether purchasing H_2 from the grid is more lucrative than investing into a local H_2 storage. High grid fees suppress FC operation with grid gas, so that operation with locally stored H_2 is more lucrative. The result for the reversible zone for practically disables gas grid connection is shown in Fig. 11. Here, one can see that, the rROL is drastically reduced compared to Fig. 7 A and a wide market price range in the reversible zone does not allow economical operation. This is because of the storage investment costs and compression energy demand. The rROL is positive only for an electricity-hydrogen-spread below 20 €/MWh, when the electrolysis operation is dominant (as shown in Fig. A4). Then storing a part of produced H_2 for conversion to electricity is lucrative due to the higher price fluctuations of 2050 in comparison to 2030. This allows for an overlap of the average price zone when both EC and FC operation are profitable (see section 3.2.1 for more details concerning fluctuations).

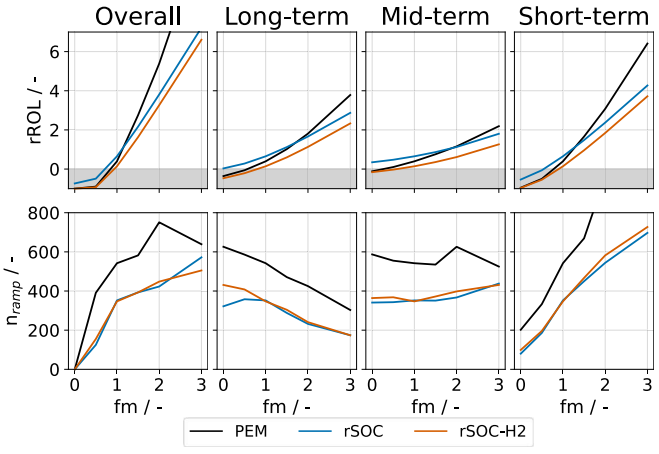

Fig. 9. Weekly share of operation in the different modes for the rSOC system in 2050 with daily to hourly fluctuations suppressed (fm = 0.001) and enhanced (fm = 2.0).

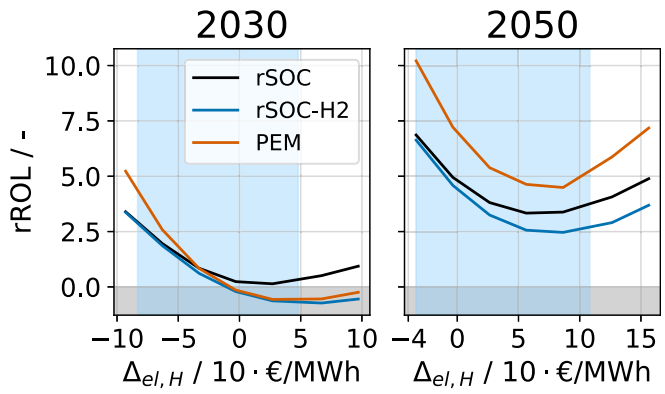

Fig. 10. Dependence of the rROL on the electricity-H2-price spread for a rSOC-, rSOC-H2 and PEM-FC-EC system under increased electricity price fluctuations (fm = 2.0), with blue highlighted reversible zone. (For interpretation of the references to colour in this figure legend, the reader is referred to the web version of this article.)

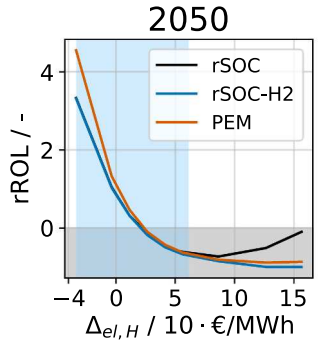

Fig. 11. Dependence of the rROL on the electricity-H2-price spread for a rSOC-, rSOC-H2 and PEM-FC-EC system at a grid fee of 123 €/MWh, with blue highlighted reversible zone. (For interpretation of the references to colour in this figure legend, the reader is referred to the web version of this article.)

The decrease of rROL and change in operation times can be seen in Fig. 12 for the year 2050. As the grid fee increases one can see a decrease of grid gas operation (GG) and increase of operation with locally stored H_2 (H2). However, also the time in warm standby increases. For a H_2-storage price of 8.0 €/kWh (1.0 €/kWh), the local storage (H2) and gas grid (GG) operation have the same operation time share at a grid fee of 33 €/MWh (15 €/MWh), as shown in Fig. 12. The corresponding optimal H_2 storage size is 0.12 GWh (530 GWh), which can be emptied in only 16 (70) hours of FC operation. The grid fee at this point is a multiple of today's grid fee of 1.059 €/MWh **[51]** for Styria in Austria. The levelized costs of aquifer underground storage facilities of around 2 €/MWh according to Lord et al. **[9]**, have to be added to the grid fee of Styria, since such large scale storage technologies need to be connected to the grid to allow long term H_2 storage. At a grid fee equal to this sum of current grid fee and levelized underground storage costs of 4 €/MWh the optimal size for local H_2 storage is 0.02 GWh (0.170 GWh). This shows that under current conditions it is worth to store H_2 locally only for very short timescales for less than three hours of FC operation. If the storage investment cost is reduced to 1 €/kWh the time for supplying the FC operation increases to 22 h. In Appendix E the influence of the storage investment costs is looked at more closely. There one can see that highly decreased storage costs would be necessary for allowing profitable systems under high gas grid fee conditions.

Finally, one can say that storing H_2 locally in pressure vessels for more than on an hourly basis is not an economical option and the presence of gas grid connection is crucial for a wide economical reversible zone.

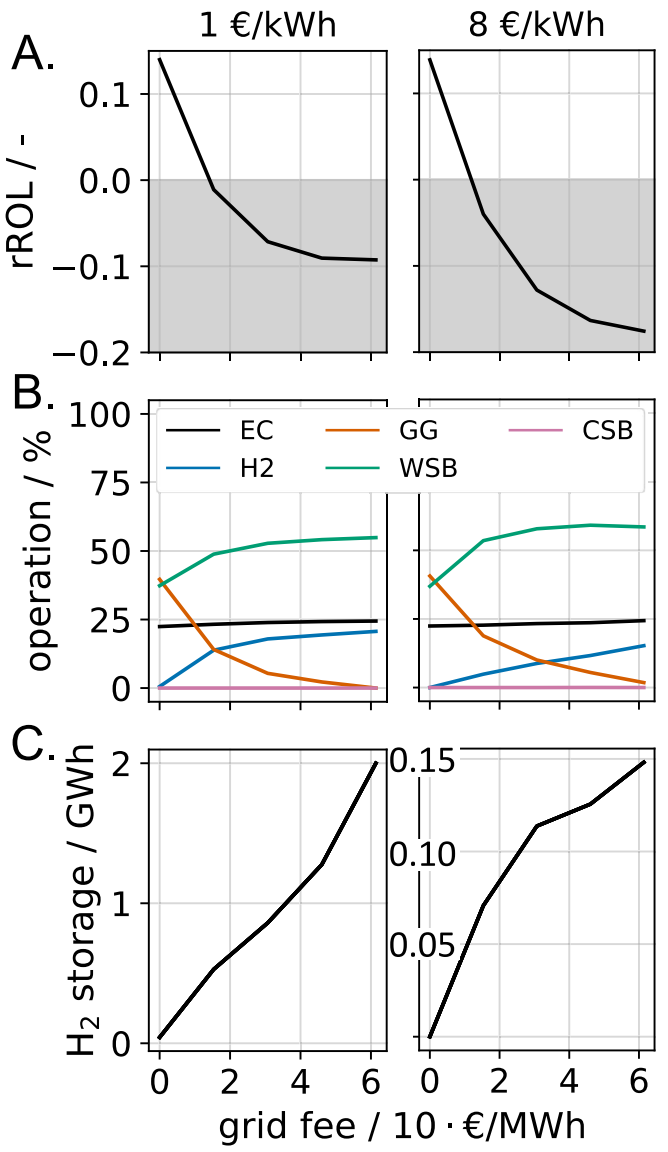

Fig. 12. Influence of the grid fee for two specific storage investment prices (1 and 8 €/kWh), in the scenario year 2050 for the 23 MW rSOC-H2 system. The influence is shown for the parameters: A. rROL, B. operation shares and C. optimal H_2-storage size.

3.2.3. The possibilities of rSOC-industry coupling and ideal rSOC system size

The benefit of coupling to industrial sites can arise from the two ways of coupling: Firstly, the utilization of industrial waste heat in EC operation. Secondly, the self-consumption of produced electricity and shifting of electricity purchase to cheaper timesteps. First, the optimal scales for the systems from the side of waste heat availability and energy demand of the industry are examined. This analysis will be followed by interpreting the results found by the optimization model for the integration scenarios ((5) in Table 3).

The investigated industries have an average waste heat stream of 2.90 MW in the case of glass production and 1.20 MW in the case of the brewery, according to section 2.4. The electricity consumption is on average 6.83 MW for glass production and 4.42 MW up to 8.55 MW for the brewery (see Fig. 6). Scaling the system to the average (minimal) available waste heat stream, according to the heat fraction in EC (12.6%, see section 2.1), would result in an electrolysis system size of 23.0 MW for glass production and 9.52 MW for the brewery (according to Fig. 6). The appropriate system scale calculated, by starting from the electricity

consumption and considering the power ratio of three between EC and FC, is 20.5 MW for glass production and 13.3 MW for the brewery.

The effect of the system size, as can be seen in Fig. 13, is the following: In the glass (brewery) industry, the rROL is constant up to a size of 23 (9.5) MW, then a steep decline in profitability follows for the IC scenario. The value where this decrease starts corresponds very well to the value calculated in the previous paragraph based on the waste heat of the industry. This means that a rSOC system smaller than this scale resulting from the industry waste heat availability has the maximum benefit from coupling. Above this scale the benefit declines for the coupling in the industry IC. In the scenario shown in Fig. 13, the system operates 75% in EC- and 25% in FC-mode. Even in scenarios with reversed operation shares (25% EC and 75% FC), the point of decreased rROL is at the same value, however, the slope of decrease is flatter. The influence in the IDH scenario is shown for the glass production in Fig. 13. Here the waste heat availability due to consumption of the district heating grid is highly reduced and therefore, the transition to a rROL-declining region is less pronounced. The advantage of the district heating network acting as FC-heat-sink, does not outweigh the lack of heat for EC operation and the connected decrease in efficiency. Even though the profiles of electricity demand and waste heat availability are different for the glass and brewery industry, the effect on the rROL is very similar. Therefore, the glass industry is chosen as a representation of industry coupling in all other presented calculations.

The increased rROL in the IDH and IC scenarios leaves the width of the reversible zone of Fig. 7 unchanged. However, it allows a wider region of the reversible zone to have a positive rROL, as shown in Fig. 14. Further details concerning the coupling to industries are contained in the Appendix D.

3.3. Influence of dynamic system parameters on the rROL

Here the rROL's dependence on parameters, that reflect dynamic limitations of the rSOC system, is discussed. The base values of these parameters are compiled in Table 1 in section 2.1. The energy consumption connected with non-active modes of the rSOC system includes the heat-up, cool-down and WSB phase. It was modulated simultaneously for all three phases from halve to triple its base value (rem times the value in Table 1). In Fig. 15 one can see the effect on the rROL which is of small significance, for scenarios with high gas grid fees and would be non-observable under low grid fees. The effect in scenario 2050 is stronger than in 2030 since WSB is of higher importance here. In scenarios with insignificant CSB or WSB times, the effect is neglectable.

Due to a vanishing number of cold start events, the heat-up time was found to have a neglectable influence in all the calculated scenarios. The CSB mode, with connected cool-down and heat-up phase, is only very

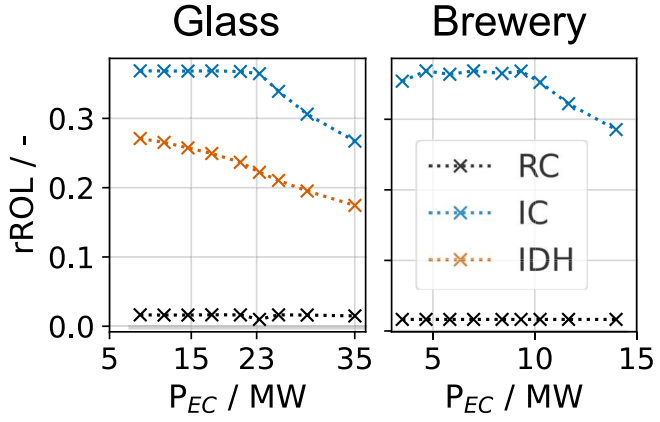

Fig. 13. Influence of rSOC system size on the rROL in the glass industry and the brewery in different coupling scenarios according to section 2.2 for the year 2030 and a spread of −33 €/MWh electricity and hydrogen price.

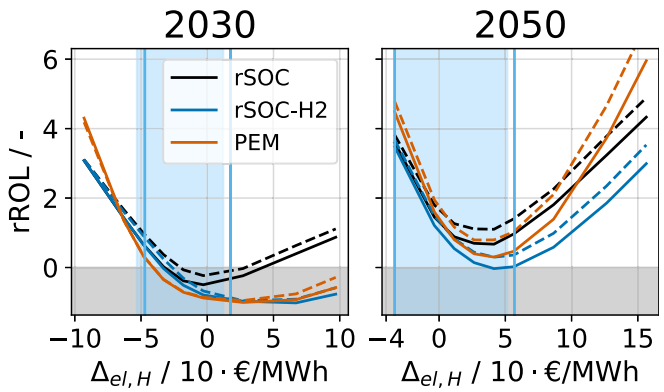

Fig. 14. Influence on the reversible zone by coupling scenario IC (dashed, vertical solid lines show boundaries of the reversible zone) in comparison to RC (solid, filled reversible zone).

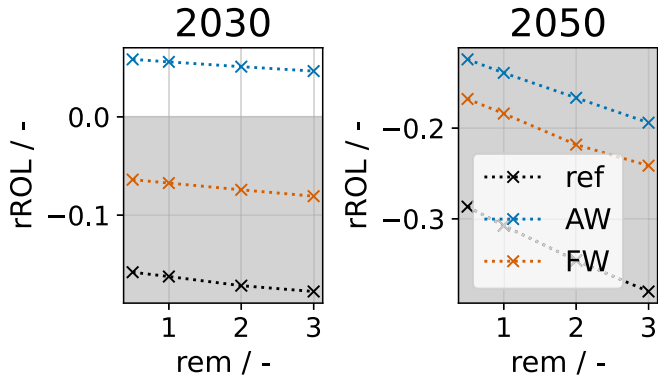

Fig. 15. Influence of the energy consumption during non-active times (WSB and CSB) of the rSOC system with high grid fees (ggf equal 202 €/MWh (2030) and 123 €/MWh (2050)).

rarely a good economic choice, the WSB is preferred. The time for ramp-to EC and ramp-to FC is far below the 1 h resolution limit of these calculations. Therefore, an influence in the model may only arise by the extension of the included non-useful time, but no impact on the rROL was observed.

3.4. Influence of investment parameters on the rROL

This section analysis the influence of parameters in the investment calculation Table 6) on the result of the ROL, which is calculated according to eq. (11). Fig. 16 shows that the specific investment costs for the stack (c_{stack}) and its lifetime (lt_{stack}) have the highest influence on the ROL calculation. With a much smaller but significant impact, the interest rate (i) and degradation over the lifetime (d_{lt}) follow. However, the influence of the degradation is not only through the investment calculation. Degradation influences additionally the optimal choice of operation and therefore the reversible zone. An estimation for this influence is presented in Appendix B. The lifetime of storage (lt_{st}) and compressor (lt_c) have only a secondary role since the connected investment costs are much lower than the ones for the stack.

Since the investment costs of system and compressor have the most significant impact on the rROL, the mechanism of influence on the calculations is clarified here. The system's operation is optimized independent from these CAPEX costs, which play a role only in the investment calculation (according to eq. (11) and (12)). Therefore, the reversible zone is not influenced by a variation of these investment costs. Changed investment costs only displace the lines of rROL, as indicated in Fig. 17, while the reversible zone stays unchanged. This means however,

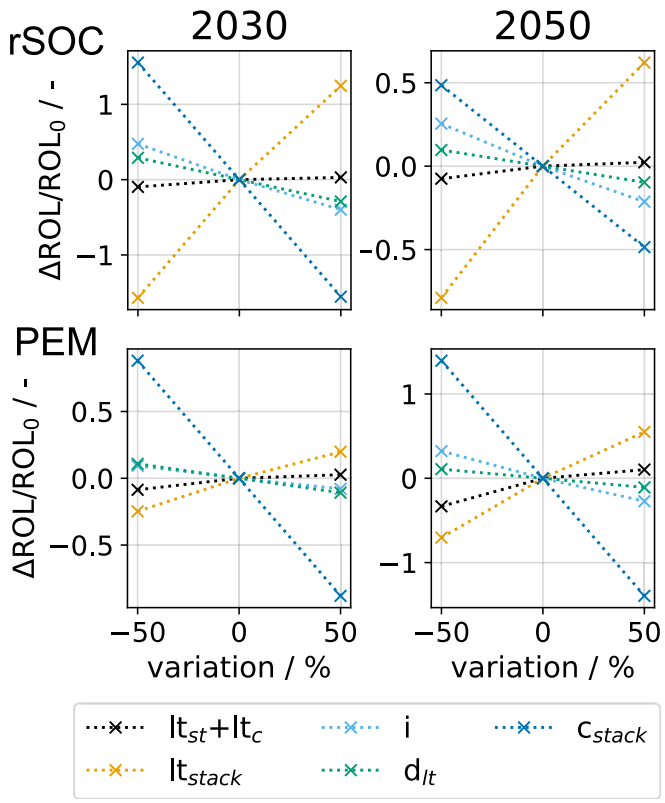

Fig. 16. Sensitivity of the ROL (eq. (11)) with respect to investment parameters for the rSOC and PEM technology.

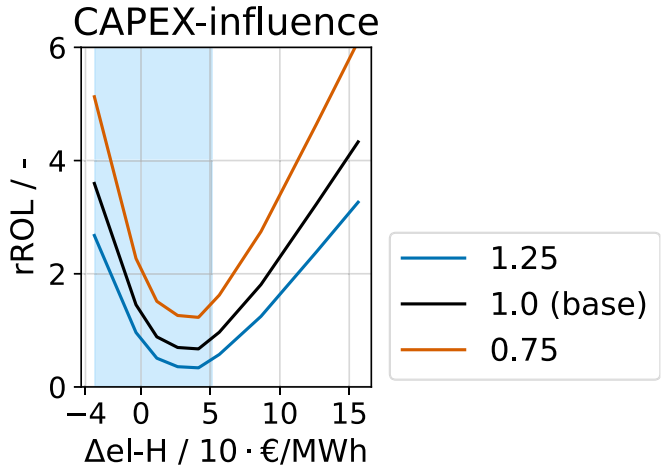

Fig. 17. Influence of the rSOC CAPEX on the rROL and reversible zone (base = Figure 7 A 2050).

that rSOC and PEM-EC/FC lines change the position with respect to each other if the deviations of CAPEX are different for these technologies.

4. Discussion

The presented investigations of rSOC and PEM-EC/FC reversible systems in section 3.1 show, that a zone for the price spread between electricity and hydrogen price exists, where both operation EC and FC operation play a significant role. This market price zone is called here the reversible zone because reversible systems have in this zone at least 10% increased operation hours compared to single-mode systems and can thus be economically more lucrative. In Fig. 7 one can see, that in 2030 a wide range of the reversible zone has a negative rROL. In this case, only a small part of the reversible zone relates to a positive investment result. Whereas, in 2050 the whole reversible zone is profitable. Outside this zone on the left (right) in Fig. 7, EC (FC) systems alone would be economically the best choice. However, there is a low chance that in the future such prices will be seen since electricity and hydrogen price will be coupled by PtHtP systems. Also, the volatility due to renewable power production increases which widens according to section 3.2.1 the reversible zone. This means, that in the future the rSOC and PEM reversible hydrogen systems are likely to find profitable application.

With the help of the present study, it can be concluded furthermore on the influences on this reversible zone and the spatial arrangement. Additionally, one can compare PEM and rSOC systems and show the impact of engineering parameters.

(1) What are the main influences on the reversible zone?

Table 7 gives an overview of the lower and upper limits of the reversible zone with positive rROL, compiling the results of section 3.1 and 3.2. In this table the base price (ggf = 0.0 and fm = 1.0) is compared to increased fluctuations and increased gas grid fees. One can see clearly, that increased fluctuations in the electricity price lead to an increased width of the economic reversible zone. Increased gas grid fees on the other hand, strongly decrease the economical reversible zone, as they decrease the rROL drastically. An exception is the case 2050 with ggf = 12.3 and fm = 2.0, since here higher grid fees only transfer operation time from FC to EC.

The influence of electrical and thermal coupling to industries (scenario IC) increases the profitability significantly and thus makes larger regions of the reversible zone profitable, as is shown in Fig. 14.

(2) Do we need spatially concentrated or delocalized reversible systems?

In section 3.2.2 one can see that the connection to a gas grid infrastructure, providing gas with low storage costs, is of high importance to allow a wide profitable reversible zone. On one hand, this means that reversible systems without gas grid connection can be profitable only for very specific market prices (narrow economic reversible zone with positive rROL and only for 2050, see Fig. 11). Having a gas grid connection allows for a wider reversible zone, making the prospects for profitability more robust. However, for injecting hydrogen into the grid comes with safety and quality regulations and compression may be necessary depending on the injection point in the grid. Therefore, injecting to gas grids relates to investment costs **[61]**, so this connection is economically non recommended below megawatt-scale EC-units and gas lines in proximity. In section 3.2.2 the optimal storage size under different gas grid fees is determined. It is found that only short-term storage of H_2 is locally feasible.

With a gas grid connection, it is not necessary to place EC- and FC-unit in one location, the units can be spatially distributed. This delocalized system has the advantage of using the gas infrastructure for distributing energy. In this way, the necessity for strengthening the electricity grid is reduced. Conversely, a concentrated reversible system

Table 7
Comparison of the positive-rROL-reversible zone electricity-hydrogen-price-difference limits for the rSOC system under changed market prices.

Parameter setup	Lower limit [€/MWh]		Upper limit [€/MWh]	
	2030	2050	2030	2050
ggf = 0.0, fm = 1.0	−53	< −34	−34	52
ggf = 0.0, fm = 2.0	−83	< −34	48	108
ggf = 12.3, fm = 2.0	–	< −34	–	133
ggf = 12.3, fm = 1.0	–	< −34	–	21

is solely dependent on the electricity grid for energy distribution that can only temporarily shift load and production. The concentrated rSOC systems offer an investment advantage by increasing the system costs compared to a pure EC system only slightly (Table 5). This means, that there can be locations where rSOC systems are economically preferred. The question of whether concentrated or delocalized reversible systems are more suitable is a question of the trade-off between the services provided for the electricity grid by delocalized systems and the investment advantage of reversible systems since the local hydrogen storage plays a subordinary role.

A strong impact on the system economy comes from the integration to consumers as shown in Fig. 13 for two industry types. For delocalized reversible systems, the locations for a good system integration are easier to find, as the coupling possibility for only one mode at once should be met. EC units can be placed by renewable production or the SOEC-technology can be placed by waste heat sources **[39]**. The FC units can independently be placed by electricity and heat consumers like industries or residential sites. Locations combining both consumption and production of energy are necessary for concentrated reversible systems to enable high efficiency of energy usage. Anyway, concentrated reversible systems may be considered for electrical- and gas-off-grid applications or emergency energy supply. However, Schöne et al. **[62]** and Cruz-Soto et al. **[63]** performed a techno-economic evaluation of power-to-hydrogen-to-power in isolated off-grid communities, where PtHtP systems need a cost reduction to be competitive with fossil-fuel-based systems.

Concentrated reversible systems are well suited for locations of seasonal fluctuating renewable production and heat demand. These conditions are given in sites which are dominated by room heat demand, like is the case for many industrial sites and residential areas. The room heating has a strong seasonal pattern, as can be seen in Fig. 6. Waste heat of the FC operation can be used for the base heat demand of the room heating and a small heat pump or electric heater may be employed to cover peak loads. In this way, the increased electrical grid load for heating can be reduced in winter. In summer, the concentrated reversible system can produce H_2, especially in regions with high potential for PV and wind power generation. This helps to reduce concurrent peak production and balances seasonal production and demand. In this application the reversible system must be competitive to alternative heating systems. However, for the required seasonal balancing of production and demand, a connection to the storage facilities of the gas grid is crucial. The gas grid needs to provide fuel for FC operation and the H_2 produced in EC operation may be injected to the grid or consumed by nearby industries.

(3) Do PEM-EC/FC- or rSOC systems perform better?

As one can learn from Fig. 12, systems with gas grid connection perform much better than with local H_2 storage. In the case of CH_4 grids, rSOC systems are therefore preferred to PEM systems. However, sites close to H_2 underground storage facilities can perform similarly well like grid-connected systems. In the case of H_2 gas grids the economic preference of PEM-EC/FC- or rSOC-H2 systems is not clear, since in Fig. 7 one finds, that in the scenario year 2030 the rSOC system and in 2050 the PEM-EC/FC system is more lucrative. This difference in the scenario years comes from the magnitude of market price fluctuations and the difference in assumed system cost according to Table 6, which is a big factor of uncertainty. From Fig. 9 one can conclude that fluctuations have a higher positive impact on the PEM system, as it can react faster and with less costs for changing the operation mode (see Table 1). This means that higher fluctuations point to PEM-EC/FC system. However, the system cost uncertainty does not allow an absolute comparison of the technologies.

(4) What is important for rSOC system engineering?

In the section about sensitivity concerning system parameters (section 3.3), one can see that the energy consumed by the rSOC system for non-active operation is significant for the economics of the system operation. The time needed to switch between operation modes on the other hand was found to be irrelevant. In the simulations no high frequent switching from cold standby to warm operation was observed in any scenario that is relevant to the application of a rSOC system. Therefore, no influence of increased heat-up time on the economics is observed. Even though the choice of 1 h for preheating is already at the lower limit of reported values. Current SOC stacks allow a heating rate of 1–10 K/min **[64,65]** which would result in a preheat time of 1 to 7 h. In section 3.4 the system's degradation was found to be of similar importance to the economics like inflation. The degradation does not only impact the investment calculation but also influences the choice of operations, which results in less reversible operation for higher degraded systems.

5. Conclusions

In this work the reversible zone, where reversible hydrogen systems have beneficial economics, is determined and studied under the influence of different market prices. The systems' degradation over the lifetime is found a significant impact on economics and is accounted for by a novel computationally inexpensive method. This method correlates active operation time and degradation with the profit made by the system.

Fluctuating electricity prices are found to be a major influencing factor for the profitability of the investment into reversible hydrogen technologies (see section 3.2.1). Higher price fluctuations on any temporal scale cause a much wider zone, when reversible systems are a good choice, and drastically increased profitability. Furthermore, the thermal and electrical coupling to industries and district heating can increase the profitability in any given market price conditions.

In section 3.2.2 the importance of costs connected with the storage of produced hydrogen is analysed in terms of gas grid fees and investment costs for local storage vessels for compressed H_2. The results show, that under high storage costs the profitable reversible zone becomes very small. Thus, it is risky to make an investment in reversible systems under such conditions. Furthermore, these investigations show that storing H2 locally is economically feasible only for timescales up to a few hours.

The observations connected with local storage and the importance of gas grid connection enable us to discuss the applicability of spatially concentrated and delocalized reversible systems, in section 4 point (2). Concentrated reversible systems show potential for integration to industrial and residential areas with waste heat availability, heat demand and renewable production. Furthermore, these systems may find application in off-grid communities and in case of energy safety. It would be interesting to study the difference in the influence of concentrated and delocalized systems on the load situation of electricity grids. This can show different aspects, for these systems application, that are not within the scope of the present studies.

The answer to the question whether PEM-EC/FC or rSOC systems perform better is impacted by the high uncertainty of future system investment costs, especially for rSOC systems. However, in the present cost scenario the economic preference depends on the specific market price and coupling scenario. This means that rSOC systems are interesting for application if the cost reduction for rSOC systems, as projected by Böhm et al. **[31]**, will be observed.

We propose future studies to make investigations concerning the spatial system arrangement including the specialities of different conversion technologies, uncertainty of investment costs and the influences on electrical distribution systems. Such combined study can generate a clearer outlook for application potentials which is crucial for planning the structure of future energy supply systems.

CRediT authorship contribution statement

David Banasiak: Writing – review & editing, Writing – original draft, Visualization, Validation, Software, Methodology, Investigation, Formal analysis, Data curation, Conceptualization. **Thomas Kienberger:** Writing – review & editing, Supervision, Funding acquisition, Conceptualization.

Declaration of competing interest

The authors declare the following financial interests/personal relationships which may be considered as potential competing interests:

Thomas Kienberger reports financial support was provided by Austrian Research Promotion Agency. If there are other authors, they declare that they have no known competing financial interests or personal relationships that could have appeared to influence the work reported in this paper.

Data availability

Data will be made available on request.

Acknowledgments

The authors would like to acknowledge the cooperation with partner in the project FIRST, especially Hans Böhm from JKU Linz for the discussions concerning investment costs. This work was financially supported by the Austrian Research Promotion Agency (FFG) with public money from the Austrian Climate and Energy Fund.

Appendix A. Market price variations for the sensitivity analysis of section 3.2

In this part of the appendix, the methodology, for changing the market prices that are shown in Fig. 4 for the analyses in section 3, is shown.

Changing the spread between electricity and hydrogen price:

To investigate the influence of the price spread between electricity and hydrogen the electricity price is shifted by a constant value. The average spread for the base scenario between the electricity and hydrogen price (eq. (13)) is −33.0 €/MWh in 2030 and 26.4 €/MWh in 2050. The average spread between electricity and grid gas price is 31.5 €/MWh in 2030 and 49.5 €/MWh in 2050.

Changing the temporal fluctuations in the electricity price:

The change of the temporal fluctuations is achieved by applying a fast Fourier transform to the electricity price time series, multiplying a section of the frequency spectrum by a spectrum fluctuation modifier (fm), and transforming this modified spectrum back to the time domain. The spectrum of the yearly time series with hourly resolution is divided into three regions as follows: **Long-term** periodicity with frequencies between 1 and 52 a^{-1}, reflecting seasonal to weekly fluctuations; **Mid-term** periodicity with frequencies between 52 and 730 a^{-1}, reflecting weekly to halve daily fluctuations; **Short-term** periodicity with frequencies between 730 and 8760 a^{-1}, reflecting halve daily to hourly fluctuations; **Overall** periodicities from 1 to 8760 a^{-1}. The spectral amplitudes of these three different frequency ranges are then multiplied by the spectral modifier (fm). The back transform of this spectrum is the new price time series with a modified long-, mid- or short-term periodicity or overall periodicity.

Variation of gas grid fee:

The grid gas price is shifted by the gas grid fee (ggf). This is equal to the difference in H_2 purchase and sales prices for the rSOC-H2- and PEM-EC/FC system. For the rSOC system the grid gas purchase price is affected, which is not directly related to the H_2 sales price. For ggf > 1 the purchase of gas from the grid is discouraged. A value smaller than one could be achieved by introducing subsidies for producing H_2.

Appendix B. Degradation

Here the dependence of the annual profit on the degradation parameter d of the reversible systems is discussed (according to eq. (9)). The way of including the degradation allows us to estimate the economic performance over the systems lifetime based on the calculation for the first year, when the system is not yet degraded. The operational and storage design optimisation is performed on a yearly hourly-resolved timeseries for different degradation values and for different operation conditions. This results in different active operation times and choice of operation modes. In Fig. A1 one can see the calculated points and the fitting curves for the resulting influence of the degradation on the annual profit for a PEM- and a rSOC system. The degradation decreases the annual profit. Furthermore, a strong dependence of the degradation-influence on the active operation time of the system can be observed. At higher active operation times the degradational influence is higher, as can be seen in Fig. A1. The least squares optimization algorithm of SciPy for Python **[66]** is used for determining the value of the fitting parameter a_1 of eq. (8). The form of the fitting function (eq. (8)) was chosen without a constant offset, since at zero operation hours, the influence should vanish. The fitted curves can be seen in Fig. A1. With this fitting curves, the degradation can be implemented in the techno-economic evaluation, without performing the operation optimisation calculations for the whole lifetime of the system, but only for an exemplary year. Furthermore, this dependence on changed system efficiency could be used as an easy way to represent systems of lower efficiency, than the ones investigated here.

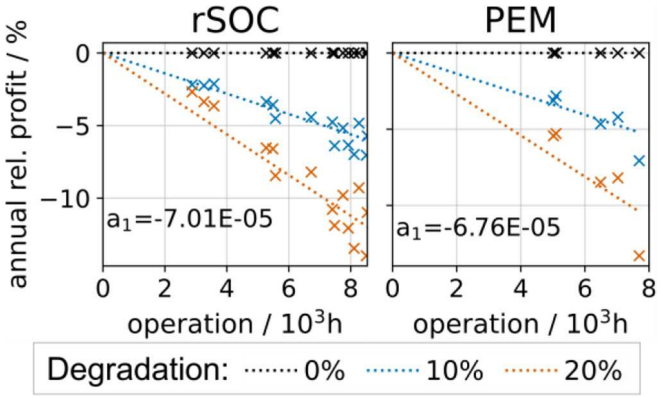

Fig. A1. Change of annual relative profit due to degradation depending on the active operation time for the rSOC- and PEM-technology. The dotted lines show the applied fitting function, with a1 the fitting parameter of eq. (8).

The degradation of the system does not only influence the economic performance, but also the optimal choice of operation modes. The change of operational choice with degradation can be various, as illustrated in Fig. A2. The left graph in Fig. A2, shows a case when the choice between electrolysis and fuel cell operation is influenced, but no increase of stand-still-time is observed. In this case the reversible zone undergoes only a displacement with respect to electricity-H_2-price spread but stays constant in its width. In the case of the right graph in Fig. A2, the fast decrease of FC-H2 and EC operation share consequently decreases the width of the reversible electricity-H_2-price zone. This means, that during the lifetime of the reversible systems, the width of the reversible zone is decreasing. In the present investigations only the reversible zone on basis of the results for the non-degraded state is studied, which is the first year of the system's application. This is justified because the influences of fluctuations and gas grid fee is indicative for any degraded state.

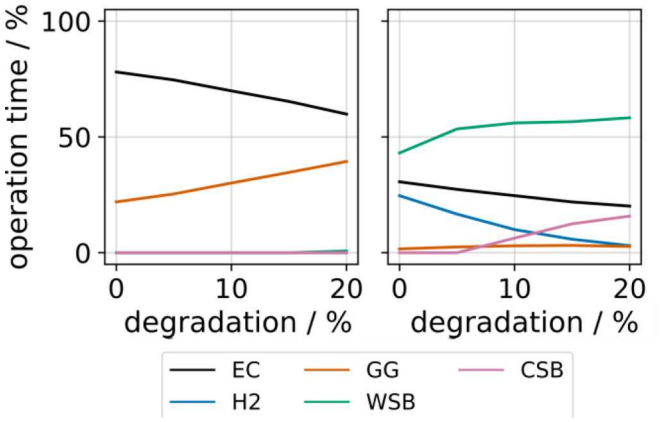

Fig. A2. Influence of degradation on the operation share exemplary for two different sets of calculation parameters.

Appendix C. Supplementary figures for the investigation of influences on the reversible zone

Here the market price dependence of the rROL together with the operation shares under high electricity price fluctuations (Fig. A3, which extends Fig. 10) and high grid gas fees (see Fig. A4, which extends Fig. 11) are discussed. Increased fluctuations flatten the operation share curves close to the EC-FC intersection point, which leads to a widening of the reversible zone. For the increased gas prices especially in 2050 the FC-H2 operation plays a significant role in contrast to the results for the base grid fee shown in Fig. 7 and Fig. A3 for base and increased fluctuations respectively. In 2030 the FC-H2 operation cannot play a significant role since price fluctuations are too low. In this case no overlap of EC and FC operation and therefore no reversible zone with respect to electricity-hydrogen price spread is seen.

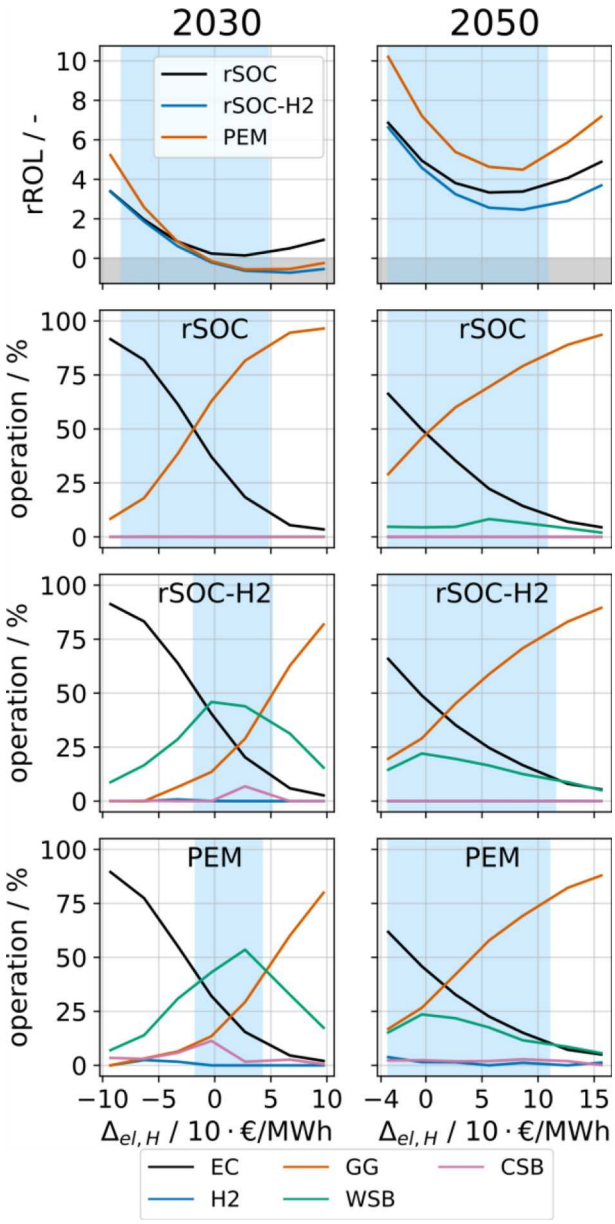

Fig. A3. Dependence of the rROL and operation shares on the electricity-H2-price spread for rSOC, rSOC-H2 and PEM-EC/FC system under overall increased electricity price fluctuations (fm = 2.0), with highlighted reversible zone.

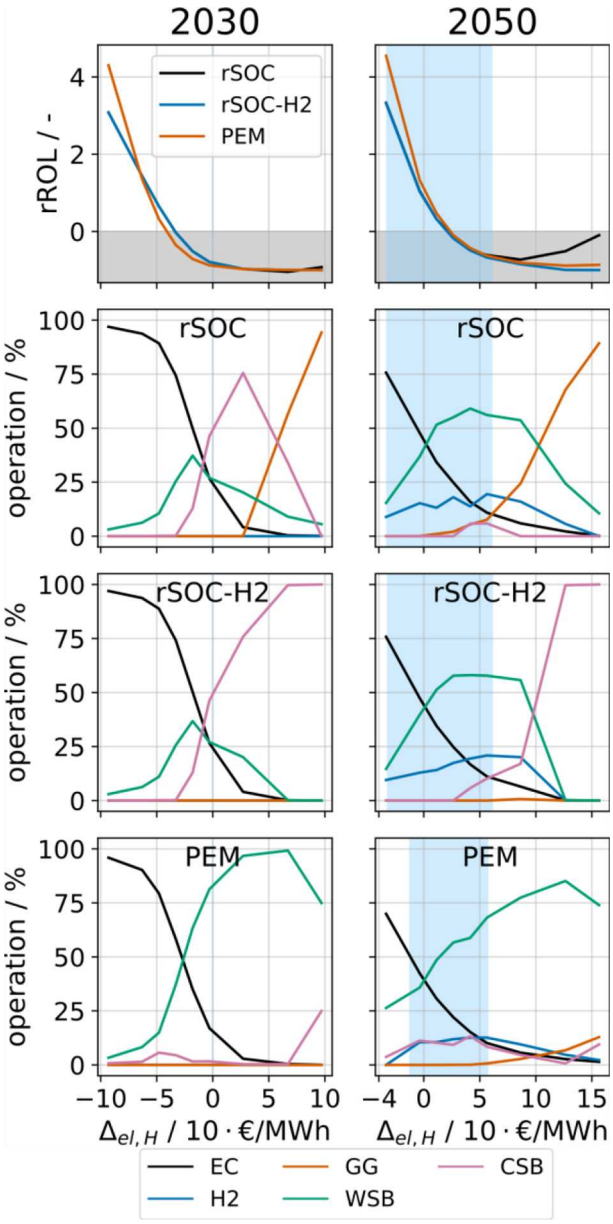

Fig. A4. Dependence of the rROL and operation shares on the electricity-H_2-price spread for rSOC, rSOC-H2 and PEM-EC/FC system under high grid gas fees and base fluctuations (fm = 1.0, ggf equal 202 €/MWh (2030) and 123 €/MWh (2050)), with highlighted reversible zone.

Appendix D. Supplement to industrial coupling

In Fig. A5 one can see the coupling to industry (IC) added in addition to the reference case (RC) to the plot of rROL and share of operations. The reversible zone is nearly unchanged for the IC-scenario. However, due to the utilization of industry waste heat and electricity self-consumption, the rROL increases. This allows in 2030 for a wider range of the reversible zone with a positive rROL. In EC operation the industry coupling influences only the rSOC systems, whereas in FC operation the PEM system gains a higher benefit from the electricity self-consumption. This means for the IC-scenario, that at the right end of the reversible zone, the PEM system gains an advantage over the rSOC system. On the left end of the reversible zone, the rSOC system gains an advantage over the PEM system.

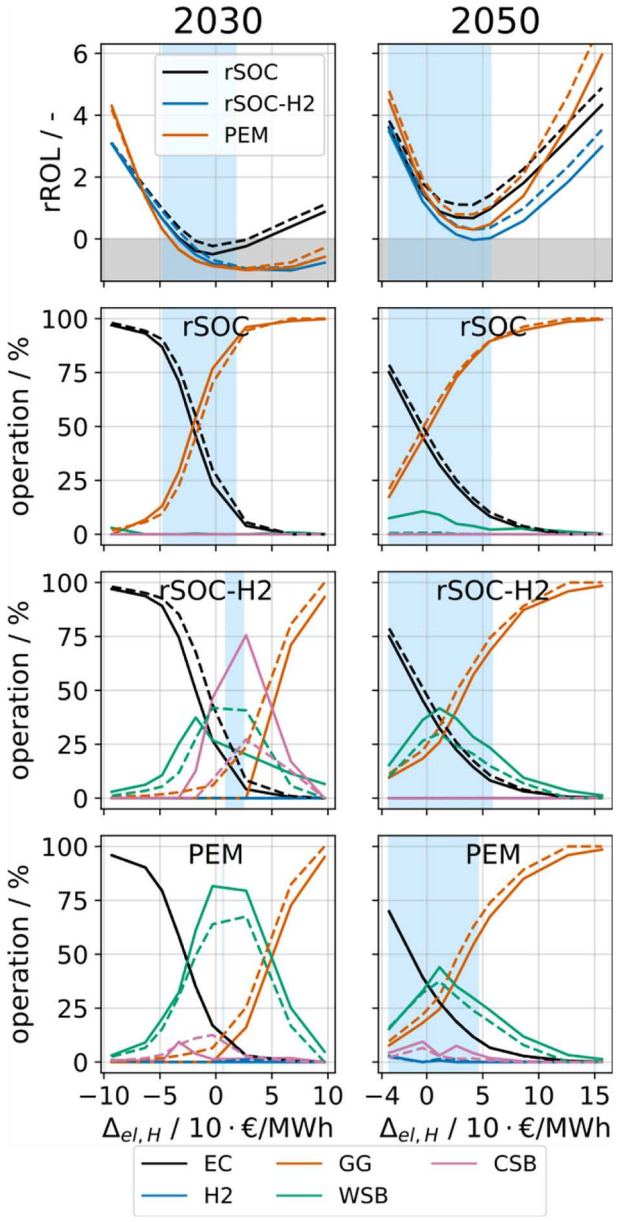

Fig. A5. Dependence of the rROL and operation share with highlighted reversible zone on the electricity-H_2-price spread for the coupling scenarios RC (solid) and IC (dashed).

Appendix E. Storage investment costs

In this investigation one can see the influence of local storage costs on the profitability of the system application. In the case with highly priced grid connection the FC-H2 operation plays especially in 2050 a significant role. The ideal storage size and the rROL is strongly influenced by the storage investment costs, as can be seen in Fig. A6. At increasing low storage investment costs from 0 to 5 €/kWh, the ideal storage size decreases drastically. Low storage costs enable more time of FC-H2 operation and reduce the standby time slightly. Therefore, the system can be operated more profitably and the rROL increases significantly with decreasing storage costs. This means that the economic performance under high grid gas prices could be improved greatly if storages with low investment costs would be available. However, this significant increase in rROL can be observed in Fig. A6, it is not enough to enable an economic self-supply of hydrogen for the RC base scenario. This figure also shows that the influence of the storage price for a variation between 0.8 and 16 €/kWh is rather small compared to the influence of the coupling scenarios, which underlines the importance of thermal system integration.

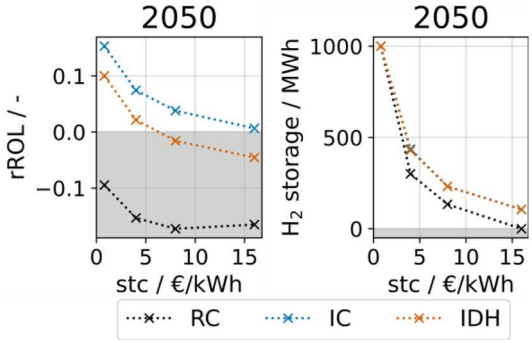

Fig. A6. rSOC-H2 system: Influence of the H_2-storage price (stc) on the rROL, operation and storage size in the 2050 scenario with ggf equal 123 €/MWh (2050).

References

[1] 2015 United Nations Treaty Collection: CHAPTER XXVII ENVIRONMETN: 7. d Paris Agreement. vol. 3156; 2024. https://treaties.un.org/Pages/ViewDetails.aspx?src=TREATY&mtdsg_no=XXVII-7-d&chapter=27. Accessed 29.02.2022.

[2] 2023 IPCC. Summary for policymakers. In: Change IPoC, editor. Climate change 2022 – Impacts, adaptation and vulnerability. Cambridge University Press; 2022. p. 3–34. https://doi.org/10.1017/9781009325844.001.

[3] Sejkora C, Kühberger L, Radner F, Trattner A, Kienberger T. Exergy as criteria for efficient Energy systems—a spatially resolved comparison of the current exergy consumption, the Current Useful Exergy Demand and Renewable Exergy Potential. Energies 2020;13:843. https://doi.org/10.3390/en13040843.

[4] Hunt JD, Byers E, Wada Y, Parkinson S, Gernaat DEHJ, Langan S, et al. Global resource potential of seasonal pumped hydropower storage for energy and water storage. Nat Commun 2020;11:947. https://doi.org/10.1038/s41467-020-14555-y.

[5] Traupmann A, Greiml M, Steinegger J, Kühberger L, Kienberger T. Analysing sector coupling technologies for Re-purposing coal-fired power plants–case study for the ENTSO-E grid. IET Energy Syst Integration 2022. https://doi.org/10.1049/esi2.12087.

[6] Amber Grid, Bulgartransgaz, Conexus, CREOS, DESFA, Elering 2023 European Hydrogen Backbone: Implementation Roadmap - Cross Boarder Projects and Costs Update November 2023. https://ehb.eu/files/downloads/EHB-2023-20-Nov-FINAL-design.pdf; 2023. Accessed 12 Dec 2023.

[7] Cerniauskas S, Jose Chavez Junco A, Grube T, Robinius M, Stolten D. Options of natural gas pipeline reassignment for hydrogen: Cost assessment for a Germany case study. Int J Hydrog Energy 2020;45:12095–107. https://doi.org/10.1016/j.ijhydene.2020.02.121.

[8] Nazir H, Muthuswamy N, Louis C, Jose S, Prakash J, Buan ME, et al. Is the H2 economy realizable in the foreseeable future? Part II: H2 storage, transportation, and distribution. Int J Hydrog Energy 2020;45:20693–708. https://doi.org/10.1016/j.ijhydene.2020.05.241.

[9] Lord AS, Kobos PH, Borns DJ. Geologic storage of hydrogen: scaling up to meet city transportation demands. Int J Hydrog Energy 2014;39:15570–82. https://doi.org/10.1016/j.ijhydene.2014.07.121.

[10] Jamal T, Shafiullah GM, Dawood F, Kaur A, Arif MT, Pugazhendhi R, et al. Fuelling the future: an in-depth review of recent trends, challenges and opportunities of hydrogen fuel cell for a sustainable hydrogen economy. Energy Rep 2023;10:2103–27. https://doi.org/10.1016/j.egyr.2023.09.011.

[11] Corigliano O, Pagnotta L, Fragiacomo P. On the Technology of Solid Oxide Fuel Cell (SOFC) Energy Systems for Stationary Power Generation: A Review. Sustainability 2022;14:15276. https://doi.org/10.3390/su142215276.

[12] Salam MA, Shaikh MAA, Ahmed K. Green hydrogen based power generation prospect for sustainable development of Bangladesh using PEMFC and hydrogen gas turbine. Energy Rep 2023;9:3406–16. https://doi.org/10.1016/j.egyr.2023.02.024.

[13] Scaccabarozzi R, Gatti M, Campanari S, Martelli E. Solid oxide semi-closed CO2 cycle: a hybrid power cycle with 75% net efficiency and zero emissions. Appl Energy 2021;290:116711. https://doi.org/10.1016/j.apenergy.2021.116711.

[14] Zainal BS, Ker PJ, Mohamed H, Ong HC, Fattah I, Rahman SA, et al. Recent advancement and assessment of green hydrogen production technologies. Renew Sust Energ Rev 2024;189:113941. https://doi.org/10.1016/j.rser.2023.113941.

[15] Mohebali Nejadian M, Ahmadi P, Houshfar E. Comparative optimization study of three novel integrated hydrogen production systems with SOEC, PEM, and alkaline electrolyzer. Fuel 2023;336:126835. https://doi.org/10.1016/j.fuel.2022.126835.

[16] Schwarze K, Geißler T, Nimtz M, Blumentritt R. Demonstration and scale-up of high-temperature electrolysis systems. Fuel Cells 2023. https://doi.org/10.1002/fuce.202300059.

[17] Rad MAV, Ghasempour R, Rahdan P, Mousavi S, Arastounia M. Techno-economic analysis of a hybrid power system based on the cost-effective hydrogen production method for rural electrification, a case study in Iran. Energy 2020;190:116421. https://doi.org/10.1016/j.energy.2019.116421.

[18] Skordoulias N, Koytsoumpa EI, Karellas S. Techno-economic evaluation of medium scale power to hydrogen to combined heat and power generation systems. Int J Hydrog Energy 2022;47:26871–90. https://doi.org/10.1016/j.ijhydene.2022.06.057.

[19] Haroon Bukhari M, Javed A, Ali Abbas Kazmi S, Ali M, Talib Chaudhary M. Techno-economic feasibility analysis of hydrogen production by PtG concept and feeding it into a combined cycle power plant leading to sector coupling in future. Energy Convers Manag 2023;282:116814. https://doi.org/10.1016/j.enconman.2023.116814.

[20] Yue M, Lambert H, Pahon E, Roche R, Jemei S, Hissel D. Hydrogen energy systems: a critical review of technologies, applications, trends and challenges. Renew Sust Energ Rev 2021;146:111180. https://doi.org/10.1016/j.rser.2021.111180.

[21] Risco-Bravo A, Varela C, Bartels J, Zondervan E. From green hydrogen to electricity: A review on recent advances, challenges, and opportunities on power-to-hydrogen-to-power systems. Renew Sust Energ Rev 2024;189:113930. https://doi.org/10.1016/j.rser.2023.113930.

[22] Escamilla A, Sánchez D, García-Rodríguez L. Assessment of power-to-power renewable energy storage based on the smart integration of hydrogen and micro gas turbine technologies. Int J Hydrog Energy 2022;47:17505–25. https://doi.org/10.1016/j.ijhydene.2022.03.238.

[23] Schwarze K, Posdziech O, Mermelstein J, Kroop S. Operational results of an 150/30 kW RSOC system in an industrial environment. Fuel Cells 2019. https://doi.org/10.1002/fuce.201800194.

[24] Königshofer B, Boškoski P, Nusev G, Koroschetz M, Hochfellner M, Schwaiger M, et al. Performance assessment and evaluation of SOC stacks designed for application in a reversible operated 150 kW rSOC power plant. Appl Energy 2021;283:116372. https://doi.org/10.1016/j.apenergy.2020.116372.

[25] Peters R, Frank M, Tiedemann W, Hoven I, Deja R, Kruse N, et al. Long-term experience with a 5/15kW-class reversible solid oxide cell system. J Electrochem Soc 2021;168:14508. https://doi.org/10.1149/1945-7111/abdc79.

[26] Santhanam S, Heddrich MP, Riedel M, Friedrich KA. Theoretical and experimental study of reversible solid oxide cell (r-SOC) systems for energy storage. Energy 2017;141:202–14. https://doi.org/10.1016/j.energy.2017.09.081.

[27] Hutty TD, Dong S, Lee R, Brown S. Long term energy storage with reversible solid oxide cells for microgrid applications. Energy Rep 2021;7:24–33. https://doi.org/10.1016/j.egyr.2021.02.059.

[28] Wang L, Zhang Y, Pérez-Fortes M, Aubin P, Lin T-E, Yang Y, et al. Reversible solid-oxide cell stack based power-to-x-to-power systems: comparison of thermodynamic performance. Appl Energy 2020;275:115330. https://doi.org/10.1016/j.apenergy.2020.115330.

[29] Paul B, Andrews J. PEM unitised reversible/regenerative hydrogen fuel cell systems: state of the art and technical challenges. Renew Sust Energ Rev 2017;79:585–99. https://doi.org/10.1016/j.rser.2017.05.112.

[30] Ito H, Miyazaki N, Ishida M, Nakano A. Efficiency of unitized reversible fuel cell systems. Int J Hydrog Energy 2016;41:5803–15. https://doi.org/10.1016/j.ijhydene.2016.01.150.

[31] Böhm H, Zauner A, Rosenfeld DC, Tichler R. Projecting cost development for future large-scale power-to-gas implementations by scaling effects. Appl Energy 2020;264:114780. https://doi.org/10.1016/j.apenergy.2020.114780.

[32] Zhao G, Kraglund MR, Frandsen HL, Wulff AC, Jensen SH, Chen M, et al. Life cycle assessment of H2O electrolysis technologies. Int J Hydrog Energy 2020;45:23765–81. https://doi.org/10.1016/j.ijhydene.2020.05.282.

[33] Gerloff N. Comparative Life-Cycle-Assessment analysis of three major water electrolysis technologies while applying various energy scenarios for a greener hydrogen production. J Energy Storage 2021;43:102759. https://doi.org/10.1016/j.est.2021.102759.

[34] FFG FIRST Fully Integrated Reversible Solid oxide cell sysTem. https://energiefors chung.at/projekt/fully-integrated-reversible-solid-oxide-cell-system/. Accessed 15 Dec 2023.

[35] Schefold J, Brisse A, Surrey A, Walter C. 80,000 current on/off cycles in a one year long steam electrolysis test with a solid oxide cell. Int J Hydrog Energy 2020;45:5143–54. https://doi.org/10.1016/j.ijhydene.2019.05.124.

[36] Nuggehalli Sampathkumar S, Aubin P, Couturier K, Sun X, Sudireddy BR, Diethelm S, et al. Degradation study of a reversible solid oxide cell (rSOC) short stack using distribution of relaxation times (DRT) analysis. Int J Hydrog Energy 2022;47:10175–93. https://doi.org/10.1016/j.ijhydene.2022.01.104.
[37] Srikanth S, Heddrich MP, Gupta S, Friedrich KA. Transient reversible solid oxide cell reactor operation – experimentally validated modeling and analysis. Appl Energy 2018;232:473–88. https://doi.org/10.1016/j.apenergy.2018.09.186.
[38] Paczona D, Sejkora C, Kienberger T. Reversible solid oxide cell systems as key elements of achieving flexibility in future energy systems. In: Sitte W, Merkle R, editors. High-temperature electrolysis. IOP Publishing; 2023. https://doi.org/10.1088/978-0-7503-3951-3ch19. 19-1-19-32.
[39] Banasiak D, Gallaun M, Rinnhofer C, Kienberger T. Integration of a rSOC-system to industrial processes. Energy Convers Managet: X 2023;20:100425. https://doi.org/10.1016/j.ecmx.2023.100425.
[40] Vialetto G, Noro M, Colbertaldo P, Rokni M. Enhancement of energy generation efficiency in industrial facilities by SOFC – SOEC systems with additional hydrogen production. Int J Hydrog Energy 2019;44:9608–20. https://doi.org/10.1016/j.ijhydene.2018.08.145.
[41] Lamagna M, Ferrario AM, Astiaso Garcia D, Mcphail S, Comodi G. Reversible solid oxide cell coupled to an offshore wind turbine as a poly-generation energy system for auxiliary backup generation and hydrogen production. Energy Rep 2022;8:14259–73. https://doi.org/10.1016/j.egyr.2022.10.355.
[42] Philipp Lettenmeier 2021 Efficiency-Electrolysis: White paper. assets.siemens-energy.com/siemens/assets/api/uuid:a33a8c39-b694-4d91-a0b5-4d8c9464e96c/efficiency-white-paper.pdf. Accessed 23 Nov 2023.
[43] Danish Energy Agency 2023 Technology Data - Renewable Fuels: Technology descriptions and projections for long-term energy system planning Version number 0011. 2024. ens.dk/en/our-services/projections-and-models/technology-data/technology-data-renewable-fuels Accessed 23 Nov 2023.
[44] Banasiak D, Gallaun M, Kienberger T. Untersuchung der Kopplung eines rSOC-Systems zur Industrie. https://iewt2023.eeg.tuwien.ac.at/download/contribution/fullpaper/155/155_fullpaper_20230214_143254.pdf; 2023.
[45] Traupmann AM. Advanced modeling and analysis of electrical grids for multi-Energy system approaches. Montanuniversität Leoben 2023:34–6. https://doi.org/10.34901/mul.pub.2023.49.
[46] Austrian Power Grid AG EXAA Spot Market Prices: Day ahead prices. https://markttransparenz.apg.at/en/markt/Markttransparenz/Uebertragung/EXAA-Spotmarkt; 2020. Accessed 25 Mar 2024.
[47] Energy Brainpool GmbH & Co. KG. EU Energy Outlook 2050 - how will Europe evolve over the next 30 years?. https://blog.energybrainpool.com/en/update-eu-energy-outlook-2050-how-will-europe-evolve-over-the-next-30-years/; 2021.
[48] Brainpool GmbH, E., Co, KG. Trends in the development of electricity prices - EU Energy outlook 2050. https://blog.energybrainpool.com/en/trends-in-the-development-of-electricity-prices-eu-energy-outlook-2050/; 2017.
[49] E-Control Systemnutzungsentgelte-Verordnung. SNE-V 2018 BGBl. In: II Nr 398/2017; Änderung BGBl II Nr 466/2022; 2018. https://www.ris.bka.gv.at/GeltendeFassung.wxe?Abfrage=Bundesnormen&Gesetzesnummer=20010107&FassungVom=2023-01-01. Accessed 08 Feb 2023.
[50] European Energy Exchange AG European Energy Exchange eex: Market Data - Natural Gas. https://www.eex.com/en/market-data/natural-gas; 2020. Accessed 25 Mar 2024.
[51] E-Control 2023 Gas-Systemnutzungsentgelte-Verordnung 2013 - Novelle 2024: GSNE-VO 2013 - Novelle 2024 Ausgegeben am 15. https://www.ris.bka.gv.at/Dokumente/BgblAuth/BGBLA_2023_II_396/BGBLA_2023_II_396.pdfsig; 2023. Dezember Accessed 23 Jan 2024.
[52] Binderbauer PJ, Kienberger T, Staubmann T. Synthetic load profile generation for production chains in energy intensive industrial subsectors via a bottom-up approach. J Clean Prod 2022;331:130024. https://doi.org/10.1016/j.jclepro.2021.130024.
[53] Binderbauer PJ. Ganymed: Application for Industrial Load Profile Simulation. Lehrstuhl für Energieverbundtechnik 2022. http://www.ganymed.ga/.
[54] Bundesverband der Energie- und Wasserwirtschaft e.V., Verband kommunaler Unternehmen e.V., GEODE 2018 Abwicklung von Standardlastprofilen Gas BDEW/VKU/GEODE-Leitfaden. https://www.bdew.de/media/documents/Leitfaden_20160630_Abwicklung-Standardlastprofile-Gas.pdf; 2024. Accessed 09 Feb 2023.
[55] Staffell I, Pfenninger S. Using bias-corrected reanalysis to simulate current and future wind power output. Energy 2016;114:1224–39. https://doi.org/10.1016/j.energy.2016.08.068.
[56] Bynum ML, Hackebeil GA, Hart WE, Laird CD, Nicholson BL, Siirola JD, et al. Pyomo — Optimization modeling in Pythonvol. 67. Springer International Publishing Cham; 2021. ISBN 978–3–030-68927-8.
[57] Hart WE, Watson J-P, Woodruff DL. Pyomo: modeling and solving mathematical programs in Python. Math Program Comput 2011;3:219–60. https://doi.org/10.1007/s12532-011-0026-8.
[58] 2023 Gurobi Optimization. Gurobi Optimization, LLC. https://www.gurobi.com; 2024.
[59] Tahan M-R. Recent advances in hydrogen compressors for use in large-scale renewable energy integration. Int J Hydrog Energy 2022;47:35275–92. https://doi.org/10.1016/j.ijhydene.2022.08.128.
[60] Hydrogen and Fuel Cell Technologies Office DOE Technical Targets for Onboard Hydrogen Storage for Light-Duty Vehicles. https://www.energy.gov/eere/fuelcells/doe-technical-targets-onboard-hydrogen-storage-light-duty-vehicles. Accessed 16 Oct 2023.
[61] Butenko Anna, Boots Maroeska. Holstein Johan Injecting green gas into the grid. Dutch Example 2012. https://doi.org/10.2139/ssrn.2581450.
[62] Schöne N, Khairallah J, Heinz B. Model-based techno-economic evaluation of power-to-hydrogen-to-power for the electrification of isolated African off-grid communities. Energy Sustain Dev 2022;70:592–608. https://doi.org/10.1016/j.esd.2022.08.020.
[63] La Cruz-Soto Jd, Azkona-Bedia I, Velazquez-Limon N, Romero-Castanon T. A techno-economic study for a hydrogen storage system in a microgrid located in Baja California, Mexico. Levelized cost of energy for power to gas to power scenarios. Int J Hydrog Energy 2022;47:30050–61. https://doi.org/10.1016/j.ijhydene.2022.03.026.
[64] Khan MZ, Mehran MT, Song R-H, Lee S-B, Lim T-H. Effects of applied current density and thermal cycling on the degradation of a solid oxide fuel cell cathode. Int J Hydrog Energy 2018;43:12346–57. https://doi.org/10.1016/j.ijhydene.2018.04.175.
[65] Zeng Z, Qian Y, Zhang Y, Hao C, Dan D, Zhuge W. A review of heat transfer and thermal management methods for temperature gradient reduction in solid oxide fuel cell (SOFC) stacks. Appl Energy 2020;280:115899. https://doi.org/10.1016/j.apenergy.2020.115899.
[66] Virtanen P, Gommers R, Oliphant TE, Haberland M, Reddy T, Cournapeau D, et al. SciPy 1.0: fundamental algorithms for scientific computing in Python. Nat Methods 2020;17:261–72. https://doi.org/10.1038/s41592-019-0686-2.

10 CONFERENCE CONTRIBUTIONS

Here an overview of the relevant conference contributions, that were created in the course of the work on this thesis, is given.

10.1 C1 NEFI 2021

At the "New Energy for Industry" conference on 6th of May 2021 a presentation was given online by David Paczona with the title "Verschaltungsmöglichkeiten eines reversible Brennstoffzellensystems für den Einsatz in der Industrie und im Energienetz". This presentation gave first insights into rSOC systems and their thermal energy streams. Furthermore, H_2 storage possibilities and a modelling approach was presented.

10.2 C2 EnInnov 2022 [88]

On 17th of February 2022 the presentation entitled "Determining best values of operational parameters for reversible Solid Oxide Cell Systems" was given online by David Paczona at the "Energy Innovation Symposium". The main content was the optimisation of recirculation rate and fuel utilisation, which was visualized in 2D contour plots showing the system efficiency.

10.3 C3 SDEWES 2022

On 9th of November 2022 the presentation entitled "Integration of a rSOC-System to Industrial Processes" was given in Paphos at the conference on sustainable development of energy, water and environment systems (SDEWES) by David Banasiak. This presentation discussed the thermal energy streams in electrolysis and fuel cell operation of a rSOC system, suggested suitable industries for a thermal coupling and evaluated with a static approach the efficiency-advantage of such a coupling.

10.4 C4 IEWT 2023 [89]

On 16th of February 2023 David Banasiak gave a presentation entitled "Untersuchung der Kopplung eines rSOC-Systems zur Industrie" at the "Internationale Energiewirtschaftstagung" (IEWT) conference in Vienna. This presentation concerned the optimal operation of a rSOC system in different integration scenarios to ambient energy systems based on the solution of a mixed integer linear optimisation problem.

10.5 C5 Österreichischer Klimatag 2023 [90]

On 12th of April 2023 David Banasiak presented the poster entitled "H2-Produktion und Flexiblität: Untersuchung eines rSOC-Systems in Wechselwirkung mit industriellen Prozessen"

at the conference “Österreichischer Klimatag” in Leoben. The poster contained different coupling scenarios for rSOC systems to ambient energy systems and operational and economic results for a optimized operation based on the solution of a mixed integer linear optimisation problem.

10.6 C6 SDEWES 2023

On 28th of September 2023 David Banasiak gave a presentation entitled “Levelized cost of hydrogen for an optimally operated rSOC-system in multi-energy systems” at the conference on sustainable development of energy, water and environment systems (SDEWES) in Dubrovnik. In this presentation the influence of degradation on the generated profit of a rSOC system with optimized operation was discussed. Furthermore, this presentation contained the optimal system sizing for integration to industries with available waste heat, the calculation of economic parameters and the levelized cost of hydrogen.

10.7 C7 EnInnov 2024 [91]

On 14th of February 2024 David Banasiak gave a presentation entitled “Reversible und räumlich getrennte Elektrolye-Brennstoffzellensysteme” at the conference “Energy Innovation Symposium” (EnInnov) in Graz. In this presentation a methodology for calculating grid supportive system powers of electrolysis and fuel cell systems was proposed, which allowed for identification of suitable sites for spatial concentrated and delocalized system types.